Title
Epithelial cell polarity and proliferation control in Drosophila melanogaster

Author
Morrison, Holly Ann

Publication Date
2010

Peer reviewed|Thesis/dissertation

Epithelial Cell Polarity and Proliferation Control in *Drosophila melanogaster*

by

Holly Ann Morrison

A dissertation submitted in partial satisfaction of the

requirements for the degree of

Doctor of Philosophy

in

Molecular and Cell Biology

in the

Graduate Division

of the

University of California, Berkeley

Committee in charge:

Professor David Bilder, Chair
Professor Iswar Hariharan
Professor G. Steven Martin
Professor Leonard Bjeldanes

Spring 2010

Epithelial Cell Polarity and Proliferation Control in *Drosophila melanogaster*

by

Holly Ann Morrison

Abstract

Epithelial Cell Polarity and Proliferation Control in *Drosophila melanogaster*

by

Holly Ann Morrison

Doctor of Philosophy in Molecular and Cell Biology

University of California, Berkeley

Professor David Bilder, Chair

The characteristic size, shape, and patterning of animal tissues and organs are regulated by the growth, division, and communication of the cells that make up those tissues. In many cases, the proper functioning of these constituent cells requires the polarized subcellular organization of proteins, lipids and cytoskeletal structures. This is especially true of apicobasally polarized epithelial cells, which make up the majority of tissues in metazoan animals, including mammals. The distinction between apical and basolateral domains in epithelial cells is essential for their roles in absorption, secretion, and protection. Furthermore, numerous diseases, including cancer, involve the loss of apicobasal polarity in epithelial tissues. Therefore, understanding the basic cell biological mechanisms controlling cell polarity is a critical step toward understanding the development and homeostasis of multicellular organisms.

The epithelia of the fruit fly *Drosophila melanogaster* have proven to be an invaluable model system for identifying the genes and cellular pathways controlling apicobasal polarity. Genes required for epithelial cell polarity include components of conserved polarity-regulating complexes and, surprisingly, regulators of the endocytic pathway. Moreover, genes in both classes are also required for proliferation control, and have been categorized as neoplastic tumor suppressor genes (nTSGs). However, the pathways by which nTSGs coordinate cell polarity and proliferation remain poorly characterized. Here I describe experiments which shed light on not only the molecular functions of individual regulators, but also how these regulators interact to accomplish concerted control of cell polarity and proliferation.

In the first part of this dissertation, I address how endocytosis could regulate epithelial cell polarity. The endocytic pathway has been demonstrated to control polarity not only in epithelial cells, but also in non-epithelial cells such as asymmetrically dividing neuroblasts in *Drosophila* and the embryo of the worm *Caenorhabditis elegans*. Surprisingly, polarity regulators have also recently been shown to control traffic through the endocytic pathway. I review the experimental data to support each side of this reciprocal regulation, and discuss several potential models for how the coordinated activities of endocytosis and polarity complexes together mediate cell polarity. In addition, I show how two of the first endocytic nTSGs to be identified – the endocytic

syntaxin *avalanche* (*avl*) and the small GTPase *Rab5* – are connected. While Rab proteins and syntaxins have well-established roles in regulating intracellular vesicle trafficking, how exactly Rab5 activity could be linked to syntaxin-mediated vesicle fusion was previously unknown. Here I provide genetic and biochemical evidence that Rab5 is molecularly coupled to Avl-mediated fusion into the endosome by Rabenosyn and Vps45, which are themselves required for endocytic polarity and proliferation control.

In the second part of this dissertation, I present experiments addressing how polarity and proliferation control could be linked, and how the known nTSGs might mediate this coregulation. In addition to controlling polarity, mutations in the endocytic and junctional nTSGs also disrupt proliferation control in the imaginal discs, though to date, the disruption in polarity has only been correlated with overproliferation; the molecular pathways linking the two phenotypes are unknown. As an approach toward discovering these pathways, I performed a forward genetic screen to identify genes that interact with the nTSG *lethal giant larvae* (*lgl*). I identified a number of regions of the genome which genetically interact with *lgl,* as well as several candidate genes. One such candidate is a gene required in the N-linked glycosylation pathway, which I show is mutated in the previously identified tumor suppressor *tumorous imaginal discs* (*tid*). I provide evidence that N-linked glycosylation is indeed required for epithelial growth control, and further demonstrate intriguing links between N-linked glycosylation and tumor suppression pathways.

Dedication

To Daisy and Dowlin Young. Your kindness changed my life.

Table of Contents

List of Figures

List of Tables

Acknowledgements

First and foremost, I owe an enormous debt of gratitude to David for his mentorship over the years. His passion for scientific discovery is inspiring, and his generosity with his time, attention and fly stocks is enabling. Every experiment David suggested, every journal article he emailed me, every sentence he edited, and every teaching opportunity he took advantage of have been invaluable contributions to my success as a graduate student. More importantly, his support and constructive criticism regarding my own ideas, experiments and writing attempts – good, bad, and ugly – have allowed me to stand behind my successes and failures, objectively evaluate them, and make the next attempts even better. Thank you for bringing out the best scientist in me.

I would also like to thank Iswar Hariharan, Steve Martin and Len Bjeldanes for their valuable comments and suggestions as members of my thesis committee. They provided much valued feedback for experimental approaches and guidance in selecting research directions. Thank you also to Barbara Meyer and Georjana Barnes for their mentorship during my rotations as a first-year student.

Every member of the Bilder lab, past and present, has helped to make my experience fulfilling and enjoyable. Thank you to the former postdocs Sally Horne-Badovinac and Thomas Vaccari for being such helpful colleagues, enjoyable lunch companions and great friends during my first years in the lab. Thanks also, of course, to Anne Classen, Lucy O'Brien and Lara Skwarek for all of their advice about life, graduate school, and everything in between. Thank you to Han Lu and Jennifer Zeitler for all of their patience, advice and training when I was just a wee first-year (and second- and third-year) student. My fellow Bilder lab graduate students have been an incredible support group – including Brandon Bunker, Saori Haigo and my wonderful bay-mate Sarah Windler – thank you for always being able to lend an ear, and for understanding when I had to delay doing the same in return. Laurent Menut, Joe Hill, Joshua Schoenfeld and Lupe Coy were helpful in too many ways to list. Special thanks to Sally for introducing me to stepography, Thomas for introducing me to the beauty of the stovetop espresso maker, to Laurent for showing me more Illustrator tricks in 10 minutes than I ever would have discovered on my own, and to Han, Jen, Anne and Saori for enabling my initial forays into the world of rock climbing.

I am also grateful to Iswar Hariharan and the members of the Hariharan lab for their generosity in sharing resources and time. The thoughtful input and advice they provided during joint lab meetings, practice talks, and random run-ins in the lunchroom, as well as many shared birthday cakes, are greatly appreciated.

I have to thank everyone at the UHS Physical Therapy clinic for helping me mitigate the various physical ailments I suffered from during graduate school – from sprained ankles to irritated IT bands. Most of all, thank you to Bryan Templeman for relieveing the dissertation writing-induced shoulder pain and teaching me correct computer-use posture.

I cannot thank my friends enough for being such a wonderful support system. I'm very grateful that I was able to share this experience with the likes of Lisa Prach and

Leslie Stanton. Being able to count on late-night conversations with Nobu Koch for much-needed comic relief and camaraderie was instrumental in helping me survive even the toughest weeks with my sanity intact. Thank you to Sam and Emily Glick for being the most supportive, kind-hearted, selfless friends I could ask for, and for sharing their guest bedroom, their HBO subscription, their wine, and most of all their friendship.

Although I am fortunate to have many wonderful people in my life, a few have been particularly significant. Thank you to Elaine Preston for being such a kind-hearted and inspirational high school science teacher, and to Professor Len Seligman for introducing me to basic scientific research and for encouraging me to attend graduate school. Finally, "Thank you" will always be an insufficient expression of my gratitude to Daisy and Dowlin Young, whose kindness and generosity set me on the path to where I am today.

Thank you to my entire family for their unconditional support over the many years of education, and for their unwavering confidence that I would succeed at whatever I set out to do. My parents have always wanted nothing but the best for me, and I am so grateful for everything that they have done to help me attain it. Thank you also to my sisters for putting up with my big-sister antics for so long, and for not holding a grudge about, well, most of them.

Above all, thank you to my best friend, confidante, and companion Steven. He has been an incredibly supportive partner, and a much needed positive influence in my life in more ways than I can enumerate. He helps me make the best of every situation, and often convinces me that the setbacks really aren't as bad as they may seem. Most of all, he helps me to not take myself too seriously, and somehow encourages me to laugh at myself without making me feel like a complete fool. Thank you, Steven, for standing by me through this experience, and for not letting me forget about the things that really matter, like enjoying good food and warm summer evening happy hours with the people I love.

Chapter 1

Introduction

In the realm of biology, cells are the universal building blocks. Animals, plants, fungi, bacteria and archaea all are composed of cells, whether single-celled organisms or complex multicellular animals. In order for an organism to survive, its constituent cells must coordinate their own activities with those of neighboring cells and the surrounding environment. Often, this coordination results in cells acquiring diverse specialized functions, such as the shmooing of mating yeast cells, the migration of neutrophils of the immune system toward pathogens, and the absorption of water from the soil by plant root hair cells. Strikingly, many specialized cellular functions require morphological changes and the presence of partitioned subcellular domains within the cells themselves. How such partitioning, or polarization, is achieved and maintained by a diversity of cell types is a fundamental question in cell biology.

Extrinsic environmental cues orient cell polarity

For many polarized cells, the extracellular environment provides extrinsic cues responsible for orienting the direction of cell polarization. Perhaps the most well-characterized example of this is the polarization of epithelial cells in response to contact with other cells or an extracellular protein matrix. In the first instance, adhesion between cells mediated by E-Cadherin distinguishes free surfaces from 'contacting' surfaces, while in the latter, contacting surfaces are created by the binding between integrin adhesion molecules and the extracellular matrix (Yeaman *et al.*, 1999). Extracellular cues also play an important role in orienting the direction of cell polarization within the plane of a tissue, as is seen by the alignment of the hairs in the vertebrate inner ear or in the process of body axis elongation during development (Zallen, 2007; McNeill, 2010). Finally, asymmetrically dividing cells such as self-renewing stem cells in the germ line of the fruit fly *Drosophila melanogaster* depend on their immediate surrounding environment, or niche, to maintain stem cell identity and the ability to divide asymmetrically (Yamashita *et al.*, 2010).

In the absence of extrinsic cues, epithelial Madin-Darby canine kidney (MDCK) cells grown in suspension express polarity markers in an unpolarized manner. However, many cells can rely entirely on intrinsic cellular cues to establish polarized axes. During its asexual reproduction, the single-celled budding yeast *Saccharomyces cerevisiae* organizes its cytoskeleton, organelles and protein trafficking to direct cellular growth toward the bud site (Drubin and Nelson, 1996). Moreover, even cells which typically orient their axis of polarity in response to extrinsic cues are fully capable of establishing a polarized morphology, albeit in a random direction. *Drosophila* neuroblasts removed from their *in vivo* environment continue to divide asymmetrically, but the axis of division is no longer along a consistent axis (Siegrist and Doe, 2006). In addition, disruptions in planar cell polarity pathways are manifested by loss of coordinated planar tissue organization, yet the individual cells establish polarized morphologies (McNeill, 2010).

Intrinsic pathways also control cell polarity

The observation that extrinsic cues are not explicitly required for all cell polarity, coupled with the intuition that extrinsic cues must ultimately impinge on intracellular

polarity pathways, argues that intrinsic cues are essential for controlling cell polarity. What are those intrinsic cues, and on which cellular pathways do they act in order to effect polarization? A large field of research has been devoted to answering these questions, and has identified complexes of proteins that are both themselves localized in specific patterns in polarized cells, and are required for cell polarity.

One of the most striking observations regarding cell polarity regulators has been their remarkable conservation, not only across evolutionarily divergent species, but across the polarized cell types. The best examples of such regulators are the *partition-defective* (*par*) genes, six of which were identified in a screen for genes required for axis specification in the *Caenorhabditis elegans* embryo (Kemphues *et al.*, 1988). Moreover, the *par* genes are conserved across vertebrate and invertebrate species and act as important polarity regulators in a variety of cells. The PAR proteins are required for the anterior-posterior asymmetry of invertebrate oocytes and the polarized migration of vertebrate cells (Suzuki and Ohno, 2006). In *C. elegans*, the PAR-1 and PAR-2 proteins are specifically localized to the cortex in the posterior half of the single-celled embryo, while a complex containing PAR-3, PAR-6 and atypical protein kinase-C (aPKC) localizes to the anterior cortex. Similarly, in the *Drosophila* oocyte, PAR-1 is found at the posterior pole, from which the aPKC complex is specifically excluded and therefore is found at the cortex in all but the most posterior of the oocyte. In migrating mammalian astrocytes, a complex of PAR6 and aPKC localizes to the leading edge and is required to orient polarized biosynthetic trafficking and the microtubule organizing center along the axis of migration (Macara, 2004; Rosse *et al.*, 2009). Finally, the aPKC-PAR6 complex is essential for apicobasal polarity in epithelial cells in both vertebrates and invertebrates (Suzuki and Ohno, 2006).

Apicobasal polarity in epithelia

It is thus apparent that while proteins that regulate cell polarity have been evolutionarily conserved, they have been adopted for use in very different cell types, and the pathways both upstream and downstream from the PARs and related proteins vary depending on the cellular context. One example which is especially prevalent and important for animal development is that of apicobasally polarized epithelia. The predominant tissue type among metazoan animals, epithelia are made up of layers of tightly associated polarized cells. In mammals, epithelia are found in the skin, lungs, intestines, and the various mucosal membranes. These sheets of cells not only provide a barrier between the external environment and the interior of the organism, but they also serve functions such as absorption and secretion. Moreover, the apicobasal polarity of epithelial cells is often essential for their functional activities (Gibson and Perrimon, 2003). Epithelial cells vary in shape, existing as cuboidal, columnar, or squamous, but share the common property of being polarized along the apicobasal axis perpendicular to the plane of the tissue, with the apical surface free or facing a lumen, and the basal surface contacting the extracellular matrix. Furthermore, epithelia may be classified as “simple,” consisting of a single monolayer of cells, while “stratified” epithelia include multiple cell layers.

In mammalian epithelial cells, particular protein complexes define the apical and basolateral domains, which are separated by the tight junctions (TJs) and the zonula adherens (Bryant and Mostov, 2008). A cytoplasmic protein complex consisting of the PDZ proteins (named for the protein family members PSD-95, Dlg and ZO-1) Discs Large (Dlg) and Scribble (Scrib) localizes to basolateral surfaces, along with Lethal Giant Larvae (Lgl). Both the Crumbs3-PATJ-PALS1 and the CDC42-PAR3-PAR6-aPKC complexes convey apical identity, though the proteins of the latter complex can also be found divided into the apical CDC42-PAR6-aPKC complex and the PAR3-aPKC tight junction complex (Bryant and Mostov, 2008). The apical zonula adherens consists of adherens junctions arrayed around the cell to form a continuous band of connection to neighboring cells; cadherins, nectins and nectin-like molecules are the major structural proteins present in the adherens junctions (Wang and Margolis, 2007). Finally, the tight junctions are found apical to the zonula adherens, and serve as a barrier to both membrane protein diffusion between the apical and basolateral membranes and to transepithelial transit between cells (Steed *et al.*, 2010).

The subcellular localization patterns of the PAR, Scribble and Crumbs protein complexes are regulated and maintained by cross-regulation between these very complexes (Gibson and Perrimon, 2003; Wang and Margolis, 2007). At early stages of polarization, aPKC and PAR6 form a complex and together bind Lgl. Cdc42 binding to PAR6 stimulates the kinase activity of aPKC, which phosphorylates Lgl, causing Lgl to dissociate from the PAR complex. aPKC-PAR6 then binds to PAR3 at the cell-cell junctions, and will continuously exclude Lgl from the apical domain. aPKC also phosphorylates the basolateral protein PAR-1b (Suzuki *et al.*, 2004), excluding it from the apical surface, while PAR-1 can phosphorylate PAR3 and destabilize the apical PAR complex (Benton and St Johnston, 2003). In addition, PALS1 and PAR6 – members of the Crumbs and PAR complexes, respectively – directly interact and reinforce localization of these two complexes to the tight junctions (Hurd *et al.*, 2003). The combined action of these complexes thus sets up mutual exclusion between polarity regulators in the apical and basolateral domains.

Early events in establishing apicobasal polarity in epithelial cells

Much insight into the cellular mechanisms governing the establishment and maintenance of polarity in epithelia has been gleaned from studies of cultured mammalian epithelial cells such as MDCK cells. MDCK cells may be cultured as single cells in suspension or as sheets of polarized cells attached to a substrate. When in isolation, MDCK cells express apical and basolateral markers throughout their plasma membrane. However, upon contact with and E-Cadherin-mediated adhesion to surrounding cells, the apical and basolateral markers are rapidly segregated to distinct domains, with basolateral markers localized to the sites of contact and apical markers redistributed away from the contacting surfaces (Wang *et al.*, 1990; Drubin and Nelson, 1996). The redistribution of polarized markers in response to cell contact is initiated by interactions between junction proteins and PAR complex proteins. The adhesion molecule JAM (junctional adhesion molecule) localizes to sites of cell-cell contact with E-Cadherin, and recruits PAR-3 to these sites (Ebnet *et al.*, 2001; Itoh *et al.*, 2001). In

addition, E-Cadherin-based contact also activates Cdc42 (Kim *et al.*, 2000), which in turn can activate aPKC through a PAR-6-dependent mechanism (Yamanaka *et al.*, 2001). Thus, the initial cell-cell contact leads to polarized localization of the apical PAR complex, which is itself essential for subsequent steps in apicobasal polarization (Suzuki *et al.*, 2001).

Notably, cell-cell contact is not sufficient to completely establish apicobasal polarity in MDCK cells. Cell adhesion to the extracellular matrix mediated by integrins is also required to segregate membrane proteins to distinct domains, and is uniquely essential for determining the orientation of the apicobasal axis (Wang *et al.*, 1990; Yeaman *et al.*, 1999). Although how integrin-mediated adhesion is relayed into downstream effects on the polarity complexes remains unclear, the small GTPases Rac and Rho, along with Myosin-II, have been shown to be required (Yu *et al.*, 2005; Yu *et al.*, 2008), suggesting that reorientation of the actin cytoskeleton in response to contact with the ECM is an essential step in apicobasal polarization.

Adhesion to neighboring cells and the ECM initiates an intracellular cascade of downstream events which polarize the cell along an apicobasal axis, including the elaboration of cell junctions, the reorientation of the cytoskeleton and the vesicle trafficking machinery, and the redistribution of cytoplasmic and surface proteins. Immediately after cell-cell adhesion, spot adherens junctions (AJs) are distributed along the contacting surfaces, but as polarization proceeds, adherens junctions coalesce into the zonula adherens at the lateral surfaces, and tight junctions (TJs) begin to form apical to the AJs (Wodarz, 2002). Cytoplasmic proteins such as ZO-1 and transmembrane proteins such as claudin, occludin, and the junctional adhesion molecule (JAM) make up the tight junctions, and homotypic binding between claudins on adjacent cells forms the basis of the transepithelial barrier function. Interestingly, there is crosstalk between the tight junction proteins such as claudin and the PAR proteins; the PAR and Crb apical polarity complexes are anchored at TJs, while PAR3 is responsible for recruiting additional proteins as the TJ is forming (Knust and Bossinger, 2002). Moreover, aPKC is essential for the formation of functional tight junctions (Suzuki *et al.*, 2001).

The progression toward full apicobasal polarity is also marked by profound changes in the organization of cytoskeletal actin structures and microtubules. In the apical domain, an unknown mechanism leads to the polymerization of actin cables and the formation of protrusions from the apical surface, termed microvilli (Yeaman *et al.*, 1999). Actin filaments also localize along the basolateral membranes and form a cortical ring at the level of the adherens junctions. Interestingly, inducing actin cytoskeleton remodeling by activating the PAR-4 kinase homolog LKB1 in some epithelial cells can lead to complete apicobasal polarization independent of cell-cell contacts (Baas *et al.*, 2004), suggesting that actin-myosin based contractility plays a key role in establishing apicobasal polarity. This suggestion is further supported by the observation that expression of activated Myosin-II regulatory light chain was also sufficient to polarize epithelial cells (Lee *et al.*, 2007; Li and Gundersen, 2008).

Similar to the changes in the actin cytoskeleton observed upon epithelial cell polarization, the microtubule network in polarized cells is organized into distinct structures. Patches of randomly oriented microtubules form in the cytosol at the apical

and basal surfaces, and long bundles of microtubules parallel the lateral membranes, with their minus-ends directed toward the apical surface (Meads and Schroer, 1995; Musch, 2004). This rearrangement of microtubules in response to polarity cues is essential for the polarized vesicle trafficking observed in apicobasally polarized cells (Musch, 2004). Many vesicle trafficking steps depend on the polarized microtubule network and microtubule motors for correct vesicle transit, although this is not an absolute requirement; in cells treated with nocodazole to depolymerize microtubules, some exocytosis of golgi-derived vesicles still occurs (Musch, 2004). More specifically, microtubules seem to be essential for trafficking of cargoes to the apical surface, while the requirement for microtubules in trafficking basolateral cargoes is thus far unclear (Li and Gundersen, 2008).

Cellular mechanisms for differentially sorting apical and basolateral proteins

The cytoskeletal polarity of polarized epithelial cells and its requirement in at least some polarized vesicle trafficking speaks to the need for polarized sorting of apical and basolateral cargoes. Polarized vesicle traffic is essential both in establishing segregated membrane domains and in maintaining apicobasal polarity. Early studies on polarization of cultured epithelial cells revealed that during the early stages of apicobasal polarity establishment, basolateral proteins are directed toward the E-Cadherin-rich sites of cell-cell contact, while apical proteins are directed toward the free surfaces (Wang *et al.*, 1990). Additional studies have led to more complete models of apicobasal protein sorting in the trans-Golgi network (TGN) and recycling endosomes (REs), perhaps through differential cargo recognition by Adaptor Protein (AP)-complex family proteins (Mellman and Nelson, 2008). Polarized cargoes are trafficked to their correct surfaces via either direct or indirect mechanisms – that is, they are either transported directly from the TGN to the apical or basolateral surfaces, or they are first delivered to one surface before being removed, sorted in REs, and transcytosed to the correct surface (Mostov *et al.*, 2000). Furthermore, cargoes trafficked "directly" from the TGN may in fact pass through various intermediate compartments, such as the recycling endosome, before being delivered to their target surfaces (Folsch *et al.*, 2009). This transit through an additional compartment before being delivered to the surface provides an additional site for sorting polarized cargoes, and different cargoes may be sorted at different steps of the secretory pathway. Some sorting certainly takes place in the Golgi/TGN or even prior to the Golgi, as apical and basolateral cargoes have been observed in distinct patches in the Golgi (Keller *et al.*, 2001; Rodriguez-Boulan and Musch, 2005). However, there is evidence that sorting also occurs in post-Golgi tubular structures or endosomal compartments (Nelson and Rodriguez-Boulan, 2004; Polishchuk *et al.*, 2004).

Whether it occurs in the trans-Golgi network or in recycling endosomes, the differential sorting of apical and basolateral cargoes implies that there are signals present on polarized proteins that dictate their localization. In the case of basolateral proteins, the cytoplasmic tails often contain a dileucine- or tyrosine-based short peptide motif (Folsch *et al.*, 2009). These motifs are recognized on proteins in the TGN or the recycling endosome by adapter proteins such as the AP-1B and AP-4 complexes, which

recruit their substrate proteins into basolateral-destined vesicles (Folsch *et al.*, 1999; Nakatsu and Ohno, 2003). Besides the AP adaptor proteins, clathrin has also been shown to be specifically required for trafficking of basolateral but not apical proteins to the membrane (Deborde *et al.*, 2008b). In addition, basolateral cargoes that contain PDZ-interacting domains can be sorted via an AP-complex-independent mechanism (Maday *et al.*, 2008).

In contrast to basolateral sorting, the polarized sorting of apical cargo relies on a much more diverse set of sorting signals, and no universal apical sorting signal has been identified. One striking feature of apical targeting is that the apical signals are not exclusively found in the cytoplasmic domain of apical proteins, but may also be present in the transmembrane or extracellular domains, or part of lipid anchors (Mostov *et al.*, 2000; Folsch *et al.*, 2009). Lipid modifications such as glycosylphosphatidylinositol (GPI) linkages may promote apical sorting by causing their associated proteins to aggregate in lipid rafts in the TGN (Paladino *et al.*, 2002), and these rafts are then preferentially sorted into apical-destined transport vesicles. Intriguingly, association with lipid rafts is not sufficient for apical transport, as apical and basolateral GDI-associated proteins are found in rafts, but protein oligomerization between apical cargoes specifically promotes apical sorting (Paladino *et al.*, 2004; Paladino *et al.*, 2007). One possible explanation for the oligomerization requirement is that the oligomerization is mediated by N-linked or O-linked glycosylation of the extracellular domains, as N-glycans have been demonstrated to be required for apical sorting of some GPI-linked cargoes (Benting *et al.*, 1999). However, it is as yet unclear whether glycosylation is absolutely required for apical sorting of all GPI-linked apical proteins.

In addition to the lipid-raft-mediated apical sorting pathway in polarized epithelial cells, raft-independent sorting pathways also exist. Beyond their putative role in promoting oligomerization of raft-associated proteins, N- and O-linked glycosylation also act as sorting signals for non-GPI-linked apical proteins (Potter *et al.*, 2006a). In particular, N-glycans have demonstrated roles in targeting both transmembrane and secreted proteins to the apical surface (Potter *et al.*, 2004). Interestingly, N-glycan-based sorting is not specific to sorting in the TGN, as it has been shown to act on proteins that traffic through post-endocytic compartments (Potter *et al.*, 2006b). However, the hypothesis that glycosylation can dictate polarized sorting remains controversial, since N-glycosylation is also important for other important aspects of protein integrity such as protein folding, ER-to-golgi trafficking, and retention at the cell surface (Vagin *et al.*, 2009). Furthermore, some N-glycans, such as E-Cadherin and the transferrin receptor, are found only on basolateral membranes, indicating that N-glycosylation is not sufficient to direct proteins to the apical surface. While the putative identification of the carbohydrate-binding lectins VIP36 and galectin-3 as sorting-mediating receptors may lend some credibility to the N-glycan sorting hypothesis, further studies are needed to clarify the significance of glycosylation for apical protein sorting. Moreover, the overall importance of N-glycosylation-mediated sorting for maintaining apicobasal polarity remains unclear (see Chapter 5).

Beyond sorting in the TGN, the differential localization of proteins in apicobasally polarized cells has also been shown to depend on the vesicle trafficking machinery itself.

The best characterized example of this is the exocyst, which was first identified in budding yeast cells as a protein complex required to target protein secretion to the growing bud site (TerBush *et al.*, 1996). The exocyst is an octermic complex comprised of Sec3, Sec5, Sec6, Sec8, Sec10, Sec15, Exo70 and Exo84 (TerBush *et al.*, 1996; Kee *et al.*, 1997). In mammalian cells, the exocyst is required for targeting vesicles from the TGN to the lateral membranes (Munson and Novick, 2006). In budding yeast cells, rather than all eight proteins acting as a complete complex assembled on golgi-derived vesicles, Sec3 and Exo70 have been proposed to act as spatial cues for exocytosis sites, and the delivery of vesicles containing the remaining six exocyst proteins promotes complex assembly and vesicle docking (Boyd *et al.*, 2004). Despite the conservation between the yeast and mammalian exocyst proteins, it seems that polarized epithelial cells use a different mechanism for exocyst-mediated vesicle targeting. During epithelial polarization, the exocyst specifically localizes to cell-cell adhesion sites rich in E-Cadherin and α-nectin (Grindstaff *et al.*, 1998; Yeaman *et al.*, 2004). Interestingly, a recent report indicates that the exocyst may be required for not only lateral protein trafficking, but also for basolateral recycling, apical recycling, and basolateral-to-apical transcytosis (Oztan *et al.*, 2007). Therefore the exocyst may be generally required for exocytic vesicle traffic, and the specificity of polarized trafficking may be provided by additional regulatory factors.

Intracellular vesicle trafficking events are regulated in part by the soluble NSF attachment protein receptor proteins (SNAREs), which include the syntaxin family of membrane fusion proteins (Chen and Scheller, 2001; Cai *et al.*, 2007). In mammalian epithelial cells, the apical and basolateral membranes contain specific syntaxins which act as target SNAREs to modulate polarized vesicle trafficking (Low *et al.*, 1996; Fujita *et al.*, 1998; Mostov *et al.*, 2000). Syntaxin-3 localizes at and controls traffic to the apical surface (ter Beest *et al.*, 2005; Sharma *et al.*, 2006), while syntaxin-4 acts at basolateral membranes (Low *et al.*, 1996). Moreover, specific v-SNAREs have been identified which specify vesicle fusion at the appropriate membranes. Cellubrevin has been implicated in syntaxin-4-mediated fusion in the basolateral domain, while TI-VAMP and VAMP8 specifically regulate fusion at the apical surface (Fields *et al.*, 2007; Pocard *et al.*, 2007).

The vesicle trafficking machinery interacts with polarity complexes

Physical interactions have been identified between the vesicle trafficking machinery and the known polarity-regulating complexes. One seminal example is the interaction between the basolateral protein Lethal giant larvae (Lgl) and syntaxins. This was first observed in yeast cells, in which the yeast homologs of Lgl, Sro7p and Sro77p, bind the plasma membrane SNARE Sec9p (Lehman *et al.*, 1999). In MDCK cells, Mlgl is associated with the lateral membrane as cells are undergoing apicobasal polarization, and binds specifically to the basolateral t-SNARE syntaxin-4 (Musch *et al.*, 2002). In addition, PALS1 is indirectly required for localization of the exocyst to MDCK cell junctions (Wang *et al.*, 2007), and in *Drosophila*, the exocyst is functionally required to maintain Crb localization to the apical domain (Blankenship *et al.*, 2007). Together, these findings suggest that crosstalk between vesicle trafficking machinery and polarity complexes significantly contributes to apicobasal polarity in epithelia. However, a

coherent picture of how the polarized cytoskeleton and vesicle trafficking pathways is linked to the polarity-regulating genes has yet to emerge.

Epithelial polarity in Drosophila

While studies in yeast and MDCK cells have yielded a great deal of insight into the process of cell polarization, much of the genetic and functional analysis of the mechanisms controlling epithelial apicobasal polarity have in fact come from work in *Drosophila* (Tepass *et al.*, 2001; Gibson and Perrimon, 2003; Bilder, 2004). The evolutionary conservation of the genes controlling epithelial apicobasal polarity combined with the genetic tractability, ease of manipulation, and power of unbiased screens in identifying genes regulating polarity have made *Drosophila* an invaluable system for further dissecting the cellular pathways controlling polarity. *Drosophila* possess three well-characterized epithelial tissues: the embryonic epidermis, the imaginal discs, and the follicle cell epithelium. The embryonic epidermis is a primary epithelium formed during cellularization of the blastoderm syncytium. Although the elaboration of apicobasal polarity during cellularization is quite different than that seen in "pre-existing" nonpolarized cells, many of the proteins required are conserved. The imaginal discs are epithelial sacs derived from the polarized embryonic epidermis. They are present during the larval stages of development, and upon metamorphosis give rise to most of the adult tissues. Finally, the follicle cell epithelium surrounds the developing oocyte in the ovary of the adult female fly. This is a self-renewing tissue, arising from division of non-epithelial somatic stem cells in the germarium, and the daughter cells produced by asymmetric stem cell division respond to environmental cues to establish apicobasal polarity.

Each of the *Drosophila* epithelia are apicobasally polarized, and many of the same polarity regulators that act in vertebrate cells are similarly required in flies. One key distinction between fly and mammalian epithelia is that while fly cells do have E-cadherin-based adherens junctions arrayed in the zonula adherens, they lack tight junctions, and instead utilize septate junctions spread along the lateral membranes between cells to prevent transepithelial diffusion. Similar to their localization in vertebrate cells, the Scrib, Dlg, and Lgl polarity proteins localize to the septate junctions along the lateral membranes (Gibson and Perrimon, 2003; Bilder, 2004). The Crumbs complex in Drosophila consists of Crumbs, Stardust (Sdt, PALS1 homolog) and PatJ, and a second complex is made up of aPKC, Bazooka (Baz, PAR3 homolog) and Par6 (Macara, 2004). The Crumbs complex is found in the apical-most domain of Drosophila epithelia, and the aPKC complex is found in the apical and junctional regions. As in vertebrate cells, the localization of the polarity complexes is mutually regulated. The Scrib module is required to restrict apical proteins from the lateral domain (Bilder and Perrimon, 2000), and this is likely through preventing Par3 and Crb localization to the basolateral domain. In addition, Baz is excluded from lateral surfaces by the activity of Par1 (Benton and St Johnston, 2003). Finally, Lgl is phosphorylated by aPKC and excluded from the apical membrane (Betschinger *et al.*, 2003). Altogether, these interactions set up a robust division between apical and basolateral membrane domains.

Diverse cellular mechanisms control epithelial cell polarity

It is satisfying that loss of function mutations in the polarity regulators such as *lgl*, *scrib*, *dlg*, *aPKC* or *Crb* lead to disrupted apicobasal polarity in the *Drosophila* epithelia (Gateff, 1978; Tepass *et al.*, 1990; Bilder and Perrimon, 2000; Wodarz *et al.*, 2000). Yet strikingly, forward genetic screens in *Drosophila* have identified additional cellular pathways that also impinge on apicobasal polarity. For instance, recent data have demonstrated a role for transcriptional regulation by the Polycomb group genes and ubiquitin-mediated protein degradation in regulating cell polarity ((Classen *et al.*, 2009) and S. Windler, pers. comm.). Furthermore, the clearest examples to date of non-classical polarity regulators implicated in cell polarity control are those required for various vesicle trafficking events. Surprisingly, not only exocytic trafficking steps are required for cell polarity. Multiple genes required for various steps of the endocytic pathway have been clearly implicated in controlling epithelial polarity, prompting new models for how apicobasal polarity is established and maintained (see Chapter 2 for detailed descriptions).

Endocytosis is the process by which cells take up cargoes from the plasma membrane or outside the cell and segregate them into internal compartments, including the lysosome, where cargoes are degraded. Genes which regulate various steps of the endocytic pathway and that have also been shown to control cell polarity include *avalanche* (*avl*), *Rab5*, *vps25*, *tsg101* and various members of the AP-2 adaptor protein complex (Wucherpfennig *et al.*, 2003; Lu and Bilder, 2005; Moberg *et al.*, 2005; Thompson *et al.*, 2005; Vaccari and Bilder, 2005; S. Windler, pers. comm.). The endosomal syntaxin *avl* and the small GTPase *Rab5* are required for fusion of endocytic vesicles into the early endosome (Lu and Bilder, 2005), although the details of how these two molecules are linked are not yet known (see Chapter 3). In addition, Vps25 and Tsg101 are members of the ESCRT complexes, which act at the later endocytic step of sorting ubiquitinated proteins into the multivesicular body (Moberg *et al.*, 2005; Thompson *et al.*, 2005; Vaccari and Bilder, 2005).

Despite the clear evidence that these additional cellular pathways are essential for maintaining cell polarity, it is not yet clear how these pathways interact with the known polarity-regulating complexes, nor is it known how their combined activity coordinately controls apicobasal polarity. However, one interesting link has developed between the endocytic pathway and polarity regulators. Emerging data indicate that not only are endocytic regulators required to maintain polarity in a number of epithelial and non-epithelial tissues, but that polarity regulators themselves can control the activity of the endocytic pathway (see Chapter 2). This suggests that controlling apicobasal polarity is a multifaceted problem that is intimately linked to multiple cellular pathways, and that identifying additional polarity regulators will shed much needed light on this complex coordination.

Drosophila neoplastic tumor suppressor genes are required for polarity and growth control

Remarkably, studies of loss of function mutants in the various polarity regulators discussed above have also revealed that many of the same genes required for

apicobasal polarity are also required for epithelial growth control (reviewed in (Hariharan and Bilder, 2006; Humbert *et al.*, 2008)). Mutations in the "junctional" regulators *scrib*, *dlg* and *lgl*, the endocytic regulators *avl*, *rab5*, *vps25* and *tsg101*, or the Polycomb group genes lead to dramatic overgrowth of the imaginal disc and follicle cell epithelial tissues, leading these genes to be designated as *Drosophila* "neoplastic tumor suppressor genes" (nTSGs). The cells that make up these tissues have unique characteristics, such as the loss of apicobasal polarity and regular epithelial architecture, the inability to differentiate, signs of metastatic behavior, and slow but persistent cell proliferation (Hariharan and Bilder, 2006). Many of the polarity-regulating genes were originally identified based on the propensity for mutants to cause tumorous phenotypes in the imaginal discs. While some light has been shed on the molecular roles of some nTSGs, the cellular pathways by which many nTSGs control cell polarity remain unclear (see Chapters 4 and 5).

The *Drosophila* nTSGs are associated with phenotypes reminiscent of those seen in human cancers. In particular, loss of both apicobasal polarity and proliferation control, along with invasive ability, are common characteristics of neoplastic human tumors (Hanahan and Weinberg, 2000; Lazebnik, 2010). The evidence for a conserved role for the *Drosophila* nTSGs in regulating mammalian cancer development is limited but growing. Several specific reports strongly suggest that at least the junctional regulators are implicated in mammalian cancers. For instance, one human *lgl* homolog, *Hugl1*, is significantly downregulated in malignant melanoma cell lines (Kuphal *et al.*, 2006). Also, the human papilloma virus (HPV) oncoprotein E6 promotes the degradation of both *scrib* and *dlg*, and *scrib* expression is decreased in HPV infection-related cervical cancer tumors (Gardiol *et al.*, 1999; Nakagawa and Huibregtse, 2000; Massimi *et al.*, 2004; Nakagawa *et al.*, 2004). Finally, Scrib and Dlg are reduced in tumors originating in breast and colon tissues (Navarro *et al.*, 2005; Gardiol *et al.*, 2006). It is also somewhat gratifying that recent studies have begun to highlight the frequency of altered endocytic trafficking in mammalian cancers (Mosesson *et al.*, 2008; Vaccari and Bilder, 2009), although there is generally little overlap between the Drosophila nTSGs and mammalian endocytic tumor suppressors. Further research will be necessary to clarify the role of endocytic regulators in controlling polarity in mammalian cells, as well as the similarities and differences between endocytic tumor suppression in fly and human epithelia.

Polarity and proliferation control may be mechanistically linked

The downstream pathways through which the polarity regulators Scrib, Dlg, and Lgl exert their effects on cell proliferation are mysterious and largely uncharacterized. There is some evidence that *scrib* may act as a tumor suppressor by promoting E-Cadherin mediated cell-cell adhesion (Qin *et al.*, 2005), and that ErbB signaling is misregulated in *lgl* mutant epithelia (Reischauer *et al.*, 2009). Interestingly, ErbB2 activation is sufficient to promote ectopic cell proliferation and disrupts apicobasal polarity in cultured epithelial cells (Muthuswamy *et al.*, 2001; Aranda *et al.*, 2006). Moreover, the observed polarity disruption, but not ectopic proliferation, requires an interaction between ErbB2, PAR6 and aPKC (Aranda *et al.*, 2006). This identifies at least

one pathway through which the junctional regulators may exert their effects on cell proliferation, although it is unclear whether this pathway is similarly controlled by Scrib, Dlg, and Lgl, and furthermore whether this relationship is evolutionarily conserved.

The observation that polarity and cell proliferation control are both disrupted in human cancer cells and Drosophila nTSG mutant tissues suggests that there may be a conserved link between polarity and proliferation. It is interesting to note that the degree of polarity loss seems to correlate with the degree of tissue neoplasia (Zeitler *et al.*, 2004). Furthermore, mimicking the polarity disruption associated with loss of *scrib* by overexpressing the apical markers Crumbs or aPKC leads to tissue overgrowth (Lu and Bilder, 2005). This exciting observation suggests that the putative link between polarity and proliferation may be causative – that is, apicobasal polarity may be an upstream component of proliferation control pathways. In order to validate this model, it will be necessary to identify additional genes that regulate both cell polarity and growth. Moreover, identifying those genes that interact with the conserved polarity complexes and the endocytic, transcriptional and degradative nTSGs will be particularly informative. Such identifications will provide a more complete picture of how polarity and growth are regulated in epithelia, a critically important question in cell biology.

Investigating the molecular roles of Drosophila tumor suppressor genes in regulating polarity

Although much has been learned about the mechanisms involved in regulating epithelial cell polarity, a number of questions remain unanswered. For instance, how does the endocytic pathway control cell polarity? In Chapter 2, we discuss recent data linking endocytic and polarity regulators, as well as potential models for how the two are integrated to effect polarity control. Furthermore, in Chapter 3, we describe the characterization of two novel endocytic regulators and Drosophila nTSGs, *rabenosyn* and *Vps45*, which provide a mechanistic link between the previously identified nTSGs *Rab5* and *avl*. Additionally, which downstream cellular pathways do the junctional regulators interact with in controlling polarity and proliferation? In Chapter 4, we describe a forward genetic screen to identify genes which genetically interact with *lgl*, and which may provide insight into the cell biological mechanisms linking polarity and proliferation control. Finally, while several of the originally identified Drosophila nTSGs such as *dlg* and *lgl* have been characterized as essential polarity regulators, another "classical nTSG" has not yet been clearly molecularly characterized. In Chapter 5, we describe the corrected identification of *tumorous imaginal discs* (*tid*), its role in the N-linked glycosylation pathway, and interactions between N-linked glycosylation and classical tumor suppressors. These data provide insight into the cellular pathways that are affected by loss of additional nTSGs, and how those may also be linked to epithelial polarity regulation.

Chapter 2

The Reciprocal Regulation between Polarity and Endocytosis

Abstract

The establishment and maintenance of polarized plasma membrane domains is essential for cellular function and proper development of organisms. The molecules and pathways involved in determining cell polarity are remarkably well conserved between animal species. Historically, exocytic mechanisms have received primary emphasis amongst trafficking routes responsible for cell polarization. Accumulating evidence now reveals that endocytosis plays an equally important role in the proper localization of key polarity proteins. Intriguingly, some polarity proteins can also regulate the endocytic machinery. Here we review emerging evidence for the reciprocal regulation between polarity proteins and endocytic pathways, and discuss possible models for how these distinct processes could interact to create separate cellular domains.

Introduction

In biology, the distinction between separate regions of individual cells is of utmost importance, as it impacts cell fate specification, cell movement, cell-based tissue function and developmental processes. Some central examples include asymmetric cell division as in self-renewing stem cell populations and dividing zygotes, cell migration during wound healing or the immune response, and apical-basal polarity of cells providing absorptive and protective functions in epithelial tissues. In each case, the asymmetric distribution of biological molecules such as proteins, RNAs, organelles or lipids along a specific axis is critical for proper polarized cellular function, whether it is in the apical-basal or anterior-posterior axis, in the plane of the tissue (planar cell polarity), or in the direction of migration. While the global organization of intracellular components and compartments is also key to functional cell polarity, we will focus on the role of determinants that influence the polarity of the plasma membrane.

How does a cell achieve distinct polarized membrane domains? Models of targeted exocytosis, including transcytosis, have been most prominent in discussions of the mechanisms underlying plasma membrane polarity (reviewed in Folsch *et al.*, 2009). However, a growing body of evidence has revealed an additional and critical role for endocytosis itself in maintaining polarized membrane domains. Moreover, proteins whose primary role seems to be in controlling cell polarity ('polarity regulators') have been found to participate in the positioning of endocytic machinery and also to regulate various steps in the endocytic pathway. We review here recent work in metazoan systems illuminating the connections between endocytosis and cell polarity, concentrating on advances in two areas: the role of canonical endocytic regulators in controlling polarity, and the role of recognized polarity regulators in controlling endocytosis.

Overview of Endocytosis and Polarity Regulators

Endocytosis is the process of transporting extracellular or membrane-bound cargoes from the plasma membrane into the cell interior via vesicular transport. A number of endocytic routes exist, but here we briefly outline a canonical endocytic pathway. Endocytic vesicles form as invaginations of the plasma membrane that subsequently pinch off, move internally, and fuse with other endocytic vesicles to form an early endosomal compartment. Cargo that enters the early endosome can take two different routes. Cargo destined for degradation remains in the early endosome as it matures into a multivesicular body (MVB), where cargo-containing vesicles invaginate into the interior of the organelle. The MVB ultimately fuses with the lysosome, where internalized cargoes are degraded. Alternatively, cargo destined for recycling rather than degradation is sorted into a specialized recycling endosome and then returned via vesicles to the plasma membrane. Notably, each of these steps is independently regulated by the interaction of multiple proteins (see Chen and Scheller, 2001; Zerial and Mcbride, 2001; Cai *et al.*, 2007 for details).

Polarity regulators, as we define them here, are those proteins that show primary and widely conserved roles in polarizing various cell types. Three key polarity modules are the Crumbs (Crumbs/Stardust/PatJ), Scribble (Scribble/Discs Large/Lethal Giant Larva) and PAR (Par6/Par3/aPKC) modules (Bilder, 2004). These are referred to as modules since not all the constituent proteins are constantly found associated within a single complex, though they functionally act together. Each of these modules localizes to a distinct sub-domain of polarized cells. For instance, in the *Caenorhabditis elegans* (*C. elegans*) embryo, the PAR module localizes to the anterior cortex, while a distinct set of PAR proteins (PAR-1, PAR-2) localize to and specify the posterior cortex (reviewed in Munro and Bowerman, 2009). Similarly, epithelial cells are polarized along an apical-basolateral axis, with the apical surface facing a free surface or lumen, and the basolateral surfaces contacting neighboring cells and the underlying extracellular matrix (Gibson and Perrimon, 2003). In such apicobasally polarized cells, the PAR and Crumbs module proteins localize to the apical domain while the Scribble module proteins localize to the basolateral domain. These segregation patterns are maintained both by complex regulatory interactions between the protein components (Bilder, 2003; Tanentzapf and Tepass, 2003), as well as interactions with additional factors – namely, small GTPases (Iden and Collard, 2008) and plasma membrane phosphoinositides (PI) (Gassama-Diagne and Payrastre, 2009).

These two seemingly independent systems – intracellular trafficking and polarity control – are now thought to work together, with recent data specifically emphasizing the importance of cross-talk between polarity proteins and endocytic regulators.

Endocytic regulators control polarity

Epithelial cells

Epithelial cells, with their distinct apical and basolateral membrane domains, have been a key system for the investigation of cell polarity. Groundbreaking work on epithelial polarity utilized cultured cell models, including Madin-Darby canine kidney (MDCK) cells (Mostov *et al.*, 2003). Exocytic mechanisms of polarity generation in MDCK cells have received the most attention, but alternatives to a 'direct' biosynthetic delivery route have been found. Most notably, some polarized proteins are initially delivered from the *trans*-Golgi network (TGN) to the basolateral surface, but are then endocytosed and re-delivered to the apical surface in a process called transcytosis (examples of apical-to-basolateral transcytosis also exist) (Tuma and Hubbard, 2003). For example, the polymeric immunoglobulin receptor (pIgR) transports its extracellular ligand dimeric immunoglobulin A (dIgA) across epithelial barriers by binding dIgA at the basal surface and then carrying it via a transcytotic pathway to the apical surface for release (Rojas and Apodaca, 2002). Transcytosis seems to require post-endocytic entry into a specialized recycling route, in which a sorting step specifies the internalized cargo for apical redelivery rather than basolateral recycling or transport to the lysosome (reviewed in van Ijzendoorn and Hoekstra, 1999). The relative importance of the endocytosis-dependent transcytotic route versus the direct route varies in different cell types. For instance, epithelial liver cells rely heavily on basolateral-to-apical transcytosis to polarize the apical membrane domain (Rodriguez-Boulan *et al.*, 2005). One might expect that blocking regulators of endocytosis or the recycling pathway would result in retention of transcytotic cargo on an inappropriate cell surface, although there are few examples where this has been examined. In MDCK cells depleted of clathrin, cell junctions form properly but basolateral proteins become mislocalized to the apical surface (Deborde *et al.*, 2008a). However, this phenotype could be attributed to the role of clathrin in sorting in the biosynthetic pathway rather than its role in endocytosis, as cells depleted of AP-2 were not reported to have polarity defects (Deborde *et al.*, 2008a). Thus, evidence for the functional importance of endocytosis in overall epithelial polarity in mammalian cells is currently inconclusive.

By contrast, striking evidence for the importance of endocytosis in regulating cell polarity has come from a number of forward genetic screens in *Drosophila*. These studies demonstrate that regulators acting at multiple stages of the endocytic pathway are required for global apicobasal polarity in the imaginal disc and follicle cell epithelia (Figure 2.2). The first to be reported, Avalanche (Avl), is a syntaxin associated with and required for entry into the early endosome (Lu and Bilder, 2005). Avl functions with Rab5, Rabenosyn-5 (Rbsn) and Vps45 to regulate this process, and epithelia lacking any of the four gene products show identical phenotypes, which include disruption of adherens junctions (AJs), mislocalization of apical proteins at basolateral surfaces and failure to maintain a regular cellular monolayer (See Chapter 3). Components of the ESCRT machinery, which control the subsequent sorting of endocytic cargoes into the multi-vesicular body (MVB) en route to the lysosome, are also required for epithelial polarity and show a similar null phenotype (Moberg *et al.*, 2005; Thompson *et al.*, 2005; Vaccari and Bilder, 2005; Herz *et al.*, 2006). Finally, recent results indicate that polarity-

regulating endocytic steps include the earliest step in the endocytic pathway, namely AP-2 dependent sorting into clathrin-coated vesicles and their scission from the plasma membrane (Windler and Bilder, 2010; G. Fletcher and B. Thompson, pers. communication). Conversely, proteins that act downstream of ESCRT sorting, including Fab1 and the AP-3/HOPS/BLOC complex which regulate entry into the lysosome, are not required for epithelial polarity (Sevrioukov *et al.*, 1999; Rusten and Stenmark, 2006; Wilkin *et al.*, 2008).

Why would canonical proteins that control the endocytic pathway be required for epithelial polarity in the fly? One possibility is that fly epithelia, like mammalian liver cells, rely on transcytosis as an apical transport route. Blocking endocytosis would prevent the post-surface-delivery internalization, sorting, and recycling required to segregate apical- from basolateral-destined cargo (Figure 2.1a). A second possibility is that polarity requires carefully controlled levels of certain transmembrane proteins that act as 'master regulators' of polarized domains or downstream signaling events. Endocytosis could function to restrict surface levels of these proteins by mediating their transport to and degradation in the lysosome (Figure 2.1b). A third possibility is that polarized exocytosis has a certain 'error rate', and endocytosis is constantly required to remove the misplaced proteins (either for lysosomal degradation or transcytosis) in order to prevent the intermixing of domains (Figure 2.1c). Current data does not allow distinction between these and other speculative models. Studies of proteins required in the recycling pathway such as Rab11 would help to distinguish between the first two models, but analyses of Rab11-depleted conditions are hampered by the general requirement of Rab11 for cell viability in *Drosophila*, and also complicated by its additional role in polarized biosynthetic delivery pathways (Emery *et al.*, 2005; Satoh *et al.*, 2005). The polarity phenotypes associated with loss of ESCRT proteins, which would be expected to have their major impact on sorting of cargo destined for degradation, lend some weight to the requirement of lysosomal transport rather than recycling. Other manipulations that would distinguish these routes have yet to be reported.

It is of some surprise that, with the exception of Rab11, fly epithelial cells lacking central regulators of endocytosis can survive, and not only carry out the physiological functions required for cell growth and division but in many cases even cause continuous, tumorous overgrowth. This indicates that the process of endocytosis *per se* is not completely blocked, and that mutant cells have alternative pathways through which membrane can be internalized. While these alternative pathways are capable of allowing sufficient function for viable cell physiology and division, what is lacking is a mechanism capable of maintaining the separation of apical and basolateral domains, which relies heavily on the canonical endocytic pathway.

Neuroblasts and Embryos

Endocytic regulators control polarity in multiple Drosophila epithelia, suggesting that this requirement is not tissue-specific and may apply to epithelial cells in general. Interestingly, there is no evidence thus far for endocytic pathways in controlling the polarity of non-epithelial *Drosophila* neuroblasts, despite the fact that other elements of the polarizing machinery (e.g. the PAR and Scribble modules) are shared between the

two cell types. For instance, the Dynamin-associated protein Dap160 controls localization of the key polarity regulator aPKC in neuroblasts, but this function appears to be independent of any endocytic functions (Chabu and Doe, 2008). Moreover, temperature-sensitive *dynamin* mutants do not alter the polarized localization of aPKC, suggesting that endocytosis may not be important for polarity in dividing neuroblasts (Chabu and Doe, 2008). One rationale for the different requirements for endocytosis in neuroblast and epithelial apicobasal polarity may be the use of divergent polarizing mechanisms. Extrinsic cues mediated by transmembrane proteins play a major role in establishing epithelial cell polarity. Although extrinsic cues can orient the axis of asymmetric neuroblast division, intrinsic cues mediated by cortical proteins are sufficient to orient neuroblast apicobasal polarity in the absence of extrinsic cues (Siegrist and Doe, 2006).

Nevertheless, endocytosis can control polarity in a non-epithelial cell. In the *C. elegans* embryo, membrane-associated polarity determinants specify the cortical anterior-posterior axis. The activity of Rho family small GTPases generates opposing PAR protein domains – PAR-6 in the anterior cortex and PAR-2 in the posterior – which in turn reinforce embryonic asymmetry. The cortical domains form in two distinct phases: establishment and maintenance. The establishment phase seems to rely primarily on RHO-1 and actomyosin contractility to localize the anterior determinants (Motegi and Sugimoto, 2006; Schonegg and Hyman, 2006). Meanwhile, CDC-42 is required specifically during the maintenance phase (Aceto *et al.*, 2006). Endocytosis from the anterior membrane is significantly enriched specifically during the polarity maintenance phase, and this is measurably reduced in embryos partially depleted of dynamin/DYN-1 (Nakayama *et al.*, 2009). This reduction is associated with a decrease in anterior PAR-6 signal and expansion of PAR-2 into the anterior region. Also, the small GTPase CDC-42 expands beyond the anterior domain during maintenance phase while RHO-1 signal decreases. Finally, the presence of PAR-6-labeled endocytic puncta near DYN-1-positive foci suggests that PAR-6 is largely removed from the cortex in a DYN-1 dependent manner (Nakayama *et al.*, 2009) and may indicate a mechanism in which cortical polarity cues are endocytosed and recycled to maintain PAR asymmetry. In budding yeast cells, efficient endocytosis is necessary to correct diffusion of Cdc42 from the bud site (Irazoqui *et al.*, 2005). Remarkably, a similar phenotype is observed in *dyn-1* RNAi-treated *C. elegans* embryos (Nakayama *et al.*, 2009). One explanation for this could be that endocytosis mitigates diffusion of CDC-42 in *C. elegans* embryos, as it does in yeast. In embryos where endocytosis is compromised, spreading of CDC-42 could also lead to dispersal of PAR-6 cortical signal. Alternatively, it is possible that a decrease in DYN-1 levels could affect vesicular traffic at another endosomal compartment, such as the Golgi (Figure 2.3), however current data does not allow distinction between these two speculations.

In addition to dynamin, the correct polarization of PAR complex proteins in *C. elegans* also requires the endocytic recycling regulator, RAB-11 (Zhang *et al.*, 2008). In RAB-11-depleted embryos, the posterior PAR-2 domain is measurably reduced and PAR-3 is no longer restricted to the anterior cortex, often even colocalizing with PAR-2 at the posterior pole. Interestingly, this contrasts with the dynamin depletion phenotype, in

which the posterior PAR-2 domain is ectopically extended into the anterior of the embryo, and suggests that different endocytic mechanisms may be controlling cortical PAR localization at opposite poles of the embryo. The exact details of this distinction are currently unresolved.

From the above examples, it is clear that while transmembrane proteins are natural targets for endocytosis-dependent localization, endocytosis can also play a key role in regulating the localized concentration of cortical proteins. Although it is not clear exactly how the PAR complex associates with the plasma membrane, binding to lipid-modified Cdc42 is one likely mechanism. Phosphoinositides may also play a role in linking polarity cues to the membrane (Wu *et al.*, 2007), raising the intriguing possibility that endocytosis may influence polarity through preferential internalization of plasma membrane domains with specific phosphoinositide content. Identifying the factors involved in tethering the PAR complex to the membrane and determining how endocytic regulators might recognize PAR-enriched domains may greatly advance our understanding of how these mechanisms cooperate and interact, whether directly or indirectly.

Oocytes

Remarkably, in addition to cortical polarity cues, endocytic machinery is also involved in the polarization of cytoplasmic molecules in non-epithelial cells. In the *Drosophila* oocyte, polarization of certain mRNAs is necessary for the specification of the embryonic anterior-posterior axis. Localization of *oskar* mRNA to the posterior of the developing oocyte is required for its translation (Kim-Ha *et al.*, 1991; Rongo *et al.*, 1995), and Oskar protein then polarizes the oocyte in part via an endocytic mechanism (Vanzo *et al.*, 2007). A long isoform of Oskar is associated with endocytic membranes at the posterior pole and is required for the observed high levels of endocytosis there (Vanzo *et al.*, 2007; Tanaka and Nakamura, 2008). When endocytosis is disrupted downstream of Oskar by loss of the Rab5 effector Rabenosyn-5 (Rbsn), the pole plasm proteins Vasa and Tudor are no longer anchored at the cortex but instead become diffusely localized in the cytosol (Tanaka and Nakamura, 2008).

Regulators of additional endocytic steps also participate in the polarization of the Drosophila oocyte. For instance, *Oskar* mRNA requires Rbsn, Rab11 and an intact microtubule array to maintain its posterior localization, and Rab11 as well as Rbsn are required for microtubule polarity (Dollar *et al.*, 2002; Tanaka and Nakamura, 2008). While this suggests an intriguing mechanism for oocyte polarization via cytoskeleton regulation, the molecular link between microtubules and Rab11 or Rbsn, as well as whether the roles of Rab11 and Rbsn in endocytic trafficking are distinct from their role in PAR module and microtubule polarity, is not known. The anterior localization of *bicoid* mRNA in the oocyte requires the ESCRT-II complex (Irion and St Johnston, 2007), but interestingly, this requirement seems independent of endosomal sorting since it is unaffected in ESCRT-I, ESCRT-III or *rabenosyn-5* mutants. Why endocytic regulators are required for the proper localization of certain mRNAs remains to be determined. Why do such a variety of metazoan cells rely on endocytosis to polarize their cytoplasm and plasma membrane? It is interesting to speculate that evolution has taken advantage of

the existing cell biological “infrastructure” of endocytic machinery present even in single-cell organisms, such as budding yeast. Even in unpolarized cells, endosomes and other vesicles are motile and linked to the cytoskeleton (Weisz and Rodriguez-Boulan, 2009), so spatial regulation of this movement could be easily adapted to generate polarity via differential trafficking of transmembrane proteins. Moreover, even without their trafficking functions, endosomes are, like other organelles, ‘singularities’ within the cell cytoplasm. These endocytic organelles could have been adopted as anchors for cytoplasmic macromolecules lacking alternative polarity-maintaining membrane attachments. Finally, endosomes have also been adapted as signaling centers during metazoan evolution; an intriguing possibility is that endosomes are sites where polarity pathways and intercellular signaling pathways can interact with each other.

Polarity regulators affect endocytosis and recycling

While evidence for endocytic regulation of cellular polarity has been rapidly accumulating, concurrent work has also revealed that polarity proteins regulate the endocytic machinery. Interesting observations from *C. elegans* first implicated polarity cues as endocytic regulators. For example, a marker for early endosomes, EEA-1, localizes to anteriorly enriched puncta in a manner that depends on PAR-3 (Andrews and Ahringer, 2007). Similarly, the *C. elegans* ortholog of dynamin, DYN-1, is enriched and maintained in the anterior cortex in a PAR-6- and PKC-3/aPKC-dependent manner (Nakayama *et al.*, 2009). The clearest evidence for a functional link emerged when the anterior PAR module and the Rho GTPase CDC-42 were shown to be required for efficient endocytosis in *C. elegans* (Balklava *et al.*, 2007). Reduced function of any of these proteins also impairs endocytic traffic in non-polarized Chinese hamster ovary (CHO) cells. Cdc42 and Par-6, in particular, are required for the uptake of clathrin-dependent cargo as well as the recycling of clathrin-independent cargo, demonstrating specific roles for polarity cues in both endocytosis and trafficking (Balklava *et al.*, 2007). These findings point toward a specific, unexpected and conserved role for PARs in regulating endocytic traffic.

Studies in *Drosophila* epithelial cells have emphasized the importance of PAR-regulated endocytosis, but have also revealed that the details of the mechanisms may vary between cell types. Disruption of Cdc42 function in the embryonic ectoderm leads to a loss of apical proteins from the plasma membrane and their accumulation in enlarged endocytic structures within affected cells (Harris and Tepass, 2008). Similar accumulations of apical cargo are observed in *par6* and *baz/par3* mutant embryos, suggesting that Cdc42 and the Par proteins function as negative regulators of apical endocytosis. Consistent with this, reducing endocytosis by disrupting Rab5 function rescued the phenotypes of Cdc42-compromised cells. Surprisingly, the compartment in which apical cargo accumulated contained markers of early endosomes, suggesting that further advancement through the endocytic pathway was blocked. Thus, in the *Drosophila* embryo Cdc42 and the PAR module appear to function in two distinct roles: negatively regulating early apical endocytosis, and positively regulating early endosome to late endosome maturation (Figure 2.2), although an additional role in regulating recycling cannot be ruled out.

Two groups independently determined that Cdc42, Par6 and aPKC control *Drosophila* epithelial organization through regulation of endocytosis, although the results of their experiments in imaginal discs differ somewhat from the observations in neuroectodermal cells. In these studies, cells lacking functional Cdc42, Par6 or aPKC contained enlarged Rab5- and Rab11-positive endosomes, as well as discontinuous AJs and E-cadherin-rich junctional extensions and puncta (Georgiou *et al.*, 2008; Leibfried *et al.*, 2008). Similar AJ discontinuities and E-cadherin-rich structures were observed in cells with disrupted shibire/Dynamin function, suggesting that the structures observed in the Cdc42-, Par6- or aPKC-compromised cells are arrested endocytic structures and that E-cadherin is endocytosed in a dynamin- and Cdc42-regulated manner. It thus seems that in the imaginal disc, in contrast to the embryonic ectoderm, the PAR proteins positively regulate scission of endocytic vesicles containing junctional cargo

from the membrane, and this contributes to the maintenance of junctions and proper localization of polarity cues.

How could polarity cues affect endocytic trafficking? One possibility is that the cortically localized Cdc42/PAR module regulates regions of endocytic activity, perhaps through specific polarized GTPase-activating proteins such as Rich1 (Wells *et al.*, 2006). Par6 and aPKC may also act in conjunction with other Cdc42 effectors after recruitment to the apical or anterior membrane. The kinase activity of aPKC could phosphorylate targets, such as endocytic regulators or adaptor proteins, which specify the rate and identity of endocytosed cargo; one example is the AP-2-interacting endocytic adaptor Numb (Nishimura and Kaibuchi, 2007; Smith *et al.*, 2007). Another possibility is that proper polarity protein function is required for cytoskeletal organization. In the imaginal disc, the phenotypic similarity between Cdc42, the Cdc42 effector Cip4, dynamin, WASp and Arp2/3 suggests that Cdc42 regulates E-Cad endocytosis in part through regulated actin polymerization (Georgiou *et al.*, 2008; Leibfried *et al.*, 2008). While this might suggest that a general misregulation of cortical actin contributes to the endocytic defects, the lack of endocytic phenotypes in tissues with disrupted cortical actin, such as those mutant for Rac or Scar, suggests that WASP and Arp2/3 regulate actin in a more specific context, perhaps in promoting Dynamin-dependent vesicle scission. The PAR module may also promote the efficient endocytic trafficking of cargo by affecting microtubule organization and/or dynamics (Schmoranzer *et al.*, 2009; reviewed in Munro, 2006). While the evidence for polarity cues organizing endocytic traffic is convincing, the details of the molecular mechanisms remain unclear. Identifying interactions, both direct and indirect, between the polarity machinery and endocytic regulators will lead to a clearer view of how certain polarity proteins act as positive or negative regulators of endocytosis in different contexts.

Discussion

The emerging data suggest a synergistic model in which polarity and endocytosis regulators mutually contribute to the proper functioning of polarized cells. Due perhaps to the apparently context-specific behavior of some molecules, no simple, central model has yet emerged. However, it seems that dialogue between the two regulator classes reinforces the proper positioning and activity of both polarity cues and endocytic machinery (Figures 2.2 and 2.3). In the clearest example, the PAR module may promote dynamin-dependent endocytosis, while dynamin-dependent endocytosis may be required to maintain correct localization of the PAR module. As work in these fields continues, similar examples are likely to arise and yield a more cohesive and complete view of the interplay between polarity and endocytosis.

The data from various experimental systems suggest that the cooperation between cell polarity and general endocytic traffic is conserved across different cell types and organisms. There is, however, variability in whether a particular polarity regulator acts positively or negatively on trafficking steps, and on what step of endocytic traffic the polarity regulators exert their influence and vice versa. Moreover, the interactions between the endocytic and polarizing proteins could be direct or indirect, and no studies have yet explicitly addressed this uncertainty. Further work will also distinguish between the possibilities of polarity regulators impacting the endocytic and trafficking pathways through actin and/or microtubule organization, or by more directly affecting endocytic regulators, perhaps through aPKC-dependent phosphorylation. Finally, the importance of the relationship between endocytosis and polarity regulators in establishing versus maintaining polarity based on other cellular cues remains ambiguous. While models derived from *in silico* and *in vivo* data in budding yeast imply that endocytosis and recycling can be an integral component of polarity maintenance mechanisms (Marco *et al.*, 2007; Slaughter *et al.*, 2009), more extensive analyses are necessary to determine the importance of endocytosis in establishing polarized axes during metazoan development.

Overall, the work reviewed here indicates that the standard cellular process of endocytosis exists in a flexible, reciprocal relationship with polarity regulators and is utilized by organisms in differing ways to organize asymmetric domains. While we have focused our discussion on animal models, it is important to note that a growing body of research emphasizes the importance of cell polarity in plants as well (reviewed in Geldner, 2009). Future advances toward elucidating polarization mechanisms will benefit from the introduction of quantitative, real-time fluorescent trafficking assays to invertebrate systems, and potent *in vivo* disruption of the endocytic pathway to vertebrate systems. Ultimately, a more complete understanding of the interplay between endocytosis and polarity and the reasons why particular cell types employ specific regulatory strategies will clarify the mechanisms necessary for proper organismal development and potentially provide new treatments for the numerous diseases associated with disruptions in cell polarity (reviewed in (Mellman and Nelson, 2008)).

Figure 2.1: Possible models for endocytosis in controlling polarity in epithelia.
(a) Newly synthesized apical proteins (dark green) could first be delivered from the Golgi network to the basolateral membrane (orange) before being endocytosed, sorted and transported to the apical membrane (light green) in a process called transcytosis. The apical membrane is separated from the basolateral membrane by cell-cell junctions (yellow). When endocytosis is blocked, these apically-destined proteins may aberrantly accumulate on basolateral surfaces, disrupting apical-basal polarity. (b) Surface levels of hypothetical 'master polarity regulators' (dark green) may normally be kept in check by endocytosis. When endocytosis is blocked, these master regulators could accumulate on the cell surface, leading to mispolarization of the cell. (c) Intrinsic exocytosis error rates or lateral diffusion between membrane domains may occasionally lead to mislocalized basolateral polarity proteins (dark red) on the apical surface, which are removed from the incorrect domain via endocytosis and degraded in the lysosome (purple compartment). Disruptions in endocytosis would lead to unmitigated delivery errors and subsequent polarity perturbation.

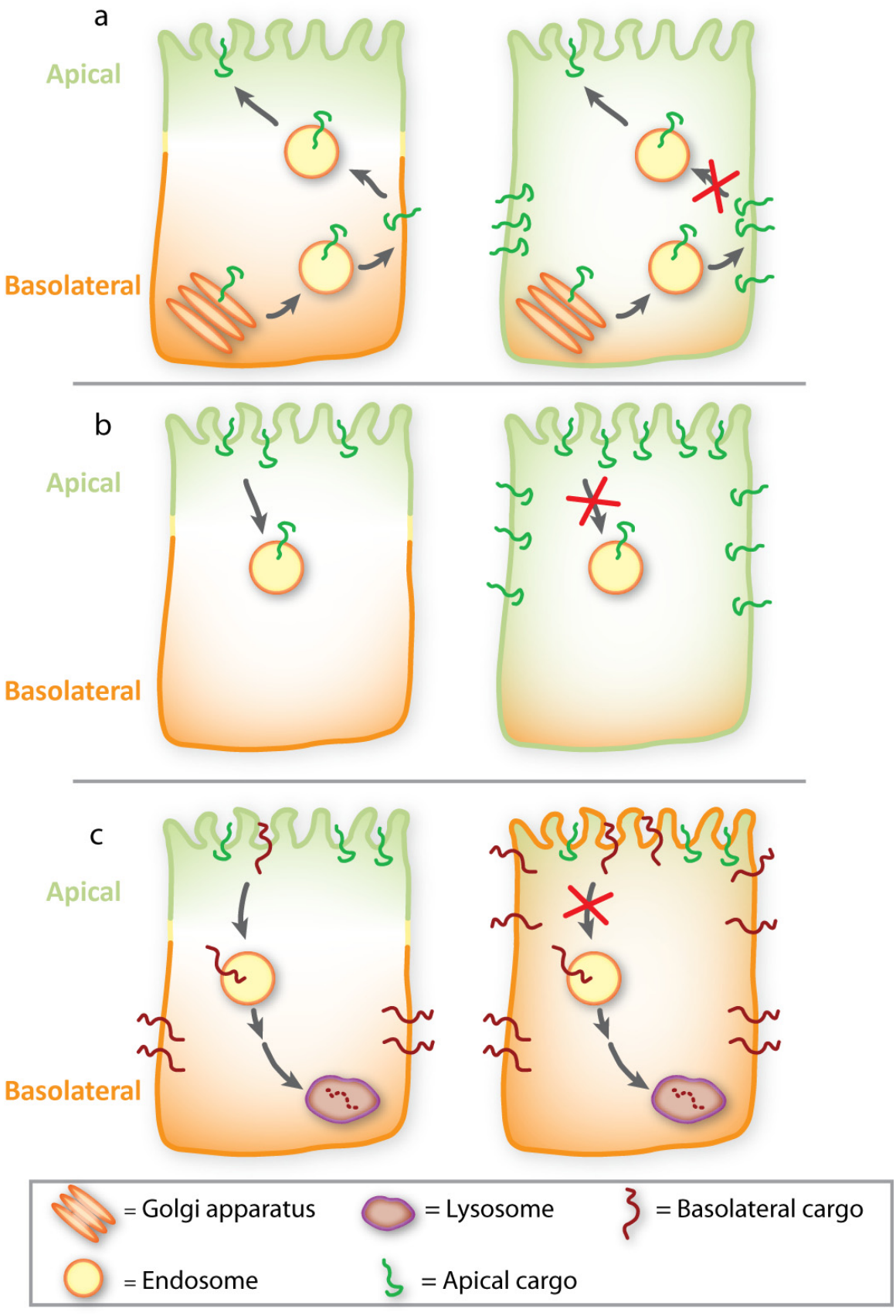
a
Apical
Basolateral
b
Apical
Basolateral
c
Apical
Basolateral
= Golgi apparatus
= Lysosome
= Basolateral cargo
= Endosome
= Apical cargo

Figure 2.2: Reciprocal regulation between polarity proteins and endocytic regulators in epithelial cells.
The plasma membrane in polarized epithelial cells is divided into apical (green) and basolateral (orange) domains, separated by cell-cell junctions (yellow). This segregation requires endocytosis, as does the apical localization of Cdc42 and the Par module. Proteins are removed from the plasma membrane by endocytosis, trafficked through the endocytic pathway (blue compartments) and then either degraded in the lysosome (pink protein) or recycled back to the plasma membrane (green). Transmembrane proteins are shown for simplicity, but the same steps could apply to peripheral membrane proteins. Key polarity regulators such as Cdc42 and Par module proteins positively or negatively (depending on the tissue context) regulate traffic from the plasma membrane to early endosomes, regulated by Dynamin (purple) and Rab5. Cdc42 and the Pars also promote the ESCRT-regulated endosome-to-MVB maturation. Green arrows represent positive regulation; red bars represent negative regulation. Gray dashed line indicates the division between endocytic steps known to regulate polarity (above) and those that don't (below); for models of the role of endocytosis in controlling epithelial polarity, see Figure 2.1. Note that only representative regulatory proteins are shown for the endocytic pathway. EE, early endosome; RE, recycling endosome; LE/MVB, late endosome/multivesicular body; Lys, lysosome.

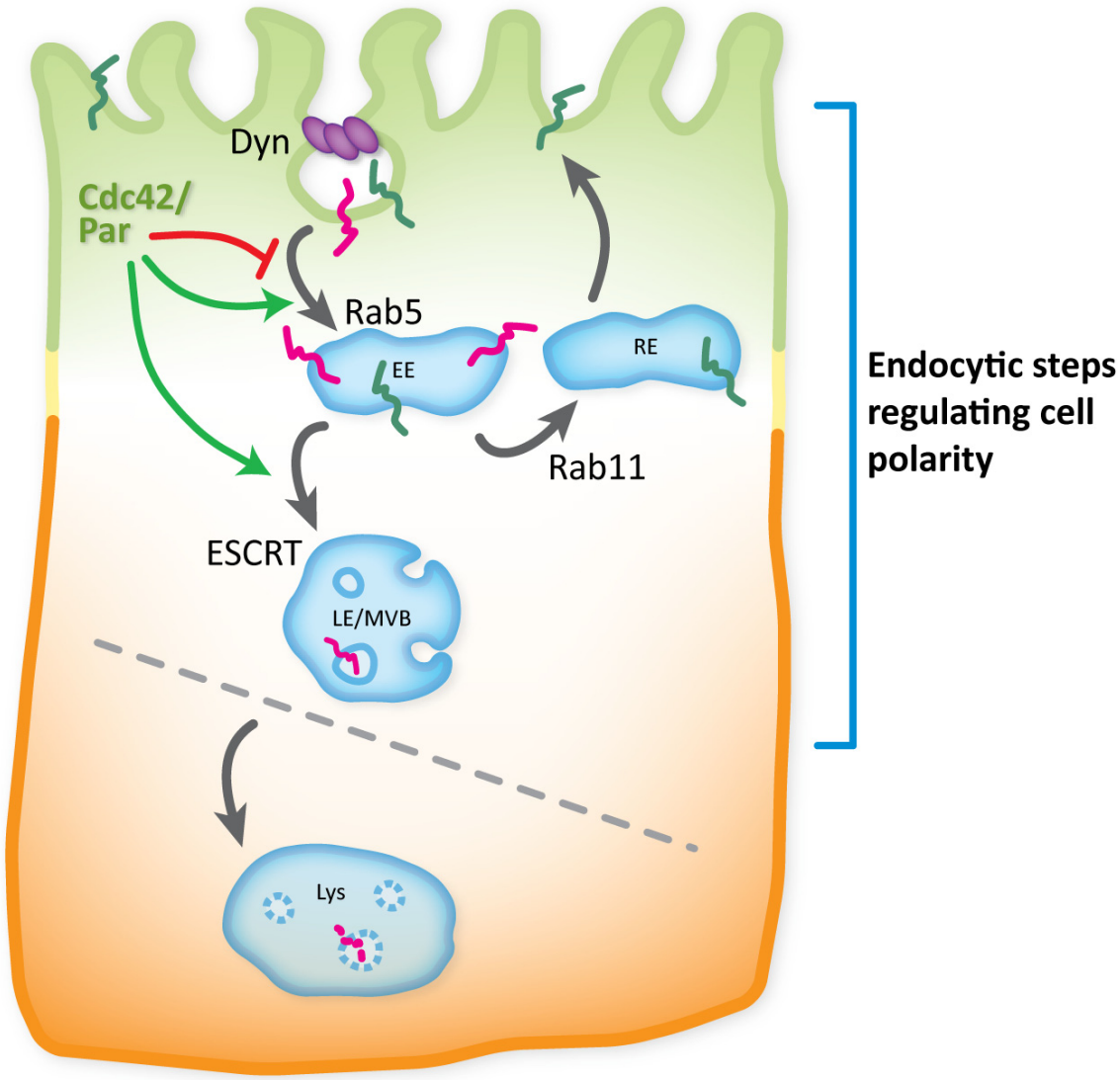
Dyn
Cdc42/
Par
Rab5
EE
RE
Rab11
ESCRT
LE/MVB
Lys
Endocytic steps
regulating cell
polarity

Figure 2.3: Reciprocal regulation between polarity proteins and endocytic regulators in non-epithelial cells.
In the *C. elegans* embryo, separate domains are marked by distinct, opposing PAR proteins, including PAR-6 in the anterior (green) and PAR-2 in the posterior (orange). Dynamin promotes the anterior enrichment of endocytosis. PAR-6 maintains the anterior enrichment of dynamin (black membrane patches) and early endosomes (green, solid arrows). PAR-6/CDC-42 may be internalized and trafficked via association with the early endosomes (gray arrows), which are enriched in the anterior. The polarizing cargo could be recycled rapidly from the early endosome, or associate with the recycling endosome and be recycled back to the anterior or posterior cortex. Speculatively, PAR-6/CDC-42 could associate with the Golgi apparatus, and dynamin could participate in vesicle scission here. Another putative function of dynamin-dependent endocytosis is preventing the expansion of PAR-2 into the anterior by promoting PAR-2 removal and recycling back to the posterior cortex, as indicated by the dotted gray arrows. EE, early endosome; RE, recycling endosome. Solid gray arrows indicate areas of the model supported by data. Dashed gray arrows indicate areas of speculation that are supported by observations in other polarized cells.

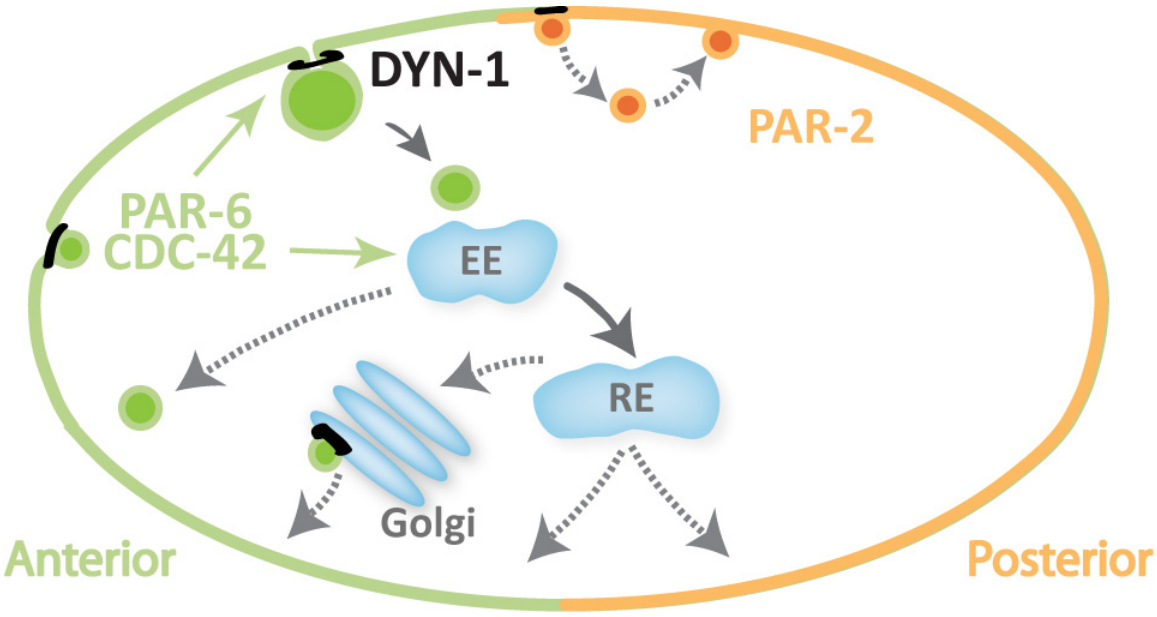
DYN-1
PAR-2
PAR-6
CDC-42
EE
RE
Golgi
Anterior
Posterior

Chapter 3

The Novel *Drosophila* Neoplastic Tumor Suppressor Genes *Rabenosyn* and *Vps45* *R*egulate Entry into the Early Endosome

Abstract
The small GTPase Rab5 has emerged as an important regulator of animal development and is essential for endocytic trafficking. However, the mechanisms that link Rab5 activation to cargo entry into early endosomes remain unclear. We show here that Drosophila Rabenosyn (Rbsn) is a Rab5 effector that bridges an interaction between Rab5 and the Sec1/Munc18-family protein Vps45, and we further identify the syntaxin Avalanche (Avl) as a target for Vps45 activity. Rbsn and Vps45, like Avl and Rab5, are specifically localized to early endosomes and are required for endocytosis. Ultrastructural analysis of *rbsn*, *Vps45*, *avl* and *Rab5* null mutant cells, which show identical defects, demonstrates that all four proteins are required for vesicle fusion to form early endosomes. These defects lead to loss of epithelial polarity in mutant tissues, which overproliferate to form neoplastic tumors. This work represents the first characterization of a Rab5 effector as a tumor suppressor, and provides *in vivo* evidence for a Rbsn-Vps45 complex on early endosomes that links Rab5 to the SNARE fusion machinery.

Introduction

The transport of protein cargoes to the numerous compartments within cells requires the budding, movement and fusion of membrane-bound vesicles. The myriad itineraries that vesicles follow require robust regulatory mechanisms to ensure specificity of delivery. One important site of regulation is at the fusion reaction itself. The core machinery that enables vesicle fusion consists of SNARE proteins, which are trans-membrane proteins located on the donor and target membranes that each contribute one of the four α-helices found in an assembled SNARE complex. Formation of a fusion-competent complex requires the incorporation of an α-helix from each of the different subfamilies of SNARE motifs, the Qa-, Qb-, Qc- and R-SNAREs (Fasshauer *et al.*, 1998). Individual SNAREs within each subfamily are localized to distinct cellular compartments, suggesting that this distribution along with intrinsic SNARE pairing propensities may contribute to membrane fusion specificity (Mcnew *et al.*, 2000; Bock *et al.*, 2001; Chen and Scheller, 2001; Ungermann and Langosch, 2005). However, the properties of SNAREs alone appear insufficient to account for the specificity seen *in vivo*, indicating that other regulators are important to ensure the integrity of intracellular traffic.

Rab proteins play a key regulatory role in SNARE-mediated fusion events. Like SNAREs, these small GTPases show distinct intracellular localization patterns and are required for specific transport steps (Stenmark and Olkkonen, 2001). Rabs are thought to influence vesicle fusion by serving as molecular switches that, when activated, recruit additional factors – "Rab effectors" – to their site of action (Zerial and Mcbride, 2001; Grosshans *et al.*, 2006). While activated Rabs generally bind to many different proteins, only a subset of these are actually direct effectors of vesicle trafficking. Identification of trafficking effectors requires a demonstration that the Rab and the effector are required for the same transport step. Genetic analyses in yeast have identified such proteins, in which loss-of-function phenotypes mimic those of mutations in specific Rabs and SNAREs (Aalto *et al.*, 1993; Tsukada *et al.*, 1999; Seals *et al.*, 2000). These trafficking effectors are structurally, and apparently functionally, diverse. Some effectors are thought to act as a physical 'tether' to mediate attachment between an incoming vesicle and its target membrane, bringing them into close proximity prior to vesicle fusion (Waters and Hughson, 2000; Whyte and Munro, 2002). Other effectors recruit proteins such as the Sec1/Munc-18 family (SM proteins), which bind and regulate the SNARE fusion complex itself (Carr *et al.*, 1999); these modes may not be mutually exclusive. Since the mechanisms by which Rab activation controls membrane fusion are varied and unclear, a thorough understanding requires the identification of Rab trafficking effectors and the molecular interactions by which they link the Rabs to the SNARE complexes.

Although yeast genetics has pioneered the determination of Rab effectors that mediate most stages of intracellular transport, an important exception is plasma membrane-to-early endosome traffic. This is a particularly significant step in metazoan organisms, where the internalization of cell surface proteins into the endosomal pathway regulates many critical cell-cell interactions, including signaling and adhesion. Current knowledge of the mechanisms underlying cargo delivery to early endosomes derives from several different approaches in mammalian cells, including biochemical

interactions and *in vitro* reconstitution of endosomal fusion reactions, which have demonstrated the central role of Rab5 in this event (Gorvel *et al.*, 1991; Bucci *et al.*, 1992; Stenmark *et al.*, 1994; Barbieri *et al.*, 1998). Intriguingly, these studies have also identified two effectors, EEA1 and Rabenosyn-5, which are recruited to endosomes by activated Rab5 and are associated, directly and indirectly respectively, with SNAREs (Mcbride *et al.*, 1999; Nielsen *et al.*, 2000). The indirect association of Rabenosyn-5 with SNAREs is through Vps45, an SM protein that binds various syntaxins *in vitro* (Nielsen *et al.*, 2000). Despite these interactions, functional studies have not demonstrated that these proteins are required for plasma membrane-to-early endosome transport *in vivo*; the identity of the Rab5 effector that mediates this trafficking step thus remains unresolved.

Drosophila has emerged as a valuable system to study endocytosis *in vivo*, in particular for the stage of early endosomal entry. Reverse genetics originally established that, as in mammalian cells, Drosophila Rab5 is required for this trafficking step (Wucherpfennig *et al.*, 2003). Recently, a forward genetic screen identified mutations in a syntaxin, called *Avalanche* (*avl*), that cause a similar endocytic phenotype to that of *Rab5* mutations (Lu and Bilder, 2005). The endocytic defects of *Rab5* and *avl* imaginal disc cells lead to a loss of epithelial architecture, and mutant tissues show dramatic overgrowth to form tumor-like cell masses; this phenotype is termed 'neoplastic'. To identify factors that link Rab5 activation to Avl-mediated vesicle fusion, we screened for new mutations that produced the same tumorous phenotype (Menut *et al.*, 2007). In this study we describe two previously uncharacterized genes, which encode the Drosophila proteins Rabenosyn (Rbsn) and Vps45, and demonstrate that both are required for plasma membrane-to-early endosome trafficking. We have further used genetics, ultrastructural analysis and biochemical interactions to link Rab5 and Avl activities through Rbsn and Vps45. Our data are consistent with a model in which Rbsn, via Vps45 binding, functions as a Rab5 effector and tumor suppressor by mediating early endosomal fusion.

Results

MENE(2L)-C identifies a novel neoplastic tumor suppressor gene

In a recent screen for mutations affecting epithelial polarity and proliferation in Drosophila, we identified many new complementation groups that control epithelial tissue architecture (Menut *et al.*, 2007). This screen used the *eyFLP*/*cell lethal* system to generate eye imaginal discs composed predominantly of homozygous mutant cells in an otherwise heterozygous animal (hereafter 'mutant eye discs'). In this assay, eye discs mutant for the *MENE(2L)-C* complementation group consist of rounded and dramatically disorganized masses of cells (Figure 3.1B, compare to 3.1A**)**. A similar phenotype is seen in the ovarian follicle cells. While wild-type follicle cells form a monolayered epithelium, *MENE(2L)-C* mutant cells multilayer and often invade the germ cell cluster (Figure 3.7). Staining for proteins normally localized to apical or lateral plasma membrane domains reveals that these domains are misspecified in *MENE(2L)-C* mutant cells. The normally apically restricted protein Atypical Protein Kinase C (aPKC) fails to remain distinct from Discs-Large-marked (Dlg) basolateral domains (Figure 3.1F, compare to 3.1E), indicating that apicobasal polarity is disrupted in these mutants. *MENE(2L)-C* mutant eye discs also show strong upregulation of Matrix Metalloprotease 1 (Mmp1) expression (Figure 3.1D, compare to WT in Figure 3.1C), which correlates with neoplastic transformation (Uhlirova and Bohmann, 2006; Menut *et al.*, 2007; Srivastava *et al.*, 2007). Finally, larvae with *MENE(2L)-C* mutant eye discs do not pupariate but continue to feed during an extended L3 stage; during this time the eye discs grow to be significantly larger than wild-type eye discs. The polarity, proliferation, and gene expression phenotypes all resemble those seen in tissues mutant for previously characterized neoplastic tumor suppressor genes (nTSGs) including *scribble (scrib)* and *Rab5* (Bilder and Perrimon, 2000; Lu and Bilder, 2005). However, complementation tests showed that *MENE(2L)-C* was not allelic to any known tumor suppressor gene. Collectively, these phenotypes therefore indicate that *MENE(2L)-C* disrupts a novel Drosophila neoplastic tumor suppressor gene.

MENE(2L)-C disrupts a protein related to human Rabenosyn-5

To identify the gene disrupted by *MENE(2L)-C* alleles, we performed complementation tests with chromosomal deficiency stocks and found a small deficiency, *Df(2L)Exel7034,* that failed to complement the two extant *MENE(2L)-C* alleles. Sequencing of genes located within the genomic region deleted in *Df(2L)Exel7034* revealed that each *MENE(2L)-C* allele carries a lesion in the gene *CG8506*, which encodes a 505 amino acid protein (Figure 3.1G). *MENE(2L)-C*$^{40\text{-}3}$ is a missense mutation altering the initiating ATG to ATA; the next in-frame ATG is located at amino acid 116. *MENE(2L)-C*^{X17} is a nonsense mutation that introduces a stop codon at amino acid 241. Both alleles show identical phenotypes in imaginal discs as well as in follicle cell epithelia, and animals either homozygous for each allele or hemizygous over *Df(2L)Exel7034* die before the second larval instar. In addition, antibodies raised against a GST-CG8506 fusion protein recognize a polypeptide of the expected molecular mass of 56kD in wild-type larval extracts; this polypeptide is absent from extracts of *MENE(2L)-*

$C^{40\text{-}3}$ tissue (Figure 3.1H). These results indicate that *MENE(2L)-*$C^{40\text{-}3}$ and *MENE(2L)-*C^{X17} are null alleles of *CG8506*.

Sequence analysis revealed that *CG8506* encodes a protein containing a number of conserved domains, including an N-terminal C2H2 zinc finger, a FYVE domain, two repeats of the tripeptide motif NPF, and several coiled-coil regions. BLAST searches indicate that CG8506 has significant homology to the human Rab5-binding protein Rabenosyn-5 (Nielsen *et al.*, 2000), which contains each of these domains, although in a different arrangement. CG8506 is shorter than Rabenosyn-5 and lacks a C-terminal helical region, the NPF motifs are N-terminal in CG8506 while they are C-terminal in Rabenosyn-5, and CG8506 contains a single coiled-coil region (Figure 3.1G). Nevertheless, these features are not found together in any other protein encoded by the fly genome. We therefore will refer to *CG8506* as Drosophila *rabenosyn* (*rbsn*).

Activated Rab5 recruits Rbsn both in vitro and in vivo

Mammalian Rabenosyn-5 has been linked to both the endocytic and the recycling pathways in part by virtue of its ability to bind simultaneously to Rab5 and Rab4 (De Renzis *et al.*, 2002; Naslavsky *et al.*, 2004). To explore whether Drosophila Rbsn might be involved in these trafficking pathways, we performed *in vitro* binding assays using recombinant Rbsn and Rab GTPases. We found that Rbsn binds to Rab5 specifically in its GTP-, but not GDP-bound form (Figure 3.1I). By contrast, we did not detect significant binding between Rbsn and Rab4 in either GTP or GDP-bound forms (Figure 3.1I). Because Rab11 has been implicated in recycling pathways (Ullrich *et al.*, 1996; Dollar *et al.*, 2002), we also tested whether Rbsn could bind to Rab11, but again failed to detect an interaction (Figure 3.1I). We conclude that Rbsn interacts specifically with the endocytic regulator Rab5 at early endosomes but not with Rab proteins that control recycling.

We also asked whether the results of our *in vitro* binding experiments reflected the protein association *in vivo*, by examining the subcellular localization pattern of Rabenosyn relative to each of the Rab proteins. In cultured Drosophila S2 cells, Rabenosyn is found in discrete puncta which partially overlap with Avl-positive endocytic compartments (Figure 3.4A). Expression of Rab5-YFP demonstrates Rbsn and Avl colocalization in Rab5-positive puncta (Figure 3.4B), indicating that Rbsn localizes to early endosomes in response to Rab5 activation. By contrast, in cells expressing activated forms of Rab4 or Rab11, Rbsn and Avl colocalize in puncta that are mostly discrete from those marked by Rab4 or Rab11 (Figure 3.8), indicating that Rbsn is not strongly recruited to recycling endosomes, consistent with our *in vitro* results.

Rbsn is required for endocytosis

The above data suggest an association between Rbsn and the endocytic pathway, and disruption of several endocytic stages has been previously shown to perturb both cell polarity and cell proliferation control (Lu and Bilder, 2005; Vaccari and Bilder, 2005). We therefore directly tested whether Rbsn was required for endocytosis. In wild-type imaginal disc cells, the apically localized transmembrane protein Notch is continuously endocytosed and lysosomally degraded; the endocytic transient

population can be visualized as intracellular cytoplasmic puncta. However, in *rbsn* cells, Notch is present at greater than wild-type levels (Figure 3.2B, compare to 3.2A); a similar elevation is seen with the apical transmembrane protein Crumbs (Crb, Figure 3.2D, compare to 3.2C). To directly analyze cargo internalization, we performed a trafficking assay in living disc tissue. This assay pulse-labels cell surface Notch using an antibody against the Notch extracellular domain; endocytosis is then allowed to occur over varying chase periods. After 10 minutes of chase in WT cells, Notch is internalized and is found in early endosomes (Figure 3.2E-E'), while after 5 hours, no Notch signal remains (Figure 3.2G-G'). In contrast, in *rbsn* mutant cells no intracellular Notch puncta are seen after 10 minutes (Figure 3.2F-F'); instead Notch remains in the cell periphery and this localization persists even after 5 hours (Figure 3.2H-H'). This pattern strongly resembles that seen in *rab5* mutants (Figure 3.7), but contrasts with that seen with the late-acting *ESCRT* mutants (Vaccari and Bilder, 2005), in which Notch accumulates in enlarged endocytic compartments; it also contrasts with mutations in 'junctional scaffold' neoplastic tumor suppressor genes such as *scrib*, where no effect on Notch endocytosis is seen (unpublished data). The activity of a Notch reporter is reduced in *rbsn* mutant discs (Figure 3.2I-J) as in *Rab5* and *avl* mutants; this is consistent with studies indicating that Notch that does not enter endosomes has reduced signaling function (Vaccari *et al.*, 2008) and suggests that Notch accumulation is not involved in the *rbsn* tumor phenotype. Together, these results establish that *rbsn* is required for an early step in the endocytic pathway.

Vps45 binds to Rbsn and regulates an early endocytic step

Our data indicate that *rbsn* has an endocytic mutant phenotype similar to *Rab5* mutants, and Rbsn colocalizes with Rab5 at early endosomes and binds directly to Rab5-GTP. These results suggest that Rbsn might regulate Rab5-dependent fusion events at the early endosome. Interestingly, the Sec-1/Munc-18 (SM) protein Vps45 has been identified as a Rabenosyn-5 interacting protein (Nielsen *et al.*, 2000). While the function of mammalian Vps45 is unknown, the yeast homolog Vps45p has a well documented requirement in biosynthetic Golgi-to-lysosome traffic, and interacts with a Rabenosyn-5 like protein Vac1p (Cowles *et al.*, 1994; Peterson *et al.*, 1999). To test whether Rbsn might associate with a Vps45-like protein, we first identified a single clear Vps45 homolog amongst the 4 SM proteins in Drosophila, which is encoded by the uncharacterized gene *CG8228* (hereafter referred to as *Vps45*). We then expressed an MBP-Vps45 fusion protein in bacteria and found, using *in vitro* binding assays, that Vps45 strongly binds to Rbsn (Figure 3.3A). These data suggest that Rab5 might regulate traffic through Rbsn-dependent Vps45 recruitment to the early endosome. The localization of Vps45 in animals has not been previously reported. To assess the *in vivo* localization of Vps45, we expressed an epitope-tagged Vps45 construct in S2 cells. In transfected cells, Vps45 shows a punctate pattern with only partial overlap to that of Rbsn and Avl (Figure 3.4A). Interestingly, upon overexpression of Rab5-YFP, Vps45 relocalizes to the resultant enlarged endosomes; most Vps45 in these cells colocalizes with both Rbsn and Avl (Figure 3.4C-D). Taken together with the *in vitro* binding data,

this result suggests that Vps45 is recruited to the early endosome in response to Rab5 activation.

Since yeast Vps45p is required for vacuolar but not endocytic traffic (Raymond *et al.*, 1992; Bryant *et al.*, 1998), we sought to determine whether the Rbsn-Vps45 interaction we observed in Drosophila was relevant for function at the early endosome. No mutations in *Vps45* have been reported in flies. However, by testing the uncharacterized neoplastic mutants isolated in our screen, we found that MENE(3R)-B alleles fail to complement deficiencies that remove Vps45. We sequenced *Vps45* and found lesions in the coding region in each of the two *MENE(3R)-B* alleles (Figure 3.3B). *MENE(3R)-B*^{JJ2} causes premature termination of the protein at amino acid 233 of the 574 amino acid coding region, and *MENE(3R)-B*^{GG11} converts valine 219 to a glutamine. Larvae homozygous for either allele die before the third instar, and the mutant eye imaginal disc phenotypes are indistinguishable, suggesting that both represent null alleles.

We next analyzed the phenotypes of *Vps45* mutant tissues. As in *rbsn* mutants, staining for Notch and Crb showed that these protein levels were elevated in *Vps45* mutant discs (Figure 3.3C-F). To test whether *Vps45* mutants might cause neoplastic transformation by blocking endocytosis in a manner similar to *rbsn* mutants, we examined Notch trafficking. Using live trafficking assays, we found that Notch was not internalized in *Vps45* mutant cells, and accumulated near the cell surface in a manner resembling that of both *rbsn* and *Rab5* mutant cells (Figure 3.3G-H'). Moreover, the cell polarity, proliferation, Mmp1 expression and Notch signaling phenotypes were indistinguishable from those of *rbsn* mutant discs (Figure 3.3I-K). These data suggest that in Drosophila, Vps45 function is indeed required for endocytic traffic and in particular for early endosomal stages.

Genetic and physical interactions between Vps45 and Avl

SM proteins are canonically thought to be trafficking regulators, able to bind to either SNARE proteins or complexes and govern fusion between vesicular and target membranes. In Golgi-to-vacuole traffic in yeast, the binding of Vps45p to Tlg2p is necessary for fusion into the vacuole (Nichols *et al.*, 1998). We tested for physical interactions between the Drosophila homologs of these proteins and confirmed a strong interaction between Vps45 and Syx16 (Figure 3.5A). However, only a small fraction of Drosophila Syx16 localizes to endosomes, and strong expression of a Syx16 RNAi transgene did not generate defects associated with disrupted endocytosis (Figure 3.9). Since similar expression of a *Vps45* RNAi transgene shows strong endocytic defects resembling that seen in null mutant tissue (Figure 3.9), we asked whether Vps45 might control endocytosis by associating with early endocytic SNAREs such as Avl. We found weak but consistent binding between Vps45 and Avl as compared to Syx1 as a negative control (Figure 3.5A); this binding was comparable to that seen with the annotated Drosophila homolog of Syx13, which interacts with Vps45 in humans and *C. elegans*.

To evaluate whether Vps45 might regulate these SNAREs *in vivo*, we turned to genetic interaction studies. Moderately reducing the protein levels of Vps45 using an RNAi construct expressed in the posterior compartment of the adult wing produces no

obvious phenotype (Figure 3.5B). However, removing one copy of the wild-type *Vps45* gene to further reduce Vps45 protein levels results in an enhanced phenotype, including aberrant vein formation and ruffling of the posterior margin (Figure 3.5C). Similar defects are also seen when Avl protein levels are reduced by RNAi (Figure 3.10), suggesting that this phenotype results from impaired endocytosis. We then used the *Vps45* RNAi sensitized background to test whether other genes might act in the *Vps45*-regulated endocytic pathway. We found that removing one copy of *Syx13* or *Syx16* did not alter the *Vps45* RNAi phenotype (Figure 3.5G, H), but removing one copy of *avl,* as well as *Rab5* and to a lesser extent *Rbsn*, resulted in an enhancement similar to that produced by the removal of one copy of *Vps45* (Figure 3.5D-F). Although weak, the interaction between *Vps45* and *rbsn* was consistent; 64% of *en>Vps45-IR; rbsn/+* wings show ectopic vein formation across the posterior cross vein, versus only 17% of *en>Vps45-IR* wings. Analogous results were seen when knocking down *avl* (Figure 3.10), further validating the interactions between these genes. Along with the strong phenotypic similarity of the mutants, these results suggest that Vps45 acts together with Rab5, Rbsn and Avl at the early endosome, and point to Avl as a regulatory target for Vps45.

Rabenosyn, Rab5, Vps45, and avl mutants block endocytosis at an identical early step

The genetic and biochemical interactions described above suggest the hypothesis that Rab5, Rbsn, Vps45 and Avl act together to promote a single stage of endocytic traffic, involving fusion of incoming endocytic vesicles into the early endosome. If this hypothesis is correct, then cells lacking any of these proteins should block endocytosis at the same step and show similar disruption of endosomal structures. Since light microscopy does not allow the resolution required to clearly distinguish these structures, we instead turned to transmission and immuno-electron microscopy to test this hypothesis. We analyzed late-stage oocytes, which are large cells with a defined endocytic pathway required for uptake of yolk proteins (Schonbaum *et al.*, 2000). By making germ-line clones, we obtained oocytes mutant for *Rab5, rbsn, Vps45,* and *avl* and found that all four mutants are defective in the formation of yolk granules. In WT oocytes, yolk granules are late endocytic structures that have a characteristic, electron-dense appearance resulting from condensation of internalized yolk proteins (Figure 3.6A). These structures are strikingly absent from mutant oocytes (Figure 3.6B-E and data not shown). Because the lack of yolk granules could point to a prior block in the endocytic pathway, we analyzed endocytic intermediates by using an antibody against the yolk proteins, which are produced outside the oocyte, to trace a known endocytic cargo within oocyte vesicular compartments. In wild-type oocytes, yolk proteins are found in numerous endocytic compartments spanning a wide size range (Figure 3.6A, (Trougakos *et al.*, 2001)). In contrast, in *Rab5*, *avl*, *rbsn* and *Vps45* mutant oocytes (Figure 3.6B-E), yolk proteins are confined to small vesicles with a narrow size distribution; these are primarily found in dense accumulations in close proximity to the plasma membrane. The diameter of the vesicles, approximately 100 nm, is consistent with both the expected size of internalized clathrin-coated vesicles and the size of vesicles present in WT oocytes (Figure 3.6A), and both electron-dense coated

and uncoated vesicles are seen. Taken together, these data indicate that endocytic vesicles still form in the absence of Avl, Rab5, Vps45, or Rbsn; these vesicles can uncoat but nevertheless cannot fuse to form later endoyctic structures. The strong phenotypic similarity seen amongst all four mutants using immuno-electron microscopy support a model in which Vps45 and Rabenosyn act with Rab5 and Avl to promote vesicle fusion into the early endosome.

Discussion

Targeted membrane trafficking steps are vital for maintaining the proper segregation of intracellular compartments and for the sorting of their protein cargoes. Here we have used forward genetics to identify and characterize two essential regulators of plasma membrane-to-early endosome traffic in Drosophila: Rbsn and Vps45. Rbsn and Vps45 are related to proteins implicated in endocytosis in mammalian cells, and their endocytic role in Drosophila is definitively demonstrated here by direct analysis of cargo trafficking in null mutant tissue. Loss of either protein disrupts the flow of information from the activated small GTPase Rab5 to the trans-SNARE complex and blocks the fusion of endocytic vesicles into the endosome. The endocytic defect further causes mispolarization of epithelial cells and consequent overproliferation to form 'neoplastic tumors.' Although we have previously shown that Rab5 acts as a Drosophila tumor suppressor (Lu and Bilder, 2005), Rab5 has many effectors that regulate cellular processes as diverse as lipid metabolism, cytoskeletal organization, and cargo recycling (Christoforidis *et al.*, 1999b; Lanzetti *et al.*, 2004; Naslavsky *et al.*, 2004). Our demonstration that Rbsn and Vps45 are effectors of the tumor suppressive-activity of Drosophila Rab5 emphasizes that growth regulation requires endosomal fusion itself. These two proteins therefore extend the list of endocytic regulators that act as tumor suppressors, confirm the critical role of endocytosis in coordinating cell polarity and cell proliferation, and provide insight into the processes controlling entry into the early endosome.

The mechanisms linking Rab-mediated vesicle targeting and SNARE-mediated vesicle fusion are among the least well understood events in cellular trafficking. We show here that Drosophila Rbsn is a Rab5 effector, binding to Rab5-GTP and localizing to early endosomes. Like Rab5, Rbsn is required for early endocytic entry, and *rbsn* and *Rab5* mutants are phenotypically indistinguishable. In particular, we have used, for the first time, high resolution immuno-electron microscopy to identify the site of cargo trapping in cells completely lacking *rbsn* and *Rab5* (as well as *Vps45* and *avl*, see below). These mutants show a striking accumulation of endocytic cargo-containing vesicles of a size consistent with plasma membrane-derived carrier vesicles; the absence of large endosomal compartments suggests that these vesicles fail to undergo fusion to form early endosomes (Rubino *et al.*, 2000). Together, the genetic, biochemical and *in vivo* phenotypic data provide strong support for a model in which Rbsn is a Rab5 effector essential for endocytic vesicles to fuse into the early endosome.

The severe endocytic block seen in *rbsn* tissue contrasts with the phenotype of mammalian cells depleted of the related human protein Rabenosyn-5 by RNA knockdown, which allow early endosomal entry but are defective in recycling cargo back to the plasma membrane (Naslavsky *et al.*, 2004). The involvement of Rabenosyn-5 in the recycling pathway is supported not only by this phenotype, but also by its ability to bind Rab5 and the recycling regulator Rab4 simultaneously, prompting a model in which Rabenosyn-5 acts to coordinate cargo transfer from the early to recycling endosomes (De Renzis *et al.*, 2002). We find that Drosophila Rbsn, despite its strong association with Rab5-GTP, does not bind to Rab proteins known to regulate recycling, and note that while Rabenosyn-5 contains separate Rab4 and Rab5 binding domains (Eathiraj *et*

al., 2005), these domains show homology to the same single domain in Drosophila Rbsn. It can be speculated that in mammalian Rabenosyn-5, duplication of the Rbsn Rab-binding domain followed by subsequent functional divergence led to its adoption into the recycling pathway, while the mammalian tethering protein and Rab5 effector EEA1 played a greater role in regulating early endosome entry (Christoforidis *et al.*, 1999a). Although such an evolutionary scenario is possible, we cannot exclude the possibility that Rbsn plays a role in Drosophila recycling, particularly since the strong endocytic defects that we observed in *rbsn* mutants are upstream of, and thus prevent analysis of, the recycling pathway.

Our analysis of *rbsn* null mutant tissue demonstrates that Rbsn is required for vesicles to fuse into the early endosome. How does Rbsn promote vesicle fusion? We find that the Drosophila SM protein Vps45, which binds to Rbsn, is required for the identical step of endocytosis as Rbsn and Rab5. We further localize Vps45 for the first time *in vivo* and find localization to early endosomes, which is increased by Rab5 overexpression. Recruitment of Vps45 by Rbsn bound to active Rab5 may create a high local concentration of Vps45 (Nielsen *et al.*, 2000); once concentrated at the endosome, Vps45 could act on SNARE proteins to enable fusion of incoming carrier vesicles. In contrast to yeast, where Vps45p is required for lysosomal delivery of biosynthetic cargo (Cowles *et al.*, 1994), we have shown that Drosophila Vps45 is required for trafficking and degradation of surface-derived cargo, thus identifying an SM protein that acts in the endocytic pathway.

While this manuscript was in preparation, Gengyo-Ando *et. al* reported that *C. elegans* oocytes lacking homologs of Vps45 or Rbsn are defective in yolk uptake, but did not distinguish the precise stage of endocytic traffic blocked; moreover, they could not identify any syntaxin required for endocytosis and therefore could not determine a functional target of Vps45 (Gengyo-ando *et al.*, 2007). Here we provide evidence that the endocytic syntaxin Avl is a key Vps45 target. We detected a clear genetic interaction specifically between *Vps45* and *avl,* as well as a weak physical interaction between Vps45 and both Avl and Syx13. While human and *C. elegans* Syx13 have been shown to bind Vps45 (Nielsen *et al.*, 2000; Gengyo-ando *et al.*, 2007), orthologous relationships with Drosophila syntaxins are ambiguous: both Drosophila Avl and Syx13 are similar to human and *C. elegans* Syx13 as well as to human Syx7. Our data demonstrate that Avl is required for the fusion event required for cargo entry into early endosomes; although RNAi experiments do not reveal a role for Drosophila Syx13 in endocytosis (unpublished data), further experiments will be needed to clarify the function of Syx13 in vesicle trafficking.

The *in vitro* physical interactions we observed between Vps45 and both Avl and Syx13 were notably weaker than that with Syx16. However, our data do not provide evidence for an endocytic role of Syx16. In addition, the significance of SM protein binding to an isolated SNARE remains unclear. While in most cases it correlates with SNARE complex assembly, in some instances this interaction is not necessary for function *in vivo* (Carpp *et al.*, 2006), and in others it is associated with inhibition of incorporation into a SNARE complex (Dulubova *et al.*, 1999; Peng and Gallwitz, 2002). Considering these scenarios, our phenotypic analysis of mutant tissues completely

lacking Vps45 demonstrates common phenotypes to those completely lacking Rab5, Avl, or Rbsn at the tissue, cellular and ultrastructural levels, indicating that Vps45 acts as a positive regulator of early endocytic SNAREs; this is also consistent with the enhancing nature of the genetic interactions. Moreover, these data argue that Avl is a component of the SNARE complex whose activity in vesicle fusion requires Vps45, establishing a functional link between Rab5 and SNAREs essential for early endosomal entry.

Taken together, our genetic, phenotypic, and biochemical analyses provide strong support for a model in which Rbsn, by binding to Vps45 and Rab5, enables incoming cargo vesicles to fuse into the early endosome. This trafficking event is required for the proper control of surface levels of transmembrane proteins and has significant consequences for tissue development. Given that plasma membrane-to-early endosome trafficking is a process by which metazoan animals can control intercellular interactions, Rbsn may be an attractive target for cellular regulation of this event. Indeed, genetic interactions hint at a role for Rbsn in modulating several cell-cell interaction and communication pathways (unpublished data); future work will reveal whether Rbsn activity is modulated in specific contexts to achieve different developmental outcomes.

Materials and Methods

Drosophila Genetics

40-3 and *X-17* were generated on an *FRT40A* chromosome, while *JJ-2* and *GG-11* alleles were generated on *FRT82B* using EMS mutagenesis (Menut *et al.*, 2007). Animals referred to in this text as *rbsn* and *Vps45* mutants are the null alleles $rbsn^{40\text{-}3}$ and $Vps45^{JJ\text{-}2}$. Other alleles used are avl^{1} and $Rab5^{2}$ (Lu and Bilder, 2005) and $scrib^{2}$ (Bilder and Perrimon, 2000). The *E(spl)mβ-LacZ* chromosome was provided by J. Posakony (University of California, San Diego, La Jolla, CA). Mutant eye discs were generated using the *eyFLP-cell lethal* system as in (Menut *et al.*, 2007). Germ line clones were produced using the ovo^{D1} system as in (Chou and Perrimon, 1996), additionally using an ovo^{D1} *FRT80* chromosome (Bänziger *et al.*, 2006). All other stocks were obtained from Bloomington Stock center (Indiana), including deficiencies used for complementation tests and genetic interactions (*Df(1)Exel6254* (Parks, 2004) removing *Syx16*, *Df(3L)BSC10* removing *Syx13*). Experiments were performed at 25°C, with the exception of the *Vps45* RNAi genetic interactions, which were maintained at room temperature.

Molecular Biology

The *40-3*, *X-17*, *JJ-2* and *GG-11* alleles were identified by sequencing PCR products amplified from genomic DNA isolated from homozygous larvae; at least two independent reactions were sequenced for each allele. Wildtype and *rbsn* mutant extracts were prepared by boiling imaginal discs generated using the *eyflp-cell lethal* system in sample buffer. The *Vps45 RNAi* transgene was generated by cloning a 723bp sequence (available upon request) from genomic clone *BACR19N07* into a modified pWIZ vector in the tail-to-tail orientation. MBP-Rabenosyn and MBP-Vps45 were generated by cloning the full coding regions into the pMAL vector. GST fusion proteins were produced by cloning the entire coding region of Rbsn or the cytoplasmic domains of Syx1a (amino acids 1-268), Syx7 (amino acids 1-258), Syx13 (amino acids 1-258) and Syx16 (amino acids 1-329) into a pGEX vector. All fusion proteins were expressed and purified from bacteria using standard protocols. Western blots were performed using standard techniques with antibodies against Rbsn (1:1000), α-Spectrin ((Dubreuil *et al.*, 1987), Developmental Studies Hybridoma Bank, Iowa City, IA), MBP (1:10,000, New England Biolabs, Ipswich, MA), or GST (1:5000, gift from M. Welch). HRP-conjugated secondary antibodies were from Jackson ImmunoResearch Laboratories, Inc. (West Grove, PA). Non-subject lanes were removed for clarity. Vps45-V5 was generated by cloning the full-length Vps45 coding region into the pMT/V5-His-TOPO® vector (Invitrogen, Carlsbad, CA).

In vitro binding assays

Wildtype Rab2, Rab4, Rab5 and Rab11 coding regions (gift of J. Zhang and M. Scott) were cloned into a pGEX vector, and the GST fusion proteins purified and loaded with GDP or GTPγS. Lysis and wash buffers used during purification contained 5 mM and 1 mM GDP, respectively, while nucleotide loading protocol was adapted from (Lu and Settleman, 1999). GTPases at a concentration of 1μM were added to 10-fold molar excess MBP-Rbsn in binding buffer (50 mM HEPES pH 7.5, 50 mM NaCl, 5 mM EDTA, 10

mM EGTA, 1 mM DTT), and washed in wash buffer (50 mM HEPES pH 7.5, 50 mM NaCl, 30 mM $MgCl_2$, 1 mM DTT). GST-Syntaxins or GST-Rbsn at 1μM were combined with MBP-Vps45 at 0.1μM in binding buffer (20 mM HEPES pH 7.4, 150 mM KoAc, 0.05% Tween-20, 1 mM DTT) and washed in wash buffer (20 mM HEPES pH 7.4, 250 mM KoAc, 0.1% Triton X-100). Bound proteins were eluted by boiling in sample buffer and analyzed by SDS-PAGE followed by immunoblotting.

Immunohistochemistry and Microscopy

Imaginal discs and ovaries were fixed and stained as described (Bilder *et al.*, 2000) with TRITC-phalloidin (Sigma-Aldrich, St. Louis, MO) and primary antibodies: Avl (Lu and Bilder, 2005), Rbsn (generated in rabbits using a GST-Rbsn fusion protein; Pocono Rabbit Farm and Laboratory, Inc, Canadensis, PA), Crb (Tepass and Knust, 1993), aPKC (Santa Cruz Biotechnology, Santa Cruz, CA), Notch (intracellular domain), Dlg, Mmp1 (Developmental Studies Hybridoma Bank, Iowa City, IA), βgal (Cappel), Syx16 (Xu *et al.*, 2002). Secondary antibodies were from Molecular Probes (Invitrogen, Carlsbad, CA). Notch endocytosis assays were performed as described in Lu and Bilder 2005. S2 cells maintained at 25ºC were transfected with Vps45-V5 (this work) and/or Rab5-YFP (gift of S. Eaton) using Cellfectin® (Invitrogen, Carlsbad, CA) according to the recommended protocol. Vps45-V5 expression was induced with 500 μM $CuSO_4$ for 20 hours. Cells were seeded on multitest slides (MP Biomedicals, Aurora, OH) then fixed and stained using the same protocol as in imaginal discs. Anti-V5 antibody was from Invitrogen (Carlsbad, CA). Confocal images shown are all single confocal cross sections, and were collected on a TCS microscope (Leica, Wetzlar, Germany) using x16/NA 0.5 or x63/NA1.4 oil lenses. Adult wings were mounted in Gary's Magic Mountant (Lawrence *et al.*, 1986) and imaged using a Z16 APO microscope (Leica, Wetzlar, Germany) with a Planapo 2.0x lens, fitted with a DFC300 FX camera. All images were edited with Adobe Photoshop 9.0, including cropping regions of interest, and assembled using Adobe Illustrator 12.0.1. For Notch, Crb, and Mmp1 static stains, mutant and wild-type discs were processed in the same tubes and confocal settings were adjusted to maintain a linear intensity range for signals in wild-type and mutant discs.

Transmission electron microscopy

Ovaries containing stage 10 oocytes were dissected and immediately transferred to fixative containing 4% formaldehyde and 0.1% glutaraldehyde in 0.1 M phosphate buffer (pH 7.4). Single oocytes were embedded in 10% gelatin, infused with 2.3 M sucrose and frozen in liquid nitrogen. Sections were cut at -110°C and picked up with a 1:1 mixture of 2.3 M sucrose and 2.0 M methyl cellulose. Sections were labeled with a rabbit antibody against yolk protein (Trougakos *et al.*, 2001), followed by 10 nm protein A gold, and observed in a JEOL-1230 electron microscope at 60-80 kV. Images were recorded with a Morada digital camera using iTEM (SIS) software.

Figure 3.1. *MENE(2L)-C* mutations disrupt Drosophila Rabenosyn, which is a Rab5 effector and neoplastic tumor suppressor. Single confocal sections of WT (A) and entirely mutant *MENE(2L)-C* (B) eye discs stained with phalloidin to mark actin. *MENE(2L)-C* discs are larger than WT discs and lack their distinctive apical enrichment of actin filaments. *MENE(2L)-C* discs express Mmp1 (D, magenta), a marker correlated with neoplastic tissue, at significantly higher levels than WT discs (C). E-F: Eye discs stained for aPKC to mark apical surfaces (green) and Dlg to mark basolateral surfaces (red). Wildtype cells have distinct aPKC and Dlg domains (E), while aPKC and Dlg are intermixed in *MENE(2L)-C* cells (F). G: Locations of the lesions in the *MENE(2L)-C*$^{40\text{-}3}$ (*40-3*) and *MENE(2L)-C*$^{X\text{-}17}$ (*X-17*) alleles are indicated. Protein domains are labeled as colored boxes according to legend, compared to human Rabenosyn-5. H: Western blot of wildtype and *MENE(2L)-C*$^{40\text{-}3}$ mutant imaginal disc extracts probed with anti-Rbsn (upper panel) or anti-α-Spectrin antibody as a loading control (lower panel). G: *In vitro* GST pulldown assays between recombinant MBP-Rbsn and GST-Rab proteins. Western blots against MBP (upper panel) to detect bound Rbsn and GST (lower panel) as a loading control. GST-Rab2 is included as a negative control, showing that Rbsn binds specifically only to Rab5-GTP. Scale bars represent 100 µm in A-D and 10 µm in E-F.

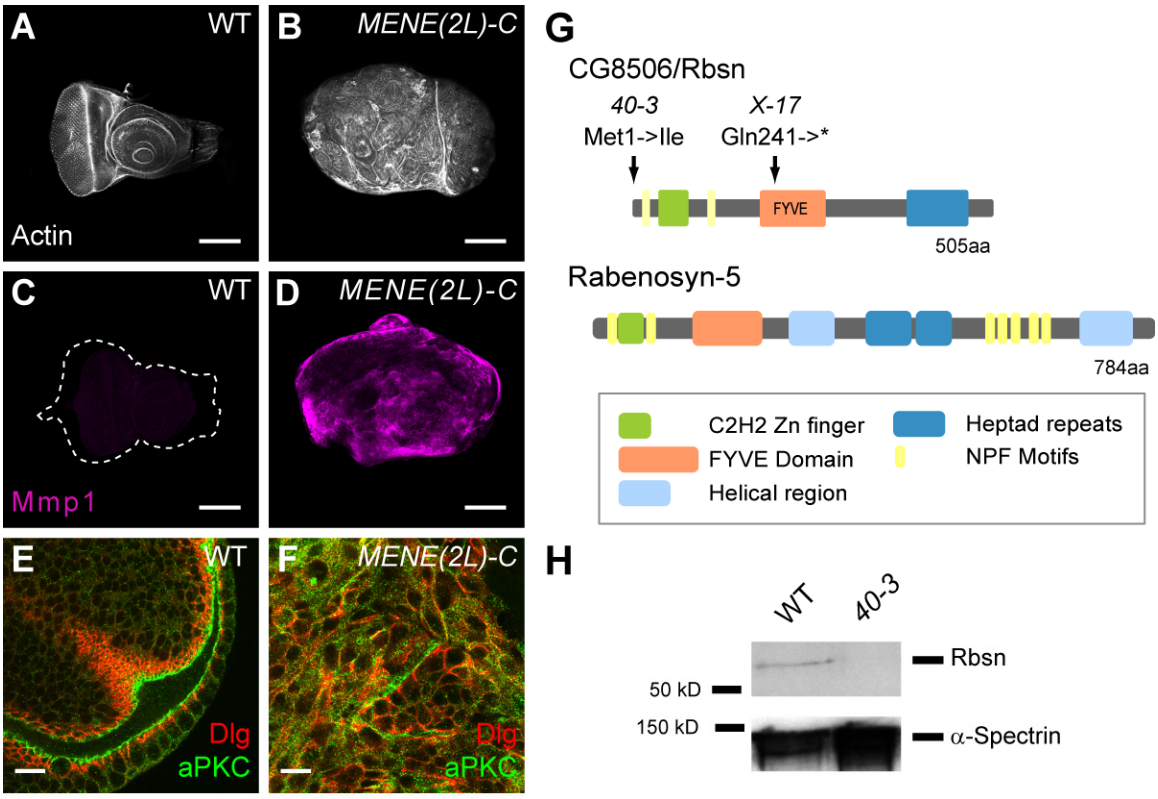
A
WT
Actin
B
MENE(2L)-C
C
WT
Mmp1
D
MENE(2L)-C
E
WT
Dlg
aPKC
F
MENE(2L)-C
Dlg
aPKC
G
CG8506/Rbsn
40-3
Met1->Ile
X-17
Gln241->*
FYVE
505aa
Rabenosyn-5
784aa
C2H2 Zn finger
FYVE Domain
Helical region
Heptad repeats
NPF Motifs
H
WT
40-3
50 kD
150 kD
Rbsn
α-Spectrin
I
5%
input
Rab2
Rab4
Rab11
Rab5
GDP
GTP
100 kD
75
Rbsn
IB: MBP
50 kD
Rab
IB: GST

Figure 3.2. Rbsn is required for uptake of endocytic cargo. The apical transmembrane proteins Notch (green, A-B) and Crumbs (Crb, cyan, C-D) are present at higher levels in *rbsn* discs (B, D) than in WT discs (A, C). E-H': Notch trafficking assays performed in WT (E, G) and *rbsn* (F, H) discs. Actin staining outlines cells (red, E-H). In WT cells, surface-labeled Notch (green) is found in internal puncta after 10 minutes (E'), and is gone from discs after 5 hours (G'). In *rbsn* cells, Notch staining is elevated and retained at the cell periphery after 10 minutes (F'), and persists over the 5 hour experiment (H'). The Notch signaling reporter, *mβ-LacZ* (green, I-J) is not ectopically activated compared to wild-type (I) in *rbsn* (J) mutant discs. Images shown are single confocal cross sections. Scale bars represent 100 µm in A-D, I-J and 10 µm in E'-H'.

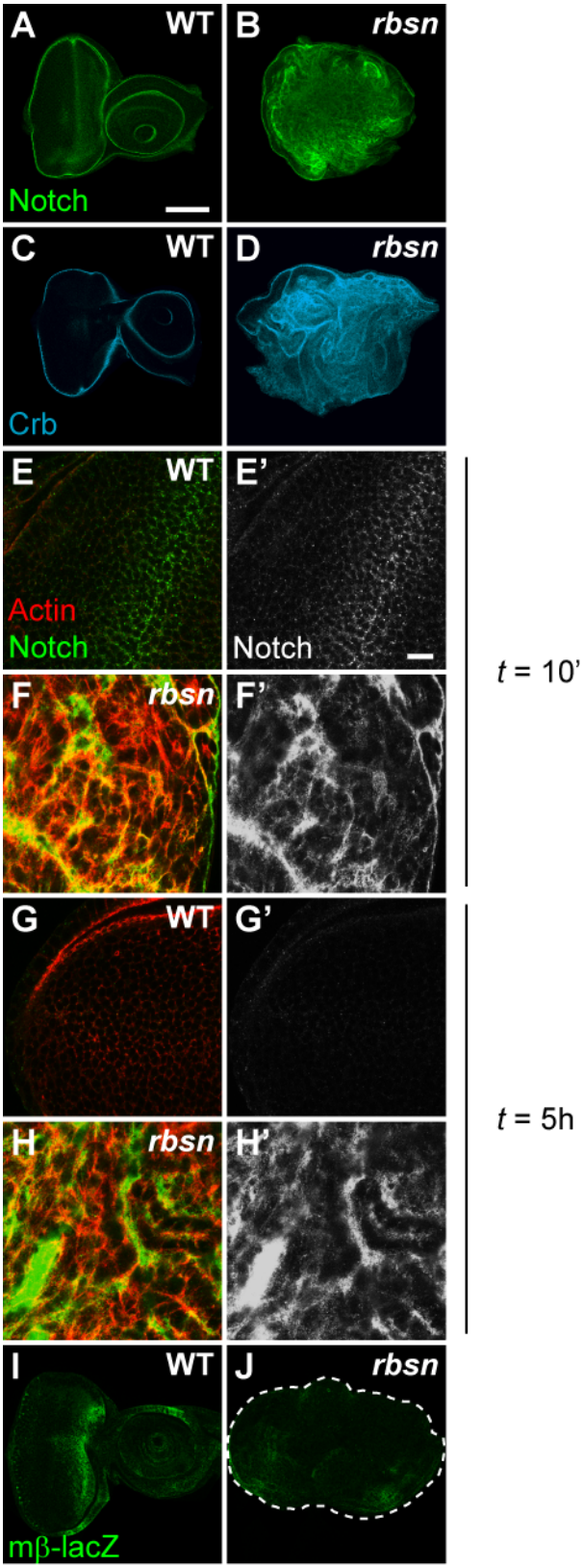
A WT
Notch
B rbsn
C WT
Crb
D rbsn
E WT
Actin
Notch
E'
Notch
F rbsn
F'
t = 10'
G WT
G'
H rbsn
H'
t = 5h
I WT
mβ-lacZ
J rbsn

Figure 3.3. Loss of Drosophila *Vps45* disrupts endocytic traffic and epithelial architecture. A: Western blots demonstrate that GST-Rbsn binds to MBP-Vps45, as detected by blotting for MBP (upper panel). GST-Rab4 is included as a negative control; anti-GST blot (lower panel) is included as a loading control. Relevant bands are indicated by *. B: Location of the *MENE(3R)-B*$^{JJ-2}$ and *MENE(3R)-B*$^{GG-11}$ mutations within the CG8228/Vps45 coding region. C-F: Compared to WT tissues (C, E), Notch (green) and Crb (cyan) levels are elevated in *Vps45* tissue (D, F). G-H': Notch trafficking assay performed as in Figure 2. *Vps45* mutants accumulate Notch (green) at the cell periphery, marked by actin staining (red), that persists after 5 hours. I-K: *Vps45* mutant discs lose epithelial architecture (actin, I) and mislocalize polarity markers (J, aPKC in green, Dlg in red), and upregulate Mmp1 (magenta, I') but do not activate Notch signaling (K, *mβ-LacZ* reporter in green; compare to WT in Figure 2I). Scale bars represent 100 µm in C-F, I, K and 10 µm in G-H', J.

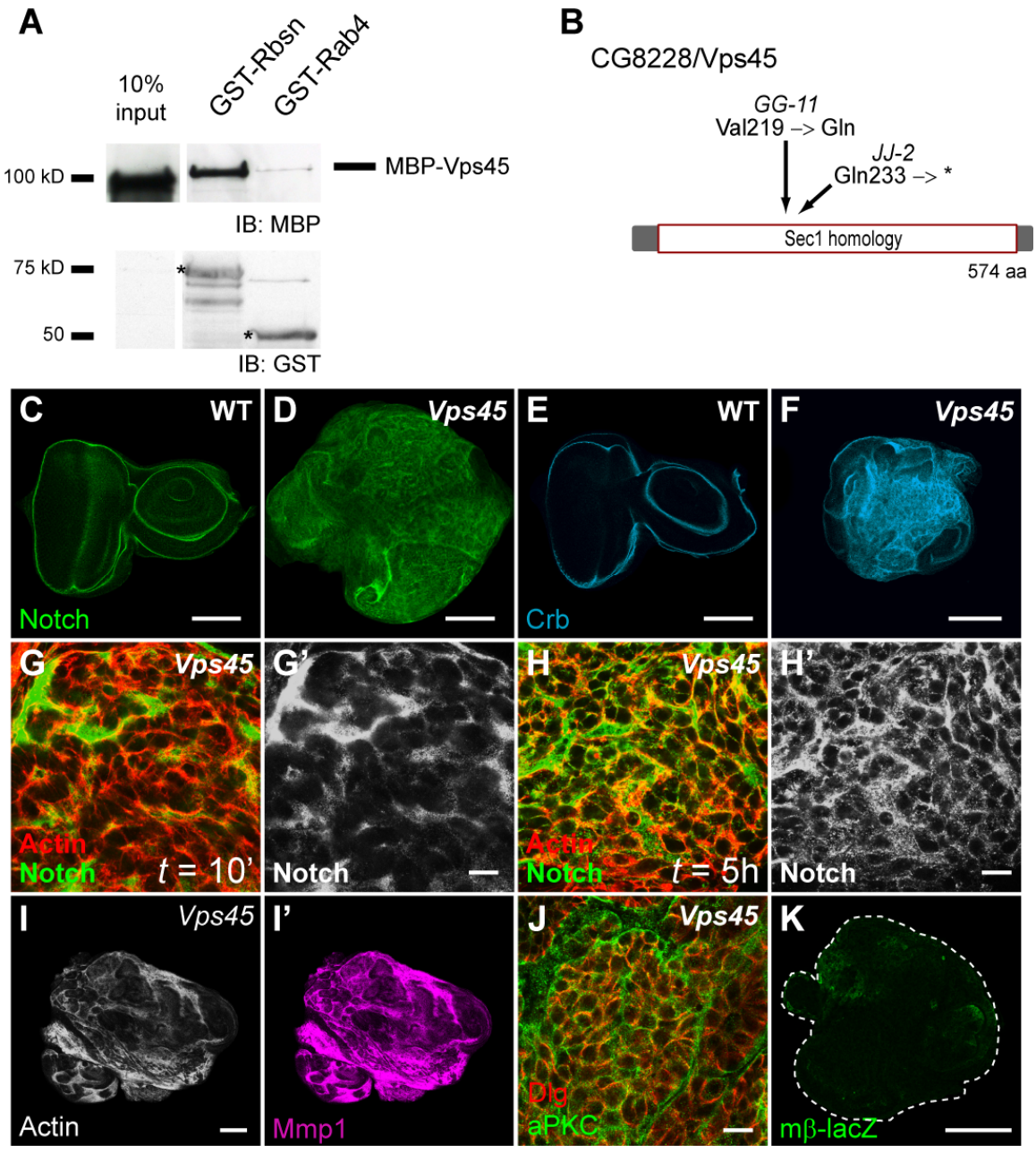
A
10% input
GST-Rbsn
GST-Rab4
100 kD
MBP-Vps45
IB: MBP
75 kD
50
IB: GST
B
CG8228/Vps45
GG-11
Val219 –> Gln
JJ-2
Gln233 –> *
Sec1 homology
574 aa
C WT
Notch
D Vps45
E WT
Crb
F Vps45
G Vps45
Actin
Notch
t = 10'
G'
Notch
H Vps45
Actin
Notch
t = 5h
H'
Notch
I Vps45
Actin
I'
Mmp1
J Vps45
Dlg
aPKC
K
mβ-lacZ

Figure 3.4. *In vivo* colocalization between Rab5, Avl, Rbsn and Vps45. Drosophila S2 cells were transfected with DNA constructs as indicated below, and then labeled to detect Rab5, Avl, Rbsn, or Vps45 as indicated in column headings. In Vps45-V5 transfected cells (A), Vps45 (green) shows partial overlap with Avl (red) and Rbsn (blue). In cells transfected with Rab5-YFP (B), Rbsn (blue) and Avl (red) are recruited to Rab5-positive structures (green). When Rab5-YFP and Vps45-V5 are cotransfected (C-D), Vps45 (blue in C, red in D) is recruited to structures labeled with Rab5 (green) and Avl (red, C) or Rbsn (blue, D). Arrowheads indicate triple colocalization, arrows in A''' indicate independent Vps45 localization. Scale bar, 5 µm.

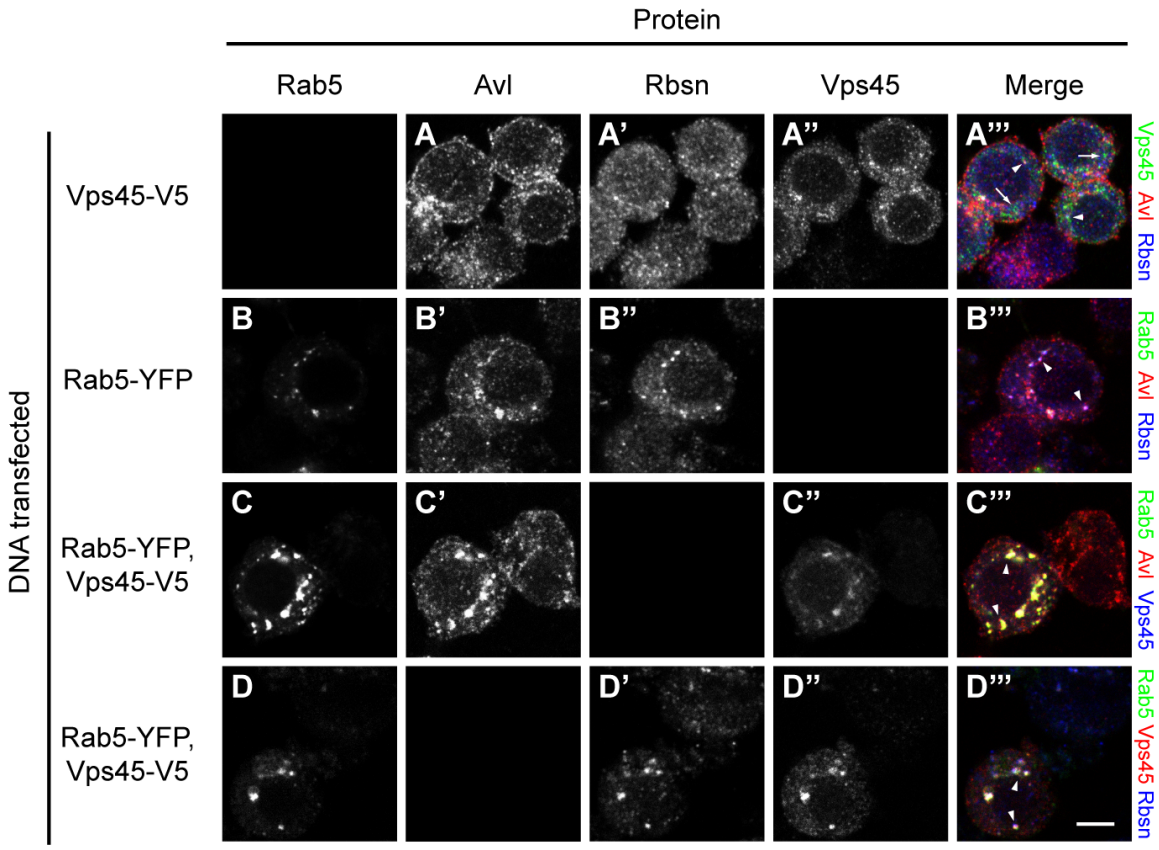
Protein
Rab5
Avl
Rbsn
Vps45
Merge
DNA transfected
Vps45-V5
Rab5-YFP
Rab5-YFP, Vps45-V5
Rab5-YFP, Vps45-V5
A
A'
A''
A'''
B
B'
B''
B'''
C
C'
C''
C'''
D
D'
D''
D'''
Vps45 Avl Rbsn
Rab5 Avl Rbsn
Rab5 Avl Vps45
Rab5 Vps45 Rbsn

Figure 3.5. Vps45 interacts with syntaxins of the endocytic pathway. A: Western blots demonstrate that MBP-Vps45 binds to Avl, GST-Syx13 and GST-Syx16 *in vitro* (upper panel). GST-Syx1a is included as a negative control. Lower panel shows loading control (anti-GST blot, with relevant bands labeled with *). B-H: Genetic interaction tests in a sensitized background generated by driving expression of a *UAS-Vps45-RNAi* transgene with the *engrailed-GAL4* driver (*en > Vps45 RNAi*). The *engrailed* expression domain is below the dashed line in B. Removal of one copy of *Vps45* (positive control, C), *avl* (D), *rbsn* (E) or *Rab5* (F), but not *Syx13* (G) or *Syx16* (H) enhances the RNAi phenotype. Note posterior cross vein modification in E (arrow). Scalebar, 0.5 mm.

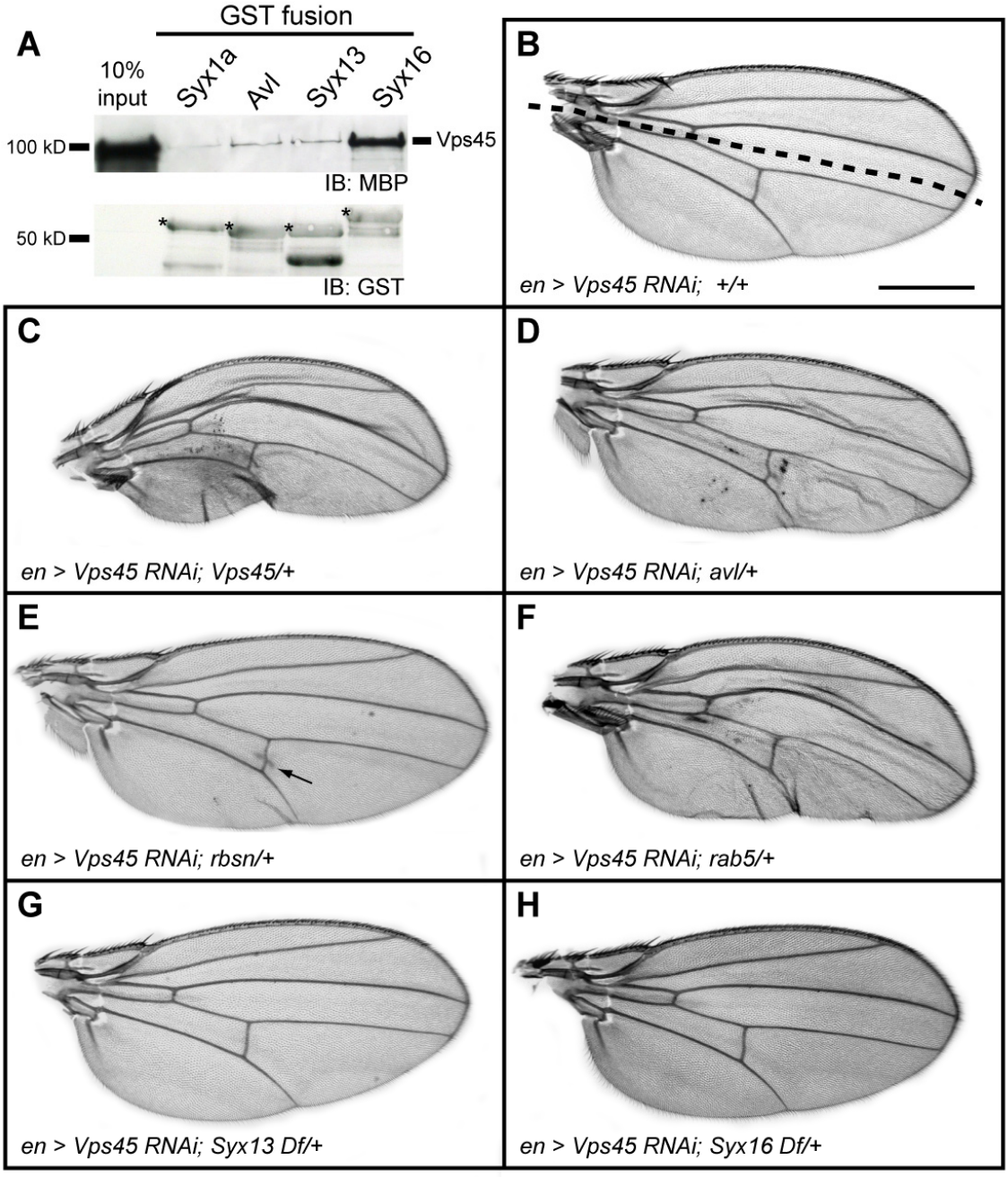
A
GST fusion
10% input
Syx1a
Avl
Syx13
Syx16
100 kD
Vps45
IB: MBP
50 kD
IB: GST
B
en > Vps45 RNAi; +/+
C
en > Vps45 RNAi; Vps45/+
D
en > Vps45 RNAi; avl/+
E
en > Vps45 RNAi; rbsn/+
F
en > Vps45 RNAi; rab5/+
G
en > Vps45 RNAi; Syx13 Df/+
H
en > Vps45 RNAi; Syx16 Df/+

Figure 3.6. ***rbsn*, *Vps45*, *avl* and *Rab5* cells accumulate endocytic vesicles but lack later endocytic structures.** Images show transmission electron micrographs of oocytes, immuno-labeled against yolk proteins produced in follicle cells and endocytosed by the oocyte, detected with gold particles (black puncta). In WT oocytes (A), yolk protein accumulates predominantly in large granules, but can also be found in immature granules (Y1); ~100nm vesicles are also evident below the plasma membrane (PM) (arrows). Yolk granules are absent in oocytes mutant for *rbsn* (B), *Vps45* (C), *avl* (D) and *Rab5* (E); instead yolk protein is found only in vesicles distributed predominantly below the PM. Some of these endocytic vesicles (EV) are uncoated, while others display a clearly visible coat (CV). Note the size difference between labeled endocytic structures found in WT tissue and vesicles found in mutant tissue. Scale, 500 nm.

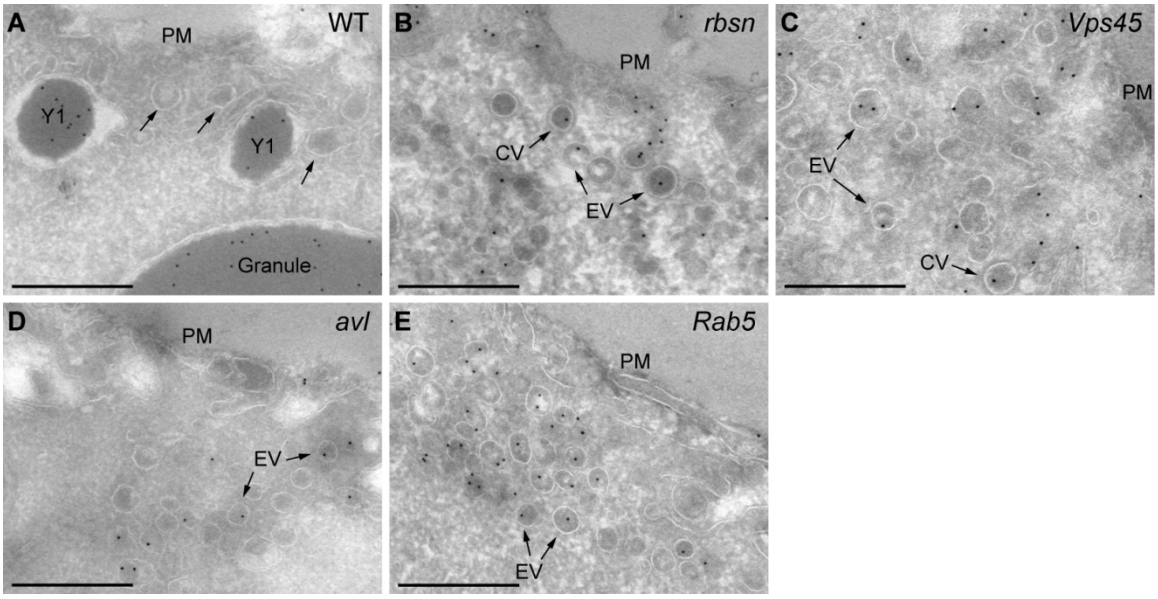
A
WT
PM
Y1
Y1
Granule
B
rbsn
PM
CV
EV
C
Vps45
PM
EV
CV
D
avl
PM
EV
E
Rab5
PM
EV

Figure 3.7. *rbsn* and *Rab5* epithelial phenotypes. A-B: In adult ovaries, WT (GFP-positive, green in A) follicle cells form an epithelial monolayer, while clones of *MENE(2L)-C* (*rbsn*, GFP-negative in B) often multilayer and invade the wild-type germ cell cluster. Cells are stained with phalloidin (red) to mark cortical actin. C-D: Notch trafficking assay in *Rab5* mutant eye imaginal discs. After 10 minutes high levels of Notch (green) are present at the cell periphery (C) and persist after 5 hours (D). Cell outlines are labeled by staining for actin (red). Follicle cell clones were generated as in (Bilder and Perrimon, 2000). Scalebars, 100 μm in A-B, 10 μm in C-D.

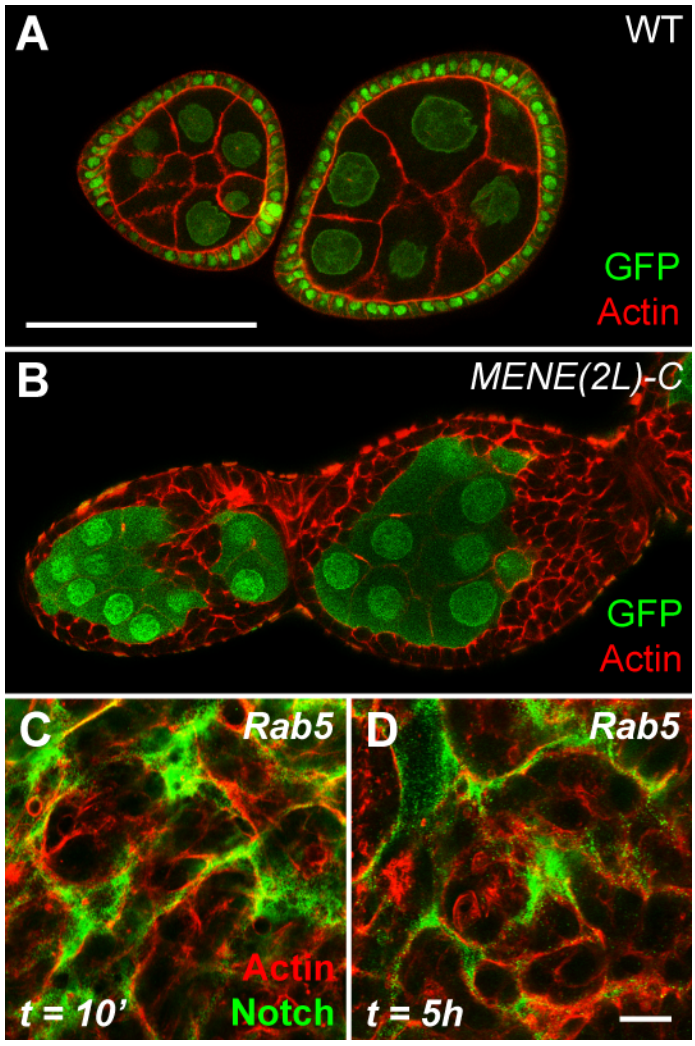
A
WT
GFP
Actin
B
MENE(2L)-C
GFP
Actin
C
Rab5
Actin
Notch
t = 10'
D
Rab5
t = 5h

Figure 3.8. Rbsn and Avl remain distinct from activated Rab4 and Rab11. Expression of YFP-tagged versions of constitutively active Rab4 (A, green) or Rab5 (B, green) in larval muscle cells under control of *MEF2-Gal4*. L3 larvae were dissected and stained for Avl (red) and Rbsn (blue). Despite some colocalization between Avl and Rbsn and Rab4 or Rab11 (arrowheads), most Avl and Rbsn does not localize to Rab4- or Rab11-positive structures (arrows). *UAS-Rab4QL-YFP* and *UAS-Rab11QL-YFP* were obtained from the Bloomington Stock Center. Scale, 10 µm.

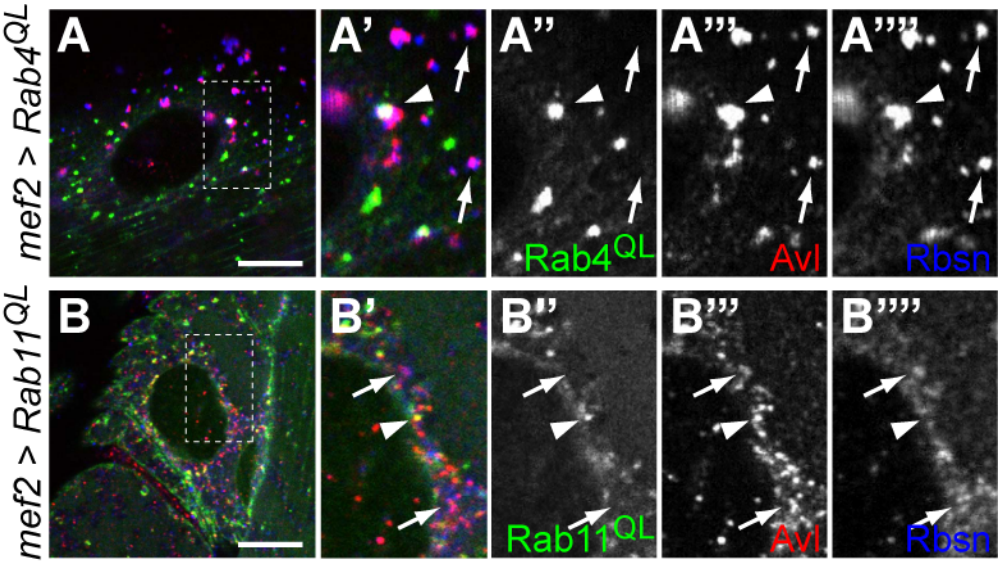
mef2 > Rab4QL
A
A'
A''
A'''
A''''
Rab4QL
Avl
Rbsn
mef2 > Rab11QL
B
B'
B''
B'''
B''''
Rab11QL
Avl
Rbsn

Figure 3.9. Subcellular localization and RNAi phenotypes suggest that Syntaxin16 does not function in early endocytosis. A: Syx16 (green, arrows) is not found in the enlarged endosomes (labeled by Avl, red) of wing imaginal discs expressing an activated form of Rab5 (Rab5DA, (Entchev *et al.*, 2000)). B-C: RNAi-mediated knockdown using *en-GAL4* to drive expression of *UAS-Dicer2* and *UAS-Syx16-IR* transgenes ((Dietzl *et al.*, 2007) produces adult wings (C) that are indistinguishable from wild-type (B). D-F': Identical coexpression of *UAS-Vps45-IR* and *UAS-Dicer2* produces defects at larval stages: wing imaginal discs lose epithelial architecture (D) and express Mmp1 (A') in addition to accumulating high levels of Notch (E') and Crb (F'). Actin (red, D-F) outlines cells, and GFP marks the e*n-Gal4* expression domain. Note the expanded Crb domains marked by yellow arrows in C'. Scalebars, 5 µm in A, 0.5 mm in B-C, 100 µm in D-E, 10 µm in F.

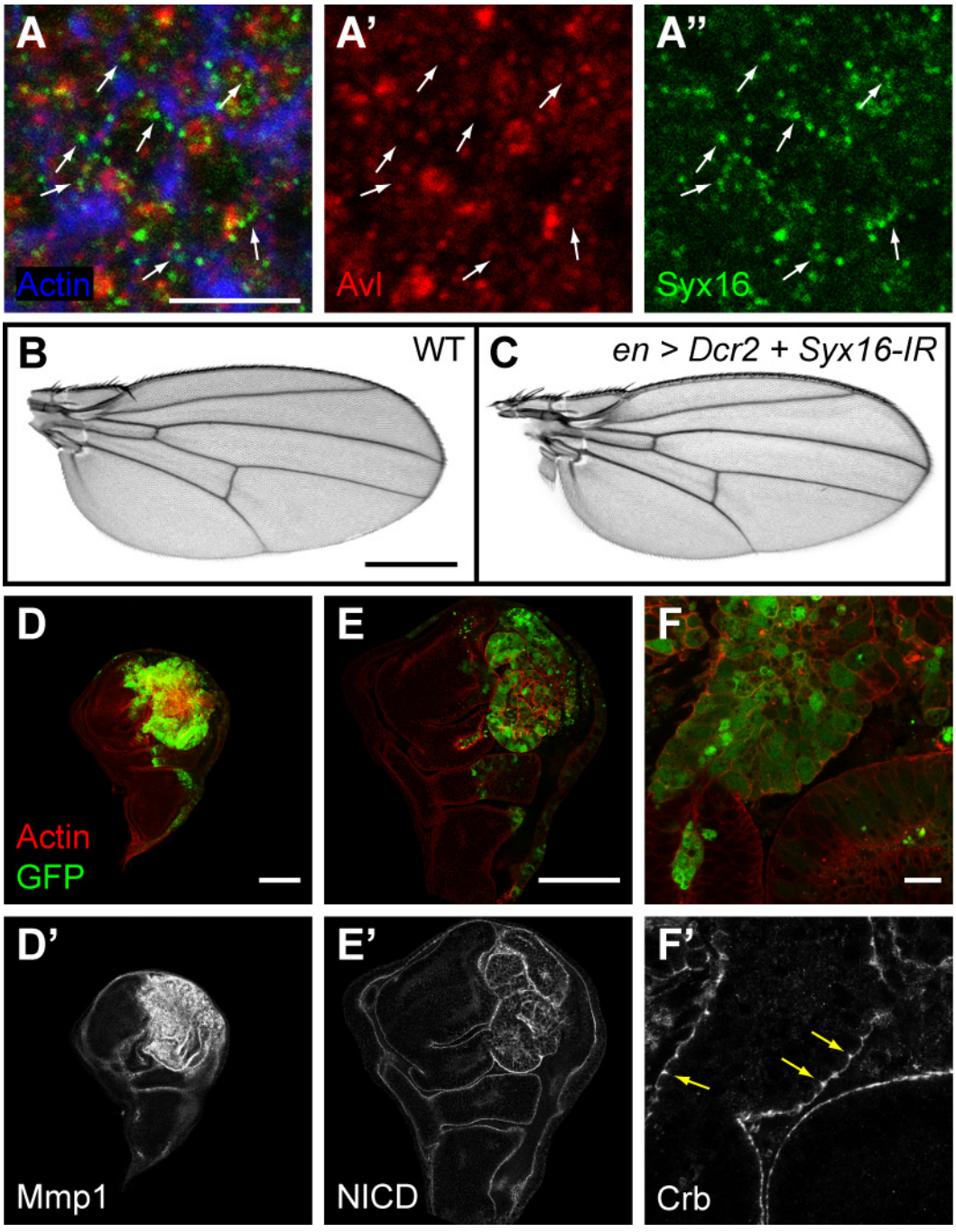
A
Actin
A'
Avl
A''
Syx16
B
WT
C
en > Dcr2 + Syx16-IR
D
Actin
GFP
E
F
D'
Mmp1
E'
NICD
F'
Crb

Figure 3.10. *rbsn*, *Vps45* and *Rab5* genetically interact with *avl*. Driving expression of a *UAS-Avl-IR* transgene (Lu and Bilder, 2005) with *en-GAL4* (A) produces a visible phenotype in the adult wing, which is enhanced by removing one copy of *avl* (B). Removing one genomic copy of *rbsn*, *Rab5*, or *Vps45* (C-E) also enhances the RNAi phenotype. Scale, 0.5 mm.

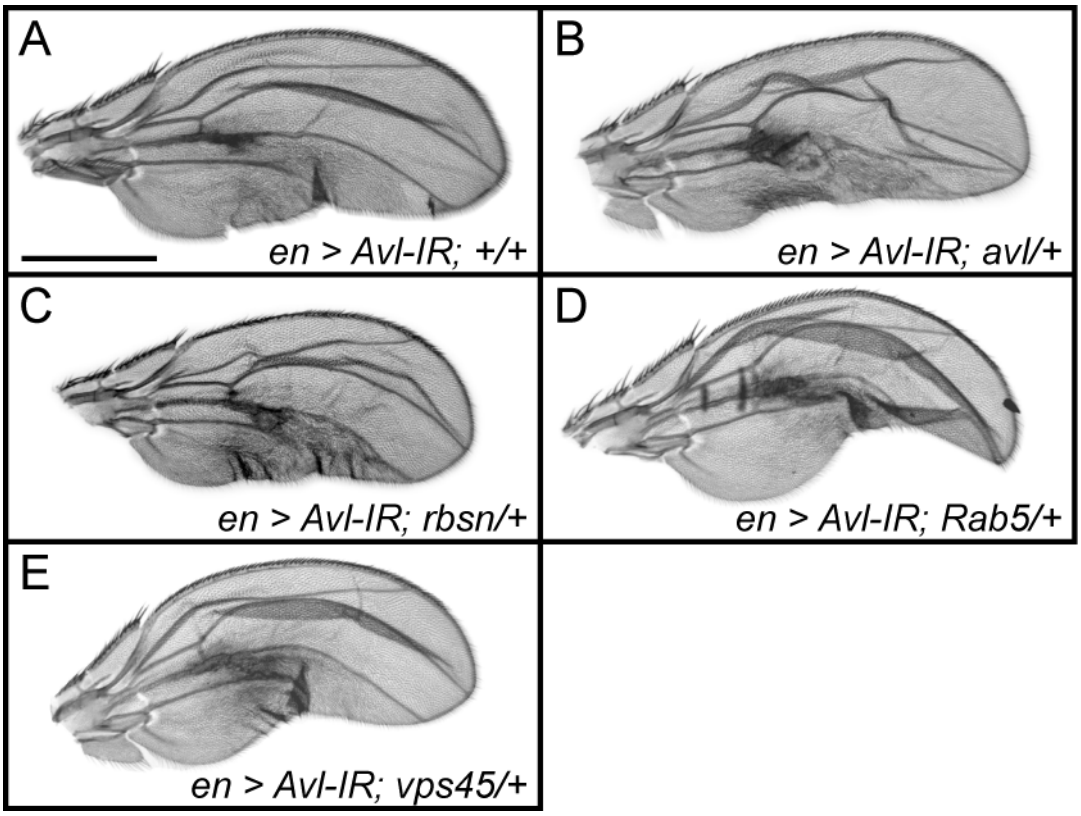
A
en > Avl-IR; +/+
B
en > Avl-IR; avl/+
C
en > Avl-IR; rbsn/+
D
en > Avl-IR; Rab5/+
E
en > Avl-IR; vps45/+

Appendix

Described herein are several additional experiments relevant to the characterization of *rbsn* and *Vps45*. In addition, we describe a series of experiments intended to provide insight into the cellular signaling pathways by which polarity and proliferation control may be coordinated.

Rescuing the *Rabenosyn* null mutant

In cloning the *rabenosyn* gene (*rbsn*), our sequencing of the $rbsn^{40\text{-}3}$ and $rbsn^{X17}$ alleles unambiguously identified lesions in the *rbsn* coding sequence (Figure 3.1). In addition, Western blot analysis using an anti-Rbsn antibody clearly indicated a loss of Rbsn protein in *rbsn* mutant tissue (Figure 3.1). To unequivocally demonstrate that loss of *rbsn* function was the only cause of the *rbsn* mutant phenotypes, we wanted to also demonstrate that ectopic expression of Rbsn could rescue *rbsn* null mutants. To address this, we generated rescue constructs that would drive ectopic *rbsn* expression under control of the GAL4-responsive Upstream Activating Sequence (*UAS-Rbsn*, T. Vaccari/C. Hsu) or a heat shock-inducible promoter (*HS-Rbsn*, C. Hsu). However, when expressed in the *rbsn* null background, none of the transgenic insertions of these two constructs rescued the larval lethality or the homozygous mutant cells generated with the eyFLP-cell lethal or the mosaic follicle cell system.

One possible explanation for the rescue constructs' inability to rescue *rbsn* mutants was that the transgenic constructs had randomly inserted into genomic regions with low expression levels and were not expressed at high enough levels to provide wild-type *rbsn* function. To test this hypothesis, we assessed the levels of Rbsn protein in wild-type imaginal discs and imaginal discs expressing either the *UAS-Rbsn* (driven by *engrailed-GAL4*) or *HS-Rbsn* constructs via Western blots. This analysis showed that Rbsn protein levels in tissue expressing the *UAS-Rbsn* or *HS-Rbsn* rescue constructs were not elevated relative to wild-type (Figure 3A.1A). We noted that the Rbsn protein levels in tissue expressing the *HS-Rbsn* construct were somewhat elevated in one experiment (Figure 3A.1B), but the increase was not as striking as we had expected. We therefore suspected that the lack of mutant rescue with these constructs was due to the lack of Rbsn expression.

We then generated an additional *rbsn* rescue construct that would take advantage of the ϕC31 integration system, which inserts transgenes into defined, highly expressed loci in the genome (Bischof *et al.*, 2007). This new construct retained the UAS promoter, but with the addition of a GFP coding sequence fusion, so that Rbsn tagged with GFP could be expressed in specific tissues under GAL4 control and easily visualized. However, we found that this construct also failed to rescue *rbsn* null mutants when expressed under control of the ubiquitously expressed *tubulin-GAL4* driver.

We then looked to see whether Rbsn-GFP was in fact being expressed under GAL4 control by examining the levels and subcellular localization of Rbsn-GFP driven by *MS1096-GAL4* in wing imaginal discs. We found that Rbsn-GFP was indeed present at very high levels in cells where *MS1096-GAL4* is expressed (Figure 3A.2). However, we also saw morphological features in these cells that indicated that the Rbsn-GFP-expressing cells were dying, suggesting that Rbsn overexpression is cytotoxic. This was

surprising, as Rab5 overexpression is not similarly cytotoxic, yet it did provide a reasonable explanation as to why this rescue construct did not rescue *rbsn* null mutant phenotypes. By overexpressing Rbsn at high levels, we were presumably overcompensating for the genomic loss of *rbsn* to such a degree that the animals were no longer *rbsn* null, yet not viable due to an uncharacterized Rbsn gain-of-function phenotype.

Generating Vps45 antibodies

As part of our analysis of the *in vivo* function of *Vps45*, we wanted to visualize the subcellular localization of Vps45 in the imaginal disc or follicle cell epithelia. To facilitate this, we attempted to generate an anti-Vps45 polyclonal antibody based on a combination of two small peptides from the Vps45 protein. Using commercial services, we obtained sera from both a rabbit and a chicken immunized with this peptide. Unfortunately, testing various sera batches that we received from these animals via Western blotting for any Vps45-specific signal failed to identify any usable antibody aliquots (Figure 3A.3). We therefore relied on expression of V5-tagged Vps45 for *in vivo* localization data as discussed previously.

Analyzing cellular signaling pathways in tissues with reduced Avl function

While completing the Rbsn and Vps45 studies, we were also interested in identifying the specific signaling pathways that might be disrupted or ectopically activated in neoplastic tumor suppressor gene (nTSG) mutant tissues, contributing to the observed cell proliferation and tissue overgrowth. To do this, we undertook a series of immunohistochemistry experiments using available reagents to evaluate the level of activation of candidate signaling pathways. So that we could directly compare the level of signaling pathway activity in nTSG mutant cells to wild type tissue, we performed the experiments in a mosaic tissue. Driving expression of an *avalanche* (*avl*) inverted repeat construct with *engrailed-GAL4* leads to *avl* knockdown specifically in the posterior compartment of the developing wing (*en>avl*-IR). The *en>avl*-IR expression leads to disrupted tissue architecture and cellular overproliferation consistent with the phenotypes we see in completely mutant eye discs (Figure 3A.5A-D). Meanwhile, the anterior compartment is relatively unaffected and retains mostly wild-type tissue morphology, although the relative contribution to the disc diminishes as the posterior *avl*-IR compartment increases in size.

We evaluated the relative levels of signaling pathway activation using assays as indicated in Table 3A.1. While many of the pathways we tested did not seem ectopically activated, the JNK pathway did show some evidence of activation in the *avl*-IR tissue relative to wild-type tissue. Using an antibody that detects phosphorylated JNK, we observed increased staining in the *avl*-IR posterior compartment relative to the anterior wild-type tissue (Figure 3A.4A, A''). This suggests that JNK pathway activation may be contributing to the *avl*-IR phenotype, which is consistent with reports that JNK activation can drive *scrib* tumor growth (Leong *et al.*, 2009).

We also observed that the regulation of Wingless expression, but not signaling, was disrupted in the *avl*-IR tissues. Similar to what we observed with pJNK, staining for

Wingless protein (Wg) also showed increased levels in the *avl*-IR tissue (Figure 3A.4A' and B-B'). However, the elevated Wg does not seem to be actively signaling, as the expression of *senseless*, a Wg signaling target, is not similarly elevated (Figure 3A.4B'). A *wingless in situ* indicated that *wingless* transcription is also elevated in the *avl*-IR tissue (Figure 3A.4C-C'), indicating that the increased Wg protein levels are not due merely to a defect in endocytic uptake and degradation. It may be that *wg* expression itself is increased due to ectopic Notch pathway activation, but this seems unlikely given that a distinct Notch target, Cut, is not elevated (Table 3A.1). The biological basis and significance of changes in the transcriptional regulation of *wingless* is therefore unclear.

Finally, we stained mosaic wing imaginal discs for markers of DNA synthesis (BrdU, Figure 3A.5E-F') and apoptosis (activated caspase-3, Figure 3A.5G-H). Elevated BrdU staining indicated that the *avl*-IR compartment is undergoing high levels of DNA synthesis, suggesting an increased rate of cell division. However, we also observed high levels of caspase-3 staining in this same compartment, suggesting that cell death is also prevalent. It was also striking that the wild-type tissue in the anterior compartment seemed to be in a state of dormancy – neither cell division nor cell death markers were observed in this compartment. This is unlike what we see in a fully wild-type wing disc, in which cell division is equally distributed across both compartments of the disc (Figure 3A.5E). This suggests that the presence of the dividing *avl*-IR tissue may have a non-autonomous growth suppression effect on the neighboring anterior compartment. Whether this truly represents a non-autonomous effect, and how that effect might be mediated is currently unknown.

To further investigate the increased cell division and death we observed in *avl*-IR tissue, we turned to fluorescence-activated cell sorting (FACS) for cell cycle analysis. In imaginal discs expressing GFP under control of *engrailed-GAL4* (*en>GFP*), the anterior and posterior compartments show similar cell cycle profiles; 25-30% of the cells are in G1, while ~50-60% are in the S- or G2-phase (Figure 3A.5K-L). This ratio is conserved in the anterior compartment in *en>avl-IR* discs (Figure 3A.5M). However, a dramatically different ratio is observed in the *en>avl-IR* posterior compartment: the vast majority of cells are in S-phase or G2 (Figure 3A.5N). However, it is unclear what this shift represents in terms of the cell cycle. Cells may be dividing so rapidly that they transit through G1 very quickly. Alternatively, they may actually be dividing quite slowly or even arresting in G2. Further investigation would be required to resolve this disparity. In addition, the results in Figure 3A.5 represent a single trial, and the experiment would need to be repeated to produce a statistically significant result. Also, the GFP-positive compartment dramatically varied in size in the *en>avl*-IR discs analyzed (Figure 3A.5I-J), which could have led to inconsistent representation of *avl*-IR cells in the cell cycle profile data. Despite these caveats, our preliminary results suggesting that cells with reduced *avl* function are shifted toward G2 correlates with data indicating that loss of *erupted* also leads to an accumulation of cells in the S- or G2 phase of the cell cycle (Gilbert *et al.*, 2009). Interestingly, the cell cycle shift in *erupted* mutant cells could be partially mitigated by decreasing STAT activity (Gilbert *et al.*, 2009). While the JAK/STAT signaling pathway is upregulated in imaginal discs from Drosophila nTSG mutants such as *scrib*, we have not tested for JAK/STAT activation in *avl*-IR discs. Furthermore, these data may

suggest that *avl* impinges on cell cycle regulators such as cyclin E, which promotes entry to S-phase and is ectopically expressed in *scrib* mutant clones in eye discs (Brumby and Richardson, 2003).

Materials and Methods

Western blots to assess expression levels of the Rbsn rescue constructs

Imaginal discs were dissected from wandering L3 larvae and homogenized in 20µL 3X sample buffer by grinding with a Kontes tissue grinder followed by boiling to denature the proteins. For *rbsn* mutant tissue, we used 18 mutant eye discs, while the wild-type, en-GAL4>UAS-Rbsn and HS-Rbsn samples contained 15 wing discs. UAS-Rbsn was generated by C. Hsu and T. Vaccari. EP-Rbsn was from W. Fisher. HS-Rbsn (made by C. Hsu and T. Vaccari) larvae were heat shocked at 37°C for one hour followed by a 2 hour recovery at 25°C before dissection. The samples were run on an SDS-PAGE gel followed by blotting to a nitrocellulose membrane via standard techniques. Anti-Rbsn ("Bleed 2") was used at a dilution of 1:1000-1:2000; loading controls Dlg or α-Spectrin were used at 1:5000 and 1:1000, respectively.

UAS-Rbsn-EGFP cloning and transgenesis

The coding sequence of Rbsn was amplified from cDNA LP18416 and ligated into the Dual Promoter (pCR®II) Invitrogen TA cloning® kit vector. Following recovery, the Rbsn coding sequence was transferred to the pBDP-UAST-EGFP vector (B. Pfeiffer) via the BglII and NotI restriction sites to generate "UAS-Rbsn-EGFP". This generated an in-frame protein fusion with EGFP at the C-terminus of Rbsn. Constructs were confirmed by direct sequencing and clone "N3" was used for subsequent injection to generate transgenic lines.

An aliquot of UAS-Rbsn-EGFP (N3) was sent to Genetic Services, Inc. for injection into flies bearing a ϕc35 integrase site on chromosome arm 3L. Two transgenic lines were recovered.

Generating and testing Vps45 antisera

Two peptides from the predicted Vps45 translation were selected for antibody generation, based on suggestions from Covance and Pocono: CEFQRKANDHKKVESIADMK ("Vps45 internal") and QFKHTKSMIKYCSTDNI ("Vps45 c-term"). Peptide synthesis, conjugation and injection were performed by Pocono Rabbit Farm and Laboratory, Inc (70-day protocol). One chicken and one rabbit were immunized, with sera collected according to Pocono's standard.

Preimmune and post-immunization bleeds from each animal were initially tested on Western blots at a dilution of 1:1000. Subsequent testing of the Chicken sera on w^{1118} embryo extract (J. Zeitler), wild-type wing discs (13 discs) or *Vps45* mutant eye discs (16 eye discs) used preimmune at 1:1000 and Bleed1 at 1:5000. Finally, bleeds 2 and 3 from each animal were tested against Drosophila tissue extracts at a dilution of 1:1000. Where appropriate, a tubulin antibody (1:5000) was used as a loading control.

Immunohistochemistry

Imaginal discs from wandering L3 larvae expressing the *avl*-IR constructs under control of *engrailed-GAL4* were dissected, fixed and imaged as previously described (Chapter 3 Materials and Methods). Antibodies and dilutions were as follows: active-JNK 1:100 (Promega #V7931), Wg 1:100 (DSHB), sens 1:1000 (H. Bellen), cut 1:100

(DSHB), active caspase-3 1:100 (Cell Signaling Technologies #9661), BrdU 1:50 (BD Biosciences), phalloidin 1:250. Secondary antibodies were from Molecular Probes.

BrdU incorporation assay

Dissect larvae in room temperature Schneider's medium. Transfer to an eppendorf tube with Schneider's media containing 0.25mg/mL BrdU. Rock on Nutator at room temperature for 90minutes (to catch $1^{st}/2^{nd}$ mitotic waves and ectopic S-phases). Wash 1x5min in room temperature Schneiders, 2x5min in PBS on ice. Fix overnight at 4°C in 1% paraformaldehyde + 0.1% Tween-20 in PBS. Wash 5x10min in PBS. DNase treat at 37°C for 30 minutes in 1X PBS, 1X DNase reaction buffer + 5µL DNase (Promega #M6101) in 100µL. Wash 2x10min with PBS-T (PBS + 0.01% Tween-20). Incubate 90 minutes at room temperature with anti-BrdU antibody in PBS-T + 10% NGS. Wash 3x10min in PBT. Incubate 1 hour at room temperature with secondary antibodies in PBS-T + 10%NGS. Wash in PBT and dissect discs onto slides.

In situ hybridization

The *in situ* probe for detecting Wingless transcripts was generated using the Wg cV cDNA from H. Lu. Briefly the cDNA was linearized by an overnight XbaI restriction digest followed by cleanup with the Qiagen PCR purification kit. RNA probes were transcribed from the cDNA using the T3 polymerase and other reagents from the Roche T7/Sp6 transcription kit. Following DNase treatment, the mRNA was fragmented and precipitated, then resuspended in hybridization buffer (50% formamide, 5x SSC, 100µg/mL ssDNA, 50µg/mL heparin, 0.1% Tween-20).

For *in situ* hybridization, L3 discs were dissected in PBS and fixed 20min in 4% paraformaldehyde. Wash 3x5min in PBS+0.1% Tween-20 (PBS-T). Resuspend in 1:1 300mM Ammonium acetate:Ethanol to dehydrate. Wash 5min in ethanol. Incubate 10min in 1:1 xylenes:ethanol. Wash 3.5min in 100% ethanol. Wash 5min in methanol. Wash 5min in 1:1 methanol: 4% paraformaldehyde in PBS. Fix again 20min in 4% paraformaldehyde/PBS. Wash 5min in PBS-T. Incubate 10min in 1:1 hybridization buffer:PBS-T. Pre-hybridize in hybridization buffer at 60°C for 2 hours. Dilute probe 1:100 in hybridization buffer, heat to 80° 5min and place on ice. Add diluted probe to discs and incubate overnight at 60°C. Next day, remove probe (may be saved and reused), Wash 6x30min with hybridization buffer at 60°C. Remove hybridization buffer incrementally by washing 3min each in 8:2 hybridization buffer:PBS-T, followed by 1:1 and 2:8. Wash 5min in PBS-T. Incubate overnight at 4°C in 1:1000 anti-DIG antibody. Wash 3x5min in PBS-T, then 2x5min in developing solution and develop with NBT+BCIP. After stain develops, wash 3x5min in PBS-T. Dissect discs to slides.

Fluorescence activated cell sorting sample preparation and analysis

Wing imaginal discs were dissected from wandering L3 larvae in room temperature 1XPBS (10 larvae per sample), including removal of trachea and other discs. Wing discs were transferred to a 6mL polystyrene tube containing 500µL of 9X Trypsin-EDTA (from 10X Trypsin-EDTA, Sigma #T4174), 1X PBS, and 0.5µg/mL Hoechst 33342 (Sigma #14533, stock 10mg/mL). Discs were dissociated by gentle rocking on a

Nutator at room temperature for ~4 hours with occasional manual shaking to break up clumps. Dissociated cells were analyzed with Hector Nolla in the UC Berkeley Cancer Research Lab Flow Cytometry Facility. Cells were analyzed for size, DNA content, and GFP fluorescence.

Figure 3A.1. Comparison of Rbsn protein levels in wild-type and Rbsn transgenic wing discs.

A: Western blot with anti-Rbsn antibody shows that Rbsn is absent from *rbsn* mutant eye discs. Compared to wild-type wing discs (iso40), driving expression of two different *UAS-Rbsn* constructs with *en-GAL4* does not lead to elevated wing disc Rbsn levels. Similarly, induction of the *HS-Rbsn* construct does not elevate wing disc Rbsn levels. α-Spectrin is used as a loading control.

B: Western blot with anti-Rbsn antibody shows that compared to wild-type wing discs (iso82), discs from larvae carrying the *HS-Rbsn* transgene that have been heat shocked contain slightly elevated levels of Rbsn protein. Dlg is used as a loading control.

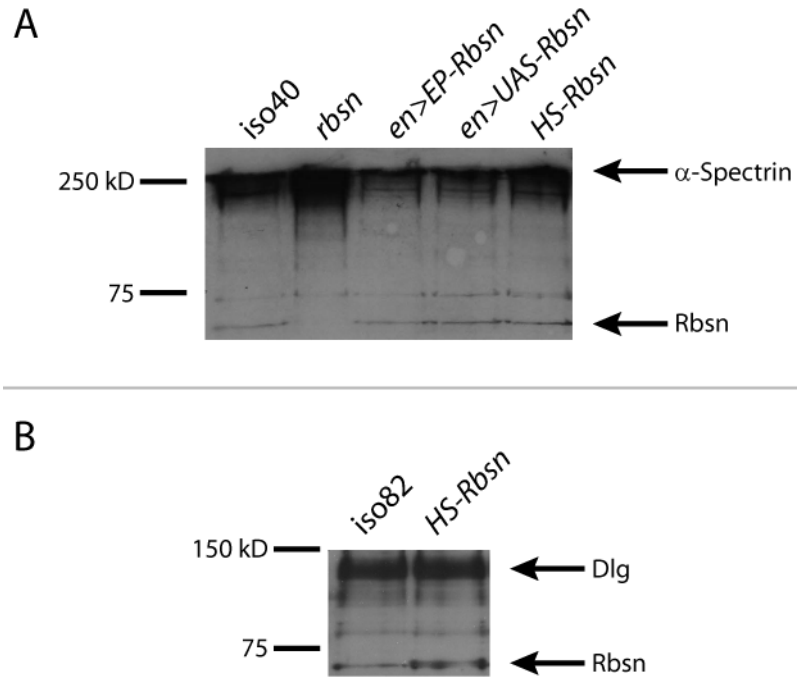
A
iso40
rbsn
en>EP-Rbsn
en>UAS-Rbsn
HS-Rbsn
250 kD
75
α-Spectrin
Rbsn
B
iso82
HS-Rbsn
150 kD
75
Dlg
Rbsn

Figure 3A.2. Overexpression of Rbsn-GFP in the imaginal wing disc.
A: In the wing imaginal disc of L3 larvae, *MS1096-GAL4* drives expression of *UAS-GFP* in the dorsal compartment of the developing wing blade. B: Driving *UAS-Rbsn-GFP* expression with *MS1096-GAL4* leads to disrupted tissue architecture. C: At the cellular level, overexpression of Rbsn-GFP as in B leads to aberrant cell morphology. Rbsn-GFP-positive structures surrounded by actin and punctate nuclei consistent with cell death are prominent. Red, actin. Green, GFP or Rbsn-GFP as indicated. Bar, 100µm in A and B, 25µm in C.

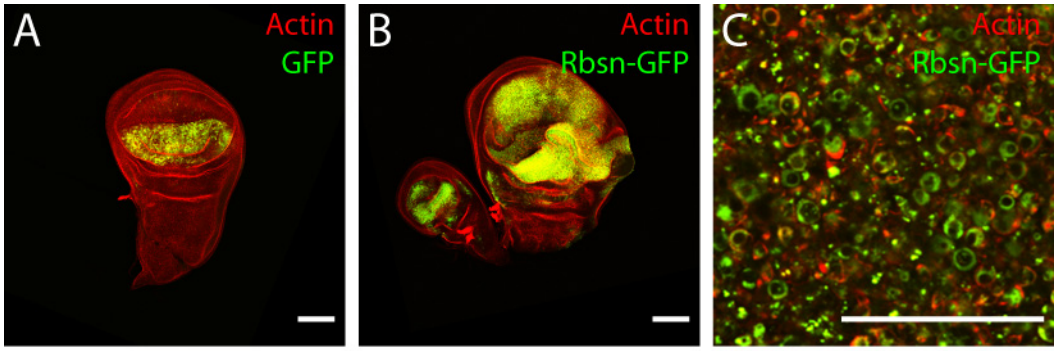
A
Actin
GFP
B
Actin
Rbsn-GFP
C
Actin
Rbsn-GFP

Figure 3A.3. Vps45 antisera show no specific activity against Drosophila tissue extracts.

A: Probing samples from wild-type wing imaginal disc tissue with preimmune or first bleed sera from an immunized chicken and rabbit does not identify any specific activity in sera from immunized animals. Expected Vps45 molecular weight: 65kD.

B: Proteins extracted from wild-type (wt) embryos, wt wing discs, or *Vps45* mutant eye discs were blotted to a membrane, then probed with either preimmunization sera ("Preimmune") or the first batch of serum collected ("Bleed 1"). Membranes were also probed with anti-tubulin as a control. Bleed 1 serum non-specifically labeled a diffuse haze in the high-molecular weight range.

C: Testing sera from the second and third bleeds from immunized rabbit. Samples were prepared as in B. Tubulin is included as a control. No Vps45-specific activity is detected.

D: Testing sera from the second and third bleeds from immunized chicken. Samples were prepared as in B. No Vps45-specific activity is detected.

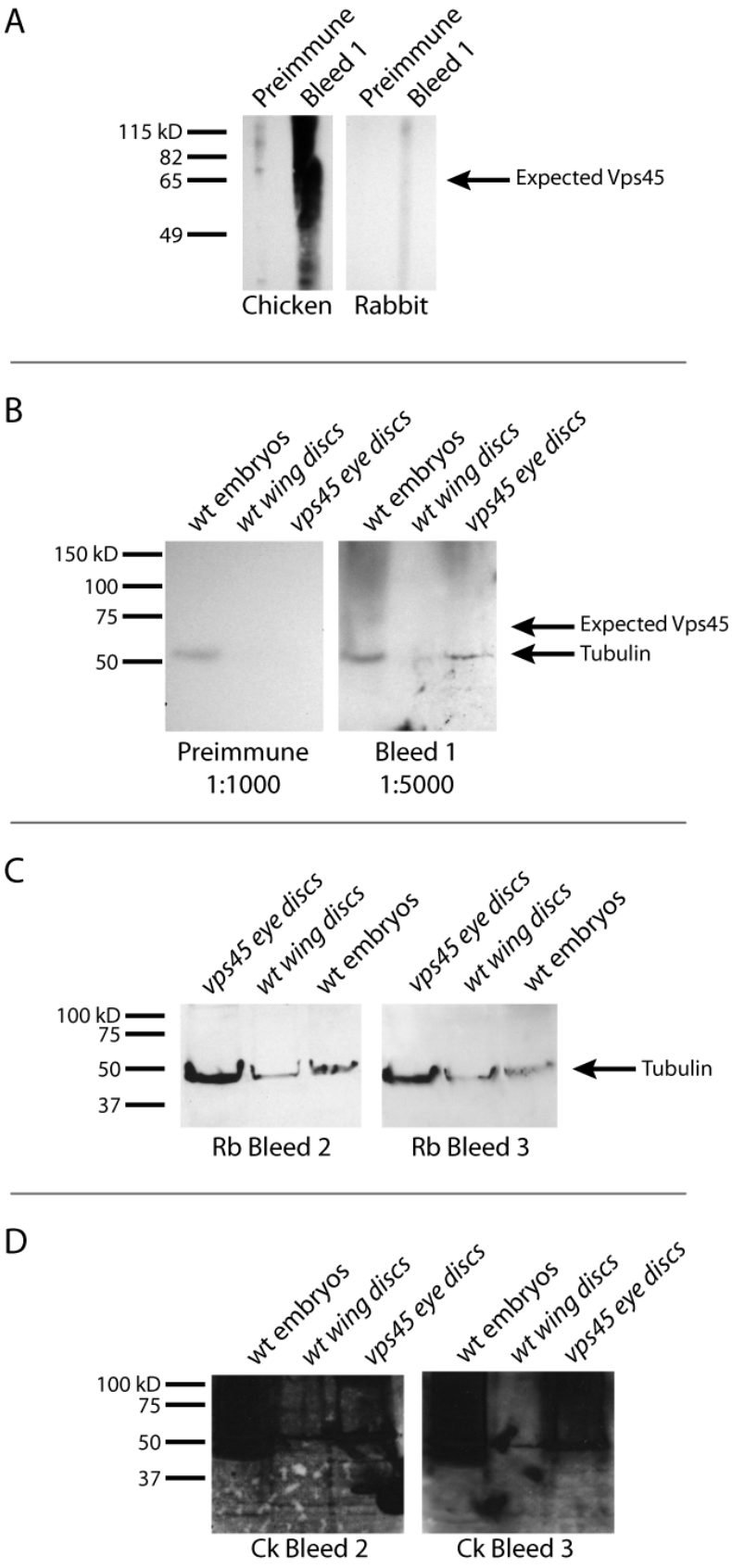
A
Preimmune
Bleed 1
Preimmune
Bleed 1
115 kD
82
65
49
Expected Vps45
Chicken
Rabbit
B
wt embryos
wt wing discs
vps45 eye discs
wt embryos
wt wing discs
vps45 eye discs
150 kD
100
75
50
Expected Vps45
Tubulin
Preimmune
1:1000
Bleed 1
1:5000
C
vps45 eye discs
wt wing discs
wt embryos
vps45 eye discs
wt wing discs
wt embryos
100 kD
75
50
37
Tubulin
Rb Bleed 2
Rb Bleed 3
D
wt embryos
wt wing discs
vps45 eye discs
wt embryos
wt wing discs
vps45 eye discs
100 kD
75
50
37
Ck Bleed 2
Ck Bleed 3

Figure 3A.4. Analysis of Wg and JNK signaling pathway readouts in *avl*-IR wing discs.
A: Imaginal wing discs expressing the *avl-IR G8+B3* transgenes under control of the *engrailed-GAL4* driver ("*en>avl*-IR") contain high levels of Wg (green, A') and phosphorylated JNK (pJNK, red, A'') proteins. *Puc-LacZ* wing discs are mostly wildtype, but contain a population of cells ectopically activating JNK (pJNK positive control, A).
B-B': Despite elevated levels of Wg protein (red), the Wg signaling target Sens (green) is not ectopically expressed in *en>avl-IR G8+B3* wing discs. Actin staining (blue) outlines cells.
C: In situ of wild-type or *en>avl-IR G8+B3* imaginal wing discs probed for *wg* mRNA. Wingless transcription is elevated in the *avl*-IR-expressing region of the disc.
Posterior is to the right in all images.

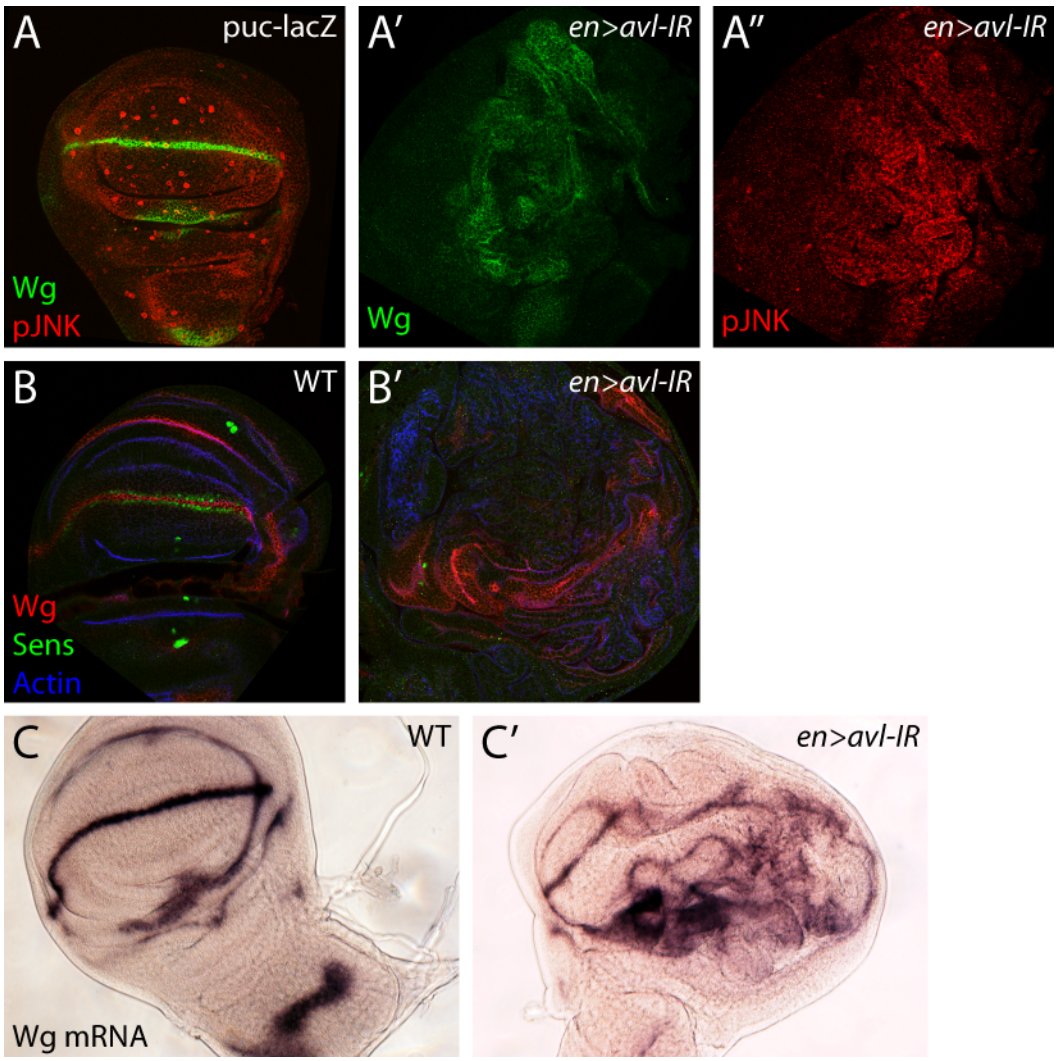
A
puc-lacZ
Wg
pJNK
A′
en>avl-IR
Wg
A″
en>avl-IR
pJNK
B
WT
Wg
Sens
Actin
B′
en>avl-IR
C
WT
Wg mRNA
C′
en>avl-IR

Figure 3A.5. Tissue architecture defects and cell cycle analysis of imaginal wing discs expressing *avl*-IR transgenes.

A-D: Driving the *avl-IR G8* transgene with *engrailed-GAL4* produces an adult wing phenotype, but no obvious phenotype in the imaginal disc (A). Expressing a stronger construct, *avl-IR B3* under *en-GAL4* control leads to tissue architecture defects (B). These tissue defects are even more severe when the *B3* transgene is expressed in combination with *avl-IR G8* (C) or a second weak transgene, *avl-IR R2-2B* (D). Actin (red) outlines cells. GFP label (green) indicates the domain of *en-GAL4* expression (A, B, D). In C, *en-GAL4* expression is to the right of the dashed line.

E-F: BrdU incorporation labels cells undergoing DNA synthesis in wild-type and *en>avl-IR G8+B3* wing discs. In the *avl*-IR discs, BrdU incorporation is reduced in the anterior compartment relative to the wild-type disc control, and is increased in the posterior compartment.

G-H: Staining for activated Caspase3 marks apoptotic cells in wild-type and *avl*-IR wing discs. Wild-type discs contain very few dying cells, while the posterior compartment of *avl*-IR discs contains an abundance of apoptotic cells.

I-J: Examples of *en>avl-IR B3* wing discs used in FACS analysis in M-N. Note the dramatic variation in phenotype and relative contribution of GFP-positive cells to the disc.

K-N: FACS analysis of *en>GFP* and *en>avl-IR B3* wing discs. X-axis is DNA content, y-axis is cell counts. GFP-negative cells in the *en>GFP* (K) and *en>avl-IR* (M) discs contain similar proportions of cells in the G1 versus S/G2 phase of the cell cycle. GFP-positive cells, however, show markedly different cell cycle distribution in *en>GFP* (L) versus *en>avl-IR* (N).

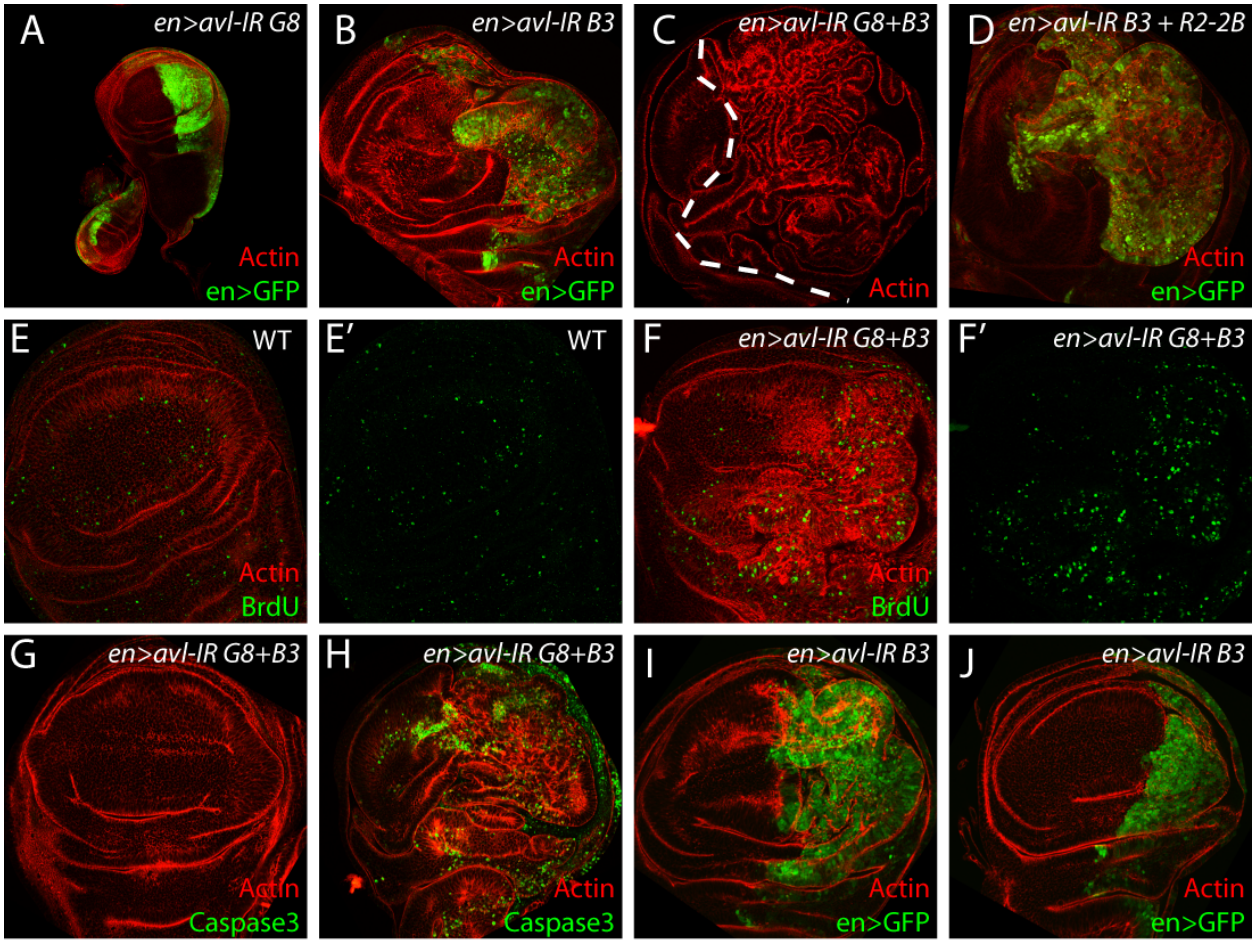
A
en>avl-IR G8
Actin
en>GFP
B
en>avl-IR B3
Actin
en>GFP
C
en>avl-IR G8+B3
Actin
D
en>avl-IR B3 + R2-2B
Actin
en>GFP
E
WT
Actin
BrdU
E′
WT
F
en>avl-IR G8+B3
Actin
BrdU
F′
en>avl-IR G8+B3
G
en>avl-IR G8+B3
Actin
Caspase3
H
en>avl-IR G8+B3
Actin
Caspase3
I
en>avl-IR B3
Actin
en>GFP
J
en>avl-IR B3
Actin
en>GFP

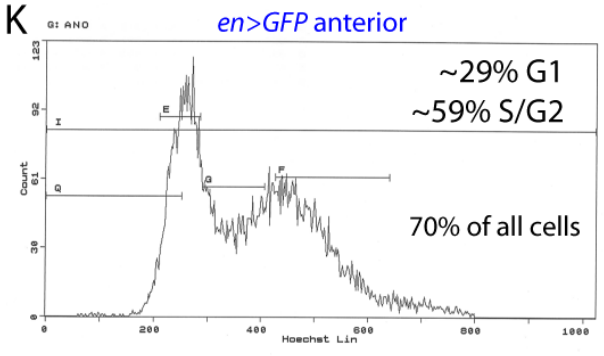
K
en>GFP anterior
~29% G1
~59% S/G2
70% of all cells
Count
Hoechst Lin

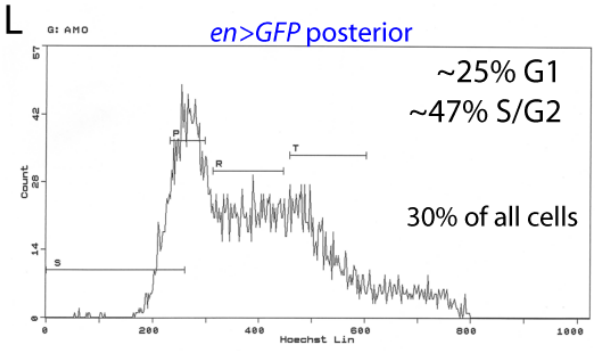
L
en>GFP posterior
~25% G1
~47% S/G2
30% of all cells
Count
Hoechst Lin

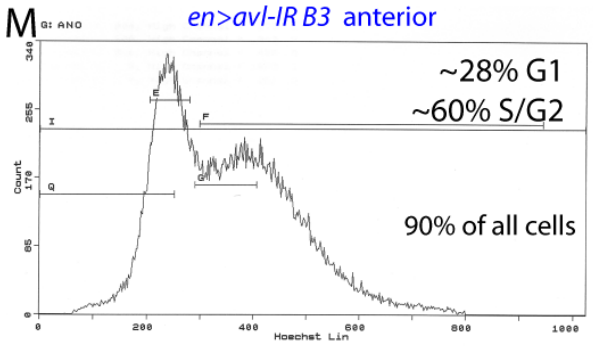
M
en>avl-IR B3 anterior
~28% G1
~60% S/G2
90% of all cells
Count
Hoechst Lin

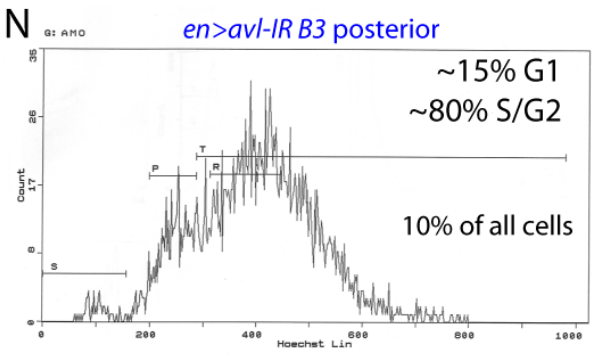
N
en>avl-IR B3 posterior
~15% G1
~80% S/G2
10% of all cells
Count
Hoechst Lin

Table 3A.1. Analysis of candidate signaling pathways in *avl*-IR wing discs.
Listed here are several signaling pathways implicated in the control of cellular proliferation in *Drosophila* and currently available assays for pathway activity. Results are given based on immunohistochemical staining on wing discs expressing the *avl-IR B3* or *avl-IR G8+B3* transgenes in the posterior compartment under *en-GAL4* control. ND, not determined. DB, results per David Bilder.

Signaling Pathway	Assay	Readout in avl-IR
JNK	pJNK antibody	slightly elevated
Unpaired	pSTAT antibody	not elevated (DB)
Notch	mβ-lacZ	not elevated (DB)
	Cut antibody	not elevated
Wingless	Wingless protein	elevated
	Wingless in situ	elevated
	Senseless antibody	not elevated
	fz3 in situ	ND - *fz3 in situ* probes not working
dMyc	Fibrillarin antibody	not clear; nucleoli maybe slightly larger
Decapentaplegic	Dpp *in situ*	not clear
	pMAD antibody	ND
	UAS-dad as inhibitor	ND
Hippo/Sav/Warts	Expanded antibody	ND
TNFα	puc-lacZ	ND
Hedgehog	Ci antibody	ND
EGFR/PVR	dpERK antibody	ND
Proliferation	BrdU incorporation	elevated in mutant tissue, eliminated in anterior of disc
Cell death	active caspase3	elevated

Chapter 4

An Unbiased Screen for Genes which Interact with *lethal giant larvae*

Abstract

Establishing and maintaining distinct subcellular domains is essential for the proper function of a myriad of cell types. In *Drosophila* epithelial cells, the tumor suppressor gene *lethal giant larvae* (*lgl*) is required for maintaining apicobasal polarity, and this function is evolutionarily conserved from flies to mammals. Previous studies in flies, yeast and mammalian systems have identified several molecular functions of Lgl. However, the exact mechanism of Lgl-mediated polarity regulation remains unclear. Here we describe a forward genetic screen for genes which genetically interact with *lgl*. Reducing Lgl activity in the developing wing by RNA interference (*lgl*-IR) results in a genetically modifiable adult phenotype. By screening 60% of the Drosophila genome using a collection of molecularly defined deficiencies, we identified 14 genomic regions that modify the *lgl*-IR phenotype. We have further refined these regions by using smaller deficiencies, and present here the identification of these narrow regions. In addition, we discuss potential candidate genes for further investigation. By testing the candidate genes, this approach may ultimately identify novel genes that act with *lgl* to regulate polarity, and clarify the mechanism of *lgl*-mediated polarity control.

Introduction

The distinction between the apical and basolateral domains in polarized epithelial cells is controlled by a variety of proteins and cellular pathways. Furthermore, many of the proteins required to maintain this domain distinction show polarized subcellular localization patterns themselves. Lethal giant larvae (Lgl) is one such protein of particular importance. Lgl localizes specifically to the basolateral domain, and is part of a module that also contains the Scribble and Discs large proteins. Remarkably, the genes encoding these three proteins were among the first to be recognized as tumor suppressor genes in Drosophila (Gateff, 1978; Bilder *et al.*, 2000). The striking finding that polarity is disrupted in *lgl* mutant epithelial cells indicated that Lgl is functionally required to maintain apicobasal polarity (Manfruelli *et al.*, 1996; Bilder *et al.*, 2000). Moreover, this requirement seems to be conserved from flies to mammals, as Lgl also localizes to lateral membranes in mammalian MDCK cells, and mice lacking the homologous Lgl1 gene have defects in cell polarity and asymmetric cell division in the developing brain (Musch *et al.*, 2002; Klezovitch *et al.*, 2004). Thus, Lgl is a functionally conserved protein that is critical for controlling cell polarity, yet the exact mechanism by which it achieves this function remains poorly understood.

Several studies have elucidated the multifaceted interactions between Lgl and other intracellular proteins, many of which have been implicated in controlling cell polarity. Perhaps the most clear of these is the interaction between Lgl and the Par6/aPKC complex. The Lgl protein contains a large domain conserved among the various Lgl homologs ("Lgl domain"), and several WD40 repeats, which act as scaffolds to facilitate protein-protein interactions (Vasioukhin, 2006). aPKC phosphorylates multiple serine residues within the conserved Lgl domain. This phosphorylation inactivates Lgl by promoting auto-inhibitory binding between the N- and C-termini of the protein. The Par6/aPKC complex localizes to the apical domain in polarized cells, and this in turn sets up polarized Lgl domains: Lgl is inactive and excluded from the apical domain, but unphosphorylated and active at the lateral cortex. Meanwhile, active Lgl excludes Par6 from the basolateral domain, reinforcing accurate apicobasal polarity.

In addition to acting in opposition with aPKC to maintain polarized intracellular domains, Lgl has also been implicated in other intracellular roles based on biochemical studies. In yeast, the Lgl homologs Sro7p and Sro77p bind to the syntaxin Sec9p (Lehman *et al.*, 1999). This is consistent with the observed binding between the mammalian homolog Lgl1 and the SNARE protein Syntaxin4 (Musch *et al.*, 2002), and suggests that Lgl may control cell polarity by regulating polarized exocytosis. On the other hand, Lgl regulates asymmetric cell division in Drosophila neuroblasts by promoting endocytosis of Sanpodo, a membrane-bound protein required for Notch signaling (Roegiers *et al.*, 2005). In addition, Lgl interacts with Myosin II in dividing neuroblasts to restrict contractile ring formation to the apical domain (Barros *et al.*, 2003), suggesting that Lgl could regulate polarity via the actin cytoskeleton. Finally, Drosophila Lgl can be found in a complex with the Fragile X Syndrome Protein FMRP, which regulates mRNA transport (Zarnescu *et al.*, 2005). Together, these studies point

to Lgl's roles in a variety of cellular pathways, including mRNA transport, the actomyosin cytoskeleton, and vesicle trafficking, both endocytic and exocytic.

Based on the various biochemical studies discussed above, it is apparent that Lgl is a fundamental and broadly used protein. However, the exact mechanism by which Lgl coordinates these processes and dictates cell polarity remains unclear. In particular, the biochemical approaches have not defined the relative importance of any one of these processes for maintaining apicobasal polarity in epithelial cells. Therefore, a genetic approach to identifying additional genes that control polarity with Lgl through these or alternative pathways is an important step toward understanding how Lgl regulates cell polarity. We present here the results of a forward genetic screen to identify such additional genes.

A previous forward genetic screen in *Drosophila* used eclosion failure and imaginal disc morphology to identify a number of growth- and polarity-regulating genes with recessive phenotypes that often strongly resemble those due to *lgl* loss of function (Menut *et al.*, 2007). Cloning these genes has identified several cellular processes that regulate polarity, such as endocytosis, protein degradation and Polycomb-mediated transcriptional control. While fruitful, that screen has not completely saturated the genome, raising the possibility that there are still polarity-regulating genes to be found. In addition, genes with pleiotropic functions, or those which negatively regulate processes that are required to maintain polarity would not have been identified in such a loss-of-function genetic screen. For example, loss of proteins in the imaginal disc which negatively regulate Lgl activity, such as aPKC, does not lead to polarity loss that produces a non-eclosion phenotype, and would not have been identified in the non-eclosion screen. We therefore turned to an alternative approach: a genetic modifier screen.

Modifier screens are a valuable complementary genetic approach to those previously used to identify polarity regulators (St Johnston, 2002). Screening for genes which dominantly enhance or suppress a sensitized genetic background avoids some of the problems inherent in recessive loss of function screens. Reducing the activity of a given pathway may still allow development to proceed fairly normally. However, further inhibition of that same pathway, for instance by reducing the dosage of additional genes in the pathway, may result in altered development. The reduced pathway activity therefore represents a sensitized genetic background in which phenotypes can be seen that would otherwise be missed in a wild-type background. These screens are particularly powerful given that one need remove only one of the two genomic copies of a gene, rather than generating homozygous mutant tissue. This is especially advantageous in the case of genes required for viability, the loss of which may lead to animal death prior to the stage of development being studied. In addition, modifier screens using large genomic deficiencies allow much more rapid screening of the entire genome than using chemical mutagenesis to generate null mutations in individual genes. Using molecularly defined deficiencies also avoids the slow step of mapping the mutations identified in chemical mutagenesis screens, although identification of the single responsible gene still remains an obstacle. Finally, if the sensitized background results in a visible phenotype, the modifier screen can identify

both enhancers and suppressors, or genes that either positively or negatively regulate the pathway of interest.

Here we describe a genetic modifier screen for genes that interact with *lgl*. We generated a sensitized background by knocking down *lgl* activity in the developing Drosophila wing by RNA interference (RNAi). We used genomic deficiencies arrayed across four chromosome arms to identify regions of the genome that contain enhancers or suppressors of the *lgl* knockdown phenotype, and further refined those genomic regions by testing smaller deficiencies. In total, we identified 13 regions of the genome containing genetic enhancers, and a single region containing a suppressor.

Results

Modifier screen design

In designing a genetic modifier screen to identify genes that interact with *lgl*, we first sought to identify a sensitized genetic background that would result in a modifiable phenotype. Flies that are heterozygous for a null mutation in *lgl* develop normally and have no visible phenotype. While this may represent a sensitized genetic background, it would not permit us to identify genes that counteract, or suppress, the reduction in *lgl* gene dosage. Instead, we generated transgenic flies carrying a construct encoding an inverted repeat targeting *lgl* under control of the Upstream Activating Sequence (UAS) promoter. When expressed, the inverted repeat forms a hairpin structure that is recognized by the RNA interference machinery, leading to downregulation of *lgl* mRNA in those cells expressing the construct. Driving expression of this construct with the *MS1096 GAL4* driver, which is expressed specifically in the dorsal compartment of the developing wing blade in the larval imaginal wing disc, leads to a robust phenotype in the adult wing. Wild-type wings are completely flat, with a stereotyped pattern of bristles and veins (Figure 4.1A). In animals in which *lgl* is knocked down in the wing (*lgl*-IR), the wings are slightly curled ventrally, which presents as a wave or ruffle in the wing blade when the wing is mounted flat (Figure 4.1B). In addition, the bristles along the wing margin are aberrantly thick and clustered together (Figure 4B', compare to WT in A'). This latter phenotype is consistent with the requirement for *lgl* in asymmetric cell division of the sensory organ precursor cells which give rise to these bristles (Langevin *et al.*, 2005), suggesting that the observed phenotypes are in fact due to an effect on *lgl* activity. Additionally, further reducing the dosage of *lgl* by removing one genomic copy of *lgl* strongly enhances the wing phenotype (Figure 4.1C), again indicating that the phenotype is due to reduced *lgl* function. Importantly, this result also suggests that the *lgl*-IR phenotype could be modified.

To determine whether the *lgl*-IR sensitized background was in fact modifiable by other genes in polarity-regulating pathways, we reduced the function of candidate genes and analyzed the effect of such reduction on the wing phenotype. Removing one copy of *scribble* leads to enhanced wing curling (Figure 4.2E), and many animals show signs of wing vein material clumping (arrow, Figure 4.2E), which is a phenotype consistent with that produced by generating *lgl* null clones in the wing (Agrawal *et al.*, 1995). Conversely, reducing aPKC activity by either removing one genomic copy of *aPKC*, or coexpressing a dominant-negative *aPKC* construct in the same tissue as the *lgl*-IR construct leads to suppression of the *lgl*-IR phenotype (Figure 4.2B-C); the wings are as flat as wild-type wings, and only show occasional wing vein defects, such as ectopic vein formation at the posterior cross vein (arrowhead, Figure 4.2). Note that coexpressing a *UAS-GFP* construct does not alter the *lgl*-IR phenotype, so the suppression seen with $aPKC^{DN}$ coexpression cannot simply be attributed to titration of the GAL4 driver (Figure 4.2D). The *scrib* and *aPKC* modification data are consistent with their defined relationships with *lgl* in regulating polarity: Scrib acts with Lgl in the basolateral domain, and removing one copy of *scrib* enhances the phenotype, while aPKC antagonizes Lgl in the apical domain, and its reduction suppresses the *lgl*-IR phenotype. These controls confirm that genes which encode proteins demonstrated to

act with Lgl in controlling polarity genetically interact with *lgl*-IR, validating our screening strategy.

Testing Candidate Genes for lgl-IR Modification

We next tested several candidate genes for *lgl*-IR modification. Those that enhanced the phenotype (Figure 4.3) included several that made sense based on their known roles in controlling polarity. These included *yurt*, a negative regulator of the Crb complex, *clathrin heavy chain* (*Chc*) and *avalanche* (*avl*), endocytic regulators required for polarity control, and *B6*, *C5*, *O9* and *RR9*, alleles identified in the MENE screen. The phenotype was also enhanced by coexpressing wild-type *Rab5* or *Hrs*, both positive regulators of the endocytic pathway, which is required for cell polarity. The observation that a mutant allele of a classic tumor suppressor gene, *tumorous imaginal discs* (*tid*) modified *lgl*-IR was somewhat surprising, and we have followed up on this interesting interaction by studying the links between *tid* and cell polarity (see Chapter 5). Another surprising enhancer was *Medea*, a *Smad4* homolog implicated in Dpp signaling. This modification is consistent with the demonstrated requirement for *lgl* in Dpp signaling (Arquier *et al.*, 2001), and could additionally indicate that Dpp target genes play a role in controlling cell polarity.

There were a number of candidate genes we tested for which heterozygosity did not modify the *lgl*-IR phenotype (Figure 4.4). Although the endocytic regulators *avl* and *Chc* enhanced the *lgl*-IR phenotype, this was not true of all endocytic regulator candidates tested. The endocytic regulator *Vps45, shibire*/*Dynamin,* and the members of the AP-2 clathrin adaptor complex *AP2α*, *AP2σ* and *AP2μ* all showed no interaction with *lgl*. In addition, several known polarity regulators did not modify the *lgl*-IR phenotype, including the apical determinant *Crumbs*, *armadillo*, a component of the adherens junction, and the cell adhesion molecule *shotgun*/*E-Cadherin*. These results emphasize that not all genes anticipated to interact with *lgl* will modify the *lgl*-IR phenotype. This is likely due to differences in both the sensitivities to gene dosage and the relative contribution of those interactions to proper cell polarity, and emphasizes an intrinsic limitation of this approach. Additional candidate genes that did not modify *lgl*-IR include genes that are required in known signaling pathways: *puckered*, a phosphatase that downregulates Jun Kinase (JNK) activity, *domeless*, the JAK/STAT signaling pathway receptor, *shaggy*, part of the β-catenin destruction complex in the Wingless/WNT signaling pathway, the E3 Ubiquitin ligase adapter *supernumerary limbs, P3C*, which disrupts the Polycomb group genes *Posterior sex combs* and *Suppressor of Zeste 2*, and *HH2*, one of the unmapped alleles from the MENE screen.

These data demonstrated that the screen could identify both *lgl*-IR enhancers and suppressors. In order to move forward with screening the Drosophila genome for additional novel modifiers, we used a collection of deficiency stocks available from the Bloomington stock center. These deficiency stocks were chosen to maximize genome coverage in a relatively small number of stocks. The deficiencies came from three large collections: the Bloomington Stock Center (BSC) collection, the DrosDel Project (ED), and the Exelixis deletion collection (Exel). Using these three collections ensured that the deficiency stocks came from defined genetic backgrounds, meaning that effects due to

differences in genetic background would be minimal. In addition, with very few exceptions, these stocks have been molecularly defined, so there is no ambiguity as to which genes are removed by each deficiency. On chromosome arm 3L, our deficiency kit of 47 stocks covered 84.22% of the 24.5 million base pairs (Mbp). On the 3R arm, 53 stocks cover 83.21% of the 27.9 Mbp. Of the 23Mbp on 2L, at least 74% is covered by 50 stocks; the coverage for this arm cannot be calculated exactly, as two of the stocks are mapped by cytology but not molecularly defined. Finally, we screened a reduced portion of 2R; with 26 deficiencies, we covered 47.68% of that chromosome arm. Altogether, the data presented here are the result of screening 60% of the total Drosophila genome for dominant *lgl*-IR modifiers.

Chromosome III Results

The results of screening both arms of chromosome 3 are presented in Table 4.1. Out of 100 deficiencies, we identified 2 that mildly suppressed (*Df(3L)Exel8104* and *Df(3L)ED4606*) and 11 which significantly enhanced the *lgl*-IR phenotype: *Df(3L)ED4483*, *Df(3L)ED4543*, *Df(3L)ED229*, *Df(3R)Exel6144*, *Df(3R)ED5416*, *Df(3R)ED5454*, *Df(3R)BSC517*, *Df(3R)BSC492*, *Df(3R)ED6232*, *Df(3R)Exel6214* and *Df(3R)BSC503*. Using smaller molecularly defined deficiency stocks within these regions, we submapped the interacting regions of these deficiencies (Table 4.4), focusing on regions that looked particularly promising based on the strength and consistency of the modification. We also compared the *lgl*-IR data to results from two other screens being done concurrently in the lab. Thomas Vaccari screened the deficiency kit for regions that could modify a *Vps25*-IR wing phenotype, and Joshua Schoenfeld screened the kit for modifiers of a phenotype due to overexpression of *Crb* in the eye (*GMR>Crb*).

Chromosome III Enhancers

The stock *Df(3L)ED4483* in the 3L/R deficiency kit covers the cytological region 69A5-69D3. Of four smaller deficiencies ("subDfs"), one enhanced the *lgl*-IR phenotype as strongly as the original Df, and one had an intermediate modification (Figure 4.5). We thus restricted the interaction region to 69C4-7. This region contains 16 genes, 8 of which are annotated only with a CG number. Annotated genes include *vihar*, *sticky*, *trailer hitch*, *Pcaf*, *eIF2-β*, *Transferrin 2* and *sosondowah*. Of these, *Transferrin2* may be an interesting candidate based on evidence that it contributes to septate junction formation (ref). Also, Vihar is a ubiquitin-conjugating protein; this could be an interesting link, given the polarity phenotypes of *slmb* mutants. In addition, expanding the interaction region to 69A5-C7, which is justified based on the strong enhancement by one of the sub-Dfs, suggests that the mirror-araucan-caupolican complex may also be a candidate modifier. We have not tested any of these candidates for an interaction. Also, note that this region was not a positive hit in the *Vps25*-IR or the *GMR-Crb* screens.

The second hit on chromosome 3L was *Df(3L)ED4543*. Using 6 subDfs, we narrowed the cytology of the interacting region from 70C6-709F4 down to 70D7-70E4. This narrow region contains 7 CG annotations and 6 annotated genes. The most intriguing candidate in this region is *big bang (bbg)*, which encodes several PDZ-domain containing proteins. Moreover, Bbg protein localizes to the apical membranes of

developing photoreceptor cells in the eye imaginal disc (Kim et al 2006). This polarized localization suggests that *bbg* may be an important polarity regulator at least in some cell types, but null alleles have not been analyzed, and we have not tested this individual candidate for *lgl*-IR modification.

The final hit on the 3L arm was *Df(3L)ED229*, cytology 76A1-76E1. We isolated the interacting region to 76B9-76C5 with 6 different subDfs. This region contains 25 protein coding genes, 12 of which are annotated only with a CG number. There are no obvious candidate genes among the annotations, and we have not focused on using alleles or smaller subDfs to further refine this region, largely because this modifier was one of the less-significant in terms of the degree of *lgl*-IR modification.

On chromosome 3R, one enhancer deficiency, *Df(3R)Exel6144,* spans from 83A6 to 83B6. Using subDfs, we refined the interacting region to 83B4-B6 (Figure 4.6). In addition to 20 snoRNAs, this region also contains 3 CG annotations and 9 characterized genes, including *Vha26*. This region also strongly enhanced the *Vps25*-IR phenotype, which was phenocopied by removing a single copy of *Vha26*. However, when we tested a *Vha26* allele for dominant modification of the *lgl*-IR phenotype, there was no interaction. A second candidate in this region is *Regena*, which seems to have a role in regenerative growth in the wing disc (M. Worley, pers. comm.); we have not tested this or any other single genes in this region for *lgl*-IR modification.

The deficiency *Df(3R)ED5416* (cytological location 85D16-85E6) strongly enhanced the *lgl*-IR, *Vps25*-IR and *GMR-Crb* phenotypes. With the *lgl*-IR modification, we used three subDfs to refine the cytological region responsible for the interaction. However, two of these three enhanced the *lgl*-IR phenotype, and as they were still relatively large Dfs, we could only refine the mapping to 85D19-E1 (Figure 4.7). This region includes *Ras85D* and *Vps45*, so we suspected that the enhancement would be attributable to one or both of these genes. However, we tested alleles of both *Ras85D* and *Vps45*, and neither interacted with *lgl*-IR. The responsible gene is thus likely one of the additional 13 annotated or 14 CG-numbered genes in this region.

Interestingly, *Df(3R)ED5454* (cytology 85E5-85F12) partially overlaps with the previous deficiency, *Df(3R)ED5416*, and also strongly enhanced the *lgl*-IR phenotype. However, subDfs that do not overlap *Df(3R)ED5416* also modify *lgl*-IR, suggesting that there is an additional gene or genes in *Df(3R)ED5454* that interact with *lgl*. Using subDfs, we mapped an interacting region to between 85F10 and 85F12. This region contains 6 microRNA coding sequences, *Fmr1* and *CG3940*. The inclusion of *Fmr1* was exciting, since Lgl and Fmr1 are known to interact in a complex regulating mRNA localization. However, removing a single copy of *Fmr1* did not enhance the *lgl*-IR phenotype. The second gene, *CG3940*, is not homologous to any known human or yeast protein. There are no alleles publicly available, so we could not directly test for an interaction between *lgl*-IR and *CG3940*. However, the modification between the region covered by *Df(3R)ED5454* and *lgl*-IR is ultimately more complicated. Two of the subDfs, *Df(3R)Exel6154* and *Df(3R)Exel6155* did not interact with *lgl*-IR, but the overlapping subDfs *Df(3R)ED5428* and *Df(3R)BSC526* did enhance the phenotype. While it is possible that this indicates that there is a gene at each end of *Df(3R)ED5454* which interacts with

lgl, we have been unable to clarify these interactions, and so have not been able to pinpoint an individual *lgl*-interacting gene or genes in this region.

For the deficiency *Df(3R)BSC517* (cytology 92C1-92F13), two of the three subDfs enhanced the *lgl*-IR phenotype as strongly as the original Df. The overlap between these two subDfs indicated the presence of modifying gene(s) is in the cytological region 92E8-92F1. Among the 15 coding regions, 9 are uncharacterized CG annotations. The remaining genes include two metallothionein genes, an odorant receptor, and *Stat92E*. Interestingly, a *Stat* reporter construct is highly expressed in *scrib* or *dlg* mutant tissue (B. Bunker, pers. comm.), and we would expect that reduced levels of *Stat* would suppress the phenotype caused by *lgl* knockdown. We did not test a *Stat* allele for *lgl*-IR modification, so this puzzle remains unsolved.

The deficiency covering 95E7-96B17 (*Df(3R)BSC492*) strongly enhanced the *lgl*-IR phenotype. Two of the four subDfs that we tested also modified *lgl*-IR, narrowing the cytological region to 95F8-96A7. One of these two subDfs more strongly recapitulated the interaction of the original Df, suggesting that the "stronger" modifier gene may in fact be in the neighboring cytological region 95E7-95F8. However, a second subDf covering this region did not modify *lgl*-IR at all. This suggested that the enhancer is in fact contained in 95F8-96A6, but with the possibility of a second enhancer present in 96A6-A7. Of the 47 genes present in this expanse, the most notable is *crb*. However, based on the molecular function of Crb, the reduction in *crb* dosage is more likely to suppress the *lgl*-IR phenotype. Rather than test individual genes for *lgl*-IR modification here, the most efficient next step would be to identify additional small deficiencies to further refine the interacting region.

With *Df(3R)ED6232* (cytology 96F10-97D2), we saw a strong enhancement of the *lgl*-IR phenotype with both this deficiency and one of the four subDfs we tested. This narrowed down the interacting region to 97B4-97D4, and the modification we saw with the subDf was just as strong as with the original large deficiency. While this section of the genome encodes over 40 genes, one of those genes is *scrib*. Because our initial candidate testing results indicated that removing one copy of *scrib* does enhance the *lgl*-IR phenotype, we attributed the modification seen with this subDf to the presence of *scrib*. While we cannot exclude the possibility that there may be other genes in this region which also interact with *lgl,* we chose to focus on the other regions identified in the modifier screen which were more likely to yield novel findings.

We used a total of four subDfs in attempting to refine the region identified in *Df(3R)Exel6214* (cytology 99D5-99E2). None of these four enhanced the *lgl*-IR phenotype nearly as strongly as the original deficiency did. While one of them did interact with *lgl*, narrowing the modifier region to 99D8-99E1, this interaction was quite weak. Note that this is in contrast to results from the *Vps25*-IR screen, in which this deficiency and three of the subDfs strongly enhanced the *Vps25*-IR phenotype (T. Vaccari, pers. comm.). We were thus unable to define a smaller region that recapitulated the original interaction; this is not likely to be due to a gap in the subDf coverage, as the subDfs were tiled across the entire original cytological region. Intriguingly, the gene *Myosin light chain 2* (*Mlc2*) is within this region, at 99E1. Given the previous reports indicating that Lgl can bind to Myosin II in dividing neuroblasts to

control polarity, this may in fact represent a significant interaction, and indicate that Lgl and Myosin together regulate polarity in the imaginal disc epithelium. However, we have not tested an *Mlc2* allele directly for *lgl*-IR modification.

The final hit on chromosome 3R was *Df(3R)BSC503* (cytology 99E3-99F6). We tested a single partially overlapping deficiency and observed a weak enhancement of the *lgl*-IR phenotype, indicating the presence of a modifier in 99F4-100A2. Among the 26 genes in this region, there were no obvious candidate genes to test. Moreover, this region was the weakest of the enhancer regions we identified in the *lgl*-IR modifier screen, and we chose to not pursue further analysis of this region.

Chromosome III Suppressors

The first of the two suppressor regions identified on chromosome III was *Df(3L)Exel8104* (cytology 65F7-66A4). We tested two subDfs in this region for *lgl*-IR modification. We found that neither of the subDfs suppressed the *lgl*-IR phenotype; however, we also could not recapitulate the suppression with Df#18. This suggested that the original observation may have been a false positive.

The second chromosome III suppressor was *Df(3L)ED4606* (cytology 72D4-73C4). Because the overlapping deficiency *Df(3L)BSC443* also showed mild suppression of the *lgl*-IR phenotype, we chose to test an array of subDfs tiling the entire 72B1-73C4 region. However, as was the case with the previously described region, we did not identify any subDf that suppressed *lgl*-IR, nor did the original deficiency suppress the phenotype upon retesting.

Because we could not identify clear suppressors among the subDfs for these two regions, we hypothesized that the relatively mild nature of the *lgl*-IR phenotype when the flies were raised at 25°C made it difficult to score anything but strong suppression. Therefore, we repeated the experiment with the putative suppressors and the corresponding subDfs at 29°C, which increases the activity of the GAL4 enzyme and presumably leads to greater *lgl*-IR knockdown, resulting in a stronger basal phenotype. Using this experimental design, the results were quite different for *Df(3L)Exel8104*. Although we did not obtain any scorable progeny for either the original deficiency or one of the subDfs, the second subDf, *Df(3L)BSC459*, actually behaved as an enhancer. This suggested that there may be an enhancer gene in this subDf that was not in the original Df. However, this is an unlikely explanation, as the neighboring Dfs in the deficiency kit which did cover this part of the subDf, *Df(3L)BSC375* and *Df(3L)ED4408*, were not scored as enhancers. We cannot reconcile this conflicting data, and additional experiments would be necessary to isolate the genetic elements responsible for the observed modifications.

In repeating the interaction assay at 29°C for *Df(3L)ED4606*, we did identify two subDfs which apparently could suppress the *lgl*-IR phenotype. However, these subDfs do not overlap. Furthermore, the experimental crosses generally did not survive well at this higher temperature, and this result is based on a non-significant number of F1 progeny and would need to be retested in order to confirm the result.

Chromosome II results

The results of screening chromosome 2L are presented in Table 4.4. Of the 50 deficiency lines screened against *lgl*-IR, we identified 1 mild suppressor, *Df(2L)ED578*, and 4 enhancers: *Df(2L)Exel6011*, *Df(2L)BSC188*, *Df(2L)ED690*, and *Df(2L)ED761*. Of these four enhancers, *Df(2L)Exel6011* was by far the strongest, resulting in pupal lethality when combined with *lgl*-IR. We therefore focused on defining the interacting region in this deficiency.

In the first pass at screening the 2L deficiency stocks, we identified *Df(2L)ED578* (cytology 28F1-29A3) as an *lgl*-IR suppressor. However, in retesting this deficiency along with four subDfs, we observed *lgl*-IR enhancement rather than suppression with the original Df. In addition, none of the four subDfs suppressed the *lgl*-IR phenotype. We therefore concluded that the original identification of *Df(2L)ED578* as a suppressor was a false positive and did not investigate this region further. Despite this conclusion, we did note that *Df(2L)ED578* included the gene *PDGF- and VEGF-receptor related (Pvr)*. This was noteworthy based on previous reports indicating that overexpression of Pvr in the wing disc led to a 'neoplastic' phenotype (Rosin *et al.*, 2004). However, when we tested for an interaction between *Pvr* and *lgl* by coexpressing a dominant-negative *Pvr* construct along with the *lgl*-IR construct, we saw no change in the *lgl*-IR phenotype. While this does not rule out an *in vivo* interaction between *lgl* and *Pvr*, it does reinforce the conclusion that the originally observed suppression was a false positive.

To narrow down the *lgl*-IR enhancing region within *Df(2L)Exel6011* (cytology 25C8-25D5), we tested two subDfs. Both of these subDfs also enhanced the *lgl*-IR phenotype to pupal lethality, though this interaction was less consistent with one of the two subDfs. We therefore defined the target interacting region as 25C10-25D5. This region includes *thick veins (tkv)*, the receptor required for the Dpp signaling pathway. However, a null allele of *tkv* does not modify the *lgl*-IR phenotype. This indicates that one of the other 26 genes in this region interacts with *lgl*, though there are no clear candidates based on their present annotations.

Finally, out of 26 deficiencies on the 2R chromosome arm, we identified a single *lgl*-IR enhancer, *Df(2R)ED1612*. Unfortunately, testing six different subDfs that together covered the entire 42A13-42E6 region did not identify any smaller deficiencies within this region that recapitulated the *lgl*-IR enhancement of the original deficiency. This could be a result of incorrect annotation in the original Df or the subDfs themselves, and this might be resolved by complementation testing between each of these deficiency stocks.

Discussion

By screening 60% of the Drosophila genome for the ability to modify the phenotype resulting from knocking down *lgl* in wing tissue during development, we identified 1 true suppressor and 13 enhancer regions. By testing smaller deficiencies within each of these regions, we defined narrower pieces of the genome that still contain *lgl*-interacting elements. Although we have not unambiguously defined the single genes within these regions that individually can modify the *lgl* knockdown phenotype, the results presented here strongly support the utility of such a screening method for identifying genes that interact with *lgl*. The utility of this approach is further supported by the interactions we observed between *lgl*-IR and both known polarity regulators (*scrib*, *aPKC*) and the tumor suppressor *tid*. Using null alleles, including those generated by either chemical or transposable element mutagenesis, or RNAi transgenes to target single genes within the interacting regions may ultimately identify specific *lgl*-interacting genes and advance our understanding of how *lgl* controls polarity in epithelial tissues.

Of all of the *lgl*-IR modifying deficiencies we identified, the two enhancers on chromosome II (*Df(2L)Exel6011* and *Df(2R)ED1612*) are certainly promising, given that they were the best enhancers we found on that chromosome. In addition, *Df(3R)ED5416* strongly enhanced *lgl*-IR, *Vps25*-IR and *GMR>Crb*, suggesting that the gene(s) responsible for the modification may be critical for polarity regulation. We were able to define a narrow interacting region, but no candidates tested thus far have recapitulated the original modification. Finally, although only a weak enhancement, the modification seen in the region containing *Mlc2* would be interesting to follow up, given the previously reported links between Lgl and Myosin II.

One important consideration in interpreting the results of this modifier screen is that the exact cellular basis of the adult wing phenotype produced by knocking down *lgl* is unclear. The margin bristle clustering and the vein material clumping observed in the control wings and several enhancers are consistent with previously reported *lgl* phenotypes. Moreover, increasing the extent of *lgl* knockdown by coexpressing *Dicer2* in the wing leads to a mild overgrowth in the wing imaginal disc reminiscent of phenotypes we see when knocking down other polarity regulators such as *avl*. Nevertheless, the adult wing phenotypes observed could be reflecting roles of *lgl* and its interacting genes in pathways unrelated to polarity control. This will be better resolved upon further characterization of the interacting genes identified, and analysis of cell polarity in tissue with null mutations in those genes.

A second concern regarding our data is that we have chosen to emphasize identifying those genes which show a strong modification of the *lgl*-IR phenotype. We made this choice partly for practical reasons, as many deficiencies showed a slight deviation from the basal *lgl*-IR phenotype. However, this was highly variable, and would have been difficult to score consistently in subsequent rounds of subDf mapping. The decision to highlight strong interactions was also based on the assumption that in a given pathway, reducing the dosage of those genes which act closest to *lgl* will modify the phenotype more strongly, such as was observed with the known polarity regulators *aPKC* and *scrib*. However, the activity of pathways through which *lgl* controls polarity

could feasibly be variably sensitive to the dosage of the constituent genes. In a similar vein, reducing the genomic dosage of a given gene may have little to no effect on the expression of that gene product, and the global cell biology would not echo the reduced gene copy.

In evaluating the various enhancers and suppressors that we identified among the deficiencies we screened, we noted that they included deficiency stocks from the BSC, Exelixis, and DrosDel projects. This was satisfying, as it indicated that our results were not biased toward a single collection, which would have suggested that there might be genetic background effects that we had not accounted for in using three different collections.

Two findings that we did not anticipate were the overrepresentation of enhancers over suppressors, and the abundance of interacting deficiencies on chromosome III relative to chromosome II. In scoring the wings of the *lgl*-IR control flies and the experimental progeny, we observed that although the *lgl*-IR phenotype was obviously non-wild-type, it was fairly mild. This was an advantage for scoring enhancement, as we could recognize even moderate shifts in the severity of the wing phenotype away from wild-type. However, the counterpoint was that we could only reliably identify as suppressors those deficiencies which would very strongly suppress the *lgl*-IR phenotype, resulting in nearly wild-type wings. In fact, in two out of the three cases where we initially scored mild suppression, that result turned out to be a false positive. Because of this, it may be more fruitful to perform a screen for suppressors at 29°C, where the basal phenotype is more severe. However, the crosses do not tend to do well at this higher temperature, and fewer scorable flies eclose, making this is a technically feasible but more arduous and less reliable strategy.

The significance of the abundance of interacting deficiencies on chromosome III relative to the second chromosome is unclear. One explanation may be that because all of the chromosome II deficiencies were maintained over a balancer carrying the dominant Curly marker, they were outcrossed before being assayed for *lgl*-IR modification. This outcrossing may have eliminated some genetic background effects and thus reduced the experimental variability. However, we did outcross and repeat the interaction tests with several of the modifiers on chromosome III, and the results were the same as we had obtained without outcrossing the deficiency stocks. Therefore we do not believe that the outcrossing had a significant impact on the screen results. We also would not expect there to be a genomic imbalance in the distribution of polarity-regulating genes, and we thus cannot further explain the observed imbalance in the distribution of *lgl*-interacting deficiencies.

Finally, it may be useful to compare the results of the *lgl*-IR modifier screen with those obtained by screening the same deficiency stocks for modifiers of other phenotypes generated by modulating additional known polarity-regulating genes, including *Vps25*-IR, or *GMR>Crb* modifiers. For example, a deficiency that suppresses all three RNAi phenotypes but not the *GMR>Crb* phenotype might simply be negatively impacting the RNAi machinery efficiency. On the other hand, a deficiency which is a hit in multiple screens might be more likely to contain a polarity-regulating gene than a deficiency that is a hit in a single screen. In general, the *lgl*-IR results closely parallel

those from the *Vps25*-IR screen (T. Vaccari) and the *slmb*-IR screen (S. Windler). While there are a few deficiencies which modulate both the *lgl*-IR and the *GMR>Crb* phenotypes in the same direction, the *GMR-Crb* screen results are generally distinct from the RNAi-based screen. Whether this is due to one of them being an RNAi-based system or actually reflects significant cell biological differences remains to be seen.

Materials and Methods

Drosophila genetics

The complete genotype of the *lgl*-IR stock is *MS1096-GAL4/FM7c/Y;; UAS-lgl-IR #9/TM3*. The following alleles were used in testing candidate genes: *scrib*^{2}*/TM6B*, *lgl*^{4}*/CyO*, *avl*^{1}*/TM6B*, *aPKC*^{k06403}*FRT42/CyO twi-GAL4 UAS-GFP*, *UAS-DaPKC CAAX CN/CyO; MKRS/TM6B* ("dominant negative"), *yrt*^{2}*/TM*, *mwh*^{1} *medea*^{1} *e*^{1}*/TM3 (Bloomington 9033)*, *tid*^{2} *kr/CyO*, *chc*^{3}*FRT19A/FM7c/Dp3658*, *B6 FRT42/CyO twi-GAL4 UAS-GFP*, *C5 FRT42/CyO twi-GAL4 UAS-GFP*, *O9 FRT42/CyO twi-GAL4 UAS-GFP*, *RR9 FRT82/TM6B*, *HH2 FRT82/TM6B*, *puc*^{E69}*/TM6B*, *sgg*^{1}*/FM7a*, *UAS-Rab5/TM3*, *UAS-Hrs* (Lloyd *et al.*, 2002), *P3C/CyO twi-GAL4 UAS-GFP*, *arm*^{YD35} *FRT101/FM7* (Loureiro and Peifer, 1998), *Crb*^{11A22}*/TM3 ftz-lacZ*, *Ras85D*^{06677}*/TM3* (Bloomington 11694), *Vps45*^{JJ2}*/TM6B*, *shi* (*shi*^{GR3} or *shi*^{FL54}), *AP2α*$^{40-31}$*/CyO*, *AP2σ*^{KG02457}*/TM6B*, *AP2μ*^{NN20}*/TM3*, *slmb*^{uu11}*/TM3*, *Vha26*^{j3E7}*/TM3* (Bloomington #10214), *shg*^{R69} *FRT42/CyO twi-GAL4 UAS-GFP*, *dFmr1*^{3}*/TM6C* (Dockendorff *et al.*, 2002), *tkv*^{4}*/CyO, UAS-DN PVR/CyO*. Either *Gla/CyO twi-GAL4 UAS-GFP* or *L/CyO* stocks were used for outcrossing stocks on chromosome II. Deficiency stocks obtained from the Bloomington stock center are listed in the Tables accompanying this chapter.

Interaction scoring

Candidates and deficiencies were assayed for genetic interaction with *lgl* by crossing the *lgl*-IR stock to the various candidate gene or Df stocks. Control flies were obtained by crossing the *lgl*-IR stock to *iso80* (isogenized FRT80) or *iso40* (isogenized FRT40) flies. All crosses were maintained at 25°C, unless otherwise noted, on standard Drosophila media. F1 flies were collected and over several days after eclosion. Non-balancer F1 flies were segregated, counted and scored against control flies. Because the MS1096-GAL4 transgene is on X and therefore subject to dosage compensation in male flies, only female flies were scored.

Interactions were scored on a scale from -3 to +3, with negative integers indicating suppression and positive integers indicating enhancement. Larger magnitudes denote stronger modification. Screening on chromosome 2R was completed with the generous help of Alejandra Figueroa-Claravega.

Imaging

Flies were frozen at -20°C and preserved in isopropanol. For imaging, the right wing was removed from female flies and mounted in Gary's Magic Mountant (Lawrence *et al.*, 1986) or Euparal (Carolina Biologicals). Wings were imaged using a Z16 APO microscope (Leica, Wetzlar, Germany) with a Planapo 2.0x lens, fitted with a DFC300 FX camera. Images were edited and assembled using Adobe Photoshop and Illustrator CS2.

Figure 4.1 Reducing *lgl* activity by expressing an RNAi construct targeting *lgl* (*lgl*-IR) leads to an adult wing phenotype.
A: Wild-type adult wings are flat with stereotyped bristle and vein patterning. B: Driving the *lgl*-IR construct with *MS1096-GAL4* in the dorsal compartment of the developing wing blade leads to aberrant wing development. Wings are curled ventrally, leading to ruffling and folding when flattened. In addition, the margin bristles are thicker and more numerous than in wild-type wings (B', compare to WT in A'). C: Further reducing *lgl* activity in the wing by removing one genomic copy of *lgl* enhances the wing phenotype ($lgl^4/+$). Wing architecture is severely disrupted, and many flies fail to eclose from their pupal cases.

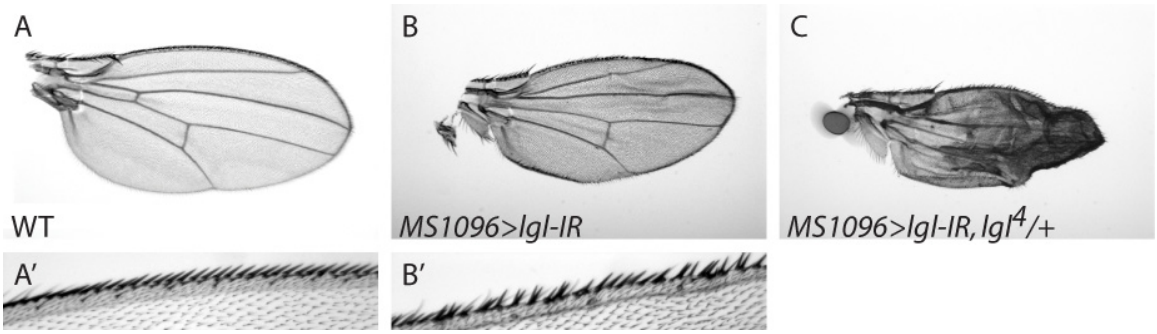
A
WT
B
MS1096>lgl-IR
C
MS1096>lgl-IR, lgl4/+
A'
B'

Figure 4.2. Known polarity regulators modify the *lgl*-IR phenotype.
Compared to the basal *lgl*-IR phenotype (*MS1096>lgl-IR*, A), reducing aPKC function by removing one genomic copy (*aPKC*/+, B) or coexpressing a dominant-negative form of *aPKC* (*UAS-aPKC*^{DN}, C) partially restores wild-type wing structure. The wings retain the ectopic margin bristles present in *lgl*-IR, but the wing blade is flat and vein pattern is mostly normal, with the occasional exception of ectopic vein formation at the posterior cross vein (arrowhead, B). The suppression seen when driving *UAS-aPKC*^{DN} is not due to titration of the *MS1096-GAL4* driver, as coexpressing a *UAS-GFP* construct does not suppress the *lgl*-IR phenotype (D). Removing a single copy of *scrib* modifies the *lgl*-IR phenotype in the opposite direction as *aPKC* (E); wing architecture is more severely disrupted than with *lgl*-IR alone, and ectopic clusters of vein material are present (arrow, E).

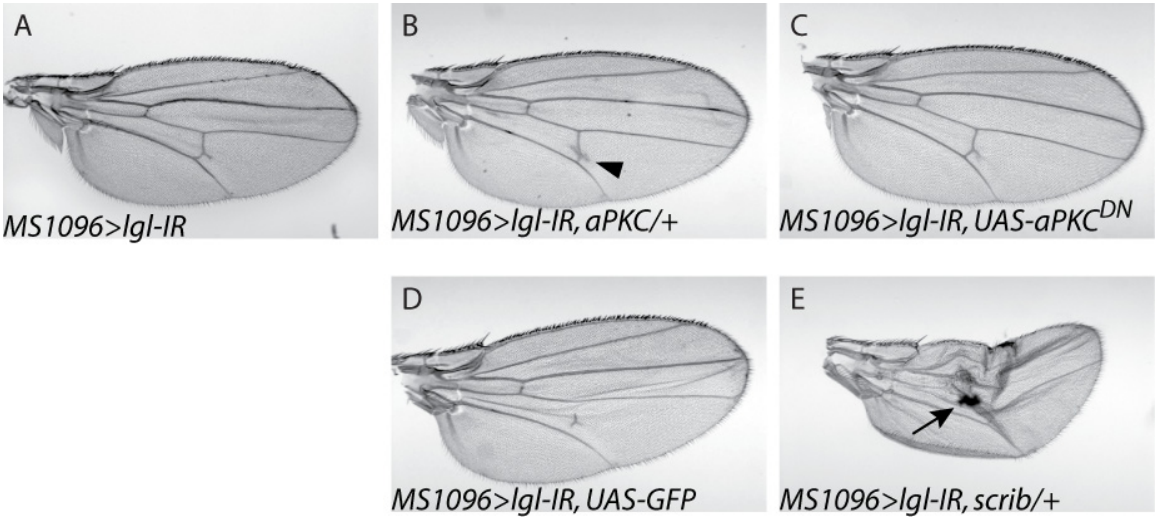
A
MS1096>lgl-IR
B
MS1096>lgl-IR, aPKC/+
C
MS1096>lgl-IR, UAS-aPKC^DN
D
MS1096>lgl-IR, UAS-GFP
E
MS1096>lgl-IR, scrib/+

Figure 4.3. Candidate genes which enhance the *lgl*-IR phenotype.
All panels are representative images of the wings present on progeny of a cross between the *lgl*-IR stock and the indicated alleles. For simplicity, panel labels give only the tested allele. As compared to the basal *lgl*-IR phenotype (iso80 control, A), the following alleles enhance the *lgl*-IR phenotype, as indicated by ectopic vein material clumping and increased wing blade ruffling: *yurt* (B), *medea* (C), *tumorous imaginal discs* (*tid*, D), *Clathrin heavy chain* (*chc*, E), *avalanche* (*avl*, F), *B6* (G), *C5* (H), *O9* (I) and *RR9* (J), the last four being alleles identified in a screen for "mutant eye disc, no eclosion" mutants. In addition, ectopic expression of *Rab5* similarly enhances the *lgl*-IR phenotype (*UAS-Rab5WT*, K). Ectopic expression of *Hrs* (L) enhances the *lgl*-IR phenotype to pupal lethality, and no adults eclose.

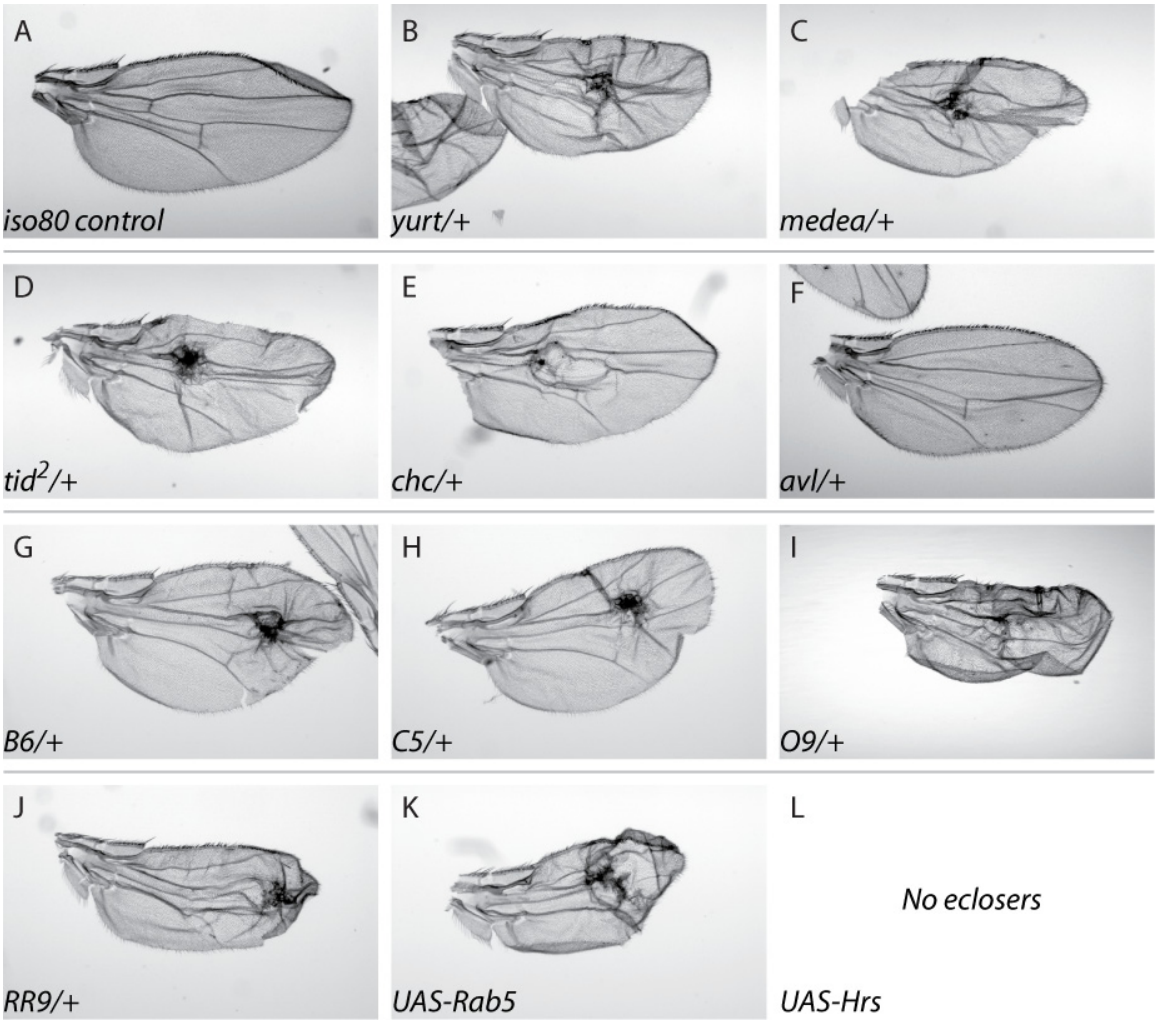
A
iso80 control
B
yurt/+
C
medea/+
D
tid2/+
E
chc/+
F
avl/+
G
B6/+
H
C5/+
I
O9/+
J
RR9/+
K
UAS-Rab5
L
No eclosers
UAS-Hrs

Figure 4.4. Candidate genes which do not modify the *lgl*-IR phenotype.
All panels are representative images of the wings present on progeny of a cross between the *lgl*-IR stock and the indicated alleles. For simplicity, panel labels give only the tested allele. As compared to the *lgl*-IR basal phenotype (iso80 control, A), the following candidate genes do not significantly enhance or suppress the *lgl*-IR phenotype: *Crumbs* (*crb*, B), *Vps45* (C), *AP2α* (D), *AP2μ* (E), *AP2σ* (F), *shibire*/*Dynamin* (*shi*, G), *armadillo* (*arm*, H), *Posterior sex combs/Suppressor of Zeste 2* (*P3C*, I), *puckered* (*puc*, J), *shotgun*/*E-Cadherin* (*shg*, K), *shaggy* (*sgg*, L), *supernumerary limbs* (*slmb*, M), and *HH2* (N), an allele identified in a screen for "mutant eye disc, no eclosion" mutants. Expressing a dominant-negative form of the receptor *domeless* (*domeΔcyt*, O) also has no effect on the *lgl*-IR phenotype.

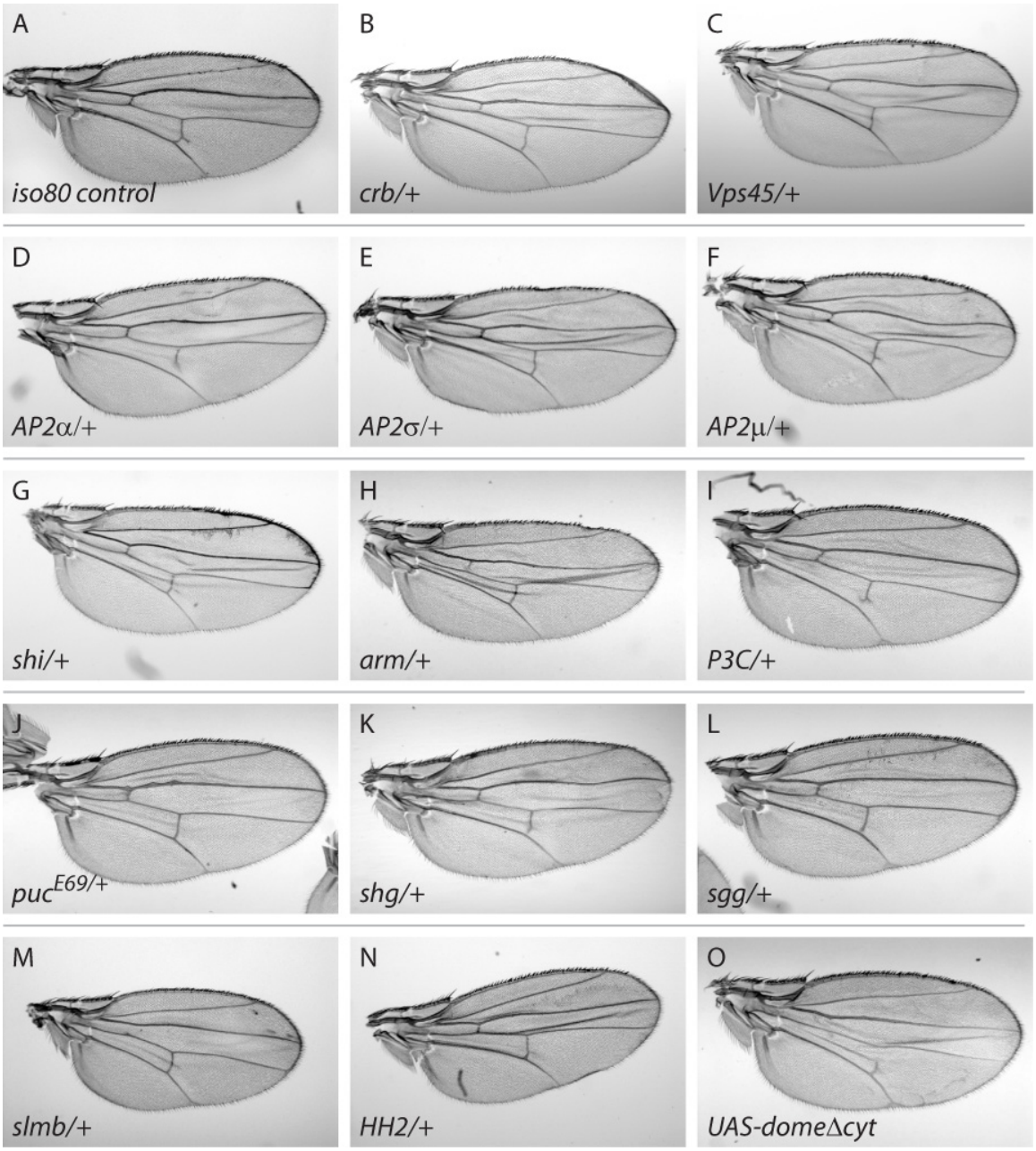
A
iso80 control
B
crb/+
C
Vps45/+
D
AP2α/+
E
AP2σ/+
F
AP2μ/+
G
shi/+
H
arm/+
I
P3C/+
J
puc^E69/+
K
shg/+
L
sgg/+
M
slmb/+
N
HH2/+
O
UAS-domeΔcyt

Table 4.1. Screening for *lgl*-IR modifiers on chromosome III.
Presented here are the results of screening deficiencies on both arms of chromosome III. Listed in cytological order, deficiencies are identified by the informal name used in our deficiency kit, the deficiency name from their respective stock collections, and the Bloomington stock number. Deficiencies were crossed to the *lgl*-IR stock, and the appropriate F1 progeny were collected and scored. The number of flies scored per deficiency interaction test cross is indicated. Score column indicates the strength of the *lgl*-IR phenotype enhancement (positive integers) or suppression (negative integers), with magnitudes of 1 (mild interaction), 2 (moderate interaction) or 3 (strong interaction). A score of zero (0) indicates that no interaction was observed. In some cases, the interaction varied between scores, and a range is indicated.

Df kit #	Deficiency	Bloomington #	Cytology	Number scored	Score
3L/R #1	Df(3L)Exel6083	7562	61A6;61B2	18	1
3L/R #2	Df(3L)ED201	8047	61B1;61C1	13	0
3L/R #3	Df(3L)ED4177	8048	61C1;61E2	8	0
3L/R #4	Df(3L)ED207	8053	61C9;62A6	20	0
3L/R #5	Df(3L)BSC181	9693	62A11;62B7	16	1-2
3L/R #6	Df(3L)ED4287	8096	62B4;62E5	18	0
3L/R #7	Df(3L)Exel6091	7570	62E8;62F5	12	1
3L/R #8	Df(3L)Exel6092	7571	62F5;63A3	23	1
3L/R #9	Df(3L)Bsc386	24410	63A3;63B8	5	0
3L/R #10	Df(3L)ED208	8059	63C1;63F5	16	1-2
3L/R #11	Df(3L)BSC368	24392	63F1;64A4	17	0
3L/R #12	Df(3L)ED4341	8060	63F6;64B9	11	0
3L/R #13	Df(3L)ED210	8061	64B9;64C13	12	0
3L/R #14	Df(3L)BSC437	24941	64E8;65A1	28	0-1
3L/R #15	Df(3L)BSC411	24915	65A2;65C1	13	0
3L/R #16	Df(3L)BSC224	9701	65D5;65E6	15	0
3L/R #17	Df(3L)BSC117	8974	65E9;65F5	14	2
3L/R #18	Df(3L)Exel8104	7929	65F7;66A4	34	-1
3L/R #19	Df(3L)BSC375	24399	66A3;66A19	8	0
3L/R #20	Df(3L)ED4408	8065	66A22;66C5	16	-1
3L/R #21	Df(3L)BSC389	24413	66C12;66D8	8	0
3L/R #22	Df(3L)ED4421	8066	66D12;67B3	8	0
3L/R #23	Df(3L)BSC391	24415	67B7;67C5	13	1
3L/R #24	Df(3L)BSC283	23668	67C7;67D5	27	0
3L/R #25	Df(3L)ED4457	9355	67E2;68A7	18	0
3L/R #26	Df(3L)ED4470	8068	68A6;68E1	16	0
3L/R #27	Df(3L)ED4475	8069	68C13;69B4	8	1
3L/R #28	Df(3L)ED4483	8070	69A5;69D3	17	3
3L/R #29	Df(3L)ED4486	8072	69C4;69F6	18	1
3L/R #30	Df(3L)ED4502	8097	70A3;70C10	15	-1-0
3L/R #31	Df(3L)ED4543	8073	70C6;70F4	40	2
3L/R #32	Df(3L)ED217	8074	70F4;71E1	27	2
3L/R #33	Df(3L)BSC443	24947	72B1;72E4	14	-1
3L/R #34	Df(3L)ED4606	8078	72D4;73C4	22	-1
3L/R #35	Df(3L)ED4685	8099	73D5;74E2	9	1
3L/R #36	Df(3L)ED4710	8100	74D1;75B11	7	2
3L/R #37	Df(3L)ED224	8080	75B1;75C6	10	1
3L/R #38	Df(3L)ED225	8081	75C1;75D4	8	1
3L/R #39	Df(3L)BSC416	24920	75D2;75E4	19	0
3L/R #40	Df(3L)ED4782	8082	75F2;76A1	9	-1
3L/R #41	Df(3L)ED229	8087	76A1;76E1	19	2-3
3L/R #42	Df(3L)ED4858	8088	76D3;77C1	6	2-3

Df kit #	Deficiency	Bloomington #	Cytology	Number scored	Score
3L/R #43	Df(3L)BSC448	24952	77C6;77E4	11	0
3L/R #44	Df(3L)ED4978	8101	78D5;79A2	15	0
3L/R #45	Df(3L)BSC223	9700	79A3;79B3	8	0
3L/R #46	Df(3L)ED230	8089	79C2;80A4	14	0
3L/R #47	Df(3L)ED5017	8102	80A4;80C2	14	0
3L/R #48	Df(3R)ED5100	9226	81F6;82E7	17	1-2
3L/R #49	Df(3R)ED5147	8967	82E7;83A1	21	1
3L/R #50	Df(3R)Exel6144	7623	83A6;83B6	26	3
3L/R #51	Df(3R)BSC464	24968	83B7;83E1	12	0
3L/R #52	Df(3R)BSC193	9620	83E5;83F4	24	0
3L/R #53	Df(3R)BSC467	24971	83F1;84B2	10	0
3L/R #54	Df(3R)ED7665	8685	84B4;84E11	13	0
3L/R #55	Df(3R)ED5230	8682	84E6;85A5	12	0
3L/R #56	Df(3R)ED5330	9077	85A5;85D1	12	1
3L/R #57	Df(3R)BSC507	25011	85D6;85D15	33	1
3L/R #58	Df(3R)ED5416	8701	85D16;85E6	1 (pupal lethal)	3
3L/R #59	Df(3R)ED5454	9080	85E5;85F12	28	3
3L/R #60	Df(3R)ED5495	9215	85F16;86C7	9	2-3
3L/R #61	Df(3R)ED5518	9084	86C7;86E13	0 (pupal lethal)	3
3L/R #62	Df(3R)ED5559	8920	86E11;87B11	5	2
3L/R #63	Df(3R)BSC486	24990	87B10;87E9	5	0
3L/R #64	Df(3R)ED5623	8921	87E3;88A4	5	1
3L/R #65	Df(3R)ED5644	9090	88A4;88C9	14	1
3L/R #66	Df(3R)ED5664	24137	88D1;88E3	12	1
3L/R #67	Df(3R)Exel6174	7653	88F1;88F7	26	0
3L/R #68	Df(3R)BSC515	25019	88F6;89A8	19	0
3L/R #69	Df(3R)Exel7328	7983	89A12;89B6	44	-1
3L/R #70	Df(3R)ED10639	9481	89B7;89B18	27	-1
3L/R #71	Df(3R)Exel6270	7737	89B18;89D8	5	1
3L/R #72	Df(3R)ED5780	8104	89E11;90C1	3	0
3L/R #73	Df(3R)ED5785	9207	90C2;90D1	15	1
3L/R #74	Df(3R)BSC510	25014	90E2;90F4	10	1
3L/R #75	Df(3R)ED2	6962	91A5;91F1	11	0
3L/R #76	Df(3R)ED5938	24139	91D4;92A11	2	0
3L/R #77	Df(3R)BSC517	25021	92C1;92F13	11	1-2
3L/R #78	Df(3R)ED10820	9486	93A4;93B12	16	0
3L/R #79	Df(3R)ED10845	9487	93B9;93D4	12	1
3L/R #80	Df(3R)ED6058	24140	93D4;93F6	25	1
3L/R #81	Df(3R)ED6076	8962	93E10;94A1	12	0
3L/R #82	Df(3R)ED6093	8924	94A2;94C4	5	2
3L/R #83	Df(3R)ED6096	8684	94B5;94E7	6	1
3L/R #84	Df(3R)BSC489	24993	94F3;95D1	13	0
3L/R #85	Df(3R)Exel6197	7676	95D8;95E1	11	1

Df kit #	Deficiency	Bloomington #	Cytology	Number scored	Score
3L/R #86	Df(3R)BSC492	24996	95E7;96B17	6	2
3L/R #87	Df(3R)BSC461	24965	96B15;96D1	21	1-2
3L/R #88	Df(3R)BSC140	9500	96F1;96F10	18	0
3L/R #89	Df(3R)ED6232	8105	96F10;97D2	8	3
3L/R #90	Df(3R)BSC497	25001	97E6;98B5	11	-1
3L/R #91	Df(3R)BSC460	24964	98B6;98D2	35	1
3L/R #92	Df(3R)Exel6210	7688	98E1;98F5	19	1
3L/R #93	Df(3R)ED6316	8925	99A5;99C1	29	2
3L/R #94	Df(3R)Exel6213	7691	99C5;99D1	26	1
3L/R #95	Df(3R)Exel6214	7692	99D5;99E2	17	2-3
3L/R #96	Df(3R)BSC503	25007	99E3;99F6	56	2-3
3L/R #97	Df(3R)Exel7378	7997	99F8;100A5	11	2
3L/R #98	Df(3R)ED6346	24142	100A5;100B1	13	1
3L/R #99	Df(3R)Exel6218	7696	100B5;100C1	8	0
3L/R #100	Df(3R)ED6361	24143	100C7;100E3	27	2

Table 4.2. Screening for *lgl*-IR modifiers on chromosome arm 2L.
Presented here are the results of screening deficiencies on the left arm of chromosome II. Listed in cytological order, deficiencies are identified by the informal name used in our deficiency kit, the deficiency name from their respective stock collections, and the Bloomington stock number. Deficiencies were outcrossed to *Gla/CTG* or *L/CyO*, then *Df/Gla* or *Df/L* flies were crossed to the *lgl*-IR stock, and the appropriate F1 progeny were collected and scored. The number of flies scored per deficiency interaction test cross is indicated. Score column indicates the strength of the *lgl*-IR phenotype enhancement (positive integers) or suppression (negative integers), with magnitudes of 1 (mild interaction), 2 (moderate interaction) or 3 (strong interaction). A score of zero (0) indicates that no interaction was observed. In some cases, the interaction varied between scores, and a range is indicated. ND, not determined.

Df kit #	Deficiency	Bloomington #	Cytology	Number scored	Score
2L Df #1	Df(2L)ED5878	9353	21B1;21B3	9	1
2L Df #2	Df(2L)BSC106	8672	21B7;21C2	20	0
2L Df #3	Df(2L)ED94	8908	21E2;21E3	12	0
2L Df #4	Df(2L)ED108	24629	21F1;22A1	18	1
2L Df #5	Df(2L)ED7762	24119	22A6;22D3	14	1
2L Df #6	Df(2L)Exel6007	7493	22D1;22E1	16	2
2L Df #7	Df(2L)ED136	9176	22F4;23A3	11	0
2L Df #8	Df(2L)ED4651	8904	23B8;23F3	15	-1
2L Df #9	Df(2L)ED247	24123	24A2;24C3	6	0
2L Df #10	Df(2L)Exel6009	7495	24C3;24C8	20	0
2L Df #11	Df(2L)BSC295	23680	24D4;24F3	-	ND
2L Df #12	Df(2L)BSC51	8470	25A1;25C3	15	0
2L Df #13	Df(2L)Exel6011	7497	25C8;25D5	0 (pupal lethal)	3
2L Df #14	Df(2L)BSC169	9560	25E5;25F3	10	0
2L Df #15	Df(2L)ED347	9272	25F5;26B5	18	1-2
2L Df #16	Df(2L)ED384	9297	26B2;26D7	12	1
2L Df #17	Df(2L)BSC354	24378	26D7;26E3	8	0
2L Df #18	Df(2L)BSC188	9615	26F1;27A2	16	1
2L Df #19	Df(2L)ED441	24126	27A1;27E1	10	0
2L Df #20	Df(2L)ED489	24127	27E4;28B1	8	0
2L Df #21	Df(2L)BSC191	9618	28C1;28D3	19	2
2L Df #22	Df(2L)Exel7034	7807	28E1;28F1	10	1
2L Df #23	Df(2L)ED578	24131	28F1;29A3	29	1
2L Df #24	Df(2L)ED629	24132	29B4;29E4	15	1
2L Df #25	Df(2L)ED678	8906	29F5;30B12	10	2
2L Df #26	Df(2L)ED690	24133	30B3;30E4	15	2-3
2L Df #27	Df(2L)BSC50	8469	30F5;31B1	10	0
2L Df #28	Df(2L)ED748	23713	31B1;32A5	5	0
2L Df #29	Df(2L)BSC230	9707	32A5;32C1	10	1
2L Df #30	Df(2L)Exel6028	7511	32D5;32E4	16	1
2L Df #31	Df(2L)BSC237	9712	32F2;33B5	11	0
2L Df #32	Df(2L)ED761	24109	33A2;33E5	11	3
2L Df #33	Df(2L)ED776	7418	33E4;34A3	17	0
2L Df #34	Df(2L)BSC277	23662	34A1;34B2	3	1
2L Df #35	Df(2L)BSC159	9594	34B4;34C4	-	ND
2L Df #36	Df(2L)BSC252	23152	34D1;34F1	14	0
2L Df #37	Df(2L)ED793	9061	34E4;35B4	16	0
2L Df #38	Df(2L)ED3	6963	35B2;35D1	13	0
2L Df #39	Df(2L)ED1054	24112	35B10;35D4	-	ND
2L Df #40	Df(2L)BSC278	23663	35E1;35F1	9	1
2L Df #41	Df(2L)ED1102	24113	35F12;36A10	15	0

Df kit #	Deficiency	Bloomington #	Cytology	Number scored	Score
2L Df #42	Df(2L)ED1161	24114	36A10;36C9	10	2
2L Df #43	Df(2L)BSC148	9507	36C8;36E3	12	0
2L Df #44	Df(2L)BSC256	23156	36E3;36F2	4	0
2L Df #45	Df(2L)BSC149	9508	36F5;36F10	18	0
2L Df #46	Df(2L)ED1203	8935	36F7;37C5	11	1
2L Df #47	Df(2L)ED1303	8679	37E5;38C6	14	1
2L Df #48	Df(2L)ED1315	9269	38B4;38F5	9	1
2L Df #49	Df(2L)ED1378	9682	38F1;39D2	11	1-2
2L Df #50	Df(2L)ED1473	9266	39B4;40A5	7	0

Table 4.3. Screening for *lgl*-IR modifiers on chromosome arm 2R.
Presented here are the results of screening deficiencies on the right arm of chromosome II. Listed in cytological order, deficiencies are identified by the informal name used in our deficiency kit, the deficiency name from their respective stock collections, and the Bloomington stock number. Deficiencies were outcrossed to *Gla/CTG* or *L/CyO*, then *Df/Gla* or *Df/L* flies were crossed to the *lgl*-IR stock, and the appropriate F1 progeny were collected and scored. The number of flies scored per deficiency interaction test cross is indicated. Score column indicates the strength of the *lgl*-IR phenotype enhancement (positive integers) or suppression (negative integers), with magnitudes of 1 (mild interaction), 2 (moderate interaction) or 3 (strong interaction). A score of zero (0) indicates that no interaction was observed. In some cases, the interaction varied between scores, and a range is indicated.

Deficiency	Bloomington #	Cytology	Number scored	Score
Df(2R)BSC630	25705	41D3;41F11	51	0
Df(2R)ED1612	8045	42A13;42E6	21	3
Df(2R)ED1715	8931	43A4;43F1	25	0
Df(2R)BSC267	24335	44A4;44F1	34	1
Df(2R)ED1770	9157	44D5;45B4	17	0-1
Df(2R)BSC280	23665	45C4;45F4	35	0
Df(2R)BSC132	9410	45F6;46B4	22	0
Df(2R)BSC152	9539	46C1;46D6	8	-1-0
Df(2R)BSC281	23666	46F1;47A9	46	0
Df(2R)BSC595	25428	47A3;47F1	20	-1
Df(2R)ED2219	8910	47D6;48B6	35	0
Df(2R)ED2247	8912	48A3;48D5	22	0
Df(2R)BSC485	24989	49B10;49E6	16	0
Df(2R)BSC273	23169	49F4;50A13	22	0
Df(2R)BSC307	23690	50B6;50C18	29	0
Df(2R)ED2436	8914	51F11;52D11	27	1-2
Df(2R)Exel6063	7545	52F6;53C4	17	0
Df(2R)BSC331	24356	53D14;54A1	29	0
Df(2R)ED3610	9066	54F1;55C8	23	0-1
Df(2R)ED3683	8918	55C2;56C4	27	0
Df(2R)ED3728	9067	56D10;56E2	15	0
Df(2R)BSC597	25430	58A2;58F1	17	0
Df(2R)BSC769	26866	59B7;59D9	18	0
Df(2R)BSC136	9424	59F5;60B6	29	0
Df(2R)BSC604	25437	60D4;60E11	34	1
Df(2R)BSC608	25441	60E11;60F2	47	0

Table 4.4 Submapping the *lgl*-IR interacting deficiencies.
Presented here are the results of screening sub-deficiencies (subDfs) for interacting deficiencies on chromosomes II and III. For both enhancers and suppressors, deficiencies are listed in cytological order, identified by the informal names of the original modifiers, the subDf names from their respective stock collections, and the Bloomington stock numbers. On chromosome II, deficiencies were outcrossed to *Gla/CTG* or *L/CyO*, then *Df/Gla* or *Df/L* flies were crossed to the *lgl*-IR stock, and the appropriate F1 progeny were collected and scored. On chromosome III, deficiencies were directly crossed to the *lgl*-IR stock. The number of flies scored per deficiency interaction test cross is indicated. Score column indicates the strength of the *lgl*-IR phenotype enhancement (positive integers) or suppression (negative integers), with magnitudes of 1 (mild interaction), 2 (moderate interaction) or 3 (strong interaction). A score of zero (0) indicates that no interaction was observed. In some cases, the interaction varied between scores, and a range is indicated. Refined cytology gives the estimated region likely to contain an *lgl*-interacting gene or genes, based on the cytology of the original deficiency and any subDfs which similarly modify the *lgl*-IR phenotype. Blm. #, Bloomington stock number. N scored, Number of flies scored.

Original modifier	Cytology	SubDf	Blm. #	N scored	Score	Refined cytology
Enhancers						
2L Df#13	25C8;25D5	Df(2L)Exel6011	7497	0 (pupal lethal)	3	25C10-25D5
	25D5;25D6	Df(2L)BSC653	25743	7	2	
	25C10;25D5	Df(2L)BSC693	26545	0 (pupal lethal)	3	
2R-8045	42A13; 42E6	Df(2R)ED1612	8045	5	2-3	
	42A14; 42C7	Df(2R)BSC326	24351	32	0	
	42A8; 42B2	Df(2R)BSC313	24339	35	0	
	42C4; 42E1	Df(2R)BSC260	23160	34	0	
	42C7; 42D6	Df(2R)Exel6050	7532	30	0	
	42D6; 42E4	Df(2R)Exel6051	7533	16	0	
	42D6; 42F1	Df(2R)BSC262	23297	25	0	
3L/R Df #28	69A5;69D3	Df(3L)ED4483	8070	16	3	69A5-C7
28a	69A5;69C7	Df(3L)BSC380	24404	7	2	
28b	69B5;69C4	Df(3L)ED215	8071	18	1	
28c	69C4;69E8	Df(3L)BSC381	24405	13	2-3	
28d	69D1;69E2	Df(3L)Exel6117	7596	9	0	
3L/R Df#31	70C6;70F4	Df(3L)ED4543	8074	6	3	70D7-E4
31a	70C6;70D2	Df(3L)ED4529	9073	9	1	
31 b	70C15;70D3	Df(3L)ED4534	9074	14	1	
31c	70D1;70D3	Df(3L)Exel6120	7599	14	0	
31d	70D3;70D4	Df(3L)Exel6121	7600	6	0	
31e	70D4;70D4	Df(3L)Exel6122	7601	12	0	
31f	70D7;70E4	Df(3L)Exel6123	7602	0 (pupal lethal)	3	
3L/R Df#41	76A1;76E1	Df(3L)ED229	8087	0 (pupal lethal)	3	76B9-C5
41a	75F7;76A5	Df(3L)ED24786	8083	16	1	
41b	76A1;76B3	Df(3L)ED4799	8085	11	1	
41c	76B3;76B9	Df(3L)Exel9007	7942	3	0	
41d	76B9;76C5	Df(3L)Exel6135	7614	25	3	
41e	76D1;76D5	Df(3L)BSC445	24949	10	0	
41f	76D3;77C1	Df(3L)ED4858	8088	11	2	
3L/R Df#50	83A6;83B6	Df(3R)Exel6144	7623	4	3	
50a	83A6;83B2	Df(3R)BSC179	23146	6	1	83B4-B6
50b	83A7;83B4	Df(3R)ED10257	9159	10	1	
50c	83B4;83B6	Df(3R)ED5177	8103	14	2-3	
3L/R Df #58	85D16;85E6	Df(3R)ED5416	8701		3	85D19-85E1
	85D16;85D24	Df(3R)BSC476	24980	19	1-2	
	85D19;85E1	Df(3R)Exel6153	7632	12	3	
	85D24;85E5	Df(3R)Exel6264	7731	7	2	
58a	85D16;85D24	Df(3R)BSC476	24980	10	2-3	
58b	85D19;85E1	Df(3R)Exel6153	7632	11	3	
58c	85E1;85E4	Df(3R)BSC468	24972	7	0	
3L/R Df #59	85E5;85F12	Df(3R)ED5454	9080	13	3	85E8-F8
	85D16-E6	Df(3R)ED5416	24136	26	1	85F10-85F12
	85E9-F1	Df(3R)Exel6154	7633	12	0	
	85F1;85F10	Df(3R)Exel6155	7634	19	1	

Original modifier	Cytology	SubDf	Blm. #	N scored	Score	Refined cytology
	85F5;85F14	Df(3R)BSC621	25696	24	3	
59a	85E1;85F8	Df(3R)ED5428	9227	1 (pupal lethal)	3	
59b	85E8;85F14	Df(3R)BSC526	25054	12	3	
59c	85F1;85F10	Df(3R)Exel6155	7634	7	1	
59d	85F10;85F16	Df(3R)Exel6265	7732	19	2-3	
3L/R Df #77	92C1;92F13	Df(3R)BSC517	25021	8	2	92E8-F1
77a	92A11;92E2	Df(3R)ED6025	8964	9	0	
77b	92E2;92F1	Df(3R)Exel6185	7664	17	1	
77c	92E8;92F13	Df(3R)BSC518	25022	7	1-2	
3L/R Df #86	95E7;96B17	Df(3R)BSC492	24996	3	3	95F8-96A7
86a	95F8;96A6	Df(3R)Exel8178	7993	13	3	
86b	95E1;95F8	Df(3R)Exel6198	7677	14	1	
86c	96A7;96C3	Df(3R)ED6220	9211	8	0	
86d	95D10;96A7	Df(3R)ED6187	9347	3	3	
3L/R Df #89	96F10;97D2	Df(3R)ED6232	8105	4	3	97B4-97D4
89a	96F9;97A6	Df(3R)Exel6204	7683	10	1-2	
89b	96F6;97B4	Df(3R)BSC495	24999	4	1	
89c	97A6;97D4	Df(3R)BSC496	25000	9	0	
89d	97A1;97B2	Df(3R)BSC512	25016	13	0	
3L/R Df #95	99D5;99E2	Df(3R)Exel6214	7692	6	2	99D8-E1
95a	99D1-2;99E1	Df(3R)X3F	2352	22	2	
95b	99D3;3Rt	Df(3R)B81	3546	8	0	
95c	99D3;99D8	Df(3R)BSC502	25006	18	0	
95d	99E1;3Rt	Df(3R)R133	2234	24	-1-0	
3L/R Df #96	99E3;99F6	Df(3R)BSC503	25007	13	1	99F4-100A2
96a	99F4;100A2	Df(3R)BSC504	25008	19	1	
Suppressors						
2L Df#23	28F1;29A3	Df(2L)ED578	24131	23	2	
	28E5;28F4	Df(2L)BSC228	9705	16	1	
	28F1;29A3	Df(2L)BSC235	9710	14	0	
	28F5;29B1	Df(2L)BSC111	8836	3	0	
	28F5;29B1	Df(2L)BSC200	9627	17	0	
3L/R Df#18	65F7-66A4	Df(3L)Exel8104	7929	25	-1	
	66A1-66B1	Df(3L)BSC459	24963	13	0	
	66A3-66A19	Df(3L)BSC375	24399	11	0	
3L/R Df#34	72D4;73C4	Df(3L)ED4606	8078	23	1	
3L/R Df#33	72B1;72E4	Df(3L)BSC443	24947	16	-1	
	72E1;72E4	Df(3L)BSC649	25739	13	0	
	72E2;73A10	Df(3L)BSC555	25117	19	0	
	71F1;72D10	Df(3L)BSC774	27346	18	1	
	73A1;73A10	Df(3L)BSC562	25124	11	0	
	73A2;73C1	Df(3L)BSC561	25123	24	0-1	
	73B5;73D1	Df(3L)Exel6130	7609	18	0-1	
	72D9;72E1	Df(3L)BSC560	25122	ND	ND	
	72D4;72F1	Df(3L)ED220	8077	ND	ND	

Chapter 5

The N-Linked Glycosylation Pathway is Required for the Control of Epithelial Architecture

Abstract

Elucidating the control of epithelial architecture has been greatly advanced by the study of genes that regulate cell polarity and proliferation in *Drosophila*, termed neoplastic tumor suppressor genes. However, despite the identification of several classes of these genes, our understanding of the molecular mechanisms linking the known tumor suppressors together remains incomplete. Identifying additional tumor suppressors and their cellular roles is therefore of great import. Here we report that phenotypes seen in the *Drosophila* tumor suppressor mutant *tumorous imaginal discs* (*tid*), previously attributed to mutations in a DnaJ homolog-encoding gene, in fact are due to mutations in the *alg3* gene. Alg3 is a mannosyltransferase required in the lipid-linked oligosaccharide biosynthesis branch of the N-linked glycosylation pathway. We show that N-linked glycosylation is disrupted in *alg3* mutant imaginal discs, and that *alg9*, an additional gene in the N-linked glycosylation pathway, shows similar imaginal disc phenotypes. Furthermore, we provide evidence linking N-linked glycosylation to known neoplastic tumor suppressor genes. *Alg3* and nTSG mutants show strong and reciprocal genetic interactions, and loss of *alg9* potentiates Ras in a cooperative tumorigenesis model. Preliminary data also indicate that the Unfolded Protein Response (UPR) is activated in *alg* and *scrib* mutant discs. We conclude that N-linked glycosylation influences cellular growth control, perhaps through polarity regulators, and further hypothesize that the UPR may connect N-linked glycosylation to some neoplastic tumor suppressor pathways, though additional experiments are required to rigorously test this hypothesis.

Introduction

Uncovering the cell biological pathways that control both cell polarity and proliferation is essential for understanding how these mechanisms contribute to overall tissue growth control. Much work has been done in *Drosophila* to elucidate the various signaling pathways and proteins required for regulating polarity and proliferation. One prominent class of genes identified as controlling these features are the neoplastic tumor suppressor genes (nTSGs). This class includes the classical polarity regulators *lethal giant larvae (lgl)*, *scribble (scrib)*, and *discs large* (*dlg),* as well as endocytic regulators such as *Rab5*, *avalanche*, *rabenosyn* and *Vps45*. Recent advances have also identified polarity-regulating roles for Ubiquitin-mediated protein degradation and Polycomb gene group-based transcriptional regulation. While these classes give us some insight to the mechanisms governing cell polarity, the available data have not yet produced a complete view of how these various pathways coalesce to enact global polarity control. We have therefore sought to identify additional genes that control cell polarity, with particular interest in those that interact with previously identified polarity regulators.

Classical studies on *Drosophila* growth regulation identified not only *dlg* and *lgl*, but also *tumorous imaginal discs* (*tid*) as malignant Drosophila tumor suppressor genes (Gateff, 1978; Löffler *et al.*, 1990). As the name implies, the imaginal discs of larvae homozygous for *tid* mutations develop into overgrown, unstructured masses and lead to developmental delays and ultimately death of the animal (Kurzik-Dumke *et al.*, 1992). Interestingly, *tid* mutant imaginal discs show a dramatically slower growth rate than wild-type discs, and are smaller than the imaginal discs from comparably aged wild-type larvae. However, the mutant larvae delay puparium formation up to 10 days, and the discs continue to grow during this extended larval phase (Kurzik-Dumke *et al.*, 1992). When transplanted into a wild-type larva, *tid* mutant discs fail to form differentiated cuticular structures. Furthermore, when transplanted into the abdomen of an adult fly, *tid* mutant imaginal disc tissue, but not brain tissue, is non-invasive but does continue to grow and eventually kills the host, which is in contrast to the arrested growth and benign nature of transplanted wild-type imaginal discs (Kurzik-Dumke *et al.*, 1992).

Genetic and cytogenetic analyses localized the *tid* gene to chromosome 2R. Northern blot analysis of mRNA from *tid* mutant larvae using a variety of cDNA probes suggested that a single transcript was lost in the mutant larvae, leading to the designation of the corresponding open reading frame as *tid* (Kurzik-Dumke *et al.*, 1995). Furthermore, *in situ* hybridization and antibody staining suggested that *tid* expression was lost in *tid* mutant imaginal discs (Kurzik-Dumke *et al.*, 1998). Therefore, the mutant phenotypes were attributed to loss of a gene, designated *tid*, with significant homology to the DnaJ proteins from yeast and humans (Kurzik-Dumke *et al.*, 1995). DnaJ proteins perform diverse functions within cells, including acting as protein chaperones and regulating the substrate specificity of Hsp70 proteins. The biochemical functions of Tid were thus presumed to be important for the function of additional "dependent proteins" (Kurzik-Dumke *et al.*, 1995).

The identification of a DnaJ protein as a tumor suppressor gene in Drosophila sparked the analysis of the role of mammalian *tid* homolog, *hTid-1*, in both normal

development and cancer cell biology. These studies have shown that *hTid-1* also behaves as a tumor suppressor gene in squamous cell and colorectal cancers in mammalian systems (Kurzik-Dumke *et al.*, 2008; Chen *et al.*, 2009), and have provided some insight into its molecular functions. The human homolog encodes three splice forms, leading to the production of three cytosolic and three mitochondrial proteins (Yin and Rozakis-Adcock, 2001; Kurzik-Dumke and Czaja, 2007), and these different isoforms have been found to interact with a variety of proteins. Tid-1 promotes the degradation of the ErbB2 oncogene in breast cancer cells (Kim *et al.*, 2004) and regulates the activity of the NF-κB transcription factor (Cheng *et al.*, 2005). Furthermore, Tid-1 directly interacts with a human interferon gamma receptor subunit (Sarkar *et al.*, 2001), the adenomatous polyposis coli (APC) tumor suppressor (Kurzik-Dumke and Czaja, 2007), the von Hippel-Lindau tumor suppressor (Bae *et al.*, 2005) and the human papilloma virus E7 oncoprotein (Schilling *et al.*, 1998). The human homolog has thus been linked to a wide variety of divergent signaling and cellular pathways.

The recent data identifying the molecular partners of *hTid-1* have provided a number of reasonable models for how *tid* may function as a tumor suppressor in *Drosophila*. However, it is not yet clear exactly which of these could explain why *tid* is required for epithelial growth control during normal development. Furthermore, previous research has not definitively demonstrated which of its molecular interactions is critical for tumor suppressor function, either in mammals or in *Drosophila*. Because the effects of loss of *tid* on cell polarity are currently unclear, whether *tid* is more likely to act with known hyperplastic or neoplastic tumor suppressor genes remains unknown. We therefore sought to carefully assess whether *tid* could control polarity in Drosophila epithelia, whether it regulates epithelial architecture by interacting with known tumor suppressors, and if so, the mechanism by which it effects that regulation.

Here we describe the results of our phenotypic and genetic analysis of *tid*, including our surprising finding that the *tumorous imaginal discs* gene was originally cloned incorrectly. Rather than disrupting the coding sequence of the DnaJ homolog, the lesions in the *tid* alleles disrupt an adjacent gene, *neighbor of tid* (*l(2)not*), which encodes an ALG3 homolog acting in the N-linked glycosylation pathway. We further investigate the mechanism of tumor suppression related to N-linked glycosylation, and speculate on the potential links between N-linked glycosylation and epithelial cell polarity.

Results

tid *alleles modify the* lgl-*IR phenotype*

In a screen for genes which genetically interact with the *Drosophila* tumor suppressor *lgl* (see Chapter 4), we found that the tid^2 allele dominantly enhanced an *lgl* RNAi (*lgl*-IR) phenotype in the adult wing. In order to confirm that the heterozygosity for *tid* was the basis for the *lgl*-IR modification, we tested an additional *tid* allele, tid^1, a deficiency that removes a genomic region containing *tid* (*Df(2R)tid*), and a PiggyBac transposon insertion upstream of the *tid* coding sequence (Figure 5.1A-E). In each instance, we found that heterozygosity for these *tid*-disrupting alleles robustly enhanced the *lgl*-IR phenotype. In addition, we asked whether *tid* heterozygosity could similarly modify the rough eye phenotype that results from expressing an activated form of the polarity regulator Crumbs (*GMR>*Crb^{Intra}). Removing one copy of *tid* in the *GMR>*Crb^{intra} background resulted in very few adult flies eclosing, and those that did bore minimal eye tissue (Figure 5.1F-H'). These results indicated that *tid* genetically interacts with two known Drosophila polarity regulators, including a tumor suppressor gene, and suggested that *tid* may in fact play a role in regulating epithelial cell polarity.

Phenotypic analysis of tid *mutant tissues in vivo*

To better characterize the *tid* loss of function phenotype, we recombined the tid^1 and tid^2 alleles onto FRT42 chromosomes. This allowed us to use the eyFLP-cell lethal system to generate homozygous mutant eye imaginal discs in an otherwise heterozygous animal (Stowers and Schwarz, 1999). Mutant eye discs generated in this manner show a much milder defect than those present in the hemizygous or tid^1/tid^2 transheterozygous animals. However, these mutant eye discs lead to pupal lethality, reminiscent of the mutant eye non-eclosion (MENE) phenotype of known polarity regulators such as *lgl* (Menut *et al.*, 2007). In hemizygous animals, eye discs are misshapen and show severely disrupted architecure (Figure 5.2C-D), while the eyFLP-cell lethal *tid* discs show only small areas of architecture disruption (Figure 5.2F-G). We also stained the hemizygous discs for Mmp1, which is a marker for activated JNK signaling and identifies neoplastic tissue. We found that small areas of the tid^1 or tid^2 discs did express Mmp1 (Figure 5.2C'-D'), suggesting that that these alleles are capable of inducing neoplastic tissue transformation similar to that seen in classic nTSG mutants.

We also analyzed the consequences of generating *tid* mutant cells in two mosaic contexts: the follicle cell epithelium, and mosaic imaginal discs. In contrast to the loss of apicobasal polarity and multilayering observed in nTSG mutant follicle cell clones (Bilder *et al.*, 2000; Lu and Bilder, 2005), *tid* mutant follicle cell clones are indistinguishable from wild-type cells (not shown). In addition, when *tid* mutant clones are generated in an otherwise wild-type eye imaginal disc, the mutant clones persist and can differentiate and seem to contribute to the adult eye (data not shown). This is again in contrast to clones of nTSG mutant cells, which grow slowly and are eliminated from the eye disc epithelium by cell competition.

The tid *phenotype is due to loss of the* neighbor of tid *gene*

The original cloning of the *tid* gene, published over a decade ago, made use of deficiency stocks and subsequent genomic walks to map the *tid* lesions to a single genomic region containing three transcribed regions (Kurzik-Dumke *et al.*, 1995). Subsequent sequencing analysis of the tid^1 and tid^2 alleles failed to identify molecular lesions within the *tid* coding sequence (Kurzik-Dumke *et al.*, 1998). These experiments did identify lesions upstream of the *tid* 5' UTR in the tid^2 allele, leading to the suggestion that the lesions were disrupting *tid* transcription. However, the genomic region containing *tid* harbors a "nested gene configuration:" the *tid* open reading frame is itself found in the intron of a second open reading frame: *neighbor of tid* (*l(2)not*) (Figure 5.2A and (Kurzik-Dumke *et al.*, 1997)). Our analysis of the region indicated that the reported location of the tid^2 lesions would in fact place them in the *l(2)not* coding sequence. A genomic rescue construct covering the entire *tid* and *l(2)not* region could rescue the tid^2 tumor phenotype (Kurzik-Dumke *et al.*, 1995), but this would also be consistent with the tumor phenotype being caused by disruptions in the *l(2)not* locus. To resolve this discrepancy, we first undertook direct sequencing of the entire genomic locus containing the *tid* and *l(2)not* open reading frames.

We used a single set of primers to amplify the entire *l(2)not* and *tid* region from genomic DNA extracted from wild-type and hemizygous tid^1 and tid^2 larvae. We then sequenced this amplicon using a collection of sequencing primers arrayed across the region. Comparing the sequences of the alleles to the wild-type DNA revealed no lesions in the *tid* coding sequence. However, we did identify lesions in both *tid* alleles in the *not* coding sequence. The tid^1 allele contains a nonsense mutation at glutamine 375, resulting in a truncation of the remaining 135 amino acids at the C-terminus of the predicted Not protein. In the tid^2 allele, we identified the same molecular lesions that were previously reported: an in-frame 24 base pair deletion that removes amino acids 36-43 of Not, and a single base pair insertion at amino acid 45 that results in a frameshift and premature termination of the Not protein at 192 amino acids (Figure 5.2A). These data raise the possibility that loss of *l(2)not* gene function may in fact be responsible for the observed phenotypes in the *tid* alleles.

To rigorously test whether loss of *l(2)not* function was the basis of the *tid* phenotype, we performed a rescue assay with the *l(2)not* coding sequence alone. We used a sequence-confirmed *l(2)not* cDNA to generate *l(2)not* rescue constructs expressed under the control of either a constitutively active tubulin promoter (*tub-Not*) or the heat shock-inducible promoter (*HS-Not*). When the rescue construct was introduced into the background of either the tid^1 or the tid^2 allele, we found that the presence of the *tub-Not* or *HS-Not* construct could rescue both the imaginal disc (Figure 5.2H-I) and the lethality phenotypes of the *tid* alleles, as well as the MENE phenotype. This strongly suggests that the *tid* gene was originally miscloned, and that the observed tumorous phenotype is actually due to loss of *l(2)not* function.

The N-linked glycosylation pathway is important for proper epithelial growth

We next sought to identify the molecular function of the protein encoded by the *l(2)not* gene. Protein BLAST searches revealed that *l(2)not* is the single fly homolog of

the yeast and human *ALG3* genes. *ALG3* (*alg*, *a*sparagine-*l*inked *g*lycosylation) encodes a mannosyltransferase required for the biosynthesis of the lipid-linked oligosaccharides in the N-linked glycosylation pathway in the ER (Aebi *et al.*, 1996; Sharma *et al.*, 2001). The oligosaccharide biosynthesis branch of, and indeed the entire the N-linked glycosylation pathway (Figure 5.3A), is quite well genetically and functionally conserved from yeast to humans (Lehle *et al.*, 2006). For this reason, and to avoid confusion with the previous *tid* annotation, we have chosen to refer hereafter to the *l(2)not* gene as *alg3*, and will refer to the tid^{1} and tid^{2} alleles as mutations in *alg3*.

We next asked whether *alg3* was a bona fide N-linked glycosylation gene in Drosophila, and furthermore, whether N-linked glycosylation is required for epithelial architecture. To address this, we first asked whether other genes required for N-linked glycosylation would interact with *lgl*-IR, as we observed with the *tid* alleles. By crossing various alleles to the *lgl*-IR stock, we found that the *lgl*-IR phenotype was enhanced by removing single copies of the mannosyltransferase *alg9*, the oligosaccharyl transferase subunit *Ost48*, or *Rft1*, the transferase required for translocating the nascent lipid-linked oligosaccharide into the ER lumen (Figure 5.4). These results strongly corroborated the earlier modification seen with the *alg3* alleles, and further solidify the potential links between N-linked glycosylation and polarity- and growth-regulating pathways.

The Alg9 protein acts at two separate steps of the lipid-linked oligosaccharide biosynthesis pathway. Through searching the public stock centers, we identified a lethal PiggyBac insertion in the coding sequence of the *Drosophila ALG9* homolog, CG11851 (hereafter $alg9^{PBac}$). Gratifyingly, the imaginal discs of homozygous $alg9^{PBac}$ larvae showed severe architectural defects similar to those of the *alg3* alleles (Figure 5.3B-D). When we recombined the $alg9^{PBac}$ onto the FRT82 chromosome and generated homozygous mutant eye discs, we saw that, like the *alg3* alleles, $alg9^{PBac}$ mutant eye discs show mild architectural defects (Figure 5.3E-G). Moreover, the eyFLP-cl $alg9^{PBac}$ eye discs also lead to the MENE pupal lethality phenotype. These findings suggest that the N-linked glycosylation pathway in general is required for proper imaginal disc architecture and development.

We next asked whether we could detect N-linked glycosylation defects in the *alg3* or *alg9* mutant discs. Chaoptin (Chp) is an N-glycosylated surface protein required for photoreceptor cell development in the eye imaginal disc, and N-glycosylation is reported to be required for Chp stability and transport to the cell surface in cultured *Drosophila* S2 cells (Hirai-Fujita *et al.*, 2008). Using immunohistochemistry, we found that in *alg3* or *alg9* homozygous mutant eye discs, Chp is still present (Figure 5.3H-J), and at least in some cells is properly transported to the cell surface, as indicated by positive antibody signal even in unpermeabilized tissues (Figure 5.3K-L). This could reflect either N-glycosylation-independent Chp trafficking, or an incomplete block of the N-glycosylation pathway. We reasoned that even a partial block in N-glycosylation would result in incomplete glycosylation on Chp molecules. We therefore turned to a biochemical assay for Chp glycosylation.

Chp protein is readily identified as a single band on a Western blot for Chp in wild-type eye imaginal discs. In *alg3* eye discs, Chp is still present at detectable levels (Figure 5.3M). However, the size is significantly smaller than wild-type Chp, which is

consistent with what has been reported for chemically deglysocylated Chp (Hirai-Fujita *et al.*, 2008). While not definitive, this does strongly suggest that the N-linked glycosylation pathway is impaired in *alg3* mutant discs. Further experiments are necessary to determine if this is also true in *alg9* discs.

Phenotypic characterization of N-glycosylation mutant tissues

Having established a relationship between *lgl* and the N-linked glycosylation pathway, we next asked whether specific cell biological pathways were disrupted by defects in N-glycosylation. Our first hypothesis was that N-glycosylation was required for polarity control in the imaginal disc epithelia. However, by staining *alg3* discs for the polarity markers aPKC and Dlg or Crb and Scrib, we found that apicobasal polarity is not obviously disrupted in these discs (Figure 5.5A-D). Similarly, the apical cadherin Cad87A retains apical localization in *alg3* discs (Figure 5.5E-H). Interestingly, staining for the junctional proteins E-Cadherin and Armadillo/β-catenin did not show polarity disruptions, but the overall levels of these proteins seemed to be much lower in *alg3* discs than in wild-type discs (Figure 5.5I-J'), suggesting that perhaps trafficking to or stability of E-cadherin-based junctions was disrupted. This was particularly appealing given the literature emphasizing the importance of N-glycosylation for E-cadherin junctional localization and stability (Liwosz *et al.*, 2006). However, on repeating the experiment, the levels of E-cadherin did not appear as drastically reduced (Figure 5.5K-L); we were also unable to detect any *E-cadherin/shotgun* loss of function-like phenotypes in *alg3* germ line clones (data not shown). Although *alg3* maternal-zygotic mutant embryos do have cuticular defects (Figure 5.5M-O), they are not specific to those expected for E-cadherin disruption. We are thus currently unable to clarify whether E-cadherin or adherens junction function is consistently impaired by disruptions in the N-linked glycosylation pathway.

In attempting to characterize the cell biological defects in *alg3* discs, we also stained the tissue for a panel of protein markers. Coracle (Cor), a protein localized to the lateral cell membranes, is properly localized in *alg3* discs (Figure 5.6A-B). However, in looking at these discs in cross section, we noticed that the cells of the peripodial membrane, which are thin squamous cells in wild-type discs, appear more cuboidal in the *alg3* discs, and the Cor signal is much stronger in the peripodium than the disc proper (Figure 5.6A-B). This could reflect changes in cell fate or signaling between the peripodium and the disc proper, but the precise significance of this finding remains to be determined. In addition, the cuboidal cells in the peripodium of *alg3* mutant discs may indicate that N-linked glycosylation plays a general role in maintaining cell shape, though the molecular targets that could mediate this activity are unclear.

We were also interested in signaling pathways with secreted ligands, since N-linked glycosylation is a modification commonly found on secreted proteins. Staining wild-type and *alg3* discs for the Wingless protein (Wg) revealed that Wg is not significantly upregulated in *alg3* wing discs, and the pattern across the wing disc is mostly preserved (Figure 5.6D). We also stained for the Wingless signaling target Senseless. We detected very low levels of Sens in the *alg3* discs, suggesting that Wg signaling may be impaired; however, it is not completely blocked, as some Sens-positive

cells are present (Figure 5.6 C-D'). Finally, we compared the levels and localization of the Notch target Cut in *alg3* eye discs. The *alg3* eye discs, despite their architectural defects, do still contain some differentiated photoreceptor cells, as indicated by the presence of Elav-positive cells (Figure 5.6E-F'). In wild-type eye discs, Cut is expressed in the interommatidial cells, but this pattern is disrupted in *alg3* discs (Figure 5.6E-F'). This suggests that there are some signaling pathways affected by the N-glycosylation defects in *alg3* discs. However, fully understanding the interaction between these pathways and the tissue growth defects will require further investigation.

N-linked glycosylation defects cooperate with neoplastic tumor suppressor pathways

Having been unable to detect obvious cellular polarity defects in *alg3* imaginal discs, we wondered whether *alg3* and *alg9*, and by extension N-linked glycosylation, might not act as neoplastic tumor suppressors. Given the interaction between the N-glycosylation genes and *lgl*, we asked whether *alg3* could modify the hypomorphic phenotype of other polarity-regulating nTSGs. There is a range of *scrib* hypomorphic alleles available that show imaginal disc phenotypes between wild-type discs and neoplastic *scrib* null discs, including hyperplastic discs with cuboidal cell shapes (Zeitler *et al.*, 2004). When we removed one copy of *alg3* in the background of the *dt6* or the *dt14* hypomorphs, we did not see any differences in the epithelial architecture. The converse experiment, however, was quite surprising. As described above, *alg3* discs show aberrant folding and disc structure. Strikingly, removing a single copy of *scrib* robustly modifies the *alg3* phenotype. These discs are not appreciably larger than *alg3* discs, but strikingly, they contain significantly more folds. This indicates that there is an interaction between N-glycosylation and *scrib in vivo* that contributes to epithelial architecture control. The observed change in global disc architecture could reflect changes in cell shape or an increase in cell proliferation. However, as we have not yet analyzed the number of cells in each of these genotypes, this discrepancy remains unresolved.

The ability of a *scrib* allele to dominantly enhance the *alg3* phenotype suggested that while disrupting N-glycosylation may not be sufficient to promote neoplastic transformation, it can cooperate with other tumor suppressor pathways. To further test this hypothesis, we used a Ras cooperation assay. Similar to the oncogenic properties of mammalian Ras^{V12}, clonal expression of Ras^{V12} in the *Drosophila* eye disc leads to cellular overproliferation (Figure 5.7B). However, when Ras^{V12} is expressed in the context of loss of an nTSG such as *scrib* using the MARCM system (Lee and Luo, 2001), dramatic neoplasia results (Figure 5.7C and Brumby and Richardson, 2003), and cells from the eye disc invade the ventral nerve cord (VNC) of the larval brain (arrows, Figure 5.7C). While eye discs containing MARCM clones of *alg9* do not show any obvious phentoypes (Figure 5.7A), *alg9* clones that also express Ras^{V12} make up a significantly higher proportion of the overall disc (Figure 5.7D). Moreover, although the *alg9-*Ras^{V12} clones do not invade the VNC as *scrib-*Ras^{V12} clones do, they are significantly different from *alg9* or Ras^{V12} alone in terms of cellular architecture, with some large clones appearing highly disorganized with potentially disrupted apicobasal polarity. This

indicates that N-linked glycosylation can cooperate with Ras^{V12} expression and promote tissue defects.

The unfolded protein response may be activated in N-linked glycosylation and nTSG mutants

One role of N-linked glycosylation is to ensure the proper folding of secreted and transmembrane substrate proteins. When unfolded proteins accumulate in the ER, the unfolded protein response (UPR) pathway is activated and leads to downstream signaling events designed to alleviate the initial stress (Davenport *et al.*, 2008). We reasoned that if N-glycosylation is reduced in *alg3* and *alg9* mutant cells, then the UPR should be activated. UPR activation begins when the Hsp70 molecule BiP relocates from binding partners such as IRE1 in the ER membrane to unfolded proteins. BiP dissociation activates IRE1, which cleaves the *Xbp1* mRNA into an active form. This splicing provides a useful assay for UPR activation: presence of spliced *Xbp1* mRNA indicates that the UPR has been activated.

To determine whether the UPR is activated in *alg3* and *alg9* discs, we isolated total RNA from the mutant discs and performed RT-PCR to detect *Xbp1* mRNA, using primers that span across the ~20bp segment that is spliced out upon UPR activation (Haecker *et al.*, 2008). In wild-type discs, we detect a single band of ~120bp, consistent with presence of the unspliced transcript (Figure 5.8A). However, in *alg3* or *alg9* discs, we detect two bands: one that is consistent with the unspliced form seen in wild-type discs, and a second, smaller band (Figure 5.8A), indicating that, as expected, the UPR is activated in *alg* mutant tissues. To test whether the UPR could be a connection between *alg* mutants and known nTSGs, we performed the same *Xbp1* splicing assay on *scrib* mutant discs. We were surprised to see that the lower band is also present in *scrib* mutant discs, suggesting that the UPR may also be activated in *scrib* mutant cells, and providing a possible explanation for the cooperativity we see between *alg3* and *scrib* in controlling imaginal disc architecture.

One confounding aspect of the *Xbp1* splicing assay was that we were uncertain whether the size difference we detected between the two bands in the *alg* samples was consistent with *Xbp1* splicing and UPR activation. We therefore repeated the assay, including a sample from discs overexpressing a dominant-negative form of BiP (Hsc70-3^{Q231S}, Elefant and Palter, 1999), which is expected to activate the UPR. However, we detected a single ~120bp band in this sample (Figure 5.8B). This indicated that either BiP^{DN} does not effectively activate the UPR, or that our assay is inefficient at detecting the *Xbp1* splicing upon UPR activation. Interestingly, the *alg3* sample in this experiment still showed a second smaller band, but this lower band was no longer present in the *scrib* sample (Figure 5.8B). The results of this series of experiments are therefore inconclusive, and the assay must be optimized to establish a reliable readout for UPR activation.

Discussion

We have shown that the lesions that identified the *Drosophila* classical growth regulator *tumorous imaginal discs* (*tid*) disrupt the *ALG3* homolog *neighbor of tid* (*l(2)not*), rather than the DnaJ homolog *tid*. We demonstrate that mutations in genes acting in the lipid-linked oligosaccharide biosynthetic pathway (*alg* mutants) lead to morphological defects in imaginal discs. We also find that N-glycosylation genes interact with the known neoplastic tumor suppressors *lgl* and *scrib*, and cooperate with the expression of Ras^{V12} to promote tissue neoplasia. Finally, preliminary data suggests that the unfolded protein response (UPR) may be activated in both *alg* and *scrib* mutant tissues, which establishes an intriguing link between cellular stress response pathways and neoplastic tumor suppressors in *Drosophila*.

During our early studies of the *tid* alleles, we were quite surprised to find that the gene responsible for the mutant phenotype had been miscloned. Previous data supporting the identification of *tid* included loss of anti-Tid antibody signal in mutant imaginal discs (Kurzik-Dumke *et al.*, 1998). However, these data clearly show Tid signal near the periphery of the mutant discs but absent from the interior, and it has been our experience that this pattern is typical of most antibodies used on neoplastic mutant tissue, as the antibodies do not penetrate very far into the tissue. Also confounding are the previously reported rescue experiments. Kurzik-Dumke *et al*. reported that a genomic construct containing both the *tid* and *l(2)not* coding regions could rescue the *tid* "tumor phenotype," while two deletion constructs – one removing part of the first *l(2)not* exon and one removing a large part of the *tid*-containing intron – did not rescue the phenotype (Kurzik-Dumke *et al.*, 1995). These data are consistent with the phenotype being due to loss of *l(2)not*, and not due to loss of *tid*.

Kurzik-Dumke and colleagues first reported the gene within gene configuration of *l(2)not* and *tid* (Kurzik-Dumke *et al.*, 1997), and have gone on to study the human homolog *Htid-1* and its role as a tumor suppressor (Kurzik-Dumke and Czaja, 2007); we are currently unable to reconcile our data with their apparent continued assumption that the growth defects in Drosophila are solely due to loss of *tid* function. While our data demonstrate that all phenotypes of the tid^1 and tid^2 alleles can be rescued by provision of Alg3, we concede that we cannot rule out a function for *tid* in epithelial growth in fly or human tissue on the basis of our data. This will require additional investigation, including generating a mutant line that disrupts *tid* function in a way that does not also disrupt *l(2)not* function.

In our investigations of the *alg3* phenotype, we became acutely aware that the tissue growth and architecture defects present in the *alg* mutants are not as dramatic as those seen in tissue lacking known neoplastic tumor suppressors. Furthermore, the imaginal discs that we have analyzed from transheterozygous or hemizygous mutant larvae regularly produce a 2-3 day delay in pupariation, in contrast to the 10-day developmental delay previously reported (Kurzik-Dumke *et al.*, 1992). One potential explanation for this difference may be our detection via complementation analysis of an uncharacterized *lgl* mutation in the tid^1 stock. Given that we have shown here that *lgl* and *tid* genetically interact, the presence of a lesion in *lgl* in the genetic background of the tid^1 mutants may have confounded the previous phenotypic analysis. As there is no

way to ascertain whether the originally analyzed *tid*^{1} stock carried this *lgl* mutation, further experiments would be required to resolve the reasons for the discrepancy between our analysis and that previously reported.

With regard to the relatively mild *alg* mutant imaginal disc phenotypes we see as compared to nTSG mutants, it is possible that the discs we have studied reflect only a hypomorphic phenotype, and that the tissue is not truly protein null, at least in the case of *alg3*. This is based on several of reasoning. The first is that development in *alg3* zygotic mutants such as the *tid*^{2}*/tid*^{1} transheterozygous larvae can proceed as far as pupal stages before dying. However, maternal zygotic mutants die during embryonic development, suggesting that a small maternal contribution of wild-type Alg3 allows larval development to proceed. The second observation came from our rescue constructs. The *HS-not* rescue construct was incorporated into the background of balanced stocks carrying the *tid* lesions. However, even without heat shocking the animals, we found that unbalanced flies – *alg3* homozygotes – eclosed. This suggests that minimal expression of *alg3* is sufficient to rescue the mutant phenotype. This further suggests that in mutant animals, either perdurant Alg3 protein or perdurant N-glycans may partially dampen the genetic loss of *alg3*, leading to a hypomorphic phenotype. Finally, we observed that *scrib* heterozygosity could modify the *alg3* phenotype. As null phenotypes are not usually subject to genetic modification, this lends additional support to our hypothesis that the imaginal discs of zygotic *alg3* mutants reflect hypomorphic phenotypes.

One way to circumvent the problem of maternally contributed perdurant protein causing a hypomorphic phenotype in zygotic mutants may be to extend the time allowed for imaginal discs to grow. Because the zygotic *alg* mutant larvae pupate, we have not been able to analyze a terminal phenotype. However, by transplanting the mutant imaginal discs into a growth-permissive environment such as the abdomen of an adult female, we may be able to observe continued disc growth. Cells in wild-type discs transplanted into the abdomen of an adult host cease to divide, but cells in discs from tumor suppressor mutants continue to proliferate and eventually kill the host. The original classification of the *tid* alleles as malignant tumor suppressors was based partly on evidence that transplanted disc fragments did undergo continuous proliferation, proving lethal to the transplant hosts (Kurzik-Dumke *et al.*, 1992). However, the disorganization of the recovered transplant tissue was not as dramatic as neoplastic mutant tissue. Moreover, in contrast to the lack of differentiation in zygotic mutant imaginal discs, when *tid* discs were transplanted into wild-type larvae and recovered after pupation, differentiation was occasionally observed (Kurzik-Dumke *et al.*, 1992); this is consistent with our detection of Elav-positive cells in *alg3* mutant eye discs. Together, these data suggest that the *alg* mutants may not be analogous to the classical nTSGs. Repetition of these experiments, including recovery and more detailed analysis of the transplanted tissue from adult hosts, will be important for both investigating the null *alg* phenotype and for clarifying whether *alg* mutants exhibit the continuous proliferation common to the known neoplastic tumor suppressor genes, or if they behave more like hyperplastic growth regulators.

We acknowledge that *alg* mutants may ultimately show distinctly different null phenotypes than the classical nTSG mutants. However, given the apparent morphological defects in mutant imaginal discs, discovering how N-linked glycosylation impinges on cellular pathways will inform our understanding of growth control in epithelia. For instance, N-linked glycosylation is not required for proper targeting of all polarized proteins, however, certain targets may have profound impacts on the downstream biology of cellular growth control.

Our preliminary results indicate that N-linked glycosylation is impaired in *alg3* mutant discs, and additional experiments to demonstrate this are straightforward. For example, repeating the Chp Western blot with tissue from additional *alg* mutants or glycosidase-treated wild-type tissue will be informative as to the consistency of this assay as a readout for N-linked glycosylation. In addition, staining wild-type and *alg* mutant imaginal disc tissues with lectins, which are biological molecules that bind to sugar moieties, may indicate a decrease in glycan prevalence in mutant tissues. In particular, the snowdrop lectin GNA or the amaryllis lectin HHA, which are specific to high-mannose glycan structures, which are the predominant structures in *Drosophila* N-glycans (ten Hagen *et al.*, 2009), may be especially useful. Furthermore, Western blot analysis to compare glycosylated proteins in wild-type and *alg* mutant tissues may also reveal global N-glycosylation defects in *alg* mutants.

The initial experiments to detect the activation of the UPR in *alg* mutant tissues are promising but require refinement in order to reliably assess UPR status. The current experimental design is non-ideal for detecting spliced and activated *Xbp1* mRNA. Performing the assay with mRNA isolated from S2 cells treated with tunicamycin or imaginal discs treated with DTT to block N-glycosylation may provide confirmation that the assay detects UPR activation. One optional modification may be to use a primer for RT-PCR that spans across the splice site, and so would detect only the presence of spliced *Xbp1* mRNA. This would provide a binary readout, as opposed to the relative contribution of two RT-PCR products. Alternatively, some researchers have used phosphorylation of eIF2α as a readout of PERK-mediated UPR activation (Haecker *et al.*, 2008), although the changes they detect in eIF2α phosphorylation state are relatively small. This may be an informative assay in the *alg* mutant discs, but we have not yet tested the assay in our hands.

Related to the detection of the UPR is the question of whether UPR activation is itself necessary for the observed tissue growth defects in *alg* and *scrib* mutant discs. Expressing a wild-type version of BiP may be sufficient to block the UPR even when unfolded proteins are present, due to saturation of the ER membrane receptors. If expressing BiP^{WT} in the context of the *alg3* mutant discs prevents the tissue growth phenotype, it would suggest that the UPR is an integral downstream component of the *alg* mutant phenotype. In addition, our preliminary finding that the UPR may also be activated in *scrib* mutant discs was quite surprising, and suggests that the UPR may also be downstream of the junctional nTSGs in controlling cell growth. This is an intriguing hypothesis, as the UPR has lately received attention in the field of mammalian cancer research. Recent findings indicate that ER stress response genes are upregulated in a variety of cancers, and additionally suggest that the UPR may play an active role in

protecting cancerous cells from apoptosis (Moenner *et al.*, 2007; Hetz, 2009). Therefore, investigating the functional contribution of the UPR to *scrib* tumor growth in *Drosophila* may be incredibly informative as to the cell biological mechanisms driving cancer cell proliferation.

The observation that *alg* mutants cooperate with *scrib* or Ras^{V12} to lead to an enhanced imaginal disc phenotype, combined with the observation that *scrib* mutants may activate the UPR, suggests that there could be biological links between tumor suppression and N-linked glycosylation. Intriguingly, this is a burgeoning area of research in the field of mammalian cancer biology. It has been recently reported that UPR activation by treatment with tunicamycin – a drug that blocks N-linked glycosylation – inhibits the accumulation of reactive oxygen species that is induced by the activation of tumor necrosis factor α (TNFα) and prevents cell death (Xue *et al.*, 2005). This may suggest that the UPR may be activated in *scrib* mutant tissues as a way of counteracting cell stress. Also, this may explain the cooperation between Ras^{V12} and the *alg9* mutant. The loss of *alg9* could lead to reduced N-glycosylation and a subsequent activation of the UPR, which could then mediate increased cell survival. This could be tested by expressing the BiP^{WT} construct to block the UPR in *alg9* mutant cells also expressing Ras^{V12} to see if this blocks Ras^{V12} cooperation. Similarly, it would be interesting to know whether activating the UPR in eye discs expressing Ras^{V12}, perhaps by coexpressing BiP^{DN}, can enhance the Ras^{V12} phenotype. Notably, promoting survival of Ras^{V12}-expressing cells by expressing the apoptosis inhibitor p35 does not lead to dramatic overgrowth (Wu *et al.*, 2010), suggesting that the cooperation between *alg9* and Ras^{V12} is not solely due to an effect on cell survival. Nevertheless, these experiments would address the necessity and sufficiency of the UPR in contributing to neoplastic tissue growth.

We have been largely interested in studying the cell biological pathways which control not just tissue growth and architecture, but also control epithelial cell polarity. Given that at least some polarized proteins rely on N-linked glycosylation for their accurate subcellular localization, N-linked glycosylation has interesting putative links to epithelial cell polarity. Our experiments to date have not identified any significant apicobasal polarity defects in *alg* mutant imaginal discs. However, as discussed above, the discs we have worked with may actually be presenting hypomorphic phenotypes. Therefore, examining the apicobasal polarity of cells in the *alg3* discs modified by removing one copy of *scrib*, the *alg9* mutant cells expressing Ras^{V12} or in discs transplanted into adult hosts may reveal a polarity defect in tissues that have progressed further toward an *alg* protein null state and possibly neoplasia.

Finally, how could N-linked glycosylation and cellular growth control be coupled? One hypothesis invokes the role of secreted galectins in binding N-glycosylated surface proteins and organizing them into lattices (Taniguchi, 2007). This lattice incorporation may inhibit the dimerization and activation of signaling receptors such as receptor tyrosine kinases (RTKs), and further preventing their endocytosis and downstream signaling to promote cell growth. In fact, it has been shown that blocking N-glycosylation of the epidermal growth factor receptor (EGFR) results in its spontaneous oligomerization and phosphorylation (Tsuda *et al.*, 2000). It is tempting to speculate

that in *alg* mutant tissues, the defects in N-linked glycosylation result in ectopic activation of signaling receptors, leading to aberrant pro-proliferative signaling. Analyzing the activation of growth-promoting signaling pathways in *alg* mutant tissues, and perhaps mutations in the single fly galectin homolog (Pace *et al.*, 2002), will be essential steps toward testing this hypothesis.

The experiments discussed here raise the interesting possibility that N-linked glycosylation may be a previously unrecognized tumor suppression mechanism. Further investigation will clarify this putative link between glycosylation, ER stress, and currently acknowledged neoplastic tumor suppressors in controlling cell polarity and proliferation.

Materials and Methods

Drosophila genetics

Drosophila were raised under standard conditions. The following stocks were used: MS1096-GAL4/FM7c;; UAS-lgl-IR #9/TM3 (MS>lgl-IR), *tid^{1}/CyO*, *tid^{2} kr/CyO*, *tid^{1} FRT42/CyO twi-GAL4 UAS-GFP*, *tid^{2} kr FRT42/CyO twi-GAL4 UAS-GFP*, *tid^{2} FRT42/CyO twi-GAL4 UAS-GFP*, *Df(2R)tid kr/CyO* (B#6148), P{EPgy2}l(2)not^{EY01896}/CyO (not^{P}, B#15380), *GMR-GAL4^{F} UAS-Crb^{intra}*/CyO (*GMR>Crb^{I}*), *Df(1)BSC537/FM7* (Ost48 Df, B25065), Df(1)Exel6236/FM7c (Rft1 Df, B7710), *PBac{w[+mC]=PB}CG11851^{c02021}/TM6B* (alg9^{PBac}, B10802), *Sp/CyO twi-GAL4 UAS-GFP; scrib^{dt14}/TM6B*, *Sp/CyO twi-GAL4 UAS-GFP; scrib^{dt6}/TM6B*, *scrib2/TM6B*, *tid^{2} FRT42/CyO twi-GAL4 UAS-GFP; scrib^{2} e FRT82/TM6C*, *UAS-Ras^{V12}/CyO*, *UAS-Ras^{V12}/CyO, alg9^{PBac} FRT82/TM6B*, *UAS-Ras^{V12}/CyO; scrib^{1}/TM6C*, *w eyFLP 1 UASGFP; tubGAL4 FRT82 tubGAL80/TM6B* (eyMARCM82), *yw eyflp; tub-Gal80, FRT40A; act>y+>Gal4 UAS-GFP^{s56T}* (eyMARCM40), *yw eyFLP; FRT42 cl/CTG* (eyFLP42cl), *UAS-BiP^{DN}* (T. Jongens), *MS1096-GAL4, w;P[hs neo; ry+]FRT 82 iso A ("iso82"), w;P[hs neo; ry+]FRT 42 iso A ("iso42"), w;P[hs neo; ry+]FRT 40A iso A ("iso40"), Sp/CyO twi-GAL4 UAS-GFP; tub-Not(2-1)*.

The original *tid^{1}* and *tid^{2}* stocks were tested for complementation to each other, a *tid*-removing deficiency (*Df(2R)tid*), and a *l(2)not* P-insertion (*not^{P}*). Both *tid* alleles failed to complement the other allele, the Df and *not^{P}*. This was also true of the FRT recombinants. Additionally, we tested the *tid* stocks for complementation to an *lgl* null allele (*lgl^{4}*). The "original" *tid^{1}* stock failed to complement *lgl*, although the *tid^{1} FRT42* recombinant did complement *lgl*, suggesting that the original allele at some point acquired a lesion in the *lgl* locus, which was eliminated during the FRT recombination. We have therefore taken care to use only *tid^{2} FRT42/tid^{1} FRT42* transheterozygotes or *tid^{2}/Df(2R)tid* hemizygotes in our analysis.

Interaction assays

The *lgl*-IR stock was crossed to alleles of candidate interactors. Non-balanced F1 female progeny were collected. Right-side wings were removed and mounted in Euparal (Carolina Biologicals) dorsal-side up and imaged using a Z16 APO microscope (Leica) with a Planapo 2.0x lens, fitted with a DFC300 FX camera.

Sequencing tid alleles

Genomic DNA was isolated from 50 hemizygous larvae per sample using the 30 Fly Prep protocol (BDGP). The *tid/not* genomic region was amplified with Phusion high fidelity DNA polymerase (NEB) using the following primers: 5'-TTAATTTTCGCCGGTTATCA-3' (l(2)not-F) and 5'-ACTCAGACCATTTTACTGCA-3' (l(2)not-R). Amplicons were gel-purified and sequenced using forward and reverse primers arrayed across the amplicon. Sequence data were aligned and analyzed using ContigExpress (Vector NTI); sequences from mutant larvae were compared to the FlyBase sequences for *l(2)not* and *tid*. Additionally, genomic DNA from rescue stocks was isolated and sequenced using primers around the individual *tid^{1}* and *tid^{2}* lesions to confirm their presence in the stocks used for rescue experiments.

Generating rescue constructs

The *not* coding sequence was amplified from cDNA FI07241 (S. Celniker) using the following primers: 5'-GCGGCCGCTATCACAGAAATGGCCCC-3' and 5'-TCTAGATTACTGCAGCTTTTTCTGTT-3'. Amplicons were gel purified and ligated into the pGEM-T Easy vector (Promega). Clones were checked for inserts, and inserts were moved into pCasperHS and pCasperTub (S. Eaton) by cleaving with NotI and XbaI. Rescue constructs were sequence verified and embryos were injected and isolated by Genetic Services, Inc. Insertions mapped to chromosome III were identified and stocked.

Making FRT recombinants

The tid^{1} and tid^{2} alleles were recombined onto the FRT42 ("iso42" stock) chromosome. Stocks were screened for the presence of FRT42 by the ability to form clones in the eye. Stocks were screened for presence of the tid lesions by complementation testing against the other allele. Additionally, the *kr* mutation was separated from tid^{2} by first crossing to an iso42 stock and isolating tid^{2} mutants lacking *kr*, then a second round of recombination was performed against iso42 to recombine the tid^{2} lesion (without *kr*) onto the FRT42 chromosome. Recombinants were verified in the same manner as the initial tid^{1} and tid^{2} recombinants. The alg^{PBac} insertion was recombined onto the FRT82 ("iso82" stock) chromosome. a$lg9^{PBac}$ presence was scored by complementation testing against a deficiency covering alg9 (B#24965). The presence of FRT82 was scored by crossing to the eyFLP82cl tester stock.

Cuticle preparations of tid maternal zygotic mutants

The tid^{2} *kr FRT42/CyO twi-GAL4 UAS-GFP* and iso42 stocks were crossed to *hs-flp slobo-lacZ/Y; FRT42* ovo^{D1}*/CyO* males. F1 progeny were heat shocked at 37°C for 2 hours over 2 consecutive days during pupal stages. F1 females carrying hs-flp and both FRT-marked chromosomes were collected and crossed to tid^{1}*/CyO twi-GAL4 UAS-GFP.* Maternal zygotic mutant embryos were selected based on lack of GFP signal and dechroionated for 5 minutes in bleach, rinsed, dried, and washed in 0.1% Triton X-100 in water. Embryos were mounted in Hoyer's media and heated overnight at 65°C. Images were collected using bright field microscopy on an Axioplan microscope.

Immunohistochemistry

Imaginal discs were dissected, fixed and stained using standard procedures. The following primary antibodies and dilutions were used: Chp 1:20 (DSHB), aPKC 1:1000 (Sigma), Dlg (4F3) 1:100, Crb 1:50 (A. Wodarz), scrib 1:100, cad87a (Fung *et al.*, 2008), E-cad 1:50 (DSHB), arm 1:100 (DSHB), Cor 1:100 (mix of 2 DSHB monoclonals), Wg 1:100 (DSHB), Sens 1:1000 (H. Bellen), Elav 1:50 (DSHB), Cut 1:100 (DSHB), phalloidin 1:250 (Sigma). Secondary fluorophore-conjugated antibodies were from Molecular Probes. For non-permeabilized Chaoptin stains, discs were processed in PBS without any detergent until after primary antibodies had been removed. Confocal images are single optical cross sections collected on a Leica TCS confocal microscope.

Chp western

For the *alg3* sample, the eye-antennal discs and optic lobes were removed from 30 wandering L3 larvae and transferred to a tube containing 1X sample buffer, then boiled 5 minutes. The iso40 sample was prepared by removing the heads from 5 adult male iso40 flies, then grinding in 60µL 1X sample buffer. Gel lanes were loaded with all of the *alg3* extract or 0.2 heads' worth in volume. Proteins were electrophoresed and blotted using standard protocols. Anti-Chp (N8A, source) was used at 1:1000. HRP-conjugated anti-mouse secondary was used at 1:5000. Blot was developed with standard ECL reagents.

Xbp1 splicing

Wing imaginal discs (15-20 per sample) were dissected from wandering L3 larvae in cold M3 media on ice and transferred to 80µL RNALater (Qiagen) and stored at 4°C overnight. Total RNA was extracted using the Qiagen RNeasy mini purification kit. RNA concentration was determined using a Nanodrop, and 400ng were treated with DNase (followed by heat inactivation) then used in a cDNA transcription reaction (SuperScript® III First-strand synthesis SuperMix for qRT-PCR, Invitrogen). Sample was treated with RNAse, then diluted 1:10 for use as template in a PCR reaction using previously published Xbp1 primers (source). PCR products were electrophoresed on a 2.5 or 3% agarose gel.

Figure 5.1. *tid* alleles genetically interact with the polarity regulators *Crb* and *lgl.*
A: Reducing *lgl* function in the dorsal compartment of the developing wing by driving an *lgl*-RNAi construct with *MS1096-GAL4* (*MS1096>lgl-IR*) leads to mild wing formation defects. When this line is crossed to the *tid* alleles tid^{1} (B) or tid^{2} (C), a P element inserted in the *not* coding sequence (not^{P}, D) or a deficiency that removes both *l(2)not* and *tid* (*Df(2R)tid*, E), the *lgl*-IR wing phenotype is noticeably enhanced.
B: Expressing an activated form of the Crb protein (Crb^{intra}) under control of the *GMR-GAL4* driver leads to a rough eye phenotype (*GMR>*Crb^{I}, G, compare to wild-type in F-F'). In this background, tid^{1} heterozygosity dramatically enhances the *GMR>*Crb^{I} phenotype, and the eye tissue is nearly completely gone.

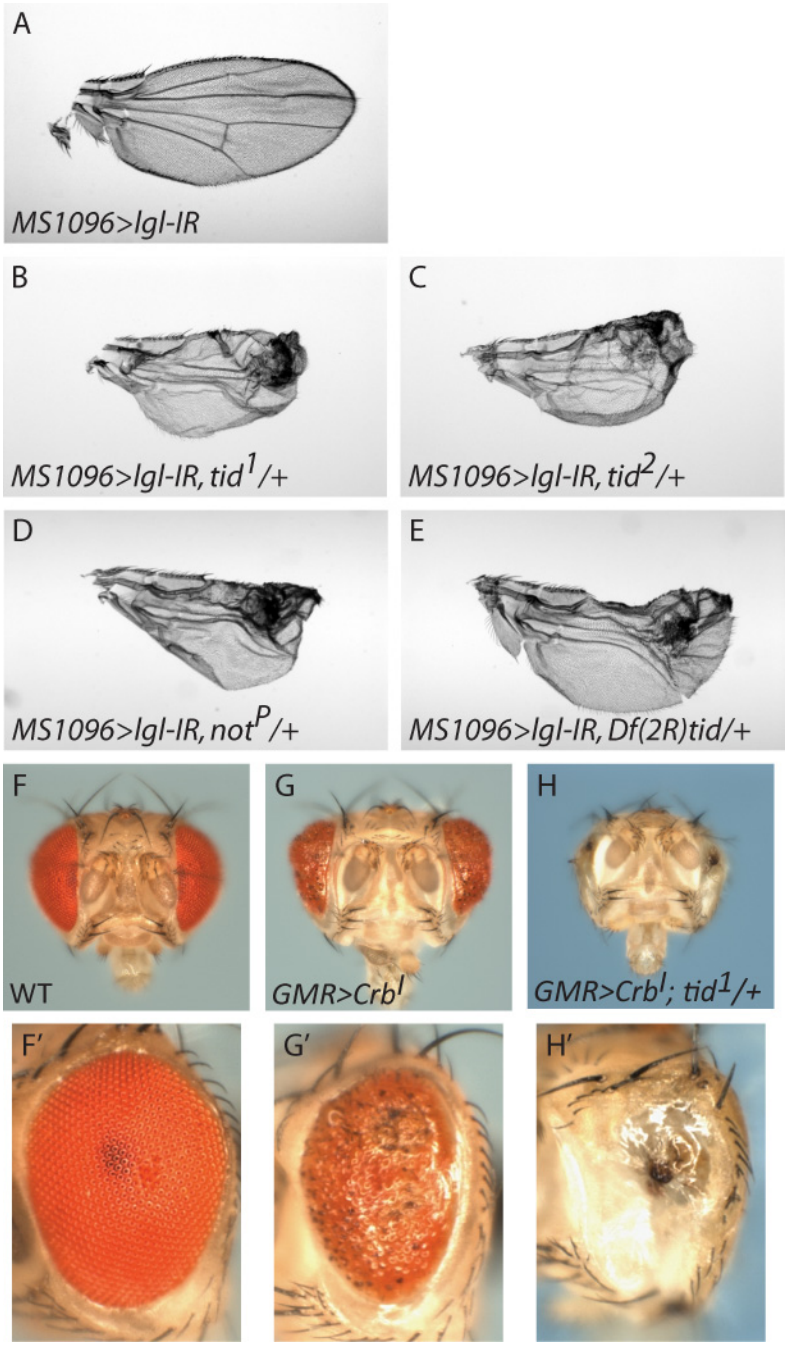
A
MS1096>lgl-IR
B
MS1096>lgl-IR, tid1/+
C
MS1096>lgl-IR, tid2/+
D
MS1096>lgl-IR, notP/+
E
MS1096>lgl-IR, Df(2R)tid/+
F
WT
G
GMR>Crb1
H
GMR>Crb1; tid1/+
F′
G′
H′

Figure 5.2. Sequencing and phenotypic characterization of *tid*^{1} and *tid*^{2}.
A: Sequencing the entire genomic region containing *l(2)not* and *tid* in genomic DNA isolated from *tid*^{1}*/Df* or *tid*^{2}*/Df* hemizygous larvae identified lesions in the *l(2)not* coding sequence in each allele.
B-D': Wild-type eye imaginal discs have a stereotyped size and shape, as shown by actin staining to outline cells (red, B), and do not express the matrix metalloprotease Mmp1, a marker of neoplastic tissue (green, B'). *tid*^{1} or *tid*^{2} hemizygous larvae show disrupted tissue morphology (C-D) and areas of the eye discs express Mmp1 (C'-D').
E-G: When homozygous eye discs are generated in otherwise heterozygous larvae using the eyFLP-cell lethal system, the *tid*^{1} and *tid*^{2} alleles lead to relatively mild tissue architecture defects, yet these animals fail to eclose, dying during early stages of pupal development.
H-I: Ectopically expressing the *not* coding sequence under control of a constitutive tubulin promoter (*tub-Not*) completely rescues the tissue architecture and growth defects of *tid*^{2}*/tid*^{1} transheterozygous larvae (I, compare to *tid*^{2}*/tid*^{1} in H). These larvae develop into adults, as opposed to the *tid*^{2}*/tid*^{1} animals, which die as pupae.
Scale bars, 100µm.

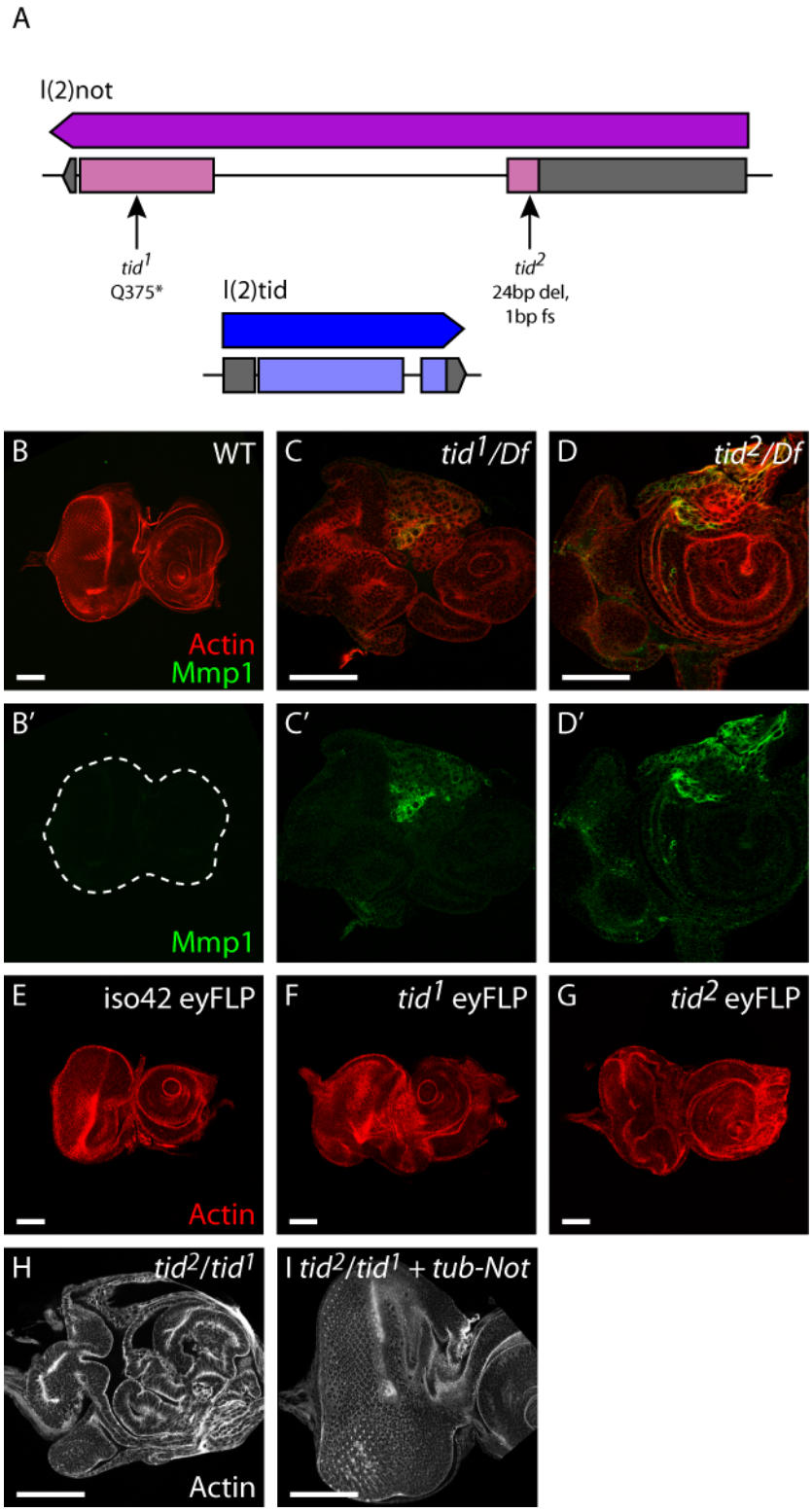
A
l(2)not
tid1
Q375*
l(2)tid
tid2
24bp del,
1bp fs
B
WT
Actin
Mmp1
C
tid1/Df
D
tid2/Df
B′
Mmp1
C′
D′
E
iso42 eyFLP
Actin
F
tid1 eyFLP
G
tid2 eyFLP
H
tid2/tid1
Actin
I tid2/tid1 + tub-Not

Figure 5.3. The N-linked glycosylation pathway is required for growth control in imaginal discs.

A: Depiction of the lipid-linked oligosaccharide synthesis steps of the N-linked glycosylation pathway. Outlined in red are *alg* mutants analyzed in this study. Red circles represent mannose monomers added in the cytosol, yellow circles represent mannose sugars added in the ER lumen. Modified from Lehle *et al*. 2006.

B-D: Larvae homozygous for a PiggyBac transposon insertion in the *alg9* locus ($alg9^{PBac}$, D) show epithelial tissue defects similar to those seen in *alg3* mutants (C). Wing imaginal discs of *alg3* or *alg9* mutants show irregular tissue folding and are misshapen compared to wild-type discs (B). *alg3* mutant shown is from tid^{2}/tid^{1} transheterozygotes. Tissues stained with phalloidin to label actin outlining the cells.

E-G: Homozygous mutant $alg9^{PBac}$ eye discs generated using the eyFLP-cell lethal system (G) show slightly irregular tissue morphology consistent with the tissue defects of *alg3* eyFLP-cell lethal discs (F). Wild-type eye disc shown in E for comparison. *alg3* discs generated with the tid^{1} allele. Tissues stained for actin to outline cells.

H-J: Discs stained for the glycosylated protein Chaoptin (Chp, green) and actin in red. Chp is present in photoreceptor cells in wild-type (H), *alg3* (I) and $alg9^{PBac}$ (J) mutant discs. *alg3* mutant is the tid^{1}/tid^{2} transheterozygote.

K-L: In nonpermeabilized tissues, an anti-Chp antibody stains photoreceptor cells in wild-type (K) and *alg3* mutant discs, indicating that Chp is being trafficked to the cell surface. *alg3* mutant is the tid^{1}/tid^{2} transheterozygote.

M: Western blot for Chaoptin (Chp) protein in wild-type and *alg3* imaginal discs. Chp is present in *alg3* discs, but is a smaller molecular weight. *alg3* mutant is the tid^{1}/tid^{2} transheterozygote.

Scale bar, 100µm.

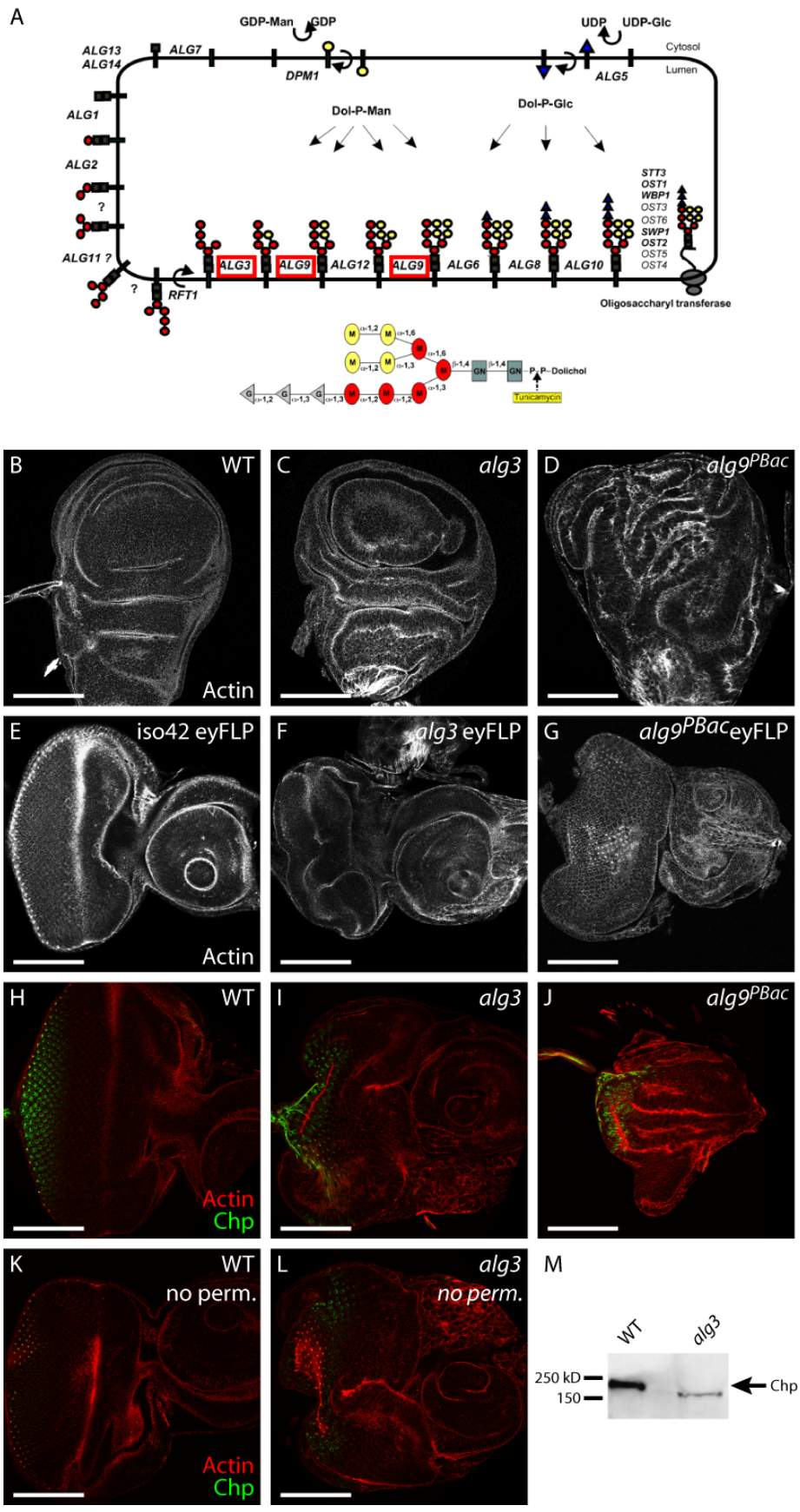
A
GDP-Man
GDP
UDP
UDP-Glc
Cytosol
Lumen
ALG13
ALG14
ALG7
DPM1
ALG5
ALG1
ALG2
Dol-P-Man
Dol-P-Glc
STT3
OST1
WBP1
OST3
OST6
SWP1
OST2
OST5
OST4
ALG11 ?
ALG3
ALG9
ALG12
ALG9
ALG6
ALG8
ALG10
RFT1
Oligosaccharyl transferase
Tunicamycin
B
WT
Actin
C
alg3
D
alg9PBac
E
iso42 eyFLP
Actin
F
alg3 eyFLP
G
alg9PBac eyFLP
H
WT
Actin
Chp
I
alg3
J
alg9PBac
K
WT
no perm.
Actin
Chp
L
alg3
no perm.
M
WT
alg3
250 kD
150
Chp

Figure 5.4. Multiple genes in the N-linked glycosylation pathway interact with *lgl*.
A: Knocking down *lgl* in the developing wing by RNA interference (*MS1096>lgl-IR*) leads to mild defects in wing morphology. Removing a single genomic copy of *alg9* (B), *Ost48* (C) or *Rft1* (D) enhances the *lgl*-IR phenotype.

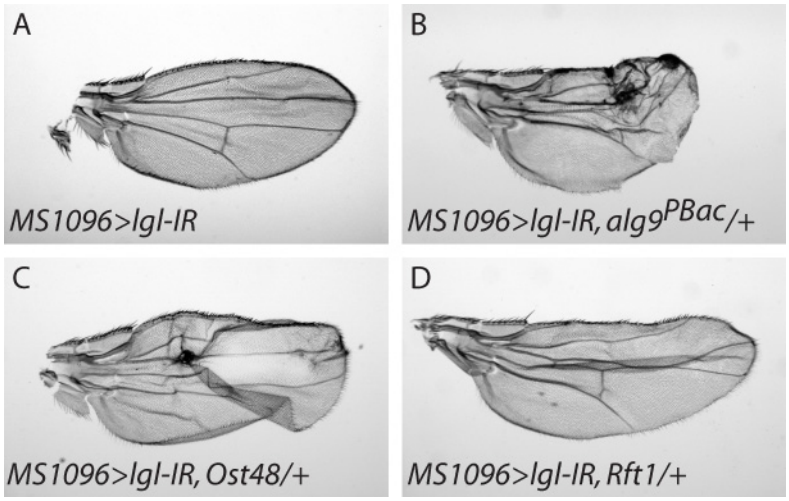
A
MS1096>lgl-IR
B
MS1096>lgl-IR, alg9PBac/+
C
MS1096>lgl-IR, Ost48/+
D
MS1096>lgl-IR, Rft1/+

Figure 5.5. Analysis of apicobasal polarity in *alg3* mutant discs.
A-D: Apicobasal polarity is conserved in *alg3* mutant wing discs. The apical markers aPKC (green, A-B) and Crumbs (Crb, green, C-D) and the basolateral markers Discs Large (Dlg, red, A-B) and Scribble (Scrib, red, C-D) label distinct domains in wild-type cells (A, C). In *alg3* mutant discs, these domain distinctions are still present (B, D).
E-H: The protein Cadherin87A (Cad87A) localizes to apical membranes in wild-type wing imaginal discs (E-F). In *alg3* mutant discs, Cad87A retains its apical localization (G-H).
I-J': Levels of the junctional proteins E-Cadherin (E-Cad, green) and Armadillo (Arm, red) were significantly reduced in *alg3* mutant discs (J-J') compared to identically stained and imaged wild-type discs (I-I'). However, this result is inconsistent, as ECad levels are not always reduced in *alg3* discs relative to wild-type (K-L).
M: Wild-type embryos secrete a complete layer of cuticle, including denticle belts. Maternal/zygotic *alg3* mutant embryos develop to late stages and can secrete cuticle, but many embryos display ventral holes in the cuticle and improperly formed denticle belts (N-O).
For each imaginal disc panel labeled *alg3,* discs are from the tid^{1}/tid^{2} transheterozygote. Scale bar, 25µm in A-D, F and H. 100µm in E, G, I-L.

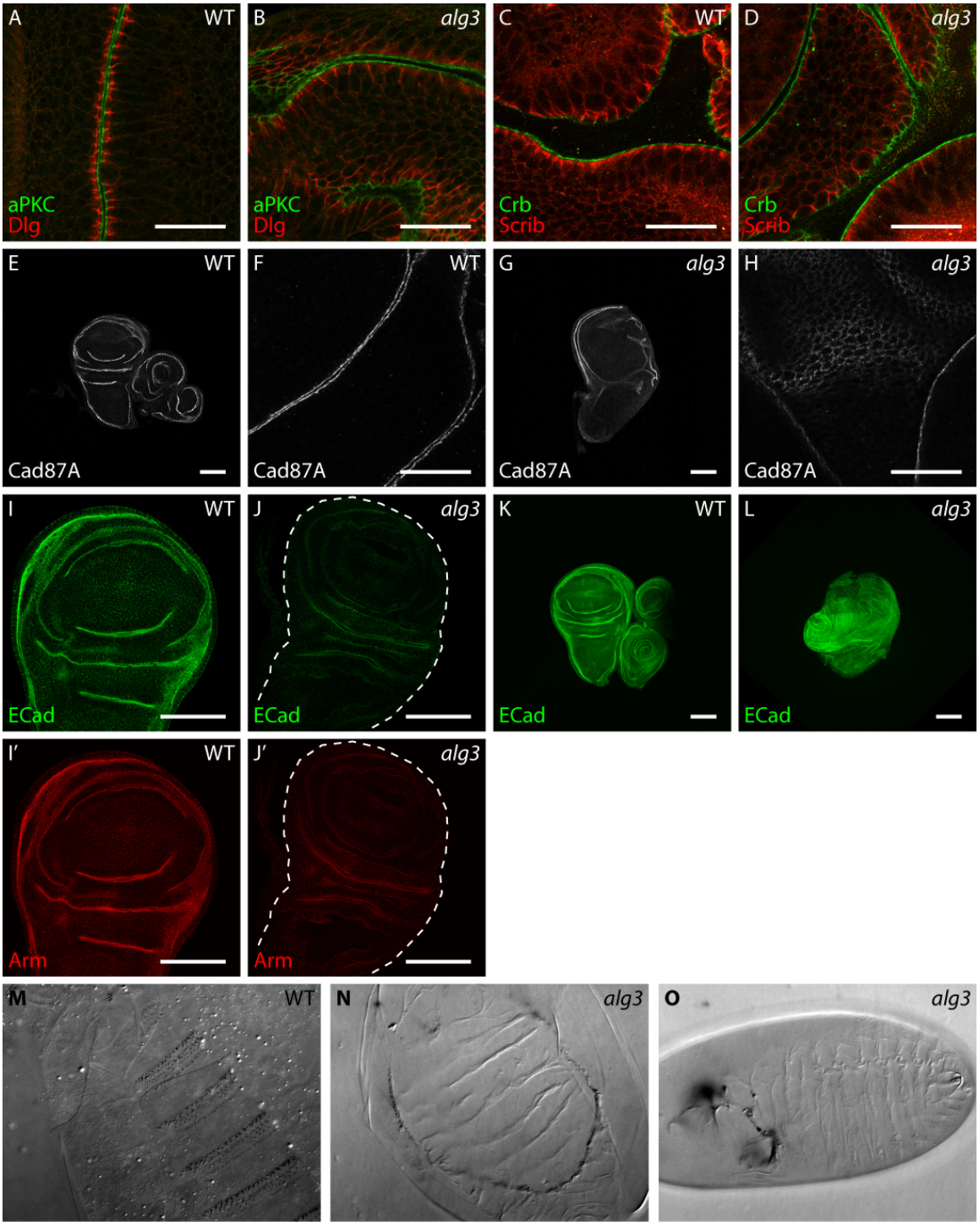
A
WT
aPKC
Dlg
B
alg3
aPKC
Dlg
C
WT
Crb
Scrib
D
alg3
Crb
Scrib
E
WT
Cad87A
F
WT
Cad87A
G
alg3
Cad87A
H
alg3
Cad87A
I
WT
ECad
J
alg3
ECad
K
WT
ECad
L
alg3
ECad
I'
WT
Arm
J'
alg3
Arm
M
WT
N
alg3
O
alg3

Figure 5.6. Signaling pathways in *alg3* mutant discs.
A-B: In wild-type imaginal wing discs, Coracle (Cor) is localized along the lateral membranes of the disc proper cells (below red dashed line) and in the squamous peripodial membrane (above red line) (A). In *alg3* mutant discs, Coracle is present on disc proper lateral membranes, though at levels much lower than are found in the peripodial membrane. In addition, cells in the peripodial membrane of *alg3* discs are much taller than in wild-type discs (B).
C-D': Wingless (Wg, green) is expressed in a stripe across the wing pouch in wild-type imaginal wing discs (C, C'). Senseless (Sens, red), a wingless signaling target, is expressed in two stripes on either side of the Wg stripe. In *alg3* mutant discs, the Wg and Sens patterns are still present, although the Sens signal is less robust (D-D').
E-F': Differentiated cells marked by Elav staining (blue) are present in wild-type and *alg3* eye imaginal discs (E, F). In wild-type discs, Cut staining (green) marks the interommatidial cells in between the differentiating photoreceptors (E'). In *alg3* discs, the patterning of differentiating photoreceptors and the expression of Cut are severely impaired (F', compare to WT in E').
For each imaginal disc panel labeled *alg3,* discs are from the tid^{1}/tid^{2} transheterozygote. Scale bar, 25µm in A-B, C', D', E' and F'. 100µm in C, D, E, F.

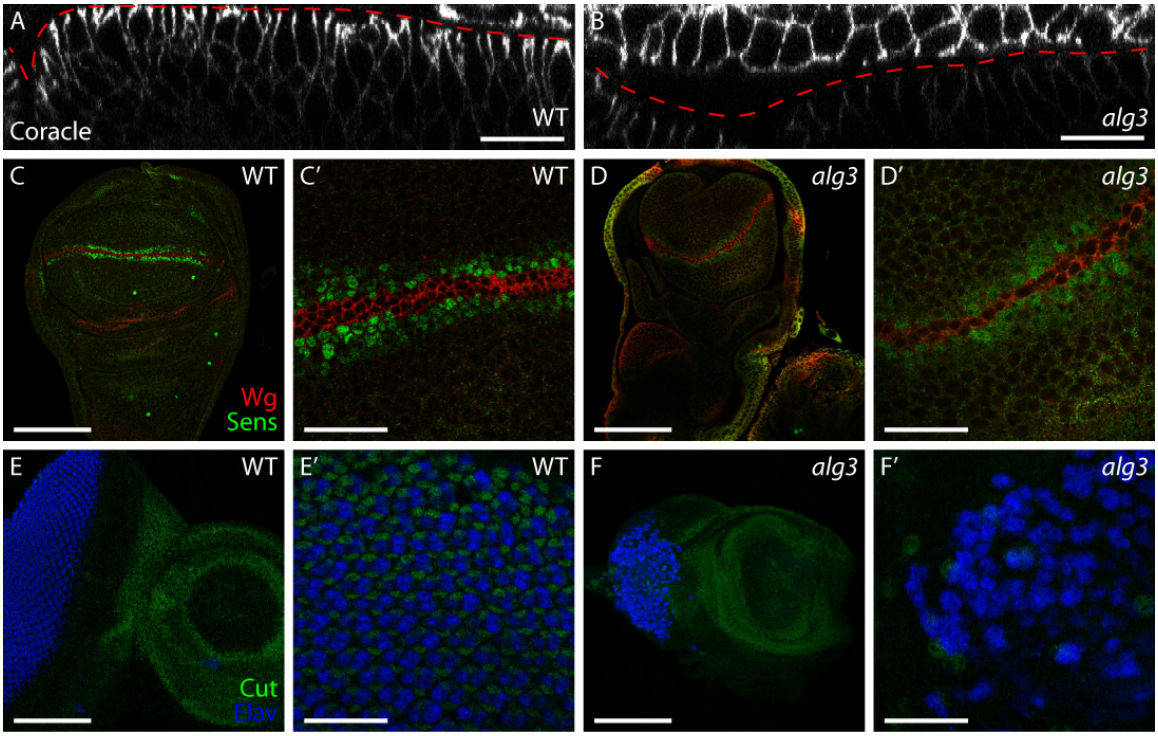
A
Coracle
WT
B
alg3
C
WT
Wg
Sens
C′
WT
D
alg3
D′
alg3
E
WT
Cut
Elav
E′
WT
F
alg3
F′
alg3

Figure 5.7. N-linked glycosylation mutants cooperate with tumor suppressor pathways.

A: Mutant clones generated with the eyMARCM system of *alg9*^{PBac} in the eye imaginal disc and the optic lobes marked with GFP do not have an obvious phenotype – the discs look essentially wild-type. Tissues are counterstained for actin (red) to outline cells. OL, optic lobes. VNC, ventral nerve cord. ID, imaginal discs.

B: eyMARCM clones marked with GFP that express Ras^{V12} but are otherwise wild-type have irregular morphologies but never invade the ventral nerve cord (VNC).

C: eyMARCM clones of a *scrib* null allele also expressing Ras^{V12} form neoplastic masses and cells invade the VNC (arrows).

D: eyMARCM clones of *alg9* also expressing Ras^{V12} do not invade the VNC, but do show dramatic overgrowth that is not present in *alg9* or Ras^{V12} clones alone (compare to A and B).

E-H: Removing a single copy of *alg3* in a *scrib*^{dt14}*/scrib*^{2} or *scrib*^{dt6}*/scrib*^{2} background does not modify the *scrib* hypomorphic phenotype (F and H, compare to *scrib* hypomorphs in E and G).

I-K: Removing a single copy of *scrib* in the *alg3* mutant background (K-L) enhances the *alg3* phenotype (I, J) to generate highly folded imaginal discs. This high degree of folding and architecture disruption is not seen in *alg3* mutant discs.

alg3 refers to the *tid*^{1}*/tid*^{2} transheterozygote. *alg3/+* refers to *tid*^{2}*/+.*

Scale bars, 100µm.

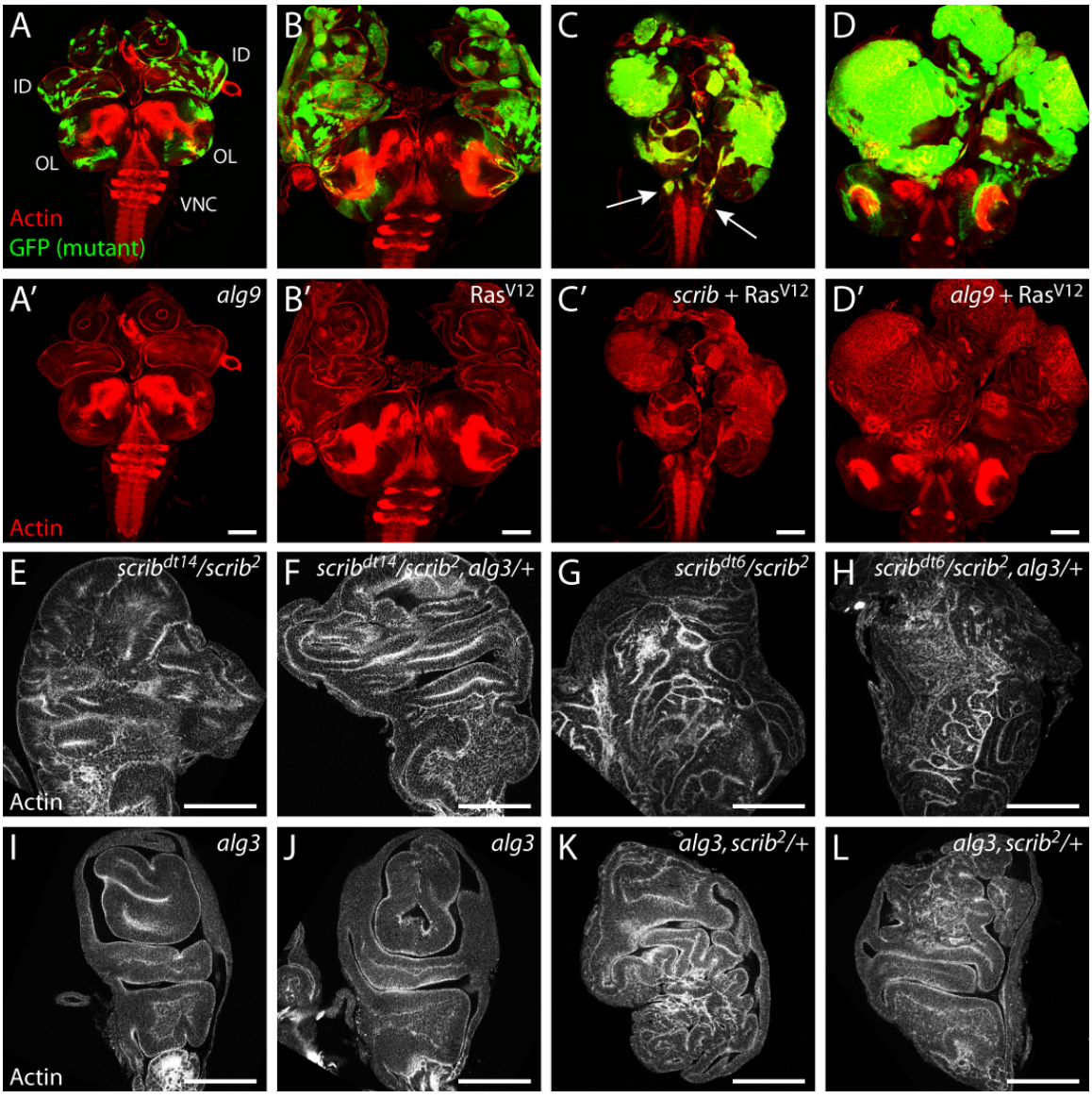
A
ID
ID
OL
OL
VNC
Actin
GFP (mutant)
B
C
D
A′
alg9
Actin
B′
RasV12
C′
scrib + RasV12
D′
alg9 + RasV12
E
scribdt14/scrib2
Actin
F
scribdt14/scrib2, alg3/+
G
scribdt6/scrib2
H
scribdt6/scrib2, alg3/+
I
alg3
Actin
J
alg3
K
alg3, scrib2/+
L
alg3, scrib2/+

Figure 5.8. The Unfolded Protein Response may be activated in *alg* and *scrib* mutant tissues.

A: Initial RT-PCR experiment to assess the activation state of the Unfolded Protein Response (UPR) based on splicing of the *Xbp1* mRNA. Under normal conditions (iso40), primers against *Xbp1* amplify a single band of ~120bp consistent with the unspliced *Xbp1* mRNA. In *alg3*, *alg9*, and *scrib* mutant tissues, the *Xbp1* primers also amplify a faint second band below the unspliced form, consistent with the presence of spliced *Xbp1* mRNA and UPR activation. *HP1* primers are included as a control. The *HP1* primers amplify an ~80bp fragment from cDNA, and a ~300bp fragment from any contaminating genomic DNA.

B: Second RT-PCR experiment to assess UPR activation. *HP1* primers are again included as a control reaction. With *Xbp1* primers, the unspliced *Xbp1* mRNA is present in wings from iso40, *scrib*, and $alg9^{PBac}$ larvae, or larvae expressing a $UAS\text{-}BiP^{DN}$ construct under control of *MS1096-GAL4* ($MS>BiP^{DN}$), which ectopically activates the UPR. No spliced *Xbp1* mRNA is present in the iso40, *scrib* or $MS>BiP^{DN}$ samples, though there is a smaller band present in the *alg9* sample.

alg3 refers to the tid^1/tid^2 transheterozygote.

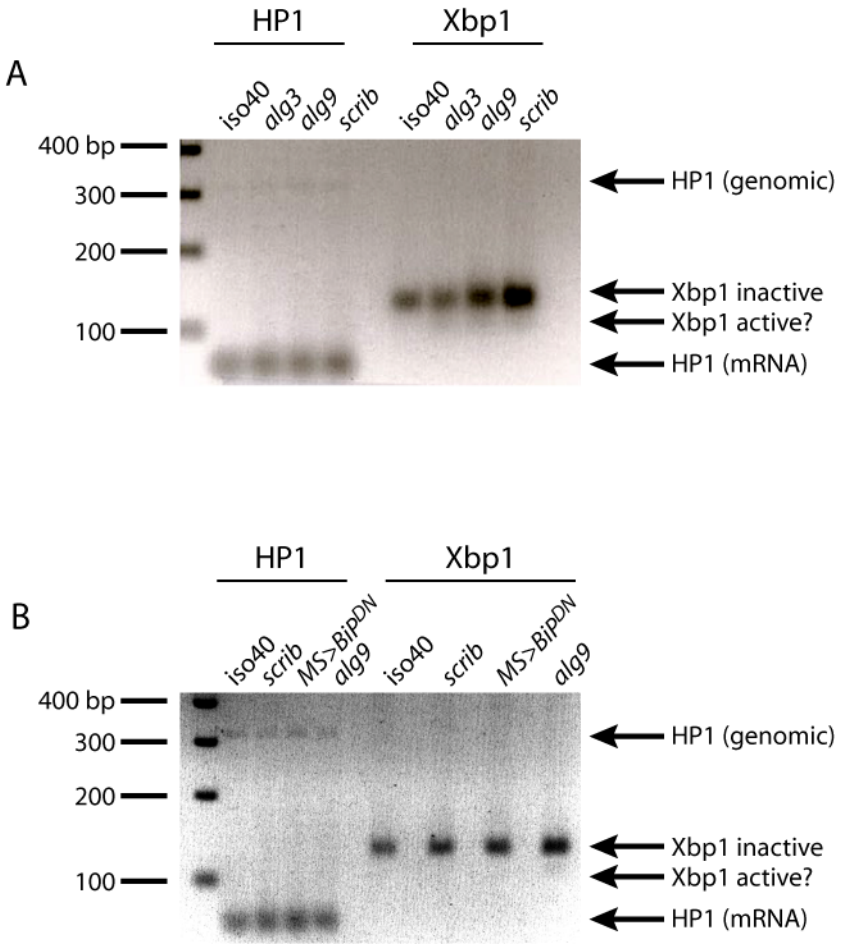
A
HP1
Xbp1
iso40
alg3
alg9
scrib
iso40
alg3
alg9
scrib
400 bp
300
200
100
HP1 (genomic)
Xbp1 inactive
Xbp1 active?
HP1 (mRNA)
B
HP1
Xbp1
iso40
scrib
MS>BiPDN
alg9
iso40
scrib
MS>BiPDN
alg9
400 bp
300
200
100
HP1 (genomic)
Xbp1 inactive
Xbp1 active?
HP1 (mRNA)

References

Aalto, M.K., Ronne, H., Nen, K., and S. (1993). Yeast syntaxins Sso1p and Sso2p belong to a family of related membrane proteins that function in vesicular transport. EMBO J. *12*, 4095-4104.

Aceto, D., Beers, M., and Kemphues, K.J. (2006). Interaction of PAR-6 with CDC-42 is required for maintenance but not establishment of PAR asymmetry in C. elegans. Dev Biol *299*, 386-397.

Aebi, M., Gassenhuber, J., Domdey, H., and te Heesen, S. (1996). Cloning and characterization of the ALG3 gene of Saccharomyces cerevisiae. Glycobiology *6*, 439-444.

Agrawal, N., Kango, M., Mishra, A., and Sinha, P. (1995). Neoplastic transformation and aberrant cell-cell interactions in genetic mosaics of lethal(2)giant larvae (lgl), a tumor suppressor gene of Drosophila. Dev Biol *172*, 218-229.

Andrews, R., and Ahringer, J. (2007). Asymmetry of early endosome distribution in C. elegans embryos. PloS one *2*, e493.

Aranda, V., Haire, T., Nolan, M.E., Calarco, J.P., Rosenberg, A.Z., Fawcett, J.P., Pawson, T., and Muthuswamy, S.K. (2006). Par6-aPKC uncouples ErbB2 induced disruption of polarized epithelial organization from proliferation control. Nat Cell Biol *8*, 1235-1245.

Arquier, N., Perrin, L., Manfruelli, P., and Semeriva, M. (2001). The Drosophila tumor suppressor gene lethal(2)giant larvae is required for the emission of the Decapentaplegic signal. Development *128*, 2209-2220.

Baas, A.F., Kuipers, J., van der Wel, N.N., Batlle, E., Koerten, H.K., Peters, P.J., and Clevers, H.C. (2004). Complete polarization of single intestinal epithelial cells upon activation of LKB1 by STRAD. Cell *116*, 457-466.

Bae, M.K., Jeong, J.W., Kim, S.H., Kim, S.Y., Kang, H.J., Kim, D.M., Bae, S.K., Yun, I., Trentin, G.A., Rozakis-Adcock, M., and Kim, K.W. (2005). Tid-1 interacts with the von Hippel-Lindau protein and modulates angiogenesis by destabilization of HIF-1alpha. Cancer Res *65*, 2520-2525.

Balklava, Z., Pant, S., Fares, H., and Grant, B.D. (2007). Genome-wide analysis identifies a general requirement for polarity proteins in endocytic traffic. Nat Cell Biol *9*, 1066-1073.

Bänziger, C., Soldini, D., Schütt, C., Zipperlen, P., Hausmann, G., and Basler, K. (2006). Wntless, a conserved membrane protein dedicated to the secretion of Wnt proteins from signaling cells. Cell *125*, 509-522.

Barbieri, M.A., Hoffenberg, S., Roberts, R., Mukhopadhyay, A., Pomrehn, A., Dickey, B.F., and Stahl, P.D. (1998). Evidence for a symmetrical requirement for Rab5-GTP in in vitro endosome-endosome fusion. J. Biol. Chem. *273*, 25850-25855.

Barros, C.S., Phelps, C.B., and Brand, A.H. (2003). Drosophila nonmuscle myosin II promotes the asymmetric segregation of cell fate determinants by cortical exclusion rather than active transport. Dev Cell *5*, 829-840.

Benting, J.H., Rietveld, A.G., and Simons, K. (1999). N-Glycans mediate the apical sorting of a GPI-anchored, raft-associated protein in Madin-Darby canine kidney cells. J Cell Biol *146*, 313-320.

Benton, R., and St Johnston, D. (2003). Drosophila PAR-1 and 14-3-3 inhibit Bazooka/PAR-3 to establish complementary cortical domains in polarized cells. Cell *115*, 691-704.
Betschinger, J., Mechtler, K., and Knoblich, J.A. (2003). The Par complex directs asymmetric cell division by phosphorylating the cytoskeletal protein Lgl. Nature *422*, 326-330.
Bilder, D. (2003). PDZ domain polarity complexes. Curr Biol *13*, R661-662.
Bilder, D. (2004). Epithelial polarity and proliferation control: links from the Drosophila neoplastic tumor suppressors. Genes Dev. *18*, 1909-1925.
Bilder, D., Li, M., and Perrimon, N. (2000). Cooperative regulation of cell polarity and growth by Drosophila tumor suppressors. Science *289*, 113-116.
Bilder, D., and Perrimon, N. (2000). Localization of apical epithelial determinants by the basolateral PDZ protein Scribble. Nature *403*, 676-680.
Bischof, J., Maeda, R.K., Hediger, M., Karch, F., and Basler, K. (2007). An optimized transgenesis system for Drosophila using germ-line-specific phiC31 integrases. Proceedings of the National Academy of Sciences of the United States of America *104*, 3312-3317.
Blankenship, J.T., Fuller, M.T., and Zallen, J.A. (2007). The Drosophila homolog of the Exo84 exocyst subunit promotes apical epithelial identity. J Cell Sci *120*, 3099-3110.
Bock, J.B., Matern, H.T., Peden, A.A., and Scheller, R.H. (2001). A genomic perspective on membrane compartment organization. Nature *409*, 839-841.
Boyd, C., Hughes, T., Pypaert, M., and Novick, P. (2004). Vesicles carry most exocyst subunits to exocytic sites marked by the remaining two subunits, Sec3p and Exo70p. J Cell Biol *167*, 889-901.
Brumby, A.M., and Richardson, H.E. (2003). scribble mutants cooperate with oncogenic Ras or Notch to cause neoplastic overgrowth in Drosophila. Embo J *22*, 5769-5779.
Bryant, D.M., and Mostov, K.E. (2008). From cells to organs: building polarized tissue. Nat Rev Mol Cell Biol *9*, 887-901.
Bryant, N.J., Piper, R.C., Gerrard, S.R., and Stevens, T.H. (1998). Traffic into the prevacuolar/endosomal compartment of Saccharomyces cerevisiae: a VPS45-dependent intracellular route and a VPS45-independent, endocytic route. Eur. J. Cell Biol. *76*, 43-52.
Bucci, C., Parton, R.G., Mather, I.H., Stunnenberg, H., Simons, K., Hoflack, B., and Zerial, M. (1992). The small GTPase Rab5 functions as a regulatory factor in the early endocytic pathway. Cell *70*, 715-728.
Cai, H., Reinisch, K., and Ferro-Novick, S. (2007). Coats, Tethers, Rabs, and SNAREs Work Together to Mediate the Intracellular Destination of a Transport Vesicle. Dev Cell *12*, 671-682.
Carpp, L.N., Ciufo, L.F., Shanks, S.G., Boyd, A., and Bryant, N.J. (2006). The Sec1p/Munc18 protein Vps45p binds its cognate SNARE proteins via two distinct modes. J. Cell Biol. *173*, 927-936.
Carr, C.M., Grote, E., Munson, M., Hughson, F.M., and Novick, P.J. (1999). Sec1p binds to SNARE complexes and concentrates at sites of secretion. J. Cell Biol. *146*, 333-344.
Chabu, C., and Doe, C.Q. (2008). Dap160/intersectin binds and activates aPKC to regulate cell polarity and cell cycle progression. Development *135*, 2739-2746.

Chen, C.Y., Chiou, S.H., Huang, C.Y., Jan, C.I., Lin, S.C., Hu, W.Y., Chou, S.H., Liu, C.J., and Lo, J.F. (2009). Tid1 functions as a tumour suppressor in head and neck squamous cell carcinoma. The Journal of pathology *219*, 347-355.
Chen, Y.A., and Scheller, R.H. (2001). SNARE-mediated membrane fusion. Nat. Rev. Mol. Cell Biol. *2*, 98-106.
Cheng, H., Cenciarelli, C., Nelkin, G., Tsan, R., Fan, D., Cheng-Mayer, C., and Fidler, I.J. (2005). Molecular mechanism of hTid-1, the human homolog of Drosophila tumor suppressor l(2)Tid, in the regulation of NF-kappaB activity and suppression of tumor growth. Molecular and cellular biology *25*, 44-59.
Chou, T.B., and Perrimon, N. (1996). The autosomal FLP-DFS technique for generating germline mosaics in Drosophila melanogaster. Genetics *144*, 1673-1679.
Christoforidis, S., Mcbride, H.M., Burgoyne, R.D., and Zerial, M. (1999a). The Rab5 effector EEA1 is a core component of endosome docking. Nature *397*, 621-625.
Christoforidis, S., Miaczynska, M., Ashman, K., Wilm, M., Zhao, L., Yip, S.-C., Waterfield, M.D., Backer, J.M., and Zerial, M. (1999b). Phosphatidylinositol-3-OH kinases are Rab5 effectors *1*, 249-252.
Classen, A.K., Bunker, B.D., Harvey, K.F., Vaccari, T., and Bilder, D. (2009). A tumor suppressor activity of Drosophila Polycomb genes mediated by JAK-STAT signaling. Nature genetics *41*, 1150-1155.
Cowles, C.R., Emr, S.D., and Horazdovsky, B.F. (1994). Mutations in the VPS45 gene, a SEC1 homologue, result in vacuolar protein sorting defects and accumulation of membrane vesicles. J. Cell Sci. *107*, 3449-3459.
Davenport, E.L., Morgan, G.J., and Davies, F.E. (2008). Untangling the unfolded protein response. Cell Cycle *7*, 865-869.
De Renzis, S., Sönnichsen, B., and Zerial, M. (2002). Divalent Rab effectors regulate the sub-compartmental organization and sorting of early endosomes *4*, 124-133.
Deborde, S., Perret, E., Gravotta, D., Deora, A., Salvarezza, S., Schreiner, R., and Rodriguez-Boulan, E. (2008a). Clathrin is a key regulator of basolateral polarity. Nature *452*, 719-723.
Deborde, S., Perret, E., Gravotta, D., Deora, A., Salvarezza, S., Schreiner, R., and Rodriguez-Boulan, E. (2008b). Clathrin is a key regulator of basolateral polarity. Nature *452*, 719-723.
Dietzl, G., Chen, D., Schnorrer, F., Su, K.C., Barinova, Y., Fellner, M., Gasser, B., Kinsey, K., Oppel, S., Scheiblauer, S., Couto, A., Marra, V., Keleman, K., and Dickson, B.J. (2007). A genome-wide transgenic RNAi library for conditional gene inactivation in Drosophila *448*, 151-156.
Dockendorff, T.C., Su, H.S., McBride, S.M.J., Yang, Z., Choi, C.H., Siwicki, K.K., Sehgal, A., and Jongens, T.A. (2002). Drosophila lacking dfmr1 activity show defects in circadian output and fail to maintain courtship interest. Neuron *34*, 973-984.
Dollar, G., Struckhoff, E., Michaud, J., and Cohen, R.S. (2002). Rab11 polarization of the Drosophila oocyte: a novel link between membrane trafficking, microtubule organization, and oskar mRNA localization and translation. Development *129*, 517-526.
Drubin, D.G., and Nelson, W.J. (1996). Origins of Cell Polarity. Cell *84*, 335-344.

Dubreuil, R., Byers, T.J., Branton, D., Goldstein, L.S., and Kiehart, D.P. (1987). Drosophilia spectrin. I. Characterization of the purified protein. J. Cell Biol. *105*, 2095-2102.
Dulubova, I., Sugita, S., Hill, S., Hosaka, M., Fernandez, I., Sudhof, T.C., and Rizo, J. (1999). A conformational switch in syntaxin during exocytosis: role of munc18. EMBO J. *18*, 4372-4382.
Eathiraj, S., Pan, X., Ritacco, C., and Lambright, D.G. (2005). Structural basis of family-wide Rab GTPase recognition by rabenosyn-5. Nature *436*, 415-419.
Ebnet, K., Suzuki, A., Horikoshi, Y., Hirose, T., Meyer Zu Brickwedde, M.K., Ohno, S., and Vestweber, D. (2001). The cell polarity protein ASIP/PAR-3 directly associates with junctional adhesion molecule (JAM). Embo J *20*, 3738-3748.
Elefant, F., and Palter, K.B. (1999). Tissue-specific expression of dominant negative mutant Drosophila HSC70 causes developmental defects and lethality. Mol Biol Cell *10*, 2101-2117.
Emery, G., Hutterer, A., Berdnik, D., Mayer, B., Wirtz-Peitz, F., Gaitan, M.G., and Knoblich, J.A. (2005). Asymmetric Rab 11 endosomes regulate delta recycling and specify cell fate in the Drosophila nervous system. Cell *122*, 763-773.
Entchev, E.V., Schwabedissen, A., and Gonzalez-Gaitan, M. (2000). Gradient formation of the TGF-beta homolog Dpp. Cell *103*, 981-991.
Fasshauer, D., Sutton, R.B., Brunger, A.T., and Jahn, R. (1998). Conserved structural features of the synaptic fusion complex: SNARE proteins reclassified as Q- and R-SNAREs. Proc. Natl. Acad. Sci. USA *95*, 15781-15786.
Fields, I.C., Shteyn, E., Pypaert, M., Proux-Gillardeaux, V., Kang, R.S., Galli, T., and Folsch, H. (2007). v-SNARE cellubrevin is required for basolateral sorting of AP-1B-dependent cargo in polarized epithelial cells. J Cell Biol *177*, 477-488.
Folsch, H., Mattila, P.E., and Weisz, O.A. (2009). Taking the scenic route: biosynthetic traffic to the plasma membrane in polarized epithelial cells. Traffic *10*, 972-981.
Folsch, H., Ohno, H., Bonifacino, J.S., and Mellman, I. (1999). A novel clathrin adaptor complex mediates basolateral targeting in polarized epithelial cells. Cell *99*, 189-198.
Fujita, H., Tuma, P.L., Finnegan, C.M., Locco, L., and Hubbard, A.L. (1998). Endogenous syntaxins 2, 3 and 4 exhibit distinct but overlapping patterns of expression at the hepatocyte plasma membrane. The Biochemical journal *329 (Pt 3)*, 527-538.
Fung, S., Wang, F., Chase, M., Godt, D., and Hartenstein, V. (2008). Expression profile of the cadherin family in the developing Drosophila brain. The Journal of comparative neurology *506*, 469-488.
Gardiol, D., Kuhne, C., Glaunsinger, B., Lee, S.S., Javier, R., and Banks, L. (1999). Oncogenic human papillomavirus E6 proteins target the discs large tumour suppressor for proteasome-mediated degradation. Oncogene *18*, 5487-5496.
Gardiol, D., Zacchi, A., Petrera, F., Stanta, G., and Banks, L. (2006). Human discs large and scrib are localized at the same regions in colon mucosa and changes in their expression patterns are correlated with loss of tissue architecture during malignant progression. International journal of cancer *119*, 1285-1290.
Gassama-Diagne, A., and Payrastre, B. (2009). Phosphoinositide signaling pathways: promising role as builders of epithelial cell polarity. Int Rev Cell Mol Biol *273*, 313-343.

Gateff, E. (1978). Malignant neoplasms of genetic origin in Drosophila melanogaster. Science (New York, N.Y.) *200*, 1448-1459.
Geldner, N. (2009). Cell polarity in plants: a PARspective on PINs. Curr Opin Plant Biol *12*, 42-48.
Gengyo-ando, K., Kuroyanagi, H., Kobayashi, T., Murate, M., Fujimoto, K., Okabe, S., and Mitani, S. (2007). The SM protein VPS-45 is required for RAB-5-dependent endocytic transport in Caenorhabditis elegans. EMBO Rep. *8*, 152-157.
Georgiou, M., Marinari, E., Burden, J., and Baum, B. (2008). Cdc42, Par6, and aPKC regulate Arp2/3-mediated endocytosis to control local adherens junction stability. Current biology : CB *18*, 1631-1638.
Gibson, M.C., and Perrimon, N. (2003). Apicobasal polarization: epithelial form and function. Curr Opin Cell Biol *15*, 747-752.
Gilbert, M.M., Beam, C.K., Robinson, B.S., and Moberg, K.H. (2009). Genetic interactions between the Drosophila tumor suppressor gene ept and the stat92E transcription factor. PloS one *4*, e7083.
Gorvel, J.P., Chavrier, P., Zerial, M., and Gruenberg, J. (1991). rab5 controls early endosome fusion in vitro. Cell *64*, 915–925.
Grindstaff, K.K., Yeaman, C., Anandasabapathy, N., Hsu, S.C., Rodriguez-Boulan, E., Scheller, R.H., and Nelson, W.J. (1998). Sec6/8 complex is recruited to cell-cell contacts and specifies transport vesicle delivery to the basal-lateral membrane in epithelial cells. Cell *93*, 731-740.
Grosshans, B.L., Ortiz, D., and Novick, P. (2006). Rabs and their effectors: achieving specificity in membrane traffic. Proc. Natl. Acad. Sci. USA *103*, 11821-11827.
Haecker, A., Bergman, M., Neupert, C., Moussian, B., Luschnig, S., Aebi, M., and Mannervik, M. (2008). Wollknauel is required for embryo patterning and encodes the Drosophila ALG5 UDP-glucose:dolichyl-phosphate glucosyltransferase. Development (Cambridge, England) *135*, 1745-1749.
Hanahan, D., and Weinberg, R.A. (2000). The hallmarks of cancer. Cell *100*, 57-70.
Hariharan, I.K., and Bilder, D. (2006). Regulation of imaginal disc growth by tumor-suppressor genes in Drosophila *40*, 335-361.
Harris, K.P., and Tepass, U. (2008). Cdc42 and Par proteins stabilize dynamic adherens junctions in the Drosophila neuroectoderm through regulation of apical endocytosis. J Cell Biol *183*, 1129-1143.
Herz, C., Aumailley, M., Schulte, C., Schlotzer-Schrehardt, U., Bruckner-Tuderman, L., and Has, C. (2006). Kindlin-1 is a phosphoprotein involved in regulation of polarity, proliferation, and motility of epidermal keratinocytes. J Biol Chem *281*, 36082-36090.
Hetz, C. (2009). The UPR as a survival factor of cancer cells: More than folding proteins? Leukemia research *33*, 880-882.
Hirai-Fujita, Y., Yamamoto-Hino, M., Kanie, O., and Goto, S. (2008). N-Glycosylation of the Drosophila neural protein Chaoptin is essential for its stability, cell surface transport and adhesive activity. FEBS letters *582*, 2572-2576.
Humbert, P.O., Grzeschik, N.A., Brumby, A.M., Galea, R., Elsum, I., and Richardson, H.E. (2008). Control of tumourigenesis by the Scribble/Dlg/Lgl polarity module. Oncogene *27*, 6888-6907.

Hurd, T.W., Gao, L., Roh, M.H., Macara, I.G., and Margolis, B. (2003). Direct interaction of two polarity complexes implicated in epithelial tight junction assembly. Nat Cell Biol *5*, 137-142.
Iden, S., and Collard, J.G. (2008). Crosstalk between small GTPases and polarity proteins in cell polarization. Nat Rev Mol Cell Biol *9*, 846-859.
Irazoqui, J.E., Howell, A.S., Theesfeld, C.L., and Lew, D.J. (2005). Opposing roles for actin in Cdc42p polarization. Mol Biol Cell *16*, 1296-1304.
Irion, U., and St Johnston, D. (2007). bicoid RNA localization requires specific binding of an endosomal sorting complex. Nature *445*, 554-558.
Itoh, M., Sasaki, H., Furuse, M., Ozaki, H., Kita, T., and Tsukita, S. (2001). Junctional adhesion molecule (JAM) binds to PAR-3: a possible mechanism for the recruitment of PAR-3 to tight junctions. J Cell Biol *154*, 491-497.
Kee, Y., Yoo, J.S., Hazuka, C.D., Peterson, K.E., Hsu, S.C., and Scheller, R.H. (1997). Subunit structure of the mammalian exocyst complex. Proc Natl Acad Sci U S A *94*, 14438-14443.
Keller, P., Toomre, D., Diaz, E., White, J., and Simons, K. (2001). Multicolour imaging of post-Golgi sorting and trafficking in live cells. Nat Cell Biol *3*, 140-149.
Kemphues, K.J., Priess, J.R., Morton, D.G., and Cheng, N.S. (1988). Identification of genes required for cytoplasmic localization in early C. elegans embryos. Cell *52*, 311-320.
Kim-Ha, J., Smith, J.L., and Macdonald, P.M. (1991). oskar mRNA is localized to the posterior pole of the Drosophila oocyte. Cell *66*, 23-35.
Kim, S.-W., Chao, T.-H., Xiang, R., Lo, J.-F., Campbell, M.J., Fearns, C., and Lee, J.-D. (2004). Tid1, the human homologue of a Drosophila tumor suppressor, reduces the malignant activity of ErbB-2 in carcinoma cells. Cancer research *64*, 7732-7739.
Kim, S.H., Li, Z., and Sacks, D.B. (2000). E-cadherin-mediated cell-cell attachment activates Cdc42. J Biol Chem *275*, 36999-37005.
Klezovitch, O., Fernandez, T.E., Tapscott, S.J., and Vasioukhin, V. (2004). Loss of cell polarity causes severe brain dysplasia in Lgl1 knockout mice. Genes & development *18*, 559-571.
Knust, E., and Bossinger, O. (2002). Composition and formation of intercellular junctions in epithelial cells. Science *298*, 1955-1959.
Kuphal, S., Wallner, S., Schimanski, C.C., Bataille, F., Hofer, P., Strand, S., Strand, D., and Bosserhoff, A.K. (2006). Expression of Hugl-1 is strongly reduced in malignant melanoma. Oncogene *25*, 103-110.
Kurzik-Dumke, U., and Czaja, J. (2007). Htid-1, the human homolog of the Drosophila melanogaster l(2)tid tumor suppressor, defines a novel physiological role of APC. Cellular signalling *19*, 1973-1985.
Kurzik-Dumke, U., Debes, A., Kaymer, M., and Dienes, P. (1998). Mitochondrial localization and temporal expression of the Drosophila melanogaster DnaJ homologous tumor suppressor Tid50. Cell stress & chaperones *3*, 12-27.
Kurzik-Dumke, U., Gundacker, D., Renthrop, M., and Gateff, E. (1995). Tumor suppression in Drosophila is causally related to the function of the lethal(2) tumorous imaginal discs gene, a dnaJ homolog. Developmental genetics *16*, 64-76.

Kurzik-Dumke, U., Horner, M., Czaja, J., Nicotra, M.R., Simiantonaki, N., Koslowski, M., and Natali, P.G. (2008). Progression of colorectal cancers correlates with overexpression and loss of polarization of expression of the htid-1 tumor suppressor. International journal of molecular medicine *21*, 19-31.
Kurzik-Dumke, U., Kaymer, M., Gundacker, D., Debes, A., and Labitzke, K. (1997). Gene within gene configuration and expression of the Drosophila melanogaster genes lethal(2) neighbour of tid [l(2)not] and lethal(2) relative of tid[l(2)rot]. Gene *200*, 45-58.
Kurzik-Dumke, U., Phannavong, B., Gundacker, D., and Gateff, E. (1992). Genetic, cytogenetic and developmental analysis of the Drosophila melanogaster tumor suppressor gene lethal(2)tumorous imaginal discs (1(2)tid). Differentiation; research in biological diversity *51*, 91-104.
Langevin, J., Le Borgne, R., Rosenfeld, F., Gho, M., Schweisguth, F., and Bellaiche, Y. (2005). Lethal giant larvae controls the localization of notch-signaling regulators numb, neuralized, and Sanpodo in Drosophila sensory-organ precursor cells. Curr Biol *15*, 955-962.
Lanzetti, L., Palamidessi, A., Areces, L., Scita, G., Fiore, D., and P, P. (2004). Rab5 is a signalling GTPase involved in actin remodelling by receptor tyrosine kinases. Nature *429*, 309-314.
Lawrence, P.A., Johnston, P., Morata, G., and Roberts, D.B. (1986). Methods of Marking Cells, Oxford: IRL Press Limited, 229-242.
Lazebnik, Y. (2010). What are the hallmarks of cancer? Nature reviews *10*, 232-233.
Lee, J.H., Koh, H., Kim, M., Kim, Y., Lee, S.Y., Karess, R.E., Lee, S.H., Shong, M., Kim, J.M., Kim, J., and Chung, J. (2007). Energy-dependent regulation of cell structure by AMP-activated protein kinase. Nature *447*, 1017-1020.
Lee, T., and Luo, L. (2001). Mosaic analysis with a repressible cell marker (MARCM) for Drosophila neural development. Trends in neurosciences *24*, 251-254.
Lehle, L., Strahl, S., and Tanner, W. (2006). Protein glycosylation, conserved from yeast to man: a model organism helps elucidate congenital human diseases. Angewandte Chemie (International ed. in English) *45*, 6802-6818.
Lehman, K., Rossi, G., Adamo, J.E., and Brennwald, P. (1999). Yeast Homologues of Tomosyn and lethal giant larvae Function in Exocytosis and Are Associated with the Plasma Membrane SNARE , Sec9. Journal of Cell Biology *146*, 125-140.
Leibfried, A., Fricke, R., Morgan, M.J., Bogdan, S., and Bellaiche, Y. (2008). Drosophila Cip4 and WASp define a branch of the Cdc42-Par6-aPKC pathway regulating E-cadherin endocytosis. Current biology : CB *18*, 1639-1648.
Leong, G.R., Goulding, K.R., Amin, N., Richardson, H.E., and Brumby, A.M. (2009). Scribble mutants promote aPKC and JNK-dependent epithelial neoplasia independently of Crumbs. BMC biology *7*, 62.
Li, R., and Gundersen, G.G. (2008). Beyond polymer polarity: how the cytoskeleton builds a polarized cell. Nat Rev Mol Cell Biol *9*, 860-873.
Liwosz, A., Lei, T., and Kukuruzinska, M.A. (2006). N-glycosylation affects the molecular organization and stability of E-cadherin junctions. J. Biol. Chem. *281*, 23138-23149.

Lloyd, T.E., Atkinson, R., Wu, M.N., Zhou, Y., Pennetta, G., and Bellen, H.J. (2002). Hrs regulates Endosome Membrane Invagination and Tyrosine Kinase Receptor Signaling in Drosophila. Cell *108*, 261-269.
Löffler, T., Wismar, J., Sass, H., Miyamoto, T., Becker, G., Konrad, L., Blondeau, M., Protin, U., Kaiser, S., and Gräf, P. (1990). Genetic and molecular analysis of six tumor suppressor genes in Drosophila melanogaster. Environmental health perspectives *88*, 157-161.
Loureiro, J., and Peifer, M. (1998). Roles of Armadillo, a Drosophila catenin, during central nervous system development. Current biology : CB *8*, 622-632.
Low, S.H., Chapin, S.J., Weimbs, T., Komuves, L.G., Bennett, M.K., and Mostov, K.E. (1996). Differential localization of syntaxin isoforms in polarized Madin-Darby canine kidney cells. Mol Biol Cell *7*, 2007-2018.
Lu, H., and Bilder, D. (2005). Endocytic control of epithelial polarity and proliferation in Drosophila. Nature cell biology *7*, 1232-1239.
Lu, Y., and Settleman, J. (1999). The Drosophila Pkn protein kinase is a Rho/Rac effector target required for dorsal closure during embryogenesis. Genes Dev. *13*, 1168-1180.
Macara, I.G. (2004). Parsing the polarity code. Nat Rev Mol Cell Biol *5*, 220-231.
Maday, S., Anderson, E., Chang, H.C., Shorter, J., Satoh, A., Sfakianos, J., Folsch, H., Anderson, J.M., Walther, Z., and Mellman, I. (2008). A PDZ-binding motif controls basolateral targeting of syndecan-1 along the biosynthetic pathway in polarized epithelial cells. Traffic *9*, 1915-1924.
Manfruelli, P., Arquier, N., Hanratty, W.P., and Semeriva, M. (1996). The tumor suppressor gene, lethal(2)giant larvae (1(2)g1), is required for cell shape change of epithelial cells during Drosophila development. Development *122*, 2283-2294.
Marco, E., Wedlich-Soldner, R., Li, R., Altschuler, S.J., and Wu, L.F. (2007). Endocytosis optimizes the dynamic localization of membrane proteins that regulate cortical polarity. Cell *129*, 411-422.
Massimi, P., Gammoh, N., Thomas, M., and Banks, L. (2004). HPV E6 specifically targets different cellular pools of its PDZ domain-containing tumour suppressor substrates for proteasome-mediated degradation. Oncogene *23*, 8033-8039.
Mcbride, H.M., Rybin, V., Murphy, C., Giner, A., Teasdale, R., and Zerial, M. (1999). Oligomeric complexes link Rab5 effectors with NSF and drive membrane fusion via interactions between EEA1 and Syntaxin 13. Cell *98*, 377-386.
McNeill, H. (2010). Planar cell polarity: keeping hairs straight is not so simple. Cold Spring Harbor perspectives in biology *2*, a003376.
Mcnew, J.A., Parlati, F., Fukuda, R., Johnston, R.J., Paz, K., Paumet, F., Sollner, T.H., and Rothman, J.E. (2000). Compartmental specificity of cellular membrane fusion encoded in SNARE proteins. Nature *407*, 153-159.
Meads, T., and Schroer, T.A. (1995). Polarity and nucleation of microtubules in polarized epithelial cells. Cell motility and the cytoskeleton *32*, 273-288.
Mellman, I., and Nelson, W.J. (2008). Coordinated protein sorting, targeting and distribution in polarized cells. Nat Rev Mol Cell Biol *9*, 833-845.

Menut, L., Vaccari, T., Dionne, H., Hill, J., Wu, G., and Bilder, D. (2007). A mosaic genetic screen for Drosophila neoplastic tumor suppressor genes based on defective pupation. Genetics *177*, 1667-1677.
Moberg, K.H., Schelble, S., Burdick, S.K., and Hariharan, I.K. (2005). Mutations in erupted, the Drosophila ortholog of mammalian tumor susceptibility gene 101, elicit non-cell-autonomous overgrowth. Dev Cell *9*, 699-710.
Moenner, M., Pluquet, O., Bouchecareilh, M., and Chevet, E. (2007). Integrated endoplasmic reticulum stress responses in cancer. Cancer Res *67*, 10631-10634.
Mosesson, Y., Mills, G.B., and Yarden, Y. (2008). Derailed endocytosis: an emerging feature of cancer. Nature reviews *8*, 835-850.
Mostov, K., Su, T., and ter Beest, M. (2003). Polarized epithelial membrane traffic: conservation and plasticity. Nat Cell Biol *5*, 287-293.
Mostov, K.E., Verges, M., and Altschuler, Y. (2000). Membrane traffic in polarized epithelial cells. Curr Opin Cell Biol *12*, 483-490.
Motegi, F., and Sugimoto, A. (2006). Sequential functioning of the ECT-2 RhoGEF, RHO-1 and CDC-42 establishes cell polarity in Caenorhabditis elegans embryos. Nat Cell Biol *8*, 978-985.
Munro, E., and Bowerman, B. (2009). Cellular Symmetry Breaking during Caenorhabditis elegans Development. Cold Spring Harb Perspect Biol *1*, a003400.
Munro, E.M. (2006). PAR proteins and the cytoskeleton: a marriage of equals. Curr Opin Cell Biol *18*, 86-94.
Munson, M., and Novick, P. (2006). The exocyst defrocked, a framework of rods revealed. Nature structural & molecular biology *13*, 577-581.
Musch, A. (2004). Microtubule organization and function in epithelial cells. Traffic *5*, 1-9.
Musch, A., Cohen, D., Yeaman, C., Nelson, W.J., Rodriguez-Boulan, E., and Brennwald, P.J. (2002). Mammalian Homolog of Drosophila Tumor Suppressor Lethal (2) Giant Larvae Interacts with Basolateral Exocytic Machinery in Madin-Darby Canine Kidney Cells. Molecular Biology of the Cell *13*, 158 -168.
Muthuswamy, S.K., Li, D., Lelievre, S., Bissell, M.J., and Brugge, J.S. (2001). ErbB2, but not ErbB1, reinitiates proliferation and induces luminal repopulation in epithelial acini. Nat Cell Biol *3*, 785-792.
Nakagawa, S., and Huibregtse, J.M. (2000). Human scribble (Vartul) is targeted for ubiquitin-mediated degradation by the high-risk papillomavirus E6 proteins and the E6AP ubiquitin-protein ligase. Molecular and cellular biology *20*, 8244-8253.
Nakagawa, S., Yano, T., Nakagawa, K., Takizawa, S., Suzuki, Y., Yasugi, T., Huibregtse, J.M., and Taketani, Y. (2004). Analysis of the expression and localisation of a LAP protein, human scribble, in the normal and neoplastic epithelium of uterine cervix. British journal of cancer *90*, 194-199.
Nakatsu, F., and Ohno, H. (2003). Adaptor protein complexes as the key regulators of protein sorting in the post-Golgi network. Cell structure and function *28*, 419-429.
Nakayama, Y., Shivas, J.M., Poole, D.S., Squirrell, J.M., Kulkoski, J.M., Schleede, J.B., and Skop, A.R. (2009). Dynamin participates in the maintenance of anterior polarity in the Caenorhabditis elegans embryo. Dev Cell *16*, 889-900.

Naslavsky, N., Boehm, M., Backlund, P.S., Jr, and Caplan, S. (2004). Rabenosyn-5 and EHD1 Interact and sequentially regulate protein recycling to the plasma membrane. Mol. Biol. Cell *15*, 2410-2422.
Navarro, C., Nola, S., Audebert, S., Santoni, M.J., Arsanto, J.P., Ginestier, C., Marchetto, S., Jacquemier, J., Isnardon, D., Le Bivic, A., Birnbaum, D., and Borg, J.P. (2005). Junctional recruitment of mammalian Scribble relies on E-cadherin engagement. Oncogene *24*, 4330-4339.
Nelson, W.J., and Rodriguez-Boulan, E. (2004). Unravelling protein sorting. Nat Cell Biol *6*, 282-284.
Nichols, B.J., Holthuis, J.C., and Pelham, H.R. (1998). The Sec1p homologue Vps45p binds to the syntaxin Tlg2p. Eur. J. Cell Biol. *77*, 263-268.
Nielsen, E., Christoforidis, S., Uttenweiler-Joseph, S., Miaczynska, M., Dewitte, F., Wilm, M., Hoflack, B., and Zerial, M. (2000). Rabenosyn-5, a novel Rab5 effector, is complexed with hVPS45 and recruited to endosomes through a FYVE finger domain. J. Cell Biol. *151*, 601-612.
Nishimura, T., and Kaibuchi, K. (2007). Numb controls integrin endocytosis for directional cell migration with aPKC and PAR-3. Dev. Cell *13*, 15-28.
Oztan, A., Silvis, M., Weisz, O.A., Bradbury, N.A., Hsu, S.C., Goldenring, J.R., Yeaman, C., and Apodaca, G. (2007). Exocyst requirement for endocytic traffic directed toward the apical and basolateral poles of polarized MDCK cells. Mol Biol Cell *18*, 3978-3992.
Pace, K.E., Lebestky, T., Hummel, T., Arnoux, P., Kwan, K., and Baum, L.G. (2002). Characterization of a novel Drosophila melanogaster galectin. Expression in developing immune, neural, and muscle tissues. The Journal of biological chemistry *277*, 13091-13098.
Paladino, S., Sarnataro, D., Pillich, R., Tivodar, S., Nitsch, L., and Zurzolo, C. (2004). Protein oligomerization modulates raft partitioning and apical sorting of GPI-anchored proteins. J Cell Biol *167*, 699-709.
Paladino, S., Sarnataro, D., Tivodar, S., and Zurzolo, C. (2007). Oligomerization is a specific requirement for apical sorting of glycosyl-phosphatidylinositol-anchored proteins but not for non-raft-associated apical proteins. Traffic *8*, 251-258.
Paladino, S., Sarnataro, D., and Zurzolo, C. (2002). Detergent-resistant membrane microdomains and apical sorting of GPI-anchored proteins in polarized epithelial cells. Int J Med Microbiol *291*, 439-445.
Parks, A.L. (2004). Systematic generation of high-resolution deletion coverage of the Drosophila melanogaster genome. Nat. Genet. *36*, 288-292.
Peng, R., and Gallwitz, D. (2002). Sly1 protein bound to Golgi syntaxin Sed5p allows assembly and contributes to specificity of SNARE fusion complexes. J. Cell Biol. *157*, 645-655.
Peterson, M.R., Burd, C.G., and Emr, S.D. (1999). Vac1p coordinates Rab and phosphatidylinositol 3-kinase signaling in Vps45p-dependent vesicle docking/fusion at the endosome. Curr. Biol. *9*, 159-162.
Pocard, T., Le Bivic, A., Galli, T., and Zurzolo, C. (2007). Distinct v-SNAREs regulate direct and indirect apical delivery in polarized epithelial cells. J Cell Sci *120*, 3309-3320.

Polishchuk, R., Di Pentima, A., and Lippincott-Schwartz, J. (2004). Delivery of raft-associated, GPI-anchored proteins to the apical surface of polarized MDCK cells by a transcytotic pathway. Nat Cell Biol *6*, 297-307.
Potter, B.A., Hughey, R.P., and Weisz, O.A. (2006a). Role of N- and O-glycans in polarized biosynthetic sorting. American journal of physiology *290*, C1-C10.
Potter, B.A., Ihrke, G., Bruns, J.R., Weixel, K.M., and Weisz, O.A. (2004). Specific N-glycans direct apical delivery of transmembrane, but not soluble or glycosylphosphatidylinositol-anchored forms of endolyn in Madin-Darby canine kidney cells. Mol Biol Cell *15*, 1407-1416.
Potter, B.A., Weixel, K.M., Bruns, J.R., Ihrke, G., and Weisz, O.A. (2006b). N-glycans mediate apical recycling of the sialomucin endolyn in polarized MDCK cells. Traffic *7*, 146-154.
Qin, Y., Capaldo, C., Gumbiner, B.M., and Macara, I.G. (2005). The mammalian Scribble polarity protein regulates epithelial cell adhesion and migration through E-cadherin. J Cell Biol *171*, 1061-1071.
Raymond, C.K., Howald-stevenson, I., Vater, C.A., and Stevens, T.H. (1992). Morphological classification of the yeast vacuolar protein sorting mutants: evidence for a prevacuolar compartment in class E vps mutants. Mol. Biol. Cell *3*, 1389-1402.
Reischauer, S., Levesque, M.P., Nusslein-Volhard, C., and Sonawane, M. (2009). Lgl2 executes its function as a tumor suppressor by regulating ErbB signaling in the zebrafish epidermis. PLoS genetics *5*, e1000720.
Rodriguez-Boulan, E., Kreitzer, G., and Musch, A. (2005). Organization of vesicular trafficking in epithelia. Nat Rev Mol Cell Biol *6*, 233-247.
Rodriguez-Boulan, E., and Musch, A. (2005). Protein sorting in the Golgi complex: shifting paradigms. Biochimica et biophysica acta *1744*, 455-464.
Roegiers, F., Jan, L.Y., and Jan, Y.N. (2005). Regulation of Membrane Localization of Sanpodo by lethal giant larvae and neuralized in Asymmetrically Dividing Cells of Drosophila Sensory Organs. Molecular Biology of the Cell *16*, 3480 -3487.
Rojas, R., and Apodaca, G. (2002). Immunoglobulin transport across polarized epithelial cells. Nat Rev Mol Cell Biol *3*, 944-955.
Rongo, C., Gavis, E.R., and Lehmann, R. (1995). Localization of oskar RNA regulates oskar translation and requires Oskar protein. Development *121*, 2737-2746.
Rosin, D., Schejter, E., Volk, T., and Shilo, B.-Z. (2004). Apical accumulation of the Drosophila PDGF/VEGF receptor ligands provides a mechanism for triggering localized actin polymerization. Development *131*, 1939-1948.
Rosse, C., Formstecher, E., Boeckeler, K., Zhao, Y., Kremerskothen, J., White, M.D., Camonis, J.H., and Parker, P.J. (2009). An aPKC-exocyst complex controls paxillin phosphorylation and migration through localised JNK1 activation. PLoS biology *7*, e1000235.
Rubino, M., Miaczynska, M., Lippe, R., and Zerial, M. (2000). Selective membrane recruitment of EEA1 suggests a role in directional transport of clathrin-coated vesicles to early endosomes *275*, 3745-3748.
Rusten, T.E., and Stenmark, H. (2006). Analyzing phosphoinositides and their interacting proteins. Nat Methods *3*, 251-258.

Sarkar, S., Pollack, B.P., Lin, K.T., Kotenko, S.V., Cook, J.R., Lewis, A., and Pestka, S. (2001). hTid-1, a human DnaJ protein, modulates the interferon signaling pathway. The Journal of biological chemistry *276*, 49034-49042.
Satoh, A.K., O'Tousa, J.E., Ozaki, K., and Ready, D.F. (2005). Rab11 mediates post-Golgi trafficking of rhodopsin to the photosensitive apical membrane of Drosophila photoreceptors. Development *132*, 1487-1497.
Schilling, B., De-Medina, T., Syken, J., Vidal, M., and Munger, K. (1998). A novel human DnaJ protein, hTid-1, a homolog of the Drosophila tumor suppressor protein Tid56, can interact with the human papillomavirus type 16 E7 oncoprotein. Virology *247*, 74-85.
Schmoranzer, J., Fawcett, J.P., Segura, M., Tan, S., Vallee, R.B., Pawson, T., and Gundersen, G.G. (2009). Par3 and dynein associate to regulate local microtubule dynamics and centrosome orientation during migration. Curr Biol *19*, 1065-1074.
Schonbaum, C.P., Perrino, J.J., and Mahowald, A.P. (2000). Regulation of the vitellogenin receptor during Drosophila melanogaster oogenesis. Mol. Biol. Cell *11*, 511-521.
Schonegg, S., and Hyman, A.A. (2006). CDC-42 and RHO-1 coordinate acto-myosin contractility and PAR protein localization during polarity establishment in C. elegans embryos. Development *133*, 3507-3516.
Seals, D.F., Eitzen, G., Margolis, N., Wickner, W.T., and Price, A. (2000). A Ypt/Rab effector complex containing the Sec1 homolog Vps33p is required for homotypic vacuole fusion. Proc. Natl. Acad. Sci. USA *97*, 9402-9407.
Sevrioukov, E.A., He, J.P., Moghrabi, N., Sunio, A., and Kramer, H. (1999). A role for the deep orange and carnation eye color genes in lysosomal delivery. in Drosophila. Mol. Cell *4*, 479-486.
Sharma, C.B., Knauer, R., and Lehle, L. (2001). Biosynthesis of Lipid-Linked Oligosaccharides in Yeast : the ALG3 Gene Encodes the Dol-P-Man:Man5GlcNAc2-PP-Dol Mannosyltransferase. Biol. Chem. *382*, 321 - 328.
Sharma, N., Low, S.H., Misra, S., Pallavi, B., and Weimbs, T. (2006). Apical targeting of syntaxin 3 is essential for epithelial cell polarity. J Cell Biol *173*, 937-948.
Siegrist, S.E., and Doe, C.Q. (2006). Extrinsic cues orient the cell division axis in Drosophila embryonic neuroblasts. Development (Cambridge, England) *133*, 529-536.
Slaughter, B.D., Das, A., Schwartz, J.W., Rubinstein, B., and Li, R. (2009). Dual modes of cdc42 recycling fine-tune polarized morphogenesis. Dev Cell *17*, 823-835.
Smith, C.A., Lau, K.M., Rahmani, Z., Dho, S.E., Brothers, G., She, Y.M., Berry, D.M., Bonneil, E., Thibault, P., Schweisguth, F., {Le Borgne}, R., and McGlade, C.J. (2007). aPKC-mediated phosphorylation regulates asymmetric membrane localization of the cell fate determinant Numb. Embo J *26*, 468-480.
Srivastava, A., Pastor-pareja, J.C., Igaki, T., Pagliarini, R., and Xu, T. (2007). Basement membrane remodeling is essential for Drosophila disc eversion and tumor invasion. Proc. Natl. Acad. Sci. USA *104*, 2721-2726.
St Johnston, D. (2002). The art and design of genetic screens: Drosophila melanogaster. Nature reviews. Genetics *3*, 176-188.
Steed, E., Balda, M.S., and Matter, K. (2010). Dynamics and functions of tight junctions. Trends Cell Biol *20*, 142-149.

Stenmark, H., and Olkkonen, V.M. (2001). The Rab GTPase family. Genome Biol. 2, REVIEWS3007.
Stenmark, H., Parton, R.G., Steele-mortimer, O., Lutcke, A., Gruenberg, J., and Zerial, M. (1994). Inhibition of rab5 GTPase activity stimulates membrane fusion in endocytosis. EMBO J. *13*, 1287-1296.
Stowers, R.S., and Schwarz, T.L. (1999). A genetic method for generating Drosophila eyes composed exclusively of mitotic clones of a single genotype. Genetics *152*, 1631-1639.
Suzuki, A., Hirata, M., Kamimura, K., Maniwa, R., Yamanaka, T., Mizuno, K., Kishikawa, M., Hirose, H., Amano, Y., Izumi, N., Miwa, Y., and Ohno, S. (2004). aPKC acts upstream of PAR-1b in both the establishment and maintenance of mammalian epithelial polarity. Curr Biol *14*, 1425-1435.
Suzuki, A., and Ohno, S. (2006). The PAR-aPKC system: lessons in polarity. J Cell Sci *119*, 979-987.
Suzuki, A., Yamanaka, T., Hirose, T., Manabe, N., Mizuno, K., Shimizu, M., Akimoto, K., Izumi, Y., Ohnishi, T., and Ohno, S. (2001). Atypical protein kinase C is involved in the evolutionarily conserved par protein complex and plays a critical role in establishing epithelia-specific junctional structures. J Cell Biol *152*, 1183-1196.
Tanaka, T., and Nakamura, A. (2008). The endocytic pathway acts downstream of Oskar in Drosophila germ plasm assembly. Development *135*, 1107-1117.
Tanentzapf, G., and Tepass, U. (2003). Interactions between the crumbs, lethal giant larvae and bazooka pathways in epithelial polarization. Nature cell biology *5*, 46-52.
Taniguchi, N. (2007). A sugar-coated switch for cellular growth and arrest. Nature chemical biology *3*, 307-309.
ten Hagen, K.G., Zhang, L., Tian, E., and Zhang, Y. (2009). Glycobiology on the fly: developmental and mechanistic insights from Drosophila. Glycobiology *19*, 102-111.
Tepass, U., and Knust, E. (1993). Crumbs and Stardust act in a genetic pathway that controls the organization of epithelia in Drosophila melanogaster. Dev. Biol. *159*, 311-326.
Tepass, U., Tanentzapf, G., Ward, R., and Fehon, R. (2001). Epithelial cell polarity and cell junctions in Drosophila. Annual review of genetics *35*, 747-784.
Tepass, U., Theres, C., and Knust, E. (1990). crumbs encodes an EGF-like protein expressed on apical membranes of Drosophila epithelial cells and required for organization of epithelia. Cell *61*, 787-799.
ter Beest, M.B., Chapin, S.J., Avrahami, D., and Mostov, K.E. (2005). The role of syntaxins in the specificity of vesicle targeting in polarized epithelial cells. Mol Biol Cell *16*, 5784-5792.
TerBush, D.R., Maurice, T., Roth, D., and Novick, P. (1996). The Exocyst is a multiprotein complex required for exocytosis in Saccharomyces cerevisiae. Embo J *15*, 6483-6494.
Thompson, B.J., Mathieu, J., Sung, H.H., Loeser, E., Rorth, P., and Cohen, S.M. (2005). Tumor suppressor properties of the ESCRT-II complex component Vps25 in Drosophila. Dev Cell *9*, 711-720.
Trougakos, I.P., Papassideri, I.S., Waring, G.L., and Margaritis, L.H. (2001). Differential sorting of constitutively co-secreted proteins in the ovarian follicle cells of Drosophila. Eur. J. Cell Biol. *80*, 271-284.

Tsuda, T., Ikeda, Y., and Taniguchi, N. (2000). The Asn-420-linked sugar chain in human epidermal growth factor receptor suppresses ligand-independent spontaneous oligomerization. Possible role of a specific sugar chain in controllable receptor activation. J Biol Chem *275*, 21988-21994.
Tsukada, M., Will, E., and Gallwitz, D. (1999). Structural and functional analysis of a novel coiled-coil protein involved in Ypt6 GTPase-regulated protein transport in yeast. Mol. Biol. Cell *10*, 63-75.
Tuma, P.L., and Hubbard, A.L. (2003). Transcytosis: crossing cellular barriers. Physiol Rev *83*, 871-932.
Uhlirova, M., and Bohmann, D. (2006). JNK- and Fos-regulated Mmp1 expression cooperates with Ras to induce invasive tumors. in Drosophila. EMBO J. *25*, 5294-5304.
Ullrich, O., Reinsch, S., Urbe, S., Zerial, M., and Parton, R.G. (1996). Rab11 regulates recycling through the pericentriolar recycling endosome. J. Cell Biol. *135*, 913-924.
Ungermann, C., and Langosch, D. (2005). Functions of SNAREs in intracellular membrane fusion and lipid bilayer mixing. J. Cell Sci. *118*, 3819-3828.
Vaccari, T., and Bilder, D. (2005). The Drosophila tumor suppressor vps25 prevents nonautonomous overproliferation by regulating notch trafficking. Dev. Cell *9*, 687-698.
Vaccari, T., and Bilder, D. (2009). At the crossroads of polarity, proliferation and apoptosis: the use of Drosophila to unravel the multifaceted role of endocytosis in tumor suppression. Molecular oncology *3*, 354-365.
Vaccari, T., Lu, H., Kanwar, R., Fortini, M.E., and Bilder, D. (2008). Endosomal entry regulates Notch receptor activation in Drosophila melanogaster. J. Cell Biol. *180*, 755-762.
Vagin, O., Kraut, J.A., and Sachs, G. (2009). Role of N-glycosylation in trafficking of apical membrane proteins in epithelia. Am J Physiol Renal Physiol *296*, F459-469.
van Ijzendoorn, S.C., and Hoekstra, D. (1999). The subapical compartment: a novel sorting centre? Trends Cell Biol *9*, 144-149.
Vanzo, N., Oprins, A., Xanthakis, D., Ephrussi, A., and Rabouille, C. (2007). Stimulation of endocytosis and actin dynamics by Oskar polarizes the Drosophila oocyte. Dev Cell *12*, 543-555.
Vasioukhin, V. (2006). Lethal giant puzzle of Lgl. Developmental neuroscience *28*, 13-24.
Wang, A.Z., Ojakian, G.K., and Nelson, W.J. (1990). Steps in the morphogenesis of a polarized epithelium. I. Uncoupling the roles of cell-cell and cell-substratum contact in establishing plasma membrane polarity in multicellular epithelial (MDCK) cysts. J Cell Sci *95 (Pt 1)*, 137-151.
Wang, Q., Chen, X.W., and Margolis, B. (2007). PALS1 regulates E-cadherin trafficking in mammalian epithelial cells. Mol Biol Cell *18*, 874-885.
Wang, Q., and Margolis, B. (2007). Apical junctional complexes and cell polarity. Kidney international *72*, 1448-1458.
Waters, M.G., and Hughson, F.M. (2000). Membrane tethering and fusion in the secretory and endocytic pathways. Traffic *1*, 588-597.
Weisz, O.A., and Rodriguez-Boulan, E. (2009). Apical trafficking in epithelial cells: signals, clusters and motors. J Cell Sci *122*, 4253-4266.

Wells, C.D., Fawcett, J.P., Traweger, A., Yamanaka, Y., Goudreault, M., Elder, K., Kulkarni, S., Gish, G., Virag, C., Lim, C., Colwill, K., Starostine, A., Metalnikov, P., and Pawson, T. (2006). A Rich1/Amot complex regulates the Cdc42 GTPase and apical-polarity proteins in epithelial cells. Cell *125*, 535-548.
Whyte, J.R.C., and Munro, S. (2002). Vesicle tethering complexes in membrane traffic. J. Cell Sci. *115*, 2627-2637.
Wilkin, M., Tongngok, P., Gensch, N., Clemence, S., Motoki, M., Yamada, K., Hori, K., Taniguchi-Kanai, M., Franklin, E., Matsuno, K., and Baron, M. (2008). Drosophila HOPS and AP-3 complex genes are required for a Deltex-regulated activation of notch in the endosomal trafficking pathway. Dev Cell *15*, 762-772.
Windler, S.L., and Bilder, D. (2010). Endocytic internalization routes required for delta/notch signaling. Curr Biol *20*, 538-543.
Wodarz, A. (2002). Establishing cell polarity in development. Nat Cell Biol *4*, E39-44.
Wodarz, A., Ramrath, A., Grimm, A., and Knust, E. (2000). Drosophila atypical protein kinase C associates with Bazooka and controls polarity of epithelia and neuroblasts. J Cell Biol *150*, 1361-1374.
Wu, H., Feng, W., Chen, J., Ling-Nga, C., Huang, S., and Zhang, M. (2007). PDZ Domains of Par-3 as Potential Phosphoinositide Signaling Integrators. Molecular Cell *28*, 886-898.
Wu, M., Pastor-Pareja, J.C., and Xu, T. (2010). Interaction between Ras(V12) and scribbled clones induces tumour growth and invasion. Nature *463*, 545-548.
Wucherpfennig, T., Wilsch-brauninger, M., and Gonzalez-gaitan, M. (2003). Role of Drosophila Rab5 during endosomal trafficking at the synapse and evoked neurotransmitter release. J. Cell Biol. *161*, 609-624.
Xu, H., Boulianne, G.L., and Trimble, W.S. (2002). Drosophila syntaxin 16 is a Q-SNARE implicated in Golgi dynamics. J. Cell Sci. *115*, 4447-4455.
Xue, X., Piao, J.-H., Nakajima, A., Sakon-Komazawa, S., Kojima, Y., Mori, K., Yagita, H., Okumura, K., Harding, H., and Nakano, H. (2005). Tumor necrosis factor alpha (TNFalpha) induces the unfolded protein response (UPR) in a reactive oxygen species (ROS)-dependent fashion, and the UPR counteracts ROS accumulation by TNFalpha. The Journal of biological chemistry *280*, 33917-33925.
Yamanaka, T., Horikoshi, Y., Suzuki, A., Sugiyama, Y., Kitamura, K., Maniwa, R., Nagai, Y., Yamashita, A., Hirose, T., Ishikawa, H., and Ohno, S. (2001). PAR-6 regulates aPKC activity in a novel way and mediates cell-cell contact-induced formation of the epithelial junctional complex. Genes Cells *6*, 721-731.
Yamashita, Y.M., Yuan, H., Cheng, J., and Hunt, A.J. (2010). Polarity in stem cell division: asymmetric stem cell division in tissue homeostasis. Cold Spring Harbor perspectives in biology *2*, a001313.
Yeaman, C., Grindstaff, K.K., and Nelson, W.J. (1999). New perspectives on mechanisms involved in generating epithelial cell polarity. Physiological reviews *79*, 73-98.
Yeaman, C., Grindstaff, K.K., and Nelson, W.J. (2004). Mechanism of recruiting Sec6/8 (exocyst) complex to the apical junctional complex during polarization of epithelial cells. J Cell Sci *117*, 559-570.
Yin, X., and Rozakis-Adcock, M. (2001). Genomic organization and expression of the human tumorous imaginal disc (TID1) gene. Gene *278*, 201-210.

Yu, W., Datta, A., Leroy, P., O'Brien, L.E., Mak, G., Jou, T.S., Matlin, K.S., Mostov, K.E., and Zegers, M.M. (2005). Beta1-integrin orients epithelial polarity via Rac1 and laminin. Mol Biol Cell *16*, 433-445.
Yu, W., Shewan, A.M., Brakeman, P., Eastburn, D.J., Datta, A., Bryant, D.M., Fan, Q.W., Weiss, W.A., Zegers, M.M., and Mostov, K.E. (2008). Involvement of RhoA, ROCK I and myosin II in inverted orientation of epithelial polarity. EMBO reports *9*, 923-929.
Zallen, J.A. (2007). Planar polarity and tissue morphogenesis. Cell *129*, 1051-1063.
Zarnescu, D.C., Jin, P., Betschinger, J., Nakamoto, M., Wang, Y., Dockendorff, T.C., Feng, Y., Jongens, T.a., Sisson, J.C., Knoblich, J.a., Warren, S.T., and Moses, K. (2005). Fragile X protein functions with lgl and the par complex in flies and mice. Developmental cell *8*, 43-52.
Zeitler, J., Hsu, C.P., Dionne, H., and Bilder, D. (2004). Domains controlling cell polarity and proliferation in the Drosophila tumor suppressor Scribble. Journal of Cell Biology *167*, 1137-1146.
Zerial, M., and Mcbride, H. (2001). Rab proteins as membrane organizers. Nat. Rev. Mol. Cell Biol. *2*, 107-117.
Zhang, H., Squirrell, J.M., and White, J.G. (2008). RAB-11 permissively regulates spindle alignment by modulating metaphase microtubule dynamics in Caenorhabditis elegans early embryos. Mol Biol Cell *19*, 2553-2565.